

DOCTOR OF PHILOSOPHY

Modelling the human accommodation
system using finite element analysis

Benjamin Coldrick

2013

Aston University

Some pages of this thesis may have been removed for copyright restrictions.

If you have discovered material in AURA which is unlawful e.g. breaches copyright, (either yours or that of a third party) or any other law, including but not limited to those relating to patent, trademark, confidentiality, data protection, obscenity, defamation, libel, then please read our [Takedown Policy](#) and [contact the service](#) immediately

Modelling the human accommodation system using finite element analysis

Benjamin James Coldrick
Doctor of Philosophy

ASTON UNIVERSITY
July 2013

©Benjamin James Coldrick, 2013

Benjamin James Coldrick asserts his moral right to be identified as the author of this thesis.

This copy of the thesis has been supplied on condition that anyone who consults it is understood to recognise that its copyright rests with its author and that no quotation from the thesis and no information derived from it may be published without proper acknowledgement.

ASTON UNIVERSITY

Modelling the human accommodation system using finite element analysis

BENJAMIN JAMES COLDRICK

Doctor of Philosophy

July 2013

The human accommodation system has been extensively examined for over a century, with a particular focus on trying to understand the mechanisms that lead to the loss of accommodative ability with age (Presbyopia). The accommodative process, along with the potential causes of presbyopia, are disputed; hindering efforts to develop methods of restoring accommodation in the presbyopic eye. One method that can be used to provide insight into this complex area is Finite Element Analysis (FEA).

The effectiveness of FEA in modelling the accommodative process has been illustrated by a number of accommodative FEA models developed to date. However, there have been limitations to these previous models; principally due to the variation in data on the geometry of the accommodative components, combined with sparse measurements of their material properties. Despite advances in available data, continued oversimplification has occurred in the modelling of the crystalline lens structure and the zonular fibres that surround the lens.

A new accommodation model was proposed by the author that aims to eliminate these limitations. A novel representation of the zonular structure was developed, combined with updated lens and capsule modelling methods. The model has been designed to be adaptable so that a range of different age accommodation systems can be modelled, allowing the age related changes that occur to be simulated.

The new modelling methods were validated by comparing the changes induced within the model to available *in vivo* data, leading to the definition of three different age models. These were used in an extended sensitivity study on age related changes, where individual parameters were altered to investigate their effect on the accommodative process. The material properties were found to have the largest impact on the decline in accommodative ability, in particular compared to changes in ciliary body movement or zonular structure. Novel data on the importance of the capsule stiffness and thickness was also established.

The new model detailed within this thesis provides further insight into the accommodation mechanism, as well as a foundation for future, more detailed investigations into accommodation, presbyopia and accommodative restoration techniques.

Keywords: Accommodation; Presbyopia; Finite element analysis (FEA); Crystalline lens; Ciliary body

Dedicated to my grandfather, David Mutton

Acknowledgments

The journey to complete this thesis has been a long one and I would never have been able to finish it without the support of the following colleagues, friends and family.

I would first like to thank my supervisor Dr Gregory Swadener and my associate supervisor Dr Leon Davies for their continued support and supervision throughout this PhD. Always available for me to ask questions, both big and small, I would not have been able to reach this stage without them. I would also like to thank AMO for their contribution to the funding of the project.

Without my friends and colleagues in MB171, in particular Tom, Joe, Jon and Alec, I would have found it hard to keep going. They have all made coming to the office an enjoyable experience over the past three years, offering both valuable input and valuable distractions! To them, I say thank you.

I must also thank my family. My father, Dr Phil Coldrick, having been through this process himself has always know what to say. My mother Becky, sister Debbie and brother Matthew have helped shape me into who I am today. For all of their love, prayers and phonecalls; I am grateful.

Finally, to my wife Becky, you know how much you mean to me. Thank you for everything, I love you.

Contents

1	Background: Accommodation and Presbyopia	23
1.1	General introduction	23
1.2	Accommodation	24
1.2.1	Historical understanding of accommodation	24
1.2.2	Current understanding of accommodation	25
1.2.3	Accommodative Apparatus	27
1.2.3.1	Crystalline Lens	28
1.2.3.2	Capsule	31
1.2.3.3	Zonules	33
1.2.3.4	Ciliary body	39
1.3	Presbyopia	40
1.3.1	Lenticular causes	41
1.3.2	Extralenticular causes	43
1.3.3	Methods of presbyopia correction	44
1.3.3.1	Accommodation intraocular lenses	44
1.3.3.2	Lens refilling	45
1.3.3.3	Femtosecond laser lentotomy	46
1.3.3.4	Scleral expansion	47
1.3.3.5	Summary	47
1.4	Aims and Objectives	47
1.4.1	Thesis structure	48
2	Background: Finite element models of accommodation	50
2.1	Introduction to Finite Element Analysis	50
2.1.1	FEA of the accommodation system	50

2.2	Geometry	54
2.2.1	Crystalline lens shape	55
2.2.1.1	Source data	55
2.2.1.2	Mathematical fit	56
2.2.2	Internal Structure	58
2.2.2.1	Homogenous models	58
2.2.2.2	Nucleus/Cortex	58
2.2.2.3	Stiffness gradient	59
2.2.3	Capsule thickness variation	59
2.2.4	Zonule Arrangement	60
2.2.4.1	Modelling the zonules	60
2.2.4.2	Force application	62
2.2.5	Other Components	62
2.2.6	Summary of geometric methods	63
2.3	Material Properties	63
2.3.1	Crystalline Lens	64
2.3.2	Capsule	67
2.3.3	Zonules	68
2.3.4	Summary of material properties	68
2.4	FEA Procedure	69
2.4.1	Models analysed	69
2.4.1.1	Boundary conditions	71
2.4.2	Verification of results	72
2.5	Results	73
2.5.1	Accommodation	73
2.5.2	Zonular forces	75
2.5.3	Presbyopia	75
2.5.3.1	Presbyopia treatments	77
2.6	Areas for Improvement	77
3	Geometry	78
3.1	Introduction	78

3.2	Measured Data	78
3.2.1	Imaging Methods	78
3.2.2	Crystalline lens measurements	79
3.2.2.1	Thickness	79
3.2.2.2	Diameter	82
3.2.2.3	Surface curvature	83
3.2.2.4	Anterior Chamber Depth	83
3.2.2.5	Other measurements	87
3.2.3	Capsule	89
3.2.4	Zonules	92
3.2.4.1	Lens attachment points	93
3.2.4.2	Ciliary body measurements	95
3.2.4.3	Zonule thickness	99
3.2.5	Summary	99
3.2.5.1	Accommodation and presbyopia theories	99
3.3	Crystalline lens model	100
3.3.1	Existing models	101
3.3.2	Model comparison	105
3.3.2.1	Data used to create models	105
3.3.2.2	How do the models compare?	107
3.3.3	Internal structure	109
3.3.4	Summary	111
3.4	Proposed capsule model	111
3.5	Proposed zonule model	112
3.5.1	Zonular Arrangement	113
3.5.2	Attachment Points on Capsule	114
3.5.2.1	APZ attachment locations	114
3.5.3	Attachment points on the ciliary body	115
3.5.3.1	Ciliary body shape	116
3.5.3.2	Ciliary body position	116
3.5.3.3	Changes with accommodation	117
3.5.3.4	Changes with age	118

3.5.4	Constructing the model	118
3.5.5	Final zonule arrangement	120
3.5.6	Zonule thickness	123
3.5.7	Summary	123
4	Material Properties	124
4.1	Introduction	124
4.2	Defining Material Behaviour	124
4.2.1	FEA Representation	125
4.2.2	Units	126
4.3	Measured Data	126
4.3.1	Crystalline lens material properties	126
4.3.1.1	Lens Spinning	126
4.3.1.2	Lens indentation	129
4.3.1.3	Lens compression and shearing	130
4.3.1.4	Acoustic methods	131
4.3.1.5	Brillouin Light Scattering	131
4.3.1.6	Comparison of results	131
4.3.2	Capsule	135
4.3.2.1	Inflation	136
4.3.2.2	Stretching	136
4.3.2.3	Atomic force microscopy	137
4.3.2.4	Other capsule tests	137
4.3.2.5	Comparison of results	138
4.3.3	Zonules	140
4.3.3.1	<i>In vitro</i> measurements	140
4.3.3.2	FEA model estimations	141
4.3.3.3	Comparison of results	141
4.3.4	Summary	142
4.3.4.1	Evidence for accommodation and presbyopia theories	142
4.4	Data used for Model	142
4.4.1	Crystalline lens	143

4.4.2	Capsule	144
4.4.3	Zonules	144
4.4.4	Summary	145
5	Procedure	146
5.1	Introduction	146
5.2	Finite element theory	146
5.2.1	Geometric non linearity	146
5.2.2	Material non linearity	147
5.2.3	Axisymmetry	147
5.3	ANSYS Modelling Procedures	147
5.3.1	Element Choice	148
5.3.2	Geometric Definition	148
5.3.2.1	Internal structure models	149
5.3.3	Material Property definition	150
5.3.4	Mesh Generation	151
5.3.5	Loads and Restraints	152
5.3.5.1	Spinning studies	152
5.3.5.2	Displacement studies	152
5.4	Results Extraction	153
5.4.1	Detailed Results	154
5.4.2	Expected changes in geometry	156
6	Modelling	158
6.1	Introduction	158
6.2	Initial model development	158
6.2.1	Internal Structure	159
6.2.1.1	Model set up	159
6.2.1.2	Results	160
6.2.2	Initial Capsule Test	163
6.2.2.1	Model set up	164
6.2.2.2	Results	164
6.2.2.3	Conclusion	165

6.2.3	Zonule testing	166
6.2.3.1	Zonule methods comparison	166
6.2.3.2	Test of base zonule model	168
6.2.3.3	Defining the thickness and movement	169
6.2.3.4	Final zonule alterations	172
6.2.4	Probabilistic Analysis	175
6.2.4.1	Comparison of lens and capsule material properties	176
6.2.4.2	Comparison of the capsule and zonule material properties	176
6.2.5	Internal structure test with zonules	178
6.2.6	Summary of the model development	180
6.3	Accommodation modelling	181
6.3.1	Models from baseline data	181
6.3.1.1	Results of baseline models	182
6.3.2	Model variations	183
6.3.3	Analysis of accommodation	186
6.3.3.1	Comparison to measured data	186
6.3.3.2	Comparison to previous FEA models	188
6.3.4	Summary of accommodaion modelling	193
6.4	Presbyopia modelling	194
6.4.1	Variations to parameters of the baseline models	194
6.4.1.1	Material Property Variation	194
6.4.1.2	Displacement Variation	195
6.4.1.3	Variation in lens attachments	195
6.4.1.4	Stiffness profile variation	195
6.4.2	Results of parameteric variations	196
6.4.2.1	29 YO	196
6.4.2.2	45 YO	198
6.4.2.3	60 YO	198
6.4.3	Further variation	198
6.4.3.1	Further Material property variation	199
6.4.3.2	Further capsule variation	199
6.4.4	Comparison to previous FEA models	199

6.4.5	Support for presbyopia theories	200
6.4.5.1	Presbyopia correction	202
6.4.6	Presbyopia modelling summary	203
6.5	Alternative Accommodation models	203
6.5.1	Model set up	204
6.5.2	Results	205
6.5.3	Analysis	205
7	Conclusion	207
7.1	Introduction	207
7.2	Comparisons to aims and objectives	207
7.2.1	Objective 1 - Development of a geometric model	207
7.2.2	Objective 2 - Selection of appropriate material properties	208
7.2.3	Objective 3 - Evaluation of proposed methods	209
7.2.3.1	Stage 1 - Development of the proposed model	209
7.2.3.2	Stage 2 - Accommodation modelling	210
7.2.4	Objective 4 - Parametric analysis	211
7.3	Answers to principal questions of the thesis	212
7.4	Suggestions for improvements and future directions	213
7.4.1	Fundamental data	213
7.4.2	FEA Modelling methods	214
7.5	Future applications	215
	References	218
A	Supporting data for Chapter 6	230
A.1	Zonule bundle data	230
A.2	Results data	231
A.3	Further details of the accommodation models in Section 6.3.2	235
B	Ciliary body image analysis tool	237
B.1	Introduction	237
B.2	Method	237
B.3	Results	240

List of Figures

1.1	The components of the human eyeball, illustrating both the structure and vision system.	23
1.2	Illustration of the changes in the accommodative structures during accommodation as according to the Helmholtz theory. The left side shows the eye in the relaxed state with the right side showing it in its accommodated state. The arrows indicate movement.	26
1.3	Illustration of the changes in the accommodative structures with accommodation as according to the Schachar theory. The left side shows the eye in the relaxed state with the right side showing it in its accommodated state. The arrows indicate movement, highlighting the differences to the Helmholtz theory shown in Figure 1.2.	26
1.4	Left: The structure of the crystalline lens, illustrating the different regions of the lens, representing the gradual addition of cells throughout life, as defined by Taylor <i>et al.</i> (1996). Right: Illustration of the suture sites on the anterior and posterior surfaces of the lens, showing the increasing complexity of the fibre end connections with age (Kuszak <i>et al.</i> , 2004).	28
1.5	Reproduction of the capsule thickness variation as illustrated by Fincham (1925), with the black area representing the capsule area. The thickness of the capsule has been exaggerated to illustrate the thickness variation.	32
1.6	Zonule arrangement according to Rohen (1979), illustrating the difference between anterior and posterior zonule groups and highlighting the region of the tension zonules.	34
1.7	Zonule arrangement according to Coleman (1986), the lens is displayed inverted to illustrate the “sling” arrangement, illustrating the changes as a result of ciliary muscle contraction.	35
1.8	Zonule arrangement according to Ludwig <i>et al.</i> (1999), illustrating the complex paths of the different zonule bundles, with the origin, insertion and possible crossing points highlighted. The overall structure is similar to that of Rohen (1979) shown in Figure 1.6.	36

1.9	Zonule arrangement according to Schachar (1992), highlighting the alternative view of the movement of the equatorial zonule with ciliary muscle contraction.	36
1.10	Zonular arrangement according to the studies of Bernal <i>et al.</i> (2006) and Nankivil <i>et al.</i> (2009), illustrating the addition of the anterior zonules interlacing the hyaloid membrane.	37
1.11	Zonular arrangement from the computer model of Goldberg (2011), primarily based on the imaging of Lütjen-Drecoll <i>et al.</i> (2010), highlighting the more detailed representation of the vitreous zonule and its connections anteriorly and posteriorly.	38
1.12	The basic shape of the ciliary body, showing the difference between the ciliary process and ciliary muscle and an illustration of the three ciliary muscle fibre types and orientations.	39
1.13	Decline in the mean accommodative amplitude with age. Adapted from Figure 2 from Pierścionek & Weale (1995) and Figure 1.5 from Sheppard (2010).	41
2.1	Comparison of the rate of curvature change in the modelling methods of Burd <i>et al.</i> (2002) (A), Hermans <i>et al.</i> (2006) (B) and Chien <i>et al.</i> (2003) (C). The change in length of the lines (in red) illustrates the curvature change, giving an indication of the smoothness of each method, with C being the smoothest. Each lens represents an eye of 29 - 30 YO.	56
2.2	Comparison between nucleus modelling methods, A represents the method used by Burd <i>et al.</i> (2002), B represents the method used by Abolmaali <i>et al.</i> (2007).	58
2.3	Zonular arrangements used in the literature. A - Burd <i>et al.</i> (2002) B - Weeber & van der Heijde (2007) C - Ljubimova <i>et al.</i> (2008) D - Liu <i>et al.</i> (2006) E - Belaidi & Pierscionek (2007) F - Abolmaali <i>et al.</i> (2007).	61
2.4	Comparison between Heys <i>et al.</i> (2004) and Weeber <i>et al.</i> (2007) stiffness variation for a 30YO lens.	66
2.5	The idealised lens profile used by Abolmaali <i>et al.</i> (2007) (Black outline), the profile shape can be seen to be an inaccurate representation of the lens where compared to an MRI image of the relaxed lens (Adapted from Figure 1 of Strenk <i>et al.</i> , 1999), principally due to the sharp point at the equator.	71
3.1	Comparison of capsule thickness variations. 0 represents the anterior pole, 100 the equator and 200 the posterior pole. The solid lines indicate the measurements of Barraquer <i>et al.</i> (2006) (20, 50 & 0 YO) and the dotted lines indicate the measurements of Fisher & Pettet (1972) (22, 37 & 77 YO).	92

3.2	Illustration of zonule groupings and nomenclature. AAZ = Anterior zonule attachment, anterior group. AEZ = Equatorial zonule attachment, anterior group, APZ = Posterior zonule attachment, anterior group, ACB = Anterior ciliary body, PCB = Posterior ciliary body.	93
3.3	Comparison between the AAZ lens attachment movements with age, the lens diameter value needed to define the Sakabe <i>et al.</i> (1998) position was taken from Strenk <i>et al.</i> (1999) and the axial length from Atchison <i>et al.</i> (2008).	94
3.4	Illustration of the AAZ, AEZ and APZ zonular attachment locations on the lens, showing the positions of Burd <i>et al.</i> (2002), Sakabe <i>et al.</i> (1998), Abolmaali <i>et al.</i> (2007) and Ljubimova <i>et al.</i> (2008). The shaded bands represent the size of the zonular attachment zones according to Streeten (1977).	95
3.5	Standard nomenclature for describing lens parameters, with definitions given in Table 3.15.	102
3.6	Example of the accommodated and relaxed form of a 20 YO lens defined using the Hermans (Red) and Giovanzana (Blue) methods. An accommodative change of 11D was assumed, as according to Duane (1922).	106
3.7	Change with age of the decrease in curvature between the relaxed and accommodated states of the Hermans and Giovanzana models.	107
3.8	The volume and surface area changes with age of the Hermans and Giovanzana models in the relaxed state.	108
3.9	Comparison between the curvature changes around the profile of a 20 YO accommodated lens modelled with the Giovanzana and Hermans methods, with the length of the red lines illustrating the amount of curvature at that point.	109
3.10	Illustration of the method used to define the capsule thickness variation. The anterior portion of a 40 YO lens is shown, with the capsule thickness increased by a factor of 10 for clarity. Detail is shown of the p45 thickness location, illustrating the perpendicular line used to generate a new set of x and y co-ordinates.	112
3.11	Proposed zonule arrangement based on analysis of the literature, showing the accommodated (Blue) and relaxed (Red) states. The schematic shows the four zonular bundles and the connections to both lens and ciliary body.	113
3.12	Illustration of the zone of Wieger, adapted from Bergua & Kuchle (2002).	115
3.13	The basic shape of the ciliary body, based on images from Pardue & Sivak (2000), Strenk <i>et al.</i> (1999) and Sheppard & Davies (2010).	116

3.14	Illustration of the method used to orientate the ciliary body model, using the equatorial line and CMT (Ciliary muscle thickness) lines. The MRI image was adapted from Figure 1 of Strenk <i>et al.</i> (1999).	119
3.15	Proposed ciliary body model with defining parameters shown.	120
3.16	Final zonular arrangement where the blue outlines represent the accommodated model and the red lines represent the relaxed model. The anterior shift of the accommodated lens is highlighted.	122
4.1	Illustration of the measurement positions within the lens in indentation studies (Left) and the locations and displacement directions used in measurement in spinning lens studies (Right).	132
4.2	Comparison of the variation in shear modulus with radial position.	133
4.3	Comparison of studies that measured nucleus and cortex properties.	134
4.4	Comparison of the studies of the capsule material properties. Fisher (1969), Krag & Andreassen (2003a), Ziebarth <i>et al.</i> (2007) and Choi <i>et al.</i> (2012).	139
5.1	Internal Structure representations. H = Homogenous, NC = Nuclues-Cortex, SA = Stiffness gradient A, SB = Stiffness Gradient B.	149
5.2	Illustration of the mesh generated for a 20 YO lens model using the free element mapping method, the colours illustrate the different material property regions that are meshed individually.	151
5.3	Illustration of the zonule node (Blue circle) connection to the capsule nodes (red circles) for the equatorial zonule, with detail on where the nodes (which form the individual elements, denoted by Black dots) are located on the model.	153
5.4	Illustration of where the displacement values for calculating thickness and movement changes are taken from.	155
5.5	Graphs showing the variation in measurements of the changes in thickness, diameter, anterior radius of curvature, posterior radius of curvature with accommodative stimulus. The dark grey regions represent the boundary between maximum and minimum values, with the light grey regions representing the variation in the measurements.	157
6.1	Mesh convergance of the thickness and anterior radius of curvature of the SB model. h = element edge length.	160

6.2	The deformation undergone by the lens after being spun at 1000 rpm, with the dotted line representing the lens before spinning and the solid line the lens after, showing the changes in thickness and curvatures.	161
6.3	The decrease in axial thickness with age of each internal structure model for lenses spun at 1000 rpm.	161
6.4	Comparison of the decrease in axial thickness for the different internal structure models at 40 and 50 YO for lenses spun at 1000 rpm.	162
6.5	The changes in the radius of curvature of the anterior and posterior surfaces of each internal structure model at 40 and 50 YO for lenses spun at 1000 rpm.	162
6.6	Comparison between the deformations undergone by an en-capsulated (Solid Grey) and de-capsulated (Solid Black) lens after being spun at 1000 rpm, with the dotted line representing the lens before spinning.	165
6.7	The three zonule models simulated in section 6.1.3.1. ZA = zonule model of Burd <i>et al.</i> (2002), ZB = The proposed zonule model without the PZ2 zonule, ZC = The complete proposed zonule model.	167
6.8	Deformations of the three zonule models from Section 6.2.3.1, showing the initial and deformed shapes for the individual displacement values given in Table A.1. ZA = Blue, ZB = Red, ZC = Green.	168
6.9	Comparison between the deformations in the three age models used in Section 6.2.3.2, with the 20 YO lens on the left, the 40 YO lens in the centre and the 50 YO lens on the right.	169
6.10	Illustration of the change in ciliary body displacement using method A based on a ciliary body displacement defined using Equation 6.2 and method B based on a ciliary body displacement defined using Equation 6.1.	170
6.11	Comparison between the deformations in the 40 YO lens with two different zonule attachment methods based on a ciliary body displacement defined using Equation 6.2. A = Angled attachments, B= Tangential attachments.	172
6.12	Illustration of the new modelling method for the PZ2 zonule in the 40 YO accommodated lens model. The black line indicates the vitreous with the dashed line indicating the altered pinning zonule.	173
6.13	Results of probabilistic analysis 1, showing that the capsule and layers 9, 4, 10 and 8 are significant parameters in regards to the total thickness change.	176

6.14	The results of probabilistic analysis 2, showing that the zonule elastic modulus was most significant for both outputs.	177
6.15	Thickness change in all internal structure models (with zonules) across all three ages. . . .	179
6.16	Thickness change of the 40 and 50 YO lens models with different internal structure models combined with the zonule structure.	179
6.17	The curvatures changes of the 40 and 50 YO models with different internal structure models combined with the zonule structure.	180
6.18	The zonular arrangements used in the 29, 45 and 60 YO models from Section 6.3.1.	182
6.19	Results of the first run of the baseline 29, 45 and 60 YO models based on the ciliary body displacement defined using Equation 6.2.	182
6.20	Deformations in the 29, 45 and 60 YO altered models (Section 6.3.2) based on a ciliary body displacement defined using Equation 6.2.	185
6.21	Comparison of the current model results to measured <i>in vivo</i> data, taken from Section 5.4.	187
6.22	Comparison between the measured force values in the current and previous FEA studies. * The two models from this study were 30 YO and 40 YO.	191
6.23	A: 1st Principal stress distribution in the 29 YO model B: Von Mises stress distribution in the 29 YO model. C: X axis strain in the 60 YO model D: y axis strain in the 60 YO model E: 1st Principal stress distribution in the 29 YO capsule F: 1st Principal strain distribution in the 29 YO Capsule. All models are shown utilising the symmetry expansion option in ANSYS, available due to the axisymmetric options used in the current models. All Stress values are in Pa.	193
6.24	Illustration of the alterations to the baseline 29 YO lens to replicate the theories of Coleman (Left model) and Schachar (Right model).	204
6.25	The deformations induced in the C_A and S_B models.	205
B.1	Comparison between the original DICOM image (Left), its rotation and histogram adjustment (Top right) and the final region of interest (Bottom right).	238
B.2	Illustration of the points used to define the top and bottom of the ciliary muscle (A) and the resulted fitted curves (B).	239

B.3 Illustration of the final measurements. The two red curves represent the original fitted muscle, with the green and yellow curves representing the dewarped curve fits. The blue curve shows the top fit of the sclera, used for the dewarping of the ciliary muscle curves. The rest of the lines represent the measurement locations. 240

B.4 Two examples of poor images, illustrating the presence of contact lenses and artefacts present. 241

List of Tables

2.1	FEA accommodation models from the literature analysed in this chapter, with a summary of the aims of each study. *Both papers report on the same study. YO = Year old.	52
2.2	Modelling methods of the key components in the FEA models in the literature. Key to methods: P: Polynomials, CS: Conic Sections, CF: Cosine function, H: Homogenous, NC: Nucleus-Cortex, SG: Stiffness gradient, F: Fincham (1925) thickness variation, BU: Burd <i>et al.</i> (2002) thickness variation, BA: Barraquer <i>et al.</i> (2006) thickness variation, 3Z: 3 Zonules, 1Z: Single zonule, 5Z: 5 zonules. There are a number of variations of each method (denoted by a *) used by different authors however, the basic methodology is the same. ** indicates the method was not explicitly stated, although a lens was modelled.	54
2.3	Summary of the different sources of material properties used in the literature. Key to letters: A Fisher (1971), B Subbaram <i>et al.</i> (2002), C Weeber <i>et al.</i> (2007), D Heys <i>et al.</i> (2004), E Van Alphen & Graebel (1991), F Wilde <i>et al.</i> (2012), G Fisher (1969), H Krag & Andreassen (2003a), I Fisher (1986). A hyphen indicates that there was no data available or the component was not modelled.	65
2.4	Summary of the models and procedures used in previous studies. Starting lens shape key: U = Un-accommodated lens, A = Accommodated lens. Deformation method Key: A = Zonule displacement, B = Vitreous Pressure, C = Force application, D = Sensitivity study.	70
3.1	Summary of the main imaging methods used in measuring accommodative components, giving detail on measurements available as well as any potential errors.	80
3.2	Summary of crystalline lens thickness measurements. Age related changes are given where possible, otherwise values are the mean value found. * indicates change per dioptre of accommodative response, A = Age.	81
3.3	Summary of crystalline lens diameter measurements. *indicates changes per dioptre otherwise measurements are the mean values found. A = Age.	84

3.4	Anterior crystalline lens radius of curvature measurements. *changes per dioptre of accommodation **measured as curvature, 1/Radius. A = Age.	85
3.5	Posterior crystalline lens radius of curvature measurements. *changes per dioptre of accommodation **measured as curvature, 1/Radius. A = Age.	86
3.6	Anterior Chamber Depth measurements *includes cornea thickness **indicates change per dioptre of accommodative response. A = Age.	88
3.7	Summary of other lens measurements. *indicates changes per dioptre of accommodation. CSA = Cross Sectional Area, A= Age (Years).	90
3.8	Capsule thickness measurement studies.	91
3.9	Measurements of the attachments of the zonular bundles to the crystalline lens.	93
3.11	Changes in key ciliary body measurements with age.	95
3.10	Summary of key ciliary body (CB) and ciliary muscle (CM) measurements. All measurements taken <i>in vivo</i> unless otherwise stated in the method column.	96
3.12	Changes in key ciliary muscle measurements with accommodation.	97
3.13	Summary of <i>in vivo</i> studies that have measured the movement of the ciliary body with age and accommodation. CM = Ciliary muscle.	98
3.14	Summary of crystalline lens modelling methods used in the literature. Whether a method is suitable is determined by 1. Ability to replicate the method 2. Ability to model based on measurable parameters.	101
3.15	Lens parameter labels and units, as illustrated in Figure 3.5.	102
3.16	Data used to create models, taken from Section 3.2. A = Age, AccAbility = the accommodative ability at Age A, taken from the data of Duane (1922).	106
3.17	Data used to define internal structure, from Dubbelman <i>et al.</i> (2003). Z = Zone, with the lens split into 8 zones along the axial length.	110
3.18	Change in internal thickness with accommodation, taken from Dubbelman <i>et al.</i> (2003).	110
3.19	Capsule thickness parameters from Barraquer <i>et al.</i> (2006) for defining Equation 3.24.	111
3.20	Parameters needed to build ciliary body model shown in Figure 3.15.	121
4.1	Summary of studies measuring the material properties of the accommodative components. All studies are <i>in vitro</i> , unless stated otherwise. *indicates diabetic samples **indicates cataract samples.	127
4.2	Comparison of Bulk modulus values from the literature. N = Nucleus, C = Cortex.	135

4.3	Comparison of the calculated spring constant and elastic modulus values from both <i>in vitro</i> and FEA models.	141
4.4	Parameters to define the shear modulus as according to Weeber.	143
4.5	Parameters to define the shear modulus values for Equation 4.8 as according to Wilde (2011).	144
5.1	Elements used for representing the different components of the accommodation model.	148
5.2	Lens areas and equivalent zones from the densitometry analysis of Dubbelman <i>et al.</i> (2003), see Section 3.2.2.1.	150
5.3	Sources of data used in plotting the graphs in Figure 5.5. A indicates age in years. All measurements indicated the change per diopter of accommodative response, with the amount of accommodative response per year, used in defining the graphs in Figure 5.5, taken from the study of Duane (1922). Each graph in Figure 5.5 is formed of a maximum and minimum range of values, hence the use of two definitions in the table.	156
6.1	Comparison between the changes in en-capsulated (C) and de-capsulated lens (DC) models in the current test and from Wilde (2011). The changes are given in terms of percentage change in thickness due to the difference in the geometric description of the lens.	164
6.2	The results of the displacement variation from Section 6.2.3.3. A *Indicates a change that was too high, a ** indicates a change that was too low, compared to measured <i>in vivo</i> data (Section 5.4.2).	171
6.3	Zonule thickness values used in thickness test, showing the difference in thickness distribution used.	171
6.4	Reaction forces calculated from the models used in Section 6.2.3.3, illustrating the reduction of force with age.	174
6.5	Results of the three iterations of zonular thickness in the 20 YO model.	175
6.6	The geometric and force changes during disaccommodation in the altered models of the 29, 45 and 60 YO models. Compared to the expected changes (Section 5.4.2) a * indicates a change that is too high and a ** indicates a change that is too low.	184

6.7	The results of the presbyopia modelling in Section 6.4, principally showing the reduction in power change as a result of variation of key parameters. Key: Baseline models are taken from (Section 6.3). For the variation models, the number indicates the age followed by the type of the variation: M = Lens material, CM = Capsule Material, LCM=Lens and capsule materials, D = Displacement, ZA = Zonule attachments, SV = Stiffness profile. E.g. 29M indicates the baseline model was given a 29 YO lens material properties.	197
A.1	Zonule displacements used in Chapter 6, divided into sections and models. All displacements in mm.	230
A.2	Zonule bundle thickness values used in Chapter 6. All values in mm.	231
A.3	Results of models using the spinning lens setup. Compared to the expected changes (Section 5.4.2) a * indicates a change that is too high and a ** indicates a change that is too low.	231
A.4	Results of models run in Section 6.2 using the zonule displacement procedure. Compared to the expected changes (Section 5.4.2) a * indicates a change that is too high and a ** indicates a change that is too low.	232
A.5	Results of studies in Section 6.3. Compared to the expected changes (Section 5.4.2) a * indicates a change that is too high and a ** indicates a change that is too low.	233
A.6	Comparison of the changes in geometry in the current model in comparison to models from previous FEA models, from Section 6.3.3.2.	233
A.7	Results of the presbyopia models run in Section 6.4	234
A.8	Material property data for the models used in Section 6.3.2.	235
A.9	Geometric data for the lens outline and internal structure used in Section 6.3.2.	235
A.10	The capsule thickness values used in Section 6.3.2.	236
A.11	Geometric data for definition of the zonules and ciliary body used in Section 6.3.2. R = Relaxed, A = Accommodated.	236

Chapter 1

Background: Accommodation and Presbyopia

1.1 General introduction

The eye is a complex organ formed of many components, all combining to allow humans to see clearly across a range of distances. This ability to clearly focus on objects at various distances is due to the crystalline lens being able to change its shape and therefore its power, a process called accommodation. It is most evident in young eyes, with the ability to accommodate being lost with age, a condition known as presbyopia. A brief overview of the general ocular structures will be given, before looking in detail at accommodation and presbyopia.

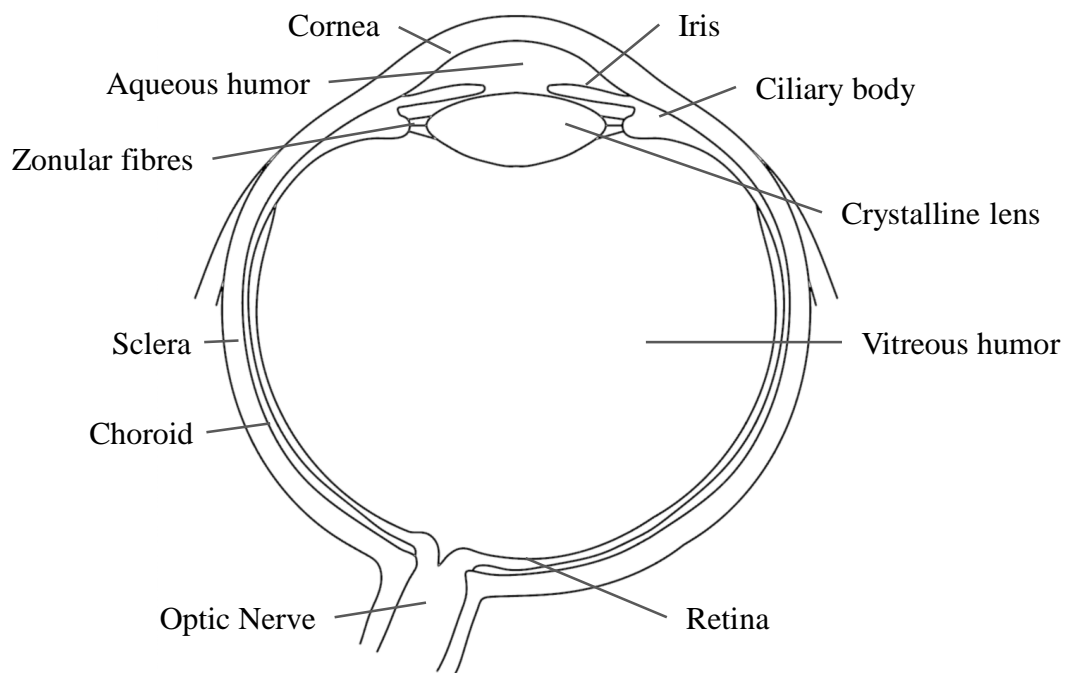


Figure 1.1: The components of the human eyeball, illustrating both the structure and vision system.

Figure 1.1 illustrates a simplified schematic of the human eye, illustrating the key components of the eyeball structure and vision system. To enable a clear image to be seen, light rays entering the eye first pass through the cornea, a transparent structure with a higher refractive index than air, causing an initial refraction of the light. The rays then pass through the anterior chamber, filled with the aqueous humor, before passing through the iris, which acts as an aperture controlling the amount of light that enters the eye by contracting and dilating on reflex. The light then passes through the crystalline lens, which controls the focusing, to be discussed further in Section 1.2.3. The lens is held in place by the zonular fibres which cross the circumferential space: the area between the lens and ciliary body. Finally, the light passes through the vitreous humor before hitting the retina, a complex structure formed of photoreceptor cells, called rods and cones. These cells convert light into the neural signals that pass through the optic nerve to the brain. The cone cells are used in well-lit conditions, while the rods are more sensitive in low light conditions.

1.2 Accommodation

The eye has two principal refractive components, the cornea, which provides approximately two thirds of the overall refractive power of the eye, and the crystalline lens, which provides the optical changes needed for accommodation, allowing constant clear focus on objects at a range of distances. Despite extensive study, there is still no universally agreed explanation on how the accommodative system functions. A summary of both the historical understanding and current understanding of accommodation will now be given, before a more detailed look at the accommodative components.

1.2.1 Historical understanding of accommodation

The first demonstration of an active accommodation process was by Scheiner (1619) (cited by Daxecker, 1992), using a double pin hole experiment, where a near and distant object were observed at the same time through these pin holes. The object focused on would appear single, while the other object appeared to double. Descartes (1637) (cited by Atchison, 1995) hypothesised that the lens could change its curvature, which allowed the lens to change its focus. He believed this was due to the fibers which held the lens in place. These speculations were furthered by the work of Young (1801), who found that accommodation still occurred after the influence of the cornea was removed, concluding that the lens was responsible for the change in power of the eye (cited by Atchison & Charman, 2010).

Cramer (1853) provided experimental evidence of the lens being responsible using Purkinje images, where he observed the increase of anterior lens curvature during accommodation. He attributed this lens change to the actions of the ciliary muscle and iris, where the ciliary muscle would contract and act on the vitreous humor, while the iris would contract and act directly on the lens (cited by Strenk *et al.*, 2005). The contribution of the iris was later invalidated by the work of von Grafe (1861), who showed an aniridic patient had accommodative ability (cited by Atchison, 1995).

Helmholtz (1855, 1924) also used Purkinje images and came up with his own theory; he stated that the change in shape of the lens was due to the ciliary muscle contracting, causing a reduction in the tension in the zonules. This allowed the lens to increase in curvature by increasing its thickness and reducing its diameter (Strenk *et al.*, 2005).

Tscherning (1895) later challenged the theory proposed by Helmholtz by suggesting that the contraction of the ciliary muscle, instead, causes the zonules to increase in tension; proposing a curvature change without a change in thickness of the lens. Due to evidence of lens thickening during accommodation, Tscherning (1909) updated his theory although he still believed the change in power was due to increasing zonular tension with ciliary muscle contraction (cited by Strenk *et al.*, 2005).

1.2.2 Current understanding of accommodation

The classical explanation of von Helmholtz (1855) is widely accepted, however, there are still other theories currently supported. A more detailed summary of these will be given here, with the evidence explored further in Chapter 3 and Chapter 4.

Helmholtz Theory

The original theory of von Helmholtz (1855) attributed some of the anterior curvature changes of the lens to the iris, however, this was later discounted by Fincham (1937) due to observations of accommodative ability in patients with aniridia (cited by Atchison, 1995). Gullstrand (1924) expanded the theory to include the actions of the choroid in aiding the contraction of the ciliary muscle (cited by Strenk *et al.*, 2005 and Charman, 2008). With these amendments the current Helmholtz theory (illustrated in Figure 1.2) is as follows; to accommodate for near objects, the ciliary muscle contracts, causing it to move closer to the lens. The zonular fibres are then relaxed, which allows the lens to form its natural, more powerful shape. The shape change is facilitated by the capsule: an elastic body surrounding the lens, which also resists the pull of the zonules. To accommodate for far objects, the ciliary muscle relaxes placing tension

The Helmholtz theory has been challenged by the emergence of the theory of Schachar (illustrated in Figure 1.3), who discounts the Helmholtz theory and proposes a theory similar to Tscherning. He proposed that the increase in power of the lens is caused by the lens forming a spindle shape, where the central portion of the lens is thicker, with the peripheral parts flattened. When the lens is in its low power, un-accommodated state, all the zonules are in tension, similar to the Helmholtz theory. However, when the ciliary muscle contracts the equatorial zonules increase in tension, while the anterior and posterior zonules relax, which is contrary to Helmholtz (Schachar, 1992).

Coleman Theory

Another theory is that of Coleman (Coleman, 1986; Coleman & Fish, 2001), who proposed the hydraulic suspension theory (also called the catenary theory). According to Coleman, the zonules, vitreous and lens create a diaphragm between the anterior chamber and the vitreous. With contraction of the ciliary muscle, a pressure gradient is created between the anterior aqueous chamber and the vitreous, forming a catenary. The contraction of the ciliary body alters the shape of the catenary by altering the fixed ends (Figure 1.7). Evidence against this theory can be found in the work of Fisher (1983), where patients without a vitreous were able to demonstrate accommodation.

Other Theories

In addition to the three theories discussed, others have been suggested. Wilson (1993) proposed that when the ciliary body is in the relaxed state the zonules simply suspend the lens, and with the contraction of the ciliary body the zonules cause a compressive force on the lens, causing it to change its shape. Santos-Neto & Alves (2011) hypothesised that the cause of accommodation was related to the change in pressure of the vitreous, brought about by the movement of the ciliary body. With a change in pressure, the posterior pole of the lens moves increasing the power of the lens. Chapter 3 explores the evidence for posterior pole movement in more detail.

1.2.3 Accommodative Apparatus

The key components of accommodation are the crystalline lens (comprising of its internal structure and capsule), the zonules and the ciliary muscle. A summary of the development, geometry, material properties and the changes that occur with age and accommodation will be given here, before a detailed analysis of each component is discussed in Chapter 3 and Chapter 4.

1.2.3.1 Crystalline Lens

The crystalline lens provides the power change in the eye through its ability to change in shape. The lens is positioned along the optical axis of the eye (see Figure 1.1) and is approximately 9 mm in diameter and 4 mm thick (in an adult), although these values will change with age and accommodation. The lens is made up of a number of layers due to the gradual addition of cells throughout life, illustrated in Figure 1.4.

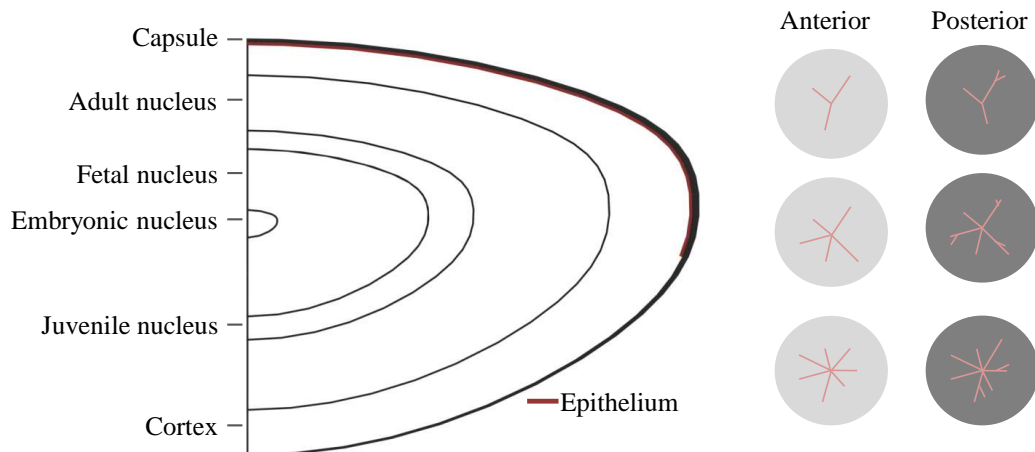


Figure 1.4: Left: The structure of the crystalline lens, illustrating the different regions of the lens, representing the gradual addition of cells throughout life, as defined by Taylor *et al.* (1996). Right: Illustration of the suture sites on the anterior and posterior surfaces of the lens, showing the increasing complexity of the fibre end connections with age (Kuszak *et al.*, 2004).

Development

The lens is first seen at 22 days gestation, and from then onwards, constantly grows. The initial lens is seen as a hollow spherical structure (the lens vesicle) made of a single layer of ectodermal cells. These cells differentiate, with the anterior cells becoming epithelial cells, differentiating into a single layer forming the initial anterior capsule. The posterior cells begin to elongate and fill this hollow structure (Stafford, 2001), becoming the primary lens fibres, filled with crystallins a protein essential for cell transparency. The primary lens fibres meet with the anterior epithelial cells, creating the embryonic nucleus. The initial lens is therefore formed of epithelial cells anteriorly (in a cube shape) and longer primary lens fibres posteriorly (Augusteyn, 2008).

From this time all additional fibres that grow (known as the secondary fibres) are not destroyed, although they lose most of their metabolic activity. These fibres originate in the anterior epithelial cells and undergo mitosis at the lens equator, where they subsequently differentiate and elongate. These new fibres layer on

top of the older cells, causing the existing fibres to move towards the centre of the lens. The fibres are compressed, losing water and increasing in protein concentration (Augusteyn, 2008).

The fibres form a u shape, rather than running in their entirety from the posterior to anterior surfaces, where the ends of the fibres meet in sutures. These suture sites appear on both sides of the lens, although as the lens ages, more suture sites appear. With age, the complexity increases, beginning with a simple 3 branch Y shape and moving onto 12 branch star structures (Kuszek *et al.*, 2004). These different suture regions are visible in a slit lamp due to the different light scattering ability of each region (Augusteyn, 2008).

Internal Structure

The layered internal structure can be seen in Figure 1.4, although commonly, the internal lens is split into two distinct sections: the nucleus and the cortex. Separating the lens into these two sections is primarily linked to the oldest fibres being compacted in the centre of the lens (the nucleus) and the rest of the lens fibres that are added on top of this (the cortex). Using this simple sectioning has been shown to be an oversimplification *in vivo* (Dubbelman *et al.*, 2003) and *in vitro* (Taylor *et al.*, 1996; Lim *et al.*, 2009).

Taylor *et al.* (1996) showed using electron microscopy on lens sections that there are a number of distinct fibre groupings within the lens, where there are observable differences in cell size and shape. These different regions can be seen with Schiempflug photography, as demonstrated by Dubbelman *et al.* (2003), utilising densitometry on the captured images. It was established that there were three distinct cortical regions surrounding the nucleus of the lens.

The variations seen in the lens due to the different cell sizes are also seen in the variation in refractive index (Glasser & Campbell, 1999; Jones *et al.*, 2005; Borja *et al.*, 2008), protein density (Fagerholm *et al.*, 1981; Pierścioneck & Chan, 1989) and material properties (Heys *et al.*, 2004; Weeber *et al.*, 2007), illustrating the complexity of the crystalline lens structure.

The refractive index contributes to the power of the lens, and is known to vary, although the exact nature of this variation is not fully known, with different results being seen *in vitro* (Glasser & Campbell, 1999; Borja *et al.*, 2008) and *in vivo* (Jones *et al.*, 2005).

Material Properties

The surface curvature and refractive index of the crystalline lens, combined with the differences in refractive index between the aqueous, lens and vitreous, all contribute to the power of the lens. However, the

power change that the lens undergoes is due to the ability to change its surface curvatures', a result of its ability to be moulded by the accommodative apparatus, which is due to its material properties. The material properties of a structure dictate how it reacts to applied forces and will control whether it will return to its original shape once a force is applied and released or whether it will break under the forces.

A number of studies have been performed to establish the material properties of the lens (see Chapter 4). As a basic overview, the lens can be seen as an almost incompressible solid that has broadly elastic behaviour, i.e. the lens can be pulled into a thinner more elliptical shape as a result of zonular action, but is able to return to its original shape when the zonules slacken. The material properties vary across the lens structure, with a young lens having a stiffer cortex than nucleus (e.g. Weeber *et al.*, 2007), although this does change with age (e.g. Heys *et al.*, 2004).

Changes with Age and Accommodation

As has been established, the lens grows continuously through life, resulting in a number of changes occurring to the geometric and material properties of the lens. During the accommodation process, the geometric properties of the lens also alter. Chapter 3 will explore the changes that occur with age and accommodation in detail, however, a brief overview will be given here.

The thickness of the lens increases with age, which has been observed *in vivo* (e.g. Koretz *et al.*, 2004; Sheppard *et al.*, 2011) and *in vitro* (e.g. Rosen *et al.*, 2006). Measurements made *in vitro* are often assumed to represent the lens in its most powerful shape, due to there being no external forces acting on the lens, similar to when the lens is in its accommodated form *in vivo*, where there are few external forces present. During accommodation, an increase in thickness is also seen (e.g. Hermans *et al.*, 2009; Sheppard *et al.*, 2011), although the amount reduces with age.

The diameter of the lens in its relaxed state remains relatively stable throughout life, with most authors finding small changes with age (e.g. Strenk *et al.*, 1999; Kasthurirangan *et al.*, 2011). *In vitro*, most authors found an increase with age (e.g. Jones *et al.*, 2005; Rosen *et al.*, 2006). During accommodation, the diameter has been seen to decrease (e.g. Hermans *et al.*, 2009; Kasthurirangan *et al.*, 2011), but as with thickness, the amount reduces with age (Sheppard *et al.*, 2011).

The curvature of the anterior and posterior surfaces also vary with age. *In vivo*, the anterior curvatures have been measured as decreasing (Koretz *et al.*, 2004; Atchison *et al.*, 2008), whilst the posterior curvatures have shown no significant change (Koretz *et al.*, 2004; Atchison *et al.*, 2008). With accommodation, both the anterior and posterior curvatures have been measured as decreasing (Hermans *et al.*, 2009; Sheppard

et al., 2011). *In vitro*, the anterior curvature has been measured as increasing with age (Rosen *et al.*, 2006) whilst the posterior curvature had no significant change (Jones *et al.*, 2005; Rosen *et al.*, 2006), with the difference between the *in vivo* and *in vitro* measurements due to the different shape the lens takes *in vitro* (see Chapter 3).

The volume change during accommodation is disputed, with *in vivo* evidence suggesting that there is both no change (Hermans *et al.*, 2009), as well as an increase (Sheppard *et al.*, 2011), potentially as a result of fluid flow into the lens (Candia *et al.*, 2010). The volume *in vitro* has been shown to increase with age (Koretz *et al.*, 2001; Rosen *et al.*, 2006), matched by measured increases of weight with age (Rosen *et al.*, 2006).

In terms of material properties, the overall stiffness of the lens has been seen to increase with age, with the stiffness profile also changing from having a stiffer cortex at a young age, to having a stiffer nucleus in old age (Fisher, 1971; Heys *et al.*, 2004; Weeber *et al.*, 2007).

The internal refractive index of the lens changes, with less variance in the refractive index across layers in the lens seen with age (de Castro *et al.*, 2011), resulting in the lens becoming more homogenous. In an older lens, any refractive index change is restricted to the cortex, while the nucleus remains constant. This results in aberrations in the lens, particularly spherical aberrations, which affect the focusing of the eye (Charman, 2008).

An interesting aspect of the refractive index changes is to do with the lens paradox, where the geometric changes that occur with age, in particular changes to surface curvatures, would suggest that the lens increases in power with age and becomes increasingly myopic (Dubbelman & Van der Heijde, 2001). However, the opposite is the case, most likely due to the changes in refractive index that occur, counter-acting the geometric changes that take place (Moffat *et al.*, 2002b).

1.2.3.2 Capsule

The capsule encases the lens and provides the link between the crystalline lens and the zonular fibres. There is debate on the exact function of the capsule during accommodation as well as its role in presbyopia, which will be discussed later. First, the development of the capsule must be discussed.

Development

The capsule develops with the lens, surrounding the developing lens forming from a basement membrane. The capsule separates the lens from the surrounding structures in the eye, only allowing water and proteins

that allow the development of the lens to pass through. The capsule grows in layers, with successive layers of lamellae formed from molecules deposited by the epithelial cells of the lens on the inner surface of the capsule, resulting in a thickening of the capsule, which continues through life (Danysh & Duncan, 2009).

Geometry

The capsule conforms to the basic lens shape discussed previously. However, its thickness around the lens varies. The classical description of this variation is from Fincham (1925) as shown in Figure 1.5, however, there are disagreements on the amount of thickness change that actually occurs, which will be discussed in Chapter 3.

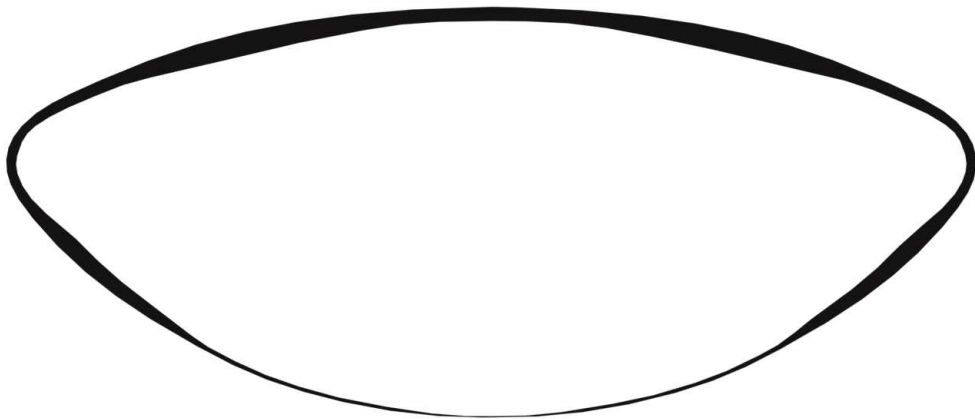


Figure 1.5: Reproduction of the capsule thickness variation as illustrated by Fincham (1925), with the black area representing the capsule area. The thickness of the capsule has been exaggerated to illustrate the thickness variation.

In summary, the capsule is thickest in its anterior section, with the thickest portion being midway between the anterior pole and the equator. The thickness reduces at the equator, before continuing to decrease posteriorly (Farnsworth & Shyne, 1979; Barraquer *et al.*, 2006). There is debate over whether the thicker sections correspond to the locations of the zonule attachments or not (Barraquer *et al.*, 2006).

Material Properties

The capsule is significantly stiffer than the lens, although the anterior and posterior sections have different properties (Krag & Andreassen, 2003a). The capsule has also been shown to exhibit non-linear behaviour, although for strains that are likely to occur *in vivo* the capsule can be assumed to have a more linear response.

Role

The original theory of Helmholtz did not differentiate between the lens and capsule, instead treating them as a single body. Fincham (1937) challenged this view, believing that the natural de-capsulated lens is in its un-accommodated form, stating that the capsule moulded the lens into its accommodated form principally due to the variation in thickness in the capsule. Others disputed this, with suggestions that the variation in thickness is not as key (Fisher, 1969). Support for the capsule moulding the lens can be seen *in vitro*, where without the capsule, the lens forms a flatter shape (Fincham, 1937; Glasser & Campbell, 1999).

An alternate theory for the capsular role during accommodation is that the capsule acts as a force distributor, taking the tractions from the zonules applied by the ciliary muscle and transferring them to the lens (Koretz & Handelman, 1982). The capsule ensures that a uniform force is applied to the lens, with greater changes anteriorly corresponding to greater anterior capsule thickness. The changes in lens shape when the zonules slacken are therefore due to the lens itself, and the complex arrangement of the internal fibres (Krag & Andreassen, 2003a).

Changes with age and accommodation

As with the lens, the capsule changes throughout life, with the anterior capsule increasing in thickness, whilst the equatorial and posterior sections show limited changes (Barraquer *et al.*, 2006).

In terms of the material properties, there are conflicting data. Fisher (1969) found that the elastic modulus decreases with age, although this was likely at deformations unlikely to be found *in vivo*. Krag & Andreassen (2003a) found that in the range of forces found *in vivo*, the stiffness of the capsule increases with age.

1.2.3.3 Zonules

The zonules surround the lens, interlacing with the capsule and ciliary body in a complex arrangement. Each zonular bundle is formed of individual fibres, with the bundles approximately 10 μm in diameter (Streeten, 1977). There has been extensive research on the zonules, although due to the difficulty in imaging them *in vivo* (a result of the obstruction of the iris combined with the small size), there is no complete agreement on the arrangement and function.

Development

The development of the zonules is still not fully understood. They can be first seen in the third fetal month, and the adult zonular arrangement can be seen towards the end of the fetal period. The zonules are believed to be synthesised from the epithelium of the ciliary body, but it is not known whether the zonules grow or undergo constant renewal throughout life (Streeten, 2003).

Arrangement

The arrangement of the zonules has been studied extensively, although there has not been agreement on the exact architecture, leading to a range of different proposals on how the zonules connect the lens and ciliary body. One of the prominent theories is that of Rohen (1979), who proposed that there are two main groups of zonules involved in accommodation. The first group consists of the anterior zonules (which run from the ciliary body to the lens) and the posterior zonules, which run from the *pars plana* (the posterior region of the ciliary body) to the anterior portion of the ciliary body. The lens is pulled into its un-accommodated state by the posterior zonules pulling on the anterior zonules, which force the lens into its flattened state. For accommodation the ciliary muscle contracts, moving the ciliary body anteriorly and inwards, bringing the second group of zonules (the tension zonules) into play. These zonules attach to the posterior and anterior zonules and take up the pull of the posterior zonules, allowing the anterior zonules to relax which allows the lens to form its most powerful shape, as shown in Figure 1.6.

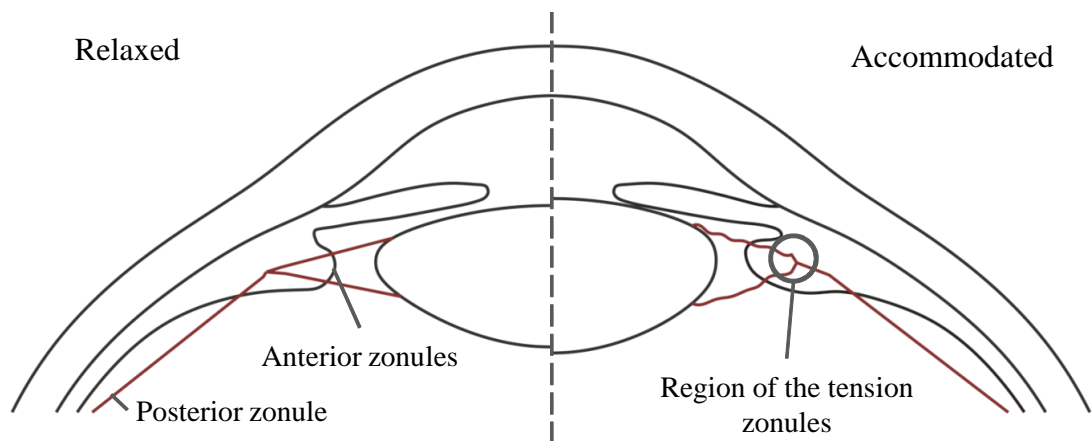


Figure 1.6: Zonule arrangement according to Rohen (1979), illustrating the difference between anterior and posterior zonule groups and highlighting the region of the tension zonules.

Coleman (1986) proposed an alternate arrangement to support the “suspension theory” of accommodation, where the anterior zonules form a “sling” that holds the lens, with support coming from the vitreous (Figure 1.7). The zonules originate near the ora seratta (a region posterior of the ciliary body) and pass

through the ciliary processes. For an un-accommodated lens, the “sling” holds the lens in its flattened state. During accommodation, the ciliary muscle moving inwards causes the central curvature of the sling to increase, causing the lens to form its more powerful shape. With the change in zonular arrangement, the vitreous, attached to the lens by Weigers ligament, helps to mould the lens into its shape.

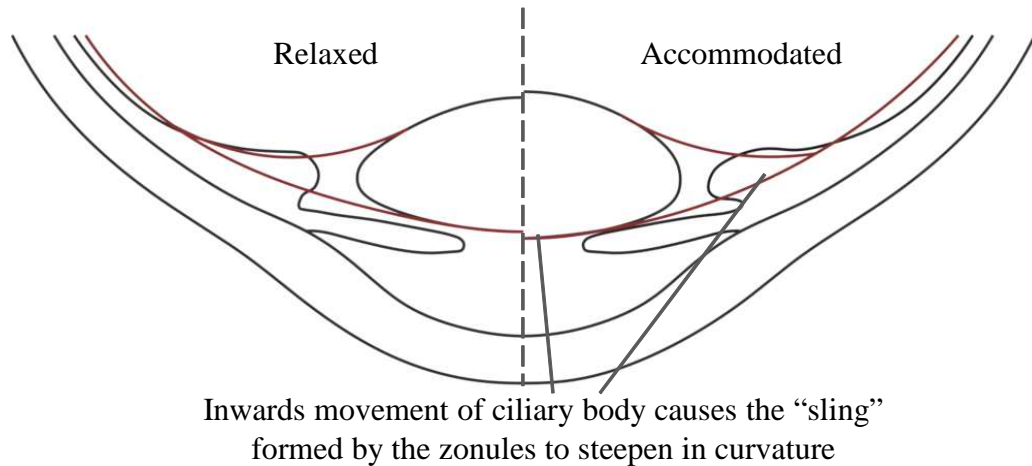


Figure 1.7: Zonule arrangement according to Coleman (1986), the lens is displayed inverted to illustrate the “sling” arrangement, illustrating the changes as a result of ciliary muscle contraction.

Ludwig *et al.* (1999) investigated the zonular arrangement using high resolution ultrasound biomicroscopy (UBM). Three different sections were taken of the eye, allowing the full spread of the zonules to be imaged, which led to Ludwig proposing that the zonules originate from three areas on the ciliary body (O1 – O3) and insert in three main and one minor band on the lens (I1 –I4), as shown in Figure 1.8. The insertion band on the equator was seen as the weakest, with many more fibres seen on the other insertion bands. Fibres were seen to run from O3 to O2 before running to different insertion bands. It was not clear whether the zonules from O3 inserted at O2, or whether they were anchored, as hypothesized by Rohen (1979). Additional fibres were seen to run from O3 directly to the lens. There were fibres seen in 3 patients that ran from O1 to I1. Predominantly, the zonules inserting at I2 come from O2. At a number of areas, highlighted as K1-K3, the zonules were seen to cross, but it was not known whether the zonules just crossed, or whether they changed direction.

The zonules were seen to run in straight courses, indicating that the zonules were taut, in the measured state of far accommodation. Not much detail was given on what was seen at near accommodation, however, what was seen indicated that the zonules were relaxed, becoming shorter and bowing.

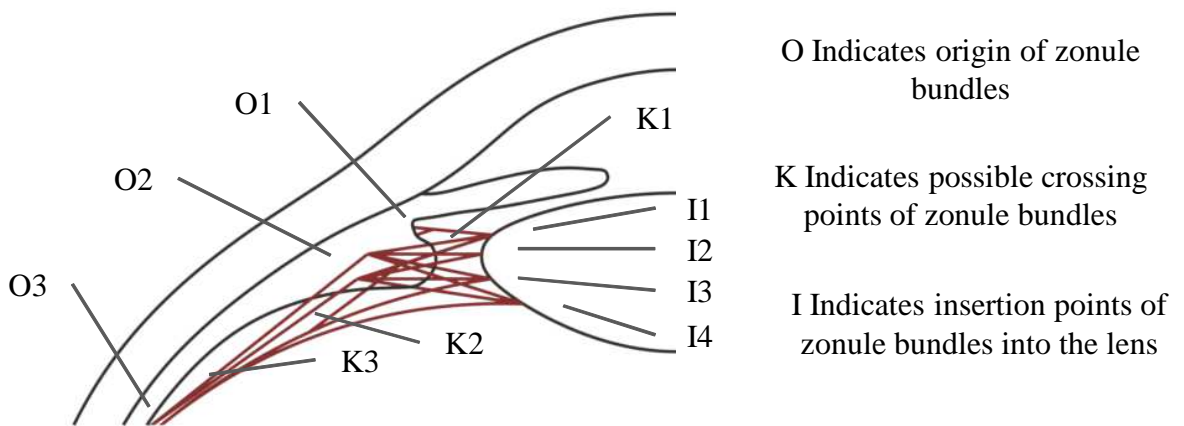


Figure 1.8: Zonule arrangement according to Ludwig *et al.* (1999), illustrating the complex paths of the different zonule bundles, with the origin, insertion and possible crossing points highlighted. The overall structure is similar to that of Rohen (1979) shown in Figure 1.6.

As discussed in Section 1.2.2, Schachar (1992) proposed an alternative accommodation theory which necessitates an alternate arrangement and action for the zonules. For this theory, the equatorial zonule increases in tension during accommodation due to the movement of the ciliary body, contrary to the Helmholtz theory. The equatorial zonules would, therefore, be under the lowest tension when the lens is in its lowest power form, but increase in tension to increase the lens power. Figure 1.9 illustrates how this arrangement looks, where the anterior and posterior zonules act purely as stabilisers, being tense during distance vision and relaxed for accommodated vision.

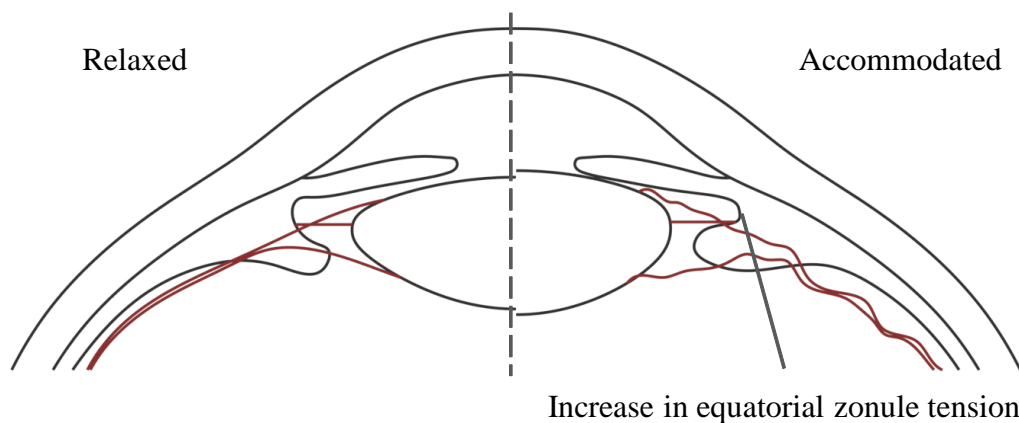


Figure 1.9: Zonule arrangement according to Schachar (1992), highlighting the alternative view of the movement of the equatorial zonule with ciliary muscle contraction.

Bernal *et al.* (2006) showed that the posterior zonules do not predominantly attach to the posterior capsule, but attach to the Weigers ligament via the anterior hyaloid membrane (Figure 1.10). The hyaloid

membrane is a thin membrane of collagen separating the vitreous from the rest of the eye, with the anterior portion separating the vitreous and lens (Bergua & Kuchle, 2002). Wiegers ligament (also known as Egger's line) is an area where the hyaloid membrane and the posterior capsule adhere to each other, forming a band around the lens, posterior of the equator, but not extending to the posterior pole (Bergua & Kuchle, 2002).

Bernal *et al.* (2006) suggested that the zonules attaching to the hyaloid membrane could affect accommodation, as unlike the anterior zonules which run a straight course from ciliary body to the lens, the posterior zonules attach to the lens via the membrane which could cause traction to be reduced. Nankivil *et al.* (2009) supported this work, showing that the posterior zonules linked with the hyaloid membrane play a role in accommodation, as even without anterior zonules, the remaining posterior zonules can still cause accommodation to occur. The overall structure according to these authors can be seen in Figure 1.10.

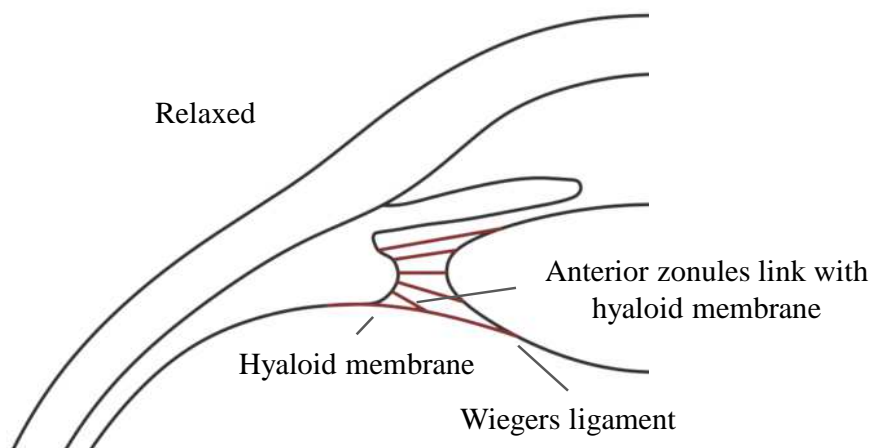


Figure 1.10: Zonular arrangement according to the studies of Bernal *et al.* (2006) and Nankivil *et al.* (2009), illustrating the addition of the anterior zonules interlacing the hyaloid membrane.

A recent computer animation was developed by Goldberg (2011) to visualise the zonular movement based on a combination of previous studies (including Rohen, 1979 and Bernal *et al.*, 2006). The majority of the detail originated from Lütjen-Drecoll *et al.* (2010) who used scanning electron microscopy (SEM) and ultrasound biomicroscopy to image the zonular groups, and strong evidence was found for a vitreous zonule primarily attached to the posterior capsule and the ora serrata (the posterior portion of the ciliary body, see Figure 1.11). There was also evidence of additional smaller attachments along the length of the vitreous zonule that may allow for finer control of the system and reduce the amount of stress at the primary attachments. These smaller attachments would also serve to stabilise and smooth the system movement. The complete arrangement proposed by Goldberg (2011) is illustrated in Figure 1.11.

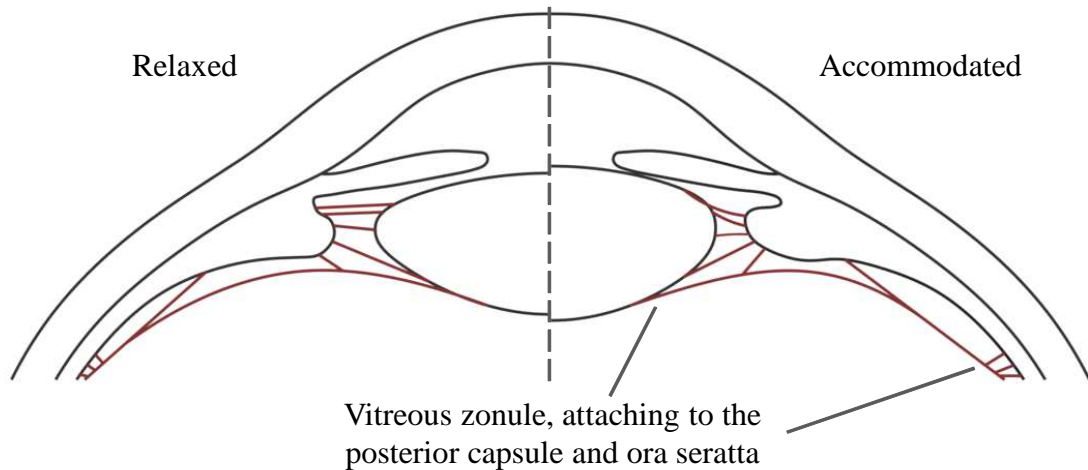


Figure 1.11: Zonular arrangement from the computer model of Goldberg (2011), primarily based on the imaging of Lütjen-Drecoll *et al.* (2010), highlighting the more detailed representation of the vitreous zonule and its connections anteriorly and posteriorly.

Few studies have analysed the insertion of the zonules into the capsule. Hiraoka *et al.* (2010) studied the insertion in monkey eyes and found that the zonules pass through the outer layer of the lens and adhere to the epithelium, actually travelling towards the poles of the lens past the initial insertion point.

Material Properties

There have been few studies into the material properties of the zonules, with each study conducted finding markedly different results for the elastic modulus of the zonular fibres, which have been found to vary between 300 mN/mm^2 (Fisher, 1986; Michael *et al.*, 2012) and 1500 mN/mm^2 (Van Alphen & Graebel, 1991), with the variation most likely due to the different mechanical testing methods (see Chapter 4).

Changes with age

The attachment positions on the capsule of the zonules have been shown to change with age. Farnsworth & Shyne (1979) demonstrated that the anterior zonules move further away from the equator with age. Sakabe *et al.* (1998) demonstrated this, but also found that the zonular free area of the lens decreases with age, indicating a spreading of the zonular attachments. Ludwig *et al.* (1999) found no age variation in the zonular arrangement, other than an increase in axial distance between the anterior and posterior attachment locations, consistent with the age related increase in lens size. In terms of material properties, the elasticity has been observed to remain stable with age, indicating the zonules retain their ability to extend and contract through life (Michael *et al.*, 2012).

1.2.3.4 Ciliary body

The ciliary body surrounds the lens and is formed of two principal sections: the *pars plicata* anteriorly and the *pars plana* posteriorly. The *pars plicata* contains the ciliary processes, folds in the ciliary body, containing the ciliary valleys. The ciliary processes are vascular structures and as was discussed in the previous section, a number of zonular fibres run through the ciliary processes. The *pars plana* runs up to the ora seratta and separates the ciliary body from the retina. The most important aspect of the ciliary body is that it contains the ciliary muscle, which is predominantly situated in the *pars plicata* region, but does extend into the *pars plana* (Figure 1.12).

Ciliary muscle

The contraction and relaxation of the ciliary muscle causes the changes in the ciliary body which, in turn, allows the zonules to control the lens. The ciliary muscle is classed as a smooth muscle (Pardue & Sivak, 2000) formed of three fibre orientations; longitudinal, radial and circular fibres. The longitudinal fibres run alongside the scleral surface, the radial run inbetween the longitudinal and circular fibres and the circular fibres run around the entire eyeball (Figure 1.12).

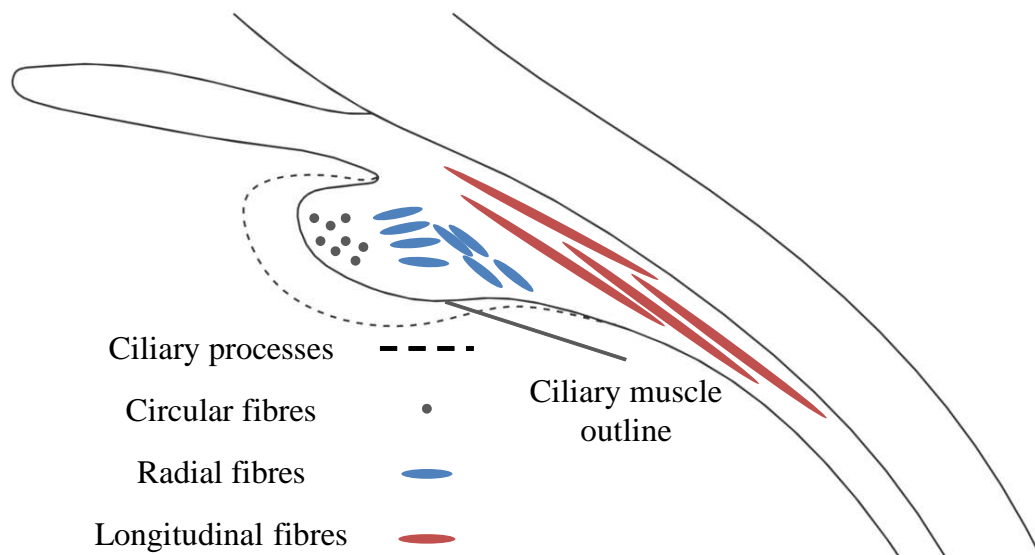


Figure 1.12: The basic shape of the ciliary body, showing the difference between the ciliary process and ciliary muscle and an illustration of the three ciliary muscle fibre types and orientations.

During accommodation it has been shown that the ciliary muscle moves anteriorly and inwards (Sheppard & Davies, 2010), which is due to the muscle contracting and causing the muscle fibres to reorganise. Some of the longitudinal fibres become orientated radially or circularly (Pardue & Sivak, 2000) causing the muscle to shorten in the longitudinal direction and thicken anteriorly. The muscle acts in a similar

manner to a sphincter, with a centripetal movement as it contracts.

Changes with age and accommodation

In the relaxed state, the thickness of the ciliary muscle has been observed to increase with age (Strenk *et al.*, 2010; Sheppard & Davies, 2011), whilst the diameter was seen to decrease (Strenk *et al.*, 2010), reducing the circumlental space (Kasthurirangan *et al.*, 2011).

During accommodation, the ciliary muscle has been shown to increase in thickness (Strenk *et al.*, 2010; Sheppard & Davies, 2011), and this thickness increase is stable with age (Strenk *et al.*, 2010; Sheppard & Davies, 2011). In terms of movement, the centripetal shift has been shown to exist throughout life (Strenk *et al.*, 1999; Stachs *et al.*, 2002) whilst measurements of the circumlental space have shown that it does not change with accommodation (Kasthurirangan *et al.*, 2011), meaning the ciliary body movement matches the lens equator movement.

1.3 Presbyopia

Presbyopia is the name given to the decline in accommodative amplitude of the eye with age. There is currently no standard definition of presbyopia but it is commonly assumed that a person is presbyopic when their inability to focus on near objects is detrimental to their everyday nearwork activities, typically when a person can achieve accommodation of 3 Dioptres or below (Weale, 2000). Figure 1.13 illustrates the decline in accommodative ability with age, and it can be seen that the decline occurs from infancy, although patients only become symptomatic from the age of 45 to 50.

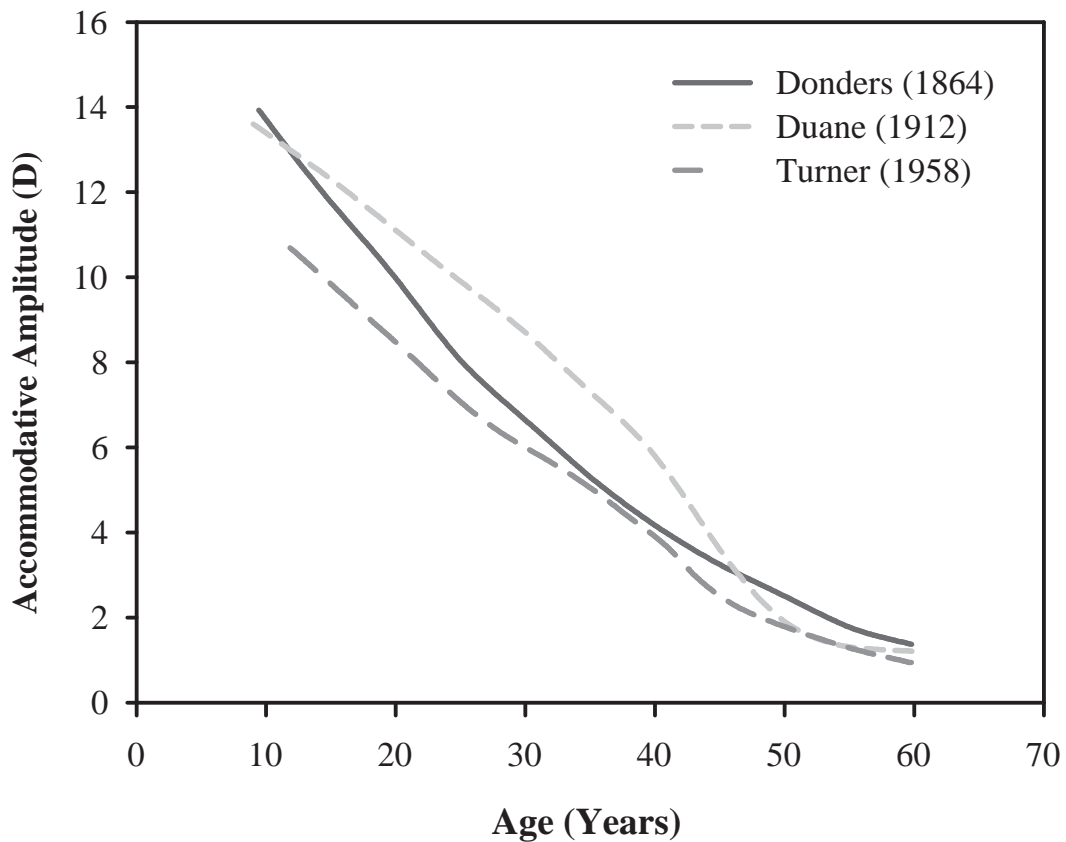


Figure 1.13: Decline in the mean accommodative amplitude with age. Adapted from Figure 2 from Pierścionek & Weale (1995) and Figure 1.5 from Sheppard (2010).

Presbyopia is clearly linked with the ageing of the eye which, as discussed in Section 1.2.3, causes many changes to occur to the accommodative components. How these changes actually contribute to the onset of presbyopia is still under debate. The theories of presbyopia development that have been suggested can be broken down into two main categories; those that attribute presbyopia development to changes within the lens; and those that attribute it to changes in components other than the lens. A summary of the main theories of presbyopia development will be discussed here, along with any sources of support, but as with the accommodative theories discussed in Section 1.2.2, further discussion will be carried out in Chapters 3 and 4.

1.3.1 Lenticular causes

There are a number of lenticular factors that change with age such as the geometry, refractive index and material properties (discussed in Section 1.2.3.1 and in Chapters 3 and 4). A number of these changes

have been hypothesised to be the cause of presbyopia.

Material property changes

Although there is debate on the nature of the stiffness changes within the lens (e.g. Fisher, 1971; Weeber *et al.*, 2007), there is an overall trend seen that the lens stiffens with age. It has been proposed that as the stiffness of the lens increases, the lens may be unable to change its shape in response to the pull of the zonules, limiting the power change of the lens. This has been demonstrated *in vitro* through lens stretching experiments (Glasser & Campbell, 1998; Manns *et al.*, 2007).

One theory that fits the above assumption is the Hess-Gullstrand theory (so termed due to the original proposals by Hess (1901) and Gullstrand (1924), cited by Atchison, 1995), which proposes that the ciliary muscle remains able to exert force on the lens throughout life, and that the amount of contraction that is needed to change the power of the lens does not change. Therefore, the reduction in accommodative amplitude is due to the stiffening of the lens, in that, with age the movement of the ciliary muscle is increasingly unused.

There is also evidence that conflicts with the Hess-Gullstrand theory; Fisher (1977) measured a reduction in the ciliary body force, and Glasser and Cambell (1998, 1999) found that older lenses required more force to deform than younger lenses. Both of these factors lend support to an alternate theory; the Duane-Fincham theory (from the studies of Duane 1925 and Fincham 1937, as cited by Atchison, 1995), which assumes that the ciliary muscle contraction is always at a maximum once the required focus is reached. As a result of lens stiffening, the capsule requires more force to be able to change the lens shape which requires the contraction, and inwards movement, of the ciliary muscle to continually increase throughout life.

Geometric changes

Even without changes to the material properties of the lens, there are a number of geometrical changes that it undergoes. Koretz & Handelman (1986) proposed the geometric theory, hypothesising that changes in lens geometry cause the apparent movement of the zonules, which would result in the forces applied by the zonules becoming more tangential, reducing the amount of force they are able to apply to the lens, causing the lens to be less affected by ciliary muscle movement. It is unlikely that the zonules actually migrate, the movement is potentially a result of both new fibres being generated in the capsule and pushing the zonules further around the lens and the thickening of the lens.

A more recent theory is the modified geometric theory from Strenk *et al.* (2005), where the loss of accommodative ability is due to the combination of lens size increase and the anterior and inwards movement of the ciliary muscle. These two factors combine to cause a reduction in the circumlental space, thereby reducing the zonular tension available for pulling on the lens. There is evidence for and against this theory from *in vivo* measurements, which will be discussed in Chapter 3.

Schachar (2006) proposed another theory of presbyopia development in line with his theory of accommodation (Section 1.2.2); the growth of the lens equator causes a loss in the force applied by the zonules, reducing the accommodative ability of the lens. The evidence for and against this theory will be discussed further in Chapter 3.

The capsule also undergoes changes, in both its thickness variation around the lens (Barraquer *et al.*, 2006) and its material properties (Krag & Andreassen, 2003a), both of which will be discussed further in Chapters 3 and 4. It is not known to what extent these capsular changes contribute to the age related decline in accommodation, but the changes cannot be ignored (Krag & Andreassen, 2003a).

Changes to the protein concentration

The protein concentration within the lens changes with age, which leads to a final lenticular theory, proposed by Truscott (2009). It was hypothesised that the increase in stiffness within the central portion of the lens is a result of the loss of α -crystallin within the lens, which by 40 years of age has been dramatically reduced. Truscott also proposed that presbyopia could be advanced in hotter climates due to the quicker loss of α -crystallin.

1.3.2 Extralenticular causes

Extralenticular theories attribute the loss of accommodation to changes in the surrounding parts of the lens; the ciliary body and the zonules. Duane (1925) (cited by Atchison, 1995) proposed that the ciliary muscle weakens with age, limiting the zonular force that can be applied. However, it has not been shown that the ciliary muscle does weaken (Fisher, 1977; Manns *et al.*, 2007), and FEA studies have shown that the force required to replicate accommodation does not change with age (e.g. Hermans *et al.*, 2008).

An alternate theory is that presbyopia is caused by a loss in the ability to relax accommodation, instead of losing accommodative ability (Bito & Miranda, 1989). This is due to the ciliary muscle losing its ability to maintain the tension required to hold the lens in its un-accommodated state, meaning that it cannot produce the shape changes needed for accommodation.

1.3.3 Methods of presbyopia correction

Even with the debate over the cause of presbyopia, there has been extensive research into methods of correcting the loss of accommodation with age. Simple static correction can be given for near distances, which can be achieved in a number of ways. The most common is the use of glasses or contact lenses, using either single or bifocal lenses. Corneal surgery can be performed as well, but as with glasses and contact lenses, corneal surgery only provides simple correction (Glasser, 2008), meaning that the dynamic range of accommodation is not restored. An increasingly popular option is the use of an intraocular lens (IOL), implanted into the capsule after the removal of the lens, however, these also only allow for similar correction to contact lenses (Sheppard *et al.*, 2010). Research using adaptive optics and a vision simulator has also demonstrated the benefits of reducing spherical aberrations in the eye as a method of improving vision (Piers *et al.*, 2007).

To attempt to restore dynamic accommodation, a number of surgical methods have been hypothesised. The first is the use of accommodating intraocular lenses (AIOLs) to implant into the capsular bag. The second is to refill the capsular bag with a synthetic material to replicate the lens, with the final method being the use of femtosecond laser surgery to alter the lens structure.

1.3.3.1 Accommodation intraocular lenses

The first type of AIOL is the single optic, where accommodation is simulated by a shift in the position of the IOL as a result of ciliary muscle contraction. A variety of designs have been developed; the Crystalens, utilising the change in vitreous pressure to push forwards the IOL, after contraction of the ciliary muscle (Cumming *et al.*, 2006), based on the Coleman theory of accommodation (see Section 1.2.2). The Ter-aflex, 1CU and Biocomfold AIOL's are based on forward movements induced by changes in the capsular bag shape, with differing methods of inducing the movement (Legeais *et al.*, 1999; Findl *et al.*, 2003; Sheppard *et al.*, 2010). Theoretical accommodative abilities of approximately 1D could be achievable with this method (Glasser, 2006), however, clinical studies have shown very varied results in implanted IOL's (Sheppard *et al.*, 2010).

An alternative to the single optic is the dual optic AIOL, using two different power optics which are separated within the capsular bag, with aqueous fluid filling the space between the optics. Different versions utilise two optics in different ways. The Synchrony AIOL contains a positive and negative optic, joined with a spring like mechanism. With the ciliary muscle relaxed, the capsule causes the spring to

be compressed, but with ciliary muscle relaxation, the capsular strain reduces, causing the spring to push the anterior optic forwards, increasing the power (McLeod *et al.*, 2007). A similar design is the Sarfarazi, which uses three haptics to join two optics and again use forward movement of the anterior optic to change power in response to capsular changes (McDonald *et al.*, 2003). An alternative design is the Turtle AIOL, which uses two optics that rotate to change its power. The two lenses reside in a frame and in response to the ciliary muscle action, rotate, changing the combined power of the optics (Hermans *et al.*, 2008). Although there has been very little clinical work in testing these dual optic designs, theoretical modelling has shown that dual optic designs have the potential for 2 - 2.5D of accommodative ability (Glasser, 2008).

There are other proposed AIOL concepts being researched. One method is to use magnets, a method developed by (Preußner *et al.*, 2001). A single optic is inserted into the capsule, along with two magnets. Two further magnets are then attached to exterior muscles, which are of opposite polarity. With the change in ciliary muscle contraction, the exterior magnets push the capsular magnets forward, changing the power.

The Nulens AIOL concept utilises changes in curvature for the power change. A haptic system is secured to the ciliary muscle comprised of an anterior plate that has a chamber fixed to it containing a silicone gel. A piston positioned posterior to the chamber is moved by the emptied capsular bag. The piston pushes the gel through the anterior plate causing a bulge and subsequent power increase. The process works on the reverse of accommodation, in that the relaxation of the ciliary muscle causes an increase in power and the contraction causes a decrease in power (Ben-Nun & Alió, 2005). Trials in monkey eyes have suggested that this AIOL could produce theoretical accommodative abilities of 40D, but there was no data on human eyes (Glasser, 2008).

The FluidVision AIOL uses a combination of hollow haptics and a single optical element. In response to ciliary body contraction and increased capsular pressure, the haptics have an increased force applied to them, causing the fluid within the AIOL to move into the optic, increasing its curvature and its power (Sheppard *et al.*, 2010).

1.3.3.2 Lens refilling

As an alternative to IOLs, lens refilling involves inserting a material within the capsule to try to replicate the natural lens as much as possible, rather than using a prefabricated optic as in an IOL (Nishi *et al.*, 2009). As with IOLs, the refilled lens is hoped to replicate the movement of a young lens in response to ciliary muscle movement.

Lens filling has two principal stages after the original lens has been removed. The first is the insertion of the material for refilling, followed by a method to seal the capsule to prevent the material from leaking. The material used needs to be suitable for injection, i.e. fluid, but then also be able to approximate the original lens's material properties once in situ. In addition, the material needs to be optically suitable (Koopmans *et al.*, 2006).

A range of methods of both injection and subsequent sealing have been developed, from simple injection of a material (e.g. Hettlich, 1996) through to endocapsular balloons (Nishi, 1989), sealing plugs (Koopmans *et al.*, 2006) and combinations of synthetic materials and IOLs (Nishi *et al.*, 2008). To date, lens refilling has only been demonstrated on animal eyes, with the principal issues holding back development of the technique, being, the change in behaviour of the capsule after lens removal and the subsequent insertion of a replacement material (Nishi *et al.*, 2009). However, lens refilling has the potential to restore greater amounts of accommodative ability, compared to AIOLs, providing the issues with aftercare are resolved (Menapace *et al.*, 2007).

1.3.3.3 Femtosecond laser lentotomy

A method that is becoming increasingly popular in vision correction is the use of laser surgery. Instead of replacing the lens with an optic or fluid, the lens is altered *in vivo*, using laser lentotomy. The first proposal was by Myers & Krueger (1998), who hypothesised that creating small incisions within the crystalline lens using nano second laser pulses would increase the flexibility of the lens. However, the initial experiments showed that the flexibility was increased, but there were substantial side effects, such as light scattering and gas bubbles (Schumacher *et al.*, 2009).

Later experiments found that femtosecond laser pulses negated the side effects found previously, in rabbit (Krueger *et al.*, 2005), porcine (Ripken *et al.*, 2008) and *in vitro* human lenses (Schumacher *et al.*, 2009); indicating that there is potential for laser surgery to restore accommodation in older lenses (59% increase in thickness in spinning studies, Schumacher *et al.* (2009)). There are still issues that need resolving, such as potential rainbow glare (Ackermann *et al.*, 2013) and whether such surgical treatments would lead to cataract development (Schumacher *et al.*, 2009). The potential benefits of laser lentotomy, such as the ability to avoid alteration of the capsule or cornea as part of the surgical treatment, will ensure that the process will be studied extensively.

1.3.3.4 Scleral expansion

A final method of accommodation restoration that has been proposed is to expand the sclera, hypothesised to restore zonular tension (Schachar, 1992). This proposal is based on the accommodative theory of Schachar (Section 1.2.2), which suggests presbyopia arises through the growth of the lens equator causing a slackening of the zonules. This method goes against the widely held theory of accommodation, and has been shown to offer little or no improvement when used (Glasser, 2008).

1.3.3.5 Summary

For the accommodative ability to be restored through the use of IOLs, lens refilling or laser lentotomy, the accommodative components that are not treated are required to function in an appropriate manner through the movement of the ciliary muscle and capsule. Therefore, a good understanding is required of how these accommodative components behave, both before and after any surgical treatment. Finite element modelling allows for different geometric, material and force descriptions to be combined into a single model, giving the potential to simulate all aspects of accommodation and accommodation restoration, which will be explored further in the next chapter.

1.4 Aims and Objectives

One avenue of research that has been used to gain a better understanding of accommodation is Finite Element Analysis (FEA), which will be explored further in Chapter 2. The overall aim of this thesis is to utilise FEA to investigate accommodation and presbyopia in more detail, by exploring the following two questions:

1. What are the principle factors that cause the crystalline lens to change its shape and therefore its power?
2. How do age changes in the material and geometric properties of the components in the accommodation system contribute to presbyopia?

These questions will be answered through the development of a new, adaptable, finite element model of the accommodation system, which is able to simulate the accommodative process in a range of different ages, as well as remove or limit the deficiencies in previous methods. To be able to explore the questions fully, a number of objectives will need to be met:

1. Development of a modelling method that can produce an age related model of the accommodative structures, improving on limitations in existing methods
2. Selection of appropriate material parameters for each accommodative component
3. Evaluation of the proposed methods to ensure that the model replicates the accommodative process
4. Completion of a detailed analysis of how altering key age related parameters affects the changes undergone during the accommodative process

1.4.1 Thesis structure

The current chapter has given the reader a broad overview of the process of accommodation and the development of presbyopia, highlighting key age related changes that are undergone in the accommodative components. Various proposals for methods of accommodation restoration were discussed, highlighting the need for a better understanding on both accommodation and presbyopia. The overall aims of the thesis were then presented, with the key objectives that need to be met; which will be addressed by the following chapters:

Chapter 2: An introduction to FEA is given, before a thorough analysis of existing accommodation FEA models is conducted in terms of four key areas; Geometry, material properties, procedures and results. The key limitations of these models are highlighted, finishing with a summary of the main improvements that will be required

Chapter 3: To develop an improved geometric model (Objective 1), the available geometric data of the relevant accommodative components required analysis. The modelling methodologies for the required components are then developed, detailing the improved and novel methods used in the proposed accommodation model.

Chapter 4: An overview of the relevant material constitutive models is given, before an analysis of the available material data of the modelled accommodative components is conducted. The appropriate material data selections are then detailed to meet Objective 2.

Chapter 5: Following the selection of appropriate geometry and material data for the proposed accommodation model, the overall experimental procedures that would be followed to answer the principal questions are defined. The FEA theories followed and how the geometric and material specifications could be combined along with the specific procedures that would be followed in the next chapter are discussed.

Chapter 6: A series of preliminary studies were conducted to ensure the methodologies proposed hitherto were suitable, before final models were analysed to meet Objective 3. With the methodology validated, the final studies into how age related changes affected presbyopia (Objective 4) were conducted.

Chapter 7: The results of the studies conducted in Chapter 6 were compared to the overall aims and objectives, with any limitations discussed. The thesis is concluded by detailing the future directions of the research.

Chapter 2

Background: Finite element models of accommodation

2.1 Introduction to Finite Element Analysis

Finite element analysis is a tool commonly used in engineering to analyse how a structure behaves when subjected to various loadings, such as internal pressure or forces. The basic principal is that a structure (or domain) is broken down into a number of finite regions, called elements, which can be used to solve equations on a smaller scale as part of a larger equation for a complete domain. By breaking a domain down into smaller elements, the complex partial differential equations governing the overall structures response to external loadings can be approximated by smaller algebraic equations. The FEA method is an approximation method, but due to being able to approximate complex geometric structures and non-linear material behaviour, it is becoming increasingly popular in investigating biomechanical problems, such as accommodation. The principals of FEA relevant to the current work will be explored further in Chapters 3 - 5.

2.1.1 FEA of the accommodation system

A number of finite element analysis models of the accommodation system have been developed, typically simulating aspects of accommodation that cannot be measured *in vivo* or *in vitro*. This has led to many of these models representing hypothetical situations, which combined with the paucity of measured data on the accommodative system has led to a number of assumptions being made. Therefore, examination of the data that has been used to develop these models is needed, to establish the key areas of modelling as well as any current limitations that can be improved on.

FEA models can be examined in terms of four key areas: the geometry, the mechanical properties, the procedure and the results. In the current chapter the literature refers to the studies listed in Table 2.1,

which also summarises the individual aims and key findings as a reference. Although not an exhaustive list, the studies in Table 2.1 have been selected for analysis as they represent a mixture of the origins of the finite element method applied to accommodation (e.g. Schachar & Bax, 2001b and Burd *et al.*, 2002), novel modelling practices (e.g. Martin *et al.*, 2005 and Ljubimova *et al.*, 2008) as well as more recent studies illustrating the current methodologies (e.g. Wilde, 2011 and Lanchares *et al.*, 2012).

Table 2.1: FEA accommodation models from the literature analysed in this chapter, with a summary of the aims of each study. *Both papers report on the same study. YO = Year old.

Study	Aim	Key Findings
Schachar & Bax (2001b)	Compare the Schachar and Helmholtz theories of accommodation	Following the Schachar theory resulted in suitable changes, using the Helmholtz theory did not
Burd <i>et al.</i> (2002)	Simulate accommodation in a 11, 29 and 45 YO lens, using updated modelling methods	The 29 and 45 YO lens model matched expected changes, but the 11 YO lens had some anomalous behaviour
Breitenfeld <i>et al.</i> (2005)	Compare the accommodative ability of a 29 YO lens before and after simulated fs-laser treatment	The fs-laser treated lens provided a marginal increase in accommodative ability
Liu <i>et al.</i> (2005)	Simulate accommodation in a 29 YO lens using updated zonule modelling methods	The power of the lens model increased with ciliary body movement
Martin <i>et al.</i> (2005)	Compare Helmholtz and Coleman theories of accommodation in a 29 YO lens	Following the Coleman theory did not provide enough power change compared to following the Helmholtz theory
Hermans <i>et al.</i> (2006)	Estimate the forces applied to a 29 YO lens during accommodation using new geometric data	The net force on the lens to achieve suitable geometric changes was 0.08 N, regardless of zonule arrangement variations
Liu <i>et al.</i> (2006)	Compare Schachar and Helmholtz theories of accommodation in a 29 YO lens using two models	Both models showed support for aspects of Schachar and Helmholtz theories
Schachar <i>et al.</i> (2006) & Abolmaali <i>et al.</i> (2007)*	Understand how geometric and material properties affect the decline of accommodative ability with age	A decline in zonular force was supported as a potential cause of presbyopia. A small decrease in accommodative ability was seen as a result of lens stiffness increases
Belaidi & Pierscionek (2007)	Investigate lens stiffness variation on the age related decline in accommodation	The change in stiffness gradient is the cause for age related accommodative loss
Weeber & van der Heijde (2007)	Investigate the change in force applied to the lens with age	Force application hardly changes with age, indicating a lenticular cause of presbyopia
Ljubimova <i>et al.</i> (2008)	Simulate accommodation in a 29 YO lens using an updated zonular model and including vitreous effects	The new model has some problems, but does behave predictably and supports the Helmholtz theory
Continued on next page...		

Table 2.1 continued

Hermans <i>et al.</i> (2008)	Determine how the force applied to the lens changes with age	Force application is preserved with age, with a small increase to a maximum value of 0.06 N found
Weeber & van der Heijde (2008)	Determine the internal changes within the lens during accommodation	Changes in lens thickness are due to change in the nucleus. Deformation in older lenses only occurs in equatorial regions and does not effect the surface curvatures
Van de Sompel <i>et al.</i> (2010)	Understand how geometric and material properties affect the decline of accommodative ability with age	The majority of the loss in accommodative ability is due to geometry changes
Riehemann <i>et al.</i> (2011)	Integrate a mechanical and optical model for simulating accommodation and presbyopia	The development of presbyopia is due to the stiffness change within the lens
Wilde (2011)	Test a new FEA model against in-vivo measurements. Laser treatment method also tested	Change in lens stiffness the most likely cause of presbyopia. Simulated laser treatment showed an increase in accommodative ability
Lanchares <i>et al.</i> (2012)	Understand how mechanical property changes with age cause presbyopia	Increase in stiffness of the nucleus and cortex supported as the cause of presbyopia

2.2 Geometry

Each component of an FEA model requires its geometry to be defined and for modelling accommodation, the typical components are the lens, capsule, zonules and ciliary body (e.g. Burd *et al.*, 2002 and Lancharas *et al.*, 2012). The key feature of an FEA model is that it needs to be a realistic representation of the structure. When modelling organic materials, which are typically complex structures without continuous contours, the geometry does need to be simplified which leads to approximations being made. For example, the components of the accommodation system are typically modelled as being rotationally symmetric, i.e. a 2-dimensional profile that is revolved around a central axis. Table 2.2 breaks down the methods used to model the key components in previous FEA models.

Table 2.2: Modelling methods of the key components in the FEA models in the literature. Key to methods: P: Polynomials, CS: Conic Sections, CF: Cosine function, H: Homogenous, NC: Nucleus-Cortex, SG: Stiffness gradient, F: Fincham (1925) thickness variation, BU: Burd *et al.* (2002) thickness variation, BA: Barraquer *et al.* (2006) thickness variation, 3Z: 3 Zonules, 1Z: Single zonule, 5Z: 5 zonules. There are a number of variations of each method (denoted by a *) used by different authors however, the basic methodology is the same. ** indicates the method was not explicitly stated, although a lens was modelled.

Study	Method of modelling			
	Lens Model	Internal Structure	Capsule	Zonule
Schachar & Bax (2001b)	P*	H	F	3Z
Burd <i>et al.</i> (2002)	P	NC	BU	3Z
Breitenfeld <i>et al.</i> (2005)	P	NC	BU	3Z
Liu <i>et al.</i> (2005)	P	NC	BU	3Z
Martin <i>et al.</i> (2005)	P	NC	BU	3Z
Hermans <i>et al.</i> (2006)	CS	NC	BU	-
Liu <i>et al.</i> (2006)	P	NC	BU	3Z*
Abolmaali <i>et al.</i> (2007)	CF	NC*	F	3Z,1Z
Belaidi & Pierscionek (2007)	P*	H,NC*	-	5Z
Weeber & van der Heijde (2007)	CS*	SG	BU	3Z*
Hermans <i>et al.</i> (2008)	CS	NC*	BU	-
Ljubimova <i>et al.</i> (2008)	P	NC	BU	3Z*
Weeber & van der Heijde (2008)	CS*	SG	BU	3Z*
Van de Sompel <i>et al.</i> (2010)	P	NC	BU	3Z
Riehemann <i>et al.</i> (2011)	-**	NC	BU	3Z
Wilde (2011)	CS	NC,SG	BA	3Z
Lancharas <i>et al.</i> (2012)	CS*	NC*	BU	-

2.2.1 Crystalline lens shape

As discussed in Chapter 1 the crystalline lens is one of the most important parts of the accommodation system, allowing the eye to keep a constant focus through the changes in shape it can achieve. There are two factors that need to be considered with the lens models, the source of the data used to define the mathematical representation and the accuracy of the mathematical method itself. The sources and mathematical methods will be discussed further in Chapter 3.

2.2.1.1 Source data

The majority of studies have used the lens measurements of Brown (1973), obtained using Scheimpflug photography of three lenses (11, 29 and 45 YO), from which a large number of lens parameters were acquired in the accommodated and un-accommodated state. Using the same method, Koretz *et al.* (1989) measured changes in lens parameters in a wider range of subjects to provide more details on the changes observed by Brown (1973). However, both Brown (1973) and Koretz *et al.* (1989) did not correct for distortions caused by the imaging method; which occur due to the optical structures in front of the sections being imaged as well as those within the instrument being used. The anterior surface will be affected by the corneal refraction, whilst the posterior surface will be affected by the refraction of the lens itself (Dubbelman *et al.*, 2001). As a result a new set of data were detailed by Dubbelman & Van der Heijde (2001), Dubbelman *et al.* (2001), Dubbelman *et al.* (2003) and Dubbelman *et al.* (2005). In these studies a larger number of subjects were used across a range of ages with measurements made across a number of accommodative stimuli, with all measurements corrected for the optical distortions mentioned previously. In all of these Scheimpflug studies, only the central surfaces of the lens can be imaged due to restrictions caused by the pupil, requiring assumptions to be made to complete the lens shape.

To avoid using partial images of the lens, alternative sources have been used. One of these was Pierścionek (1993), where the shape data was obtained from photographs of two lenses in a lens stretching device. This has the obvious disadvantage of giving data on the lens *in vitro*, although it can be assumed that an *in vitro* lens can be similar to an *in vivo* lens at full accommodation (Rosen *et al.*, 2006). It is likely that external forces are present (such as from the vitreous and iris), however, it is assumed that these are negligible compared to the capsule and zonule forces. An alternative to *in vitro* whole lens imaging is the use of Magnetic Resonance Imaging (MRI) which can provide data for the whole lens *in vivo*, although typically at a lower resolution, with Strenk *et al.* (1999) being a commonly used data source.

2.2.1.2 Mathematical fit

Although there have been a number of different studies used to provide the geometric data, there have been only three types of mathematical fit used (Methods A – C, Table 2.2 and Figure 2.1).

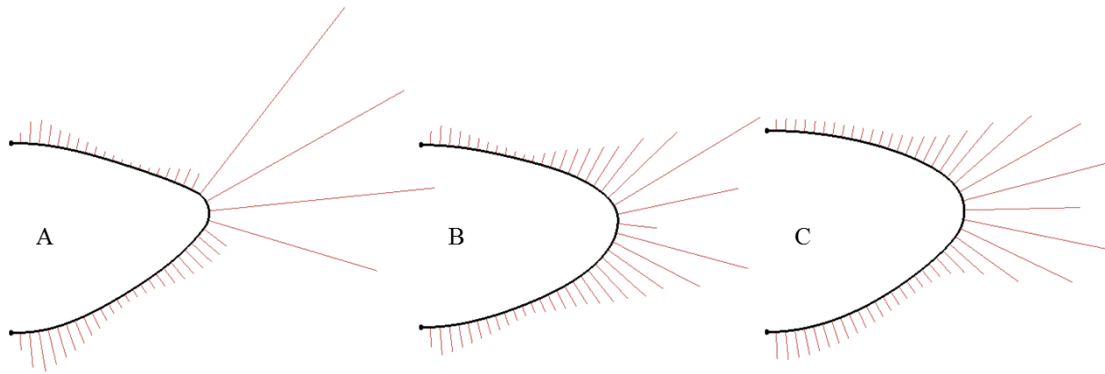


Figure 2.1: Comparison of the rate of curvature change in the modelling methods of Burd *et al.* (2002) (A), Hermans *et al.* (2006) (B) and Chien *et al.* (2003) (C). The change in length of the lines (in red) illustrates the curvature change, giving an indication of the smoothness of each method, with C being the smoothest. Each lens represents an eye of 29 - 30 YO.

Polynomials

Polynomials provide a simple mathematical fit for curved surfaces, which means it can be complicated to fit them to a shape like the crystalline lens. As such, they have typically been fitted to the central optical surfaces and a different method used to complete the lens shape. The most prolific version of this was developed by Burd *et al.* (2002), where fifth order polynomials were fitted to the thickness and curvature data from Brown (1973) to describe the anterior and posterior surfaces of the lens. As the data do not give a complete lens profile, a circular cap was used to close the profile between the anterior and posterior surfaces. The point representing the equator, which the circular arc passed through, was taken from MRI images (Strenk *et al.*, 1999). Other authors using this method are limited to replicating the same age lenses as Burd due to not being able to adapt the method.

Schachar & Bax (2001a) also used the data of Brown (1973), but no details were given on how the lens profile was completed apart from that four 14th order polynomials were used to describe the lens outline. An alternative method was used by Belaidi & Pierscionek (2007), using data from Pierścionek (1993) to fit second order polynomials, producing a rotationally-symmetric 3-dimensional model instead of the typical 2-dimensional model.

The main problem with the polynomial method is the general need to have additional mathematical de-

scriptions to produce a complete lens profile. This results in a discontinuous outline (shown in Figure 2.1) which is not ideal for an accurate FEA model. Polynomial methods are also limited in adaptability as the defining parameters are not measurable.

Conic sections

Using updated scheinpflug photography data (Dubbelman & Van der Heijde, 2001, Dubbelman *et al.*, 2001, Dubbelman *et al.*, 2003 and Dubbelman *et al.*, 2005), Hermans *et al.* (2006) developed their own mathematical description of the lens utilising conic sections (a curve resulting from the intersection of a plane and a cone). Two conic sections were used to describe the central surfaces, using the curvature values measured at particular points on the lens as well as the lens thickness. To complete the profile two additional conics were used to describe the outer anterior and posterior surfaces, which had the same derivatives where they joined the first two conics. The complete lens profile could be created from measured lens parameters. Weeber & van der Heijde (2007) used this method to model the central surfaces, but used a circular fillet to complete the profile using averages of the data of Dubbelman *et al.* (2005) and the equatorial point from Strenk *et al.* (1999).

As with the method of Burd *et al.* (2002) additional data are needed to complete the lens outlines, due to the lack of a complete data set from the Scheimpflug photographs. The increase in the number of curves required will also add to the discontinuities in the model, although a smoother outline is achieved with this method than with polynomials (Figure 2.1). The main advantage of this method is in its adaptability, as it is defined using measurable lens parameters allowing a range of ages to be produced simply.

Cosine functions

Chien *et al.* (2003) undertook a study investigating a number of different methods of fitting a curve to the lens data of Fincham (1937). The eventual method that was chosen was a cosine function, which was validated by fitting it to five MRI images of the lens (from Strenk *et al.*, 1999, Lizak *et al.*, 2000 and Krueger, 2002). The method splits the lens model into two curves which meet at its equator. Subsequently, Abolmaali *et al.* (2007) used the results of the five MRI fits in their FEA model.

Using this method gives a smoother lens outline than with a polynomial method (Figure 2.1) due to there being only two curves, however, the method is limited in adaptability due to not relating the constants to measurable values of the lens. Therefore, as with the Burd *et al.* (2002) model, only the same lens outlines can be produced as defined by Chien *et al.* (2003).

2.2.2 Internal Structure

As described in Chapter 1 the lens is not a single homogenous body but is actually formed of a number of internal layers that are developed throughout life. This variation within the lens is an important aspect of computer models as it will dictate how the material properties are distributed throughout the lens (Chapter 4).

2.2.2.1 Homogenous models

The most basic representation of the internal structure is to model the lens as being a homogenous body. Schachar & Bax (2001a) used this method, although this was amongst the first FEA accommodation models and therefore had a number of simplifications. In later models, this method is utilised as a comparison to more complex models (Abolmaali *et al.*, 2007; Belaidi & Pierscionek, 2007; Wilde, 2011).

2.2.2.2 Nucleus/Cortex

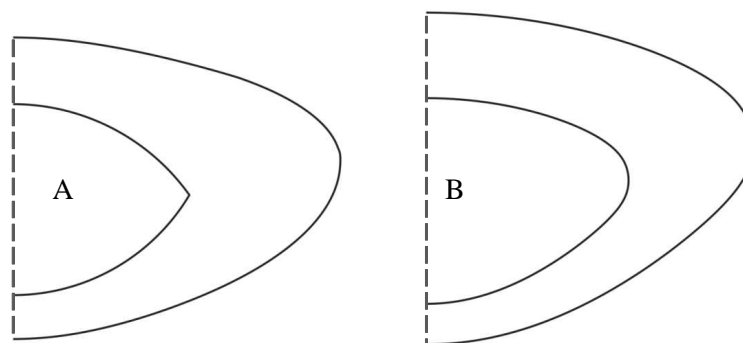


Figure 2.2: Comparison between nucleus modelling methods, A represents the method used by Burd *et al.* (2002), B represents the method used by Abolmaali *et al.* (2007).

Using method E the lens is assumed to be made of two distinct regions, the nucleus and the cortex, and was the most common method used in the literature. Using these two regions was an assumption made by Fisher (1971) when analysing the material properties of the lens, discussed further in Chapter 4, which appears to be the origin of the use of this method in FEA models.

The methods of splitting the lens into the nucleus and cortex have varied. The most basic is the use of two arcs which meet at a point, as used by Burd *et al.* (2002) (Figure 2.2), where the points defining the nucleus shape were taken from Brown (1973). A more complex description was developed by Hermans

et al. (2008), based on enhanced scheinplflug photography (Hermans *et al.*, 2007), where four curves were used to enclose the nucleus. Lanchares *et al.* (2012) developed a different four curve model, which could be seen as a hybrid of the Burd *et al.* (2002) and Hermans *et al.* (2008) methods as it causes the nucleus to come together at a point, but the more complex four curves allowed for better positioning of the nucleus equator. As with the lens outline, the method adopted by Burd *et al.* (2002) has subsequently been widely used. The main disadvantage with this method is the representation of the nucleus as having a sharp point at its widest point, which does not match what is seen *in vivo* (Hermans *et al.*, 2007).

An alternative to having a separate mathematical description of the nucleus shape is to represent it as a percentage reduction of the outer lens shape (Figure 2.2). Two methods have been used, a percentage reduction based on *in vivo* thickness data (Abolmaali *et al.*, 2007) and a percentage reduction based on volume (Belaidi & Pierscionek, 2007). Both methods result in a nucleus shape that is the same as the lens outline, which as shown by Hermans *et al.* (2007) may not be the case. Simply shrinking the outer lens shape down will also not allow for alteration to the proportions of the nucleus, which can be achieved through the mathematical modelling option.

2.2.2.3 Stiffness gradient

In an attempt to accurately model the internal structure Weeber & van der Heijde (2007) segmented the lens into 10 shells, each 10% smaller than the previous, based on stiffness measurements made in a previous study (Weeber *et al.*, 2007). Wilde (2011) later adopted a similar method, although the stiffness distribution was taken from their own stiffness measurements and how the lens was segmented was not clear. Segmenting the lens allows for a much more complex and realistic representation of the distribution of material properties within the lens, allowing more complex changes that occur with age to be modelled.

2.2.3 Capsule thickness variation

The variation in capsule thickness was discussed in Section 1.2.3.2, with the classical description illustrated in Figure 1.5. Representing this variation is important in analysing how the lens changes shape, which can be seen in the literature as the thickness variation has been implemented by the majority of authors, with the differential between them being the source of data used.

The predominant source of the capsule variation has been the thickness measurements of Fisher & Pettet (1972) (Method BU in Table 2.2), which was adapted by Burd *et al.* (2002) who fitted fifth order

polynomials to the data to combine a capsule thickness variation with the lens outline method discussed previously. The data set from Fisher & Pettet (1972) only had data for certain ages, therefore Burd *et al.* (2002) interpolated the data to obtain values for the missing ages. As with the lens outline this method cannot be adjusted and can only be used on the models developed by Burd *et al.* (2002). Weeber & van der Heijde (2007) and Hermans *et al.* (2006) also adapted the data, using it to develop a thickness variation that would be included directly in the element formulation, although details were not given on how the data was adopted.

Another source of data is that of Fincham (1925) (Method F in Table 2.2), first used by Schachar & Bax (2001a) but no details were given on how. This source was also fitted by Chien *et al.* (2003) when developing his mathematical lens description, which was subsequently used by Abolmaali *et al.* (2007).

The final data source (denoted method BA in Table 2.2) is a more recent study by Barraquer *et al.* (2006) used by Wilde (2011). This provided data similar to method BU and was adapted to fit the method of modelling the lens.

2.2.4 Zonule Arrangement

Due to the complications in imaging the zonules and the resultant uncertainty on the arrangement of the zonules (e.g. Rohen, 1979 and Nankivil *et al.*, 2009, as discussed in Chapter 1), there is little variation in the modelling of the zonules in the models discussed hitherto.

There have been two methods of applying zonular force to the lens; modelling the fibres and applying forces directly to the capsule. If the fibres are modelled the attachment points on the capsule and ciliary body need to be defined, whereas for applying force directly to the capsule only the capsule attachment positions are needed. The different zonular models are illustrated in Figure 2.3.

2.2.4.1 Modelling the zonules

Of the authors that have selected to model the zonules (see Table 2.2), the predominant method has been to use three zonular groups; split into an anterior, equatorial and posterior set. The typical arrangement, first modelled by Burd *et al.* (2002) (denoted the 3Z method in Table 2.2 and A in Figure 2.3), has an attachment for each set on the capsule and then has them all attach to a single point replicating the ciliary body. Burd *et al.* (2002) used the data of Farnsworth & Shyne (1979) to position the anterior zonules relative to the equator. An assumption was made that the posterior zonules attach to the lens at the same

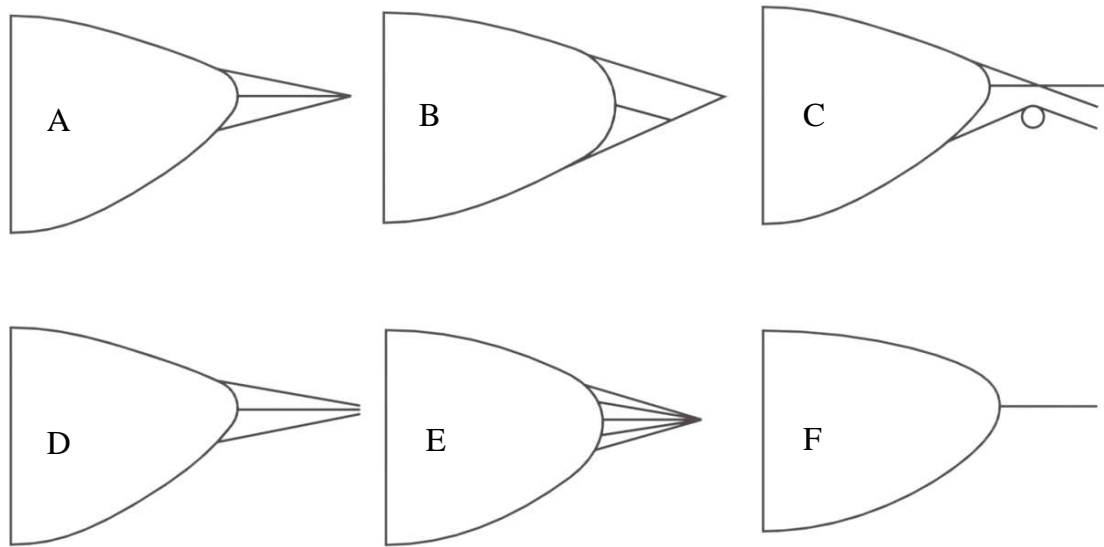


Figure 2.3: Zonular arrangements used in the literature. A - Burd *et al.* (2002) B - Weeber & van der Heijde (2007) C - Ljubimova *et al.* (2008) D - Liu *et al.* (2006) E - Belaidi & Pierscionek (2007) F - Abolmaali *et al.* (2007).

distance from the equator as the anterior zonules, with the equatorial zonules attaching at the widest point on the lens. The ciliary body position was taken from the MRI measurements of Strenk *et al.* (1999). The 3Z method has been utilised by the majority of studies, even though it is a simplistic representation of the complex zonular arrangement.

There have been some attempts to improve on the 3Z method. Liu *et al.* (2006) used the same data for the capsule attachments but represented the zonules as attaching to the ciliary body in three separate locations. It was not clear how these locations were chosen but it appears that the three ciliary body attachments were aligned vertically (D in Figure 2.3). The purpose was to replicate Schachar's theory of accommodation by moving the anterior and posterior zonules in opposition to the equatorial zonule. Weeber & van der Heijde (2007) represented the equatorial zonule as connecting to the posterior zonule, to provide an axial pull, an effort to represent the tensor zonules from Rohen (1979) (B in Figure 2.3).

Ljubimova *et al.* (2008) developed a more complicated model using three zonular groups (C in Figure 2.3). The anterior and equatorial capsule attachments were specified as with Burd *et al.* (2002), however, the posterior attachment was positioned using data from Gorban & Dgiliashvili (1993), which resulted in a posterior attachment closer to the equator. The ciliary body attachments were also developed further; the equatorial zonule attached horizontally to the ciliary body as with Burd however, the anterior and posterior zonules were modelled as attaching to the ora serrata, although the whole length of them was not modelled.

This resulted in a more posteriorly sloped attachment to the anterior zonule, whilst the posterior zonule was modelled as having to pass over the vitreous before sloping posteriorly. The use of this arrangement gave a more horizontal application of force by the posterior zonule.

Another method (denoted the 1Z method in Table 2.2 and F in Figure 2.3) used in modelling the zonules was to only model a single equatorial zonule (Abolmaali *et al.*, 2007) to replicate the accommodative theory of Schachar. The zonule ran from the equatorial point of the capsule to a single point representing the ciliary body movement, an oversimplified version of the zonular arrangement.

2.2.4.2 Force application

The alternative to modelling the zonules is to apply tractions or forces directly to the lens, reducing the complexity of the model. Both the attachment locations and the direction of force application are still required.

Hermans *et al.* (2006) was the first model in the literature to adopt this method. The locations of the force were defined by Streeten (1977), where the zonular attachments were positioned further apart than the data used in other studies. To be able to apply a force, an area to apply it over needed to be defined. Ludwig (2001) provided the data for the width of the anterior and posterior zonules and the equatorial width was assumed to be the same as the posterior width. The directions of application were not specified. This method was later adopted by Hermans *et al.* (2008) and Lanchares *et al.* (2012).

Belaidi & Pierscionek (2007) (Denoted the 5Z method in Table 2.2 and E in Figure 2.3) used an alternative model, using five zonules to distribute force (rather than a displacement) to the lens, all loaded at a single point representing the ciliary body. This was chosen as previous studies had shown using 3 zonules resulted in discontinuities at the zonular attachments when the lens models were deformed (Burd *et al.*, 2002; Martin *et al.*, 2005). How the zonules were spaced was not specified.

2.2.5 Other Components

Although the Helmholtz theory attributes the lens changes to the ciliary muscle, zonules and lens, other theories hypothesise that the vitreous has a role (e.g. Coleman & Fish, 2001). Martin *et al.* (2005) and Liu *et al.* (2006) created a simple model replicating these ideas by representing the vitreous as a pressure on the posterior lenticular surface.

Ljubimova *et al.* (2008) modelled a representation of the vitreous itself, assuming that the vitreous acted as a support for the lens during accommodation and resisted posterior zonule force. The vitreous model was used to develop the posterior zonule arrangement as well as applying a force to the posterior lens surface.

2.2.6 Summary of geometric methods

The lack of a complete description of the components of the accommodative structure has led to a number of different methods being used to model it. Although there are modelling methods used to replicate the lens and capsule that appear to be suitable, careful consideration will be needed to ensure that the appropriate changes with age are accounted for. The two areas that improvement is needed in are the internal structure modelling and the zonular arrangement.

The internal structure is key as it dictates the distribution of material properties through the lens, which has been shown to vary in a more complicated way than a simple nucleus-cortex split (e.g. Weeber *et al.* 2007). There was evidence for the majority of thickness change occurring in the central part of the lens (Dubbelman *et al.*, 2003), therefore if the nucleus-cortex method is adopted, the oversimplification of the shape could have negative effects on the results. Adopting a stiffness gradient method could be a solution for this but further work is needed on how to implement this effectively.

Even with the increase in data on the arrangement of the zonules (see Section 1.2.3.3), the same methods of representation have persisted in the literature, in particular the 3 zonule method, which can lead to discontinuities or areas of high stress in deformed models (e.g. Breitenfeld *et al.*, 2005; Hermans *et al.*, 2008; Weeber & van der Heijde, 2008). To fully understand how the lens behaves in accommodation, a more detailed representation is needed to establish whether controlling the zonules in separate groups will give a more realistic response.

2.3 Material Properties

Each component that is represented in an FEA model requires its material properties to be defined, as these dictate how a body will deform under external loading conditions. Different assumptions have been made in the literature on how the materials in the accommodative system can be defined, which has resulted in a number of different sources being used for the material data (see Table 2.3). A comprehensive overview

of material properties and the sources covered in this review will be given in Chapter 4, however, a basic understanding of the main types of material properties that can be defined is needed here.

For modelling the accommodative components, it has generally been assumed that the components are linear elastic, isotropic materials. Elastic materials will deform under a load but return to their original shape. If a material is isotropic, the material properties are the same in all directions, whereas for anisotropic materials the properties vary with position and direction of loading. Depending on the assumptions made as to how the material behaves, different material properties are required to define the material behaviour.

To define an isotropic elastic material for an FEA study, the only properties needed are the elastic modulus and Poisson's ratio. Poisson's ratio defines how a material reacts to compression; it is the ratio of the contraction of a material to the extension in the direction of the load. Anisotropic materials require additional properties to be defined to dictate how the properties vary throughout the component. A smaller set of studies have represented the components as having hyper-elasticity, which requires the shear modulus and bulk modulus to be defined.

In the models analysed, the differences in the models have been mainly due to the source of the material properties, with different sources using different testing techniques to define the material properties of different components.

2.3.1 Crystalline Lens

As discussed in Section 2.2.2 three methods have been adopted to represent the internal structure of the lens; as being homogenous, having a nucleus and cortex and as having a stiffness gradient. These geometric representations dictate how the material properties are distributed through the lens and are often adopted due to the data source used.

The first major study into the material properties of the lens was by Fisher (1971) (Source A in Table 2.3) who conducted spinning lens tests to establish the Young's modulus of the nucleus and cortex. Spinning individual lenses resulted in changes in the axial thickness and equatorial diameter; these changes were used to infer the Young's modulus of the nucleus and cortex. The study gave age related results, showing that the nucleus had a lower Young's modulus than the cortex in a young lens, but with an older lens this reduced. These properties were adopted by a range of authors as the basis of their accommodation models (see Table 2.3). The study of Fisher (1971) has since been shown to have a number of inaccuracies due to oversimplification (Burd *et al.*, 2006), leading to an improved version (Burd *et al.*, 2011) which will be

Table 2.3: Summary of the different sources of material properties used in the literature. Key to letters: A Fisher (1971), B Subbaram *et al.* (2002), C Weeber *et al.* (2007), D Heys *et al.* (2004), E Van Alphen & Graebel (1991), F Wilde *et al.* (2012), G Fisher (1969), H Krag & Andreassen (2003a), I Fisher (1986). A hyphen indicates that there was no data available or the component was not modelled.

Study	Source of Material Properties		
	Lens	Capsule	Zonules
Schachar & Bax (2001b)	-	G,H	-
Burd <i>et al.</i> (2002)	A	G	I,E
Breitenfeld <i>et al.</i> (2005)	A	G	I,E
Liu <i>et al.</i> (2005)	A	G	-
Martin <i>et al.</i> (2005)	A	G	I,E
Hermans <i>et al.</i> (2006)	A	G	-
Liu <i>et al.</i> (2006)	A	G	-
Abolmaali <i>et al.</i> (2007)	B,D	G,H	E
Belaidi & Pierscionek (2007)	A	G	-
Weeber & van der Heijde (2007)	A,C	G	E
Hermans <i>et al.</i> (2008)	A,C,D	G	-
Ljubimova <i>et al.</i> (2008)	A,D	G	E
Weeber & van der Heijde (2008)	C	G	E
Van de Sompel <i>et al.</i> (2010)	A,B,D,E	G	-
Riehemann <i>et al.</i> (2011)	C	-	-
Wilde (2011)	F	G,H	I,E
Lanchares <i>et al.</i> (2012)	A	G	-

discussed in Chapter 4.

Subbaram *et al.* (2002) (Source B in Table 2.3) also measured the material properties of the nucleus and cortex, although in this case Brillouin light scattering was used to establish the Bulk modulus. The Bulk modulus cannot be used alone in modelling the mechanics of a material, therefore, where this was used, another source was needed to give the shear modulus, which could be combined with the bulk modulus to define the elastic modulus. In the studies that used the Bulk modulus data of Subbaram *et al.* (2002), the shear modulus values given by Heys *et al.* (2004) were used to calculate the elastic modulus of the nucleus and cortex.

As an alternative to assuming that the lens can be separated into a nucleus and cortex, some studies measured the stiffness across the lens. The first of these studies was Heys *et al.* (2004) (Source D in Table 2.3) where a controlled force indentation test was used to measure the Shear modulus of sectioned lenses. Measurements were taken of the shear modulus across the lens sections with the results indicating that the nucleus was less stiff than the cortex in a young lens, but by 40 YO this reverses (see Figure 2.4).

A similar test was run by Weeber *et al.* (2007) (Source C in Table 2.3) where an indenter was inserted into lens sections and then oscillated to obtain a dynamic response. This test produced a shear modulus

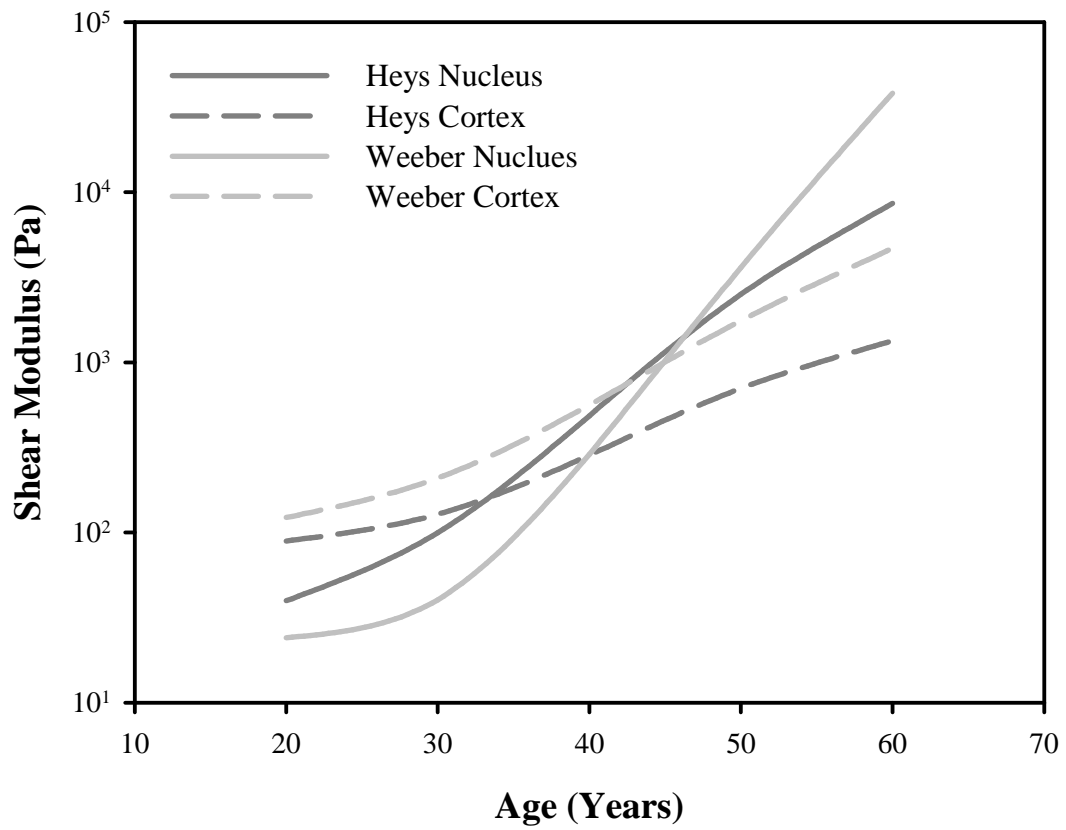


Figure 2.4: Comparison between Heys *et al.* (2004) and Weeber *et al.* (2007) stiffness variation for a 30YO lens.

value at different locations across the lens, showing a similar trend to the results of Heys *et al.* (2004) (see Figure 2.4).

A more recent study was conducted by Wilde *et al.* (2012) (Source F in Table 2.3), using an updated and improved lens spinning test on de-capsulated lenses. Inverse FEA modelling was used to establish the values of shear modulus that caused the FEA lens to deform as much as the lenses in the test rig. Different stiffness distributions were tested, but the overall trend followed that of Heys *et al.* (2004) and Weeber *et al.* (2007).

As discussed, the method the author employs to define the material behaviour dictates the material properties that can be used. Each of these sources give the data in terms of the shear modulus, which can only be inputted as a value under certain assumptions in an FEA model. Typically, the lens regions were modelled as being linear elastic, isotropic materials, which requires the input of the elastic modulus and Poisson's ratio. To obtain the elastic modulus from the shear modulus values, authors have assumed that the materials are homogenous and isotropic. This means that the following relationships apply between

the elastic constants:

$$E = 2G(1 + \nu) = 3K(1 - 2\nu) \quad (2.1)$$

Where E is the elastic modulus, G is the shear modulus, K is bulk modulus and ν is the Poisson's ratio. Typically, the Poisson's ratio has been defined as nearly 0.5 (e.g. Burd *et al.* (2002) used 0.49 whilst Abolmaali *et al.* (2007) used 0.49999999), which is due to the assumed incompressibility of the lens.

However, some authors (Wilde, 2011; Lanchares *et al.*, 2012) have assumed that the components are hyper-elastic (See Chapter 4), meaning that the shear modulus values can be inputted. For these materials, the bulk modulus is also required, rather than the Poisson's ratio. Wilde (2011) defined the bulk modulus as being 1000 times greater than the shear modulus to ensure incompressibility was accounted for. Lanchares *et al.* (2012) used the data of Fisher (1971) but did not specify how the bulk modulus was calculated.

2.3.2 Capsule

In the FEA models analysed, two studies have been used for the capsule material properties (see Table 2.3), both of which tested capsules *in vitro* separated from the lens. The earliest was by Fisher (1969) (denoted source G in Table 2.3) where a section of the anterior capsule was tested by inflating it with a fluid pressure. This allowed the relationship between pressure and volume to be recorded which allowed the calculation of the Young's modulus of the capsule. Additional tests were carried out to establish the Poisson's ratio.

More recently, Krag *et al.* (1997) and Krag & Andreassen (2003b) (Denoted source H in Table 2.3) carried out tests on rings of capsular samples. The samples were stretched by two supports at a constant speed until rupture, allowing load vs strain graphs to be plotted which were used to calculate the elastic stiffness. The results showed that the capsule behaved in a non-linear fashion.

As with the lens most studies represented the capsule as a linear elastic isotropic material using the material properties from the sources given, combined with a Poisson's ratio of 0.47 as defined by Fisher (1969). However, Wilde (2011) used a constitutive model derived by Burd (2009) to model the material properties of the capsule, although the Young's modulus was the base property used. The Young's modulus was adapted from the studies of Fisher (1969) and Krag & Andreassen (2003a), but to be able to use both sources an in plane Poisson's ratio was found.

Lanchares *et al.* (2012) represented the capsule with an anisotropic hyper-elastic constitutive model, similar to the one used for the lens substance, but with additional properties to define the behaviour of the capsule in the preferential direction of deformation. Again, the study of Krag & Andreassen (2003a) was used to provide the data, but the method of adapting the data was not given.

2.3.3 Zonules

In the FEA models analysed, two studies have been directly referenced for the zonule elastic modulus: Fisher (1986) (denoted source I in Table 2.3) and Van Alphen & Graebel (1991) (denoted source E in Table 2.3). Both papers provide data on the elastic modulus of the zonular fibres, Fisher reported a value of 0.35 N/mm^2 , whilst Van Alphen reported a value of 1.5 N/mm^2 , although different methods were used to establish these values (see Chapter 4).

However, some authors have not used the data, instead due to the zonular modelling method used, they have derived a stiffness value suitable for their own studies. Burd *et al.* (2002) developed a model where each zonule bundle (anterior, equatorial and posterior) was represented by a thin sheet of material with zero circumferential stiffness. The thickness of these sheets was set in a ratio, then a preliminary FEA model was run where the stiffness of the sheets was varied until the equatorial displacement of the lens model matched the displacement measured by Strenk *et al.* (1999); these stiffness values were then used in the subsequent models. The process was later adapted by Breitenfeld *et al.* (2005) and Wilde (2011). Liu *et al.* (2005) proposed an alternate version where the zonules could be modelled as springs, with each zonular group assigned a separate spring stiffness, based on data from Fisher (1977) and Rao & Wang (2002).

2.3.4 Summary of material properties

The lack of data on the material properties of the components of the accommodation system has led to a number of simplifications and assumptions in early FEA models. However, more recent studies have been able to utilise more comprehensive data, in particular on the stiffness gradients within the lens, which will need to be an essential feature of any future models. Future models will ideally incorporate the non-linear behaviour of both the lens and capsule, and if possible, investigate whether incorporating anisotropy is possible.

A decision will need to be made on how the zonules are represented, as there is a paucity of data on both

structure and material properties. Similar to the steps taken hitherto, methods of adapting existing material data to new zonular representations may need to be investigated.

2.4 FEA Procedure

After defining the geometry and material properties the next stage is to define the boundary conditions and load steps that will be used to simulate accommodation. The boundary conditions include the restraints that will hold the lens in place as well as the loads that will be applied. Due to variations in aims and modelling methods used in previous studies, a number of models were created which are defined in Table 2.4 (Page 70).

2.4.1 Models analysed

The models created in each study depend on the aims of the study as well as the accommodative theory being followed (Table 2.1). Here, the models will be discussed in terms of age and starting shape. The standard method of deciding the starting shape was to model the lens in its most stress free state, which will be different depending on the accommodative theory followed. If the Helmholtz theory was followed, the lens was assumed to be stress free in its accommodated form. If the Schachar theory was followed, the lens was assumed to be in its lowest stress state in its relaxed, un-accommodated form (Chapter 1).

Some studies investigated the causes of presbyopia, which required modelling lenses of different ages, typically a young (≈ 20 YO), middle aged (≈ 45 YO) and old lens (≈ 60 YO). The geometric method chosen needed to be able to accurately model the lens at these ages which has been the case in the majority of studies, although some studies were limited to set ages (e.g. those based on Burd *et al.*, 2002) limiting their range. Abolmaali *et al.* (2007) produced an idealised lens to represent a young lens using the Chien *et al.* (2003) mathematical description, based on assumed geometrical data for a young lens. The resulting lens is shown in Figure 2.5 and it appears to be an inaccurate model of the lens, in particular compared to the other lens models used in the same study which were of the form illustrated in Figure 2.1.

Some authors have analysed more than just the deformations in different ages. Breitenfeld *et al.* (2005) analysed the differences between a normal lens and a lens altered to represent changes that could be made with laser treatment (see Section 1.3.3.3), an approach later followed by Wilde (2011). Both studies

Table 2.4: Summary of the models and procedures used in previous studies. Starting lens shape key: U = Un-accommodated lens, A = Accommodated lens. Deformation method Key: A = Zonule displacement, B = Vitreous Pressure, C = Force application, D = Sensitivity study.

Study	Starting Lens Shape	Model Ages (Years)	Deformation Method	Additional Information
Schachar & Bax (2001b)	U, A	19, 29	A	-
Burd <i>et al.</i> (2002)	A	11, 29, 45	A	-
Breitenfeld <i>et al.</i> (2005)	A	29	A	One model with fs-laser cuts
Liu <i>et al.</i> (2005)	A	45	A	-
Martin <i>et al.</i> (2005)	A	6, 29, 45	A, B	Vitreous pressure included on some models
Hermans <i>et al.</i> (2006)	A	29	C	3 zonular force methods
Liu <i>et al.</i> (2006)	A	45	A, B	3 zonular arrangements used
Abolmaali <i>et al.</i> (2007)	U	45	D	Additional idealised lens model used
Belaidi & Pierscionek (2007)	A	27, 46	A	-
Weeber & van der Heijde (2007)	A	20, 40, 60	A	Although three ages were modelled, only the geometry of a 40 YO lens was used
Hermans <i>et al.</i> (2008)	A	11, 29, 45	C	-
Ljubimova <i>et al.</i> (2008)	A	29	A, B	-
Weeber & van der Heijde (2008)	A	20, 40, 60	A	Although three ages were modelled, only the geometry of a 40 YO lens was used
Van de Sompel <i>et al.</i> (2010)	A	29, 45	A	45 YO lens tested with modified material and geometric properties
Riehemann <i>et al.</i> (2011)	A	45	A	Stiffness of lens varied to simulate presbyopia, optical modelling using ray tracing performed
Wilde (2011)	A	29, 45	A	Additional models with fs-laser cuts
Lanchares <i>et al.</i> (2012)	A	30, 40, 50	C	-

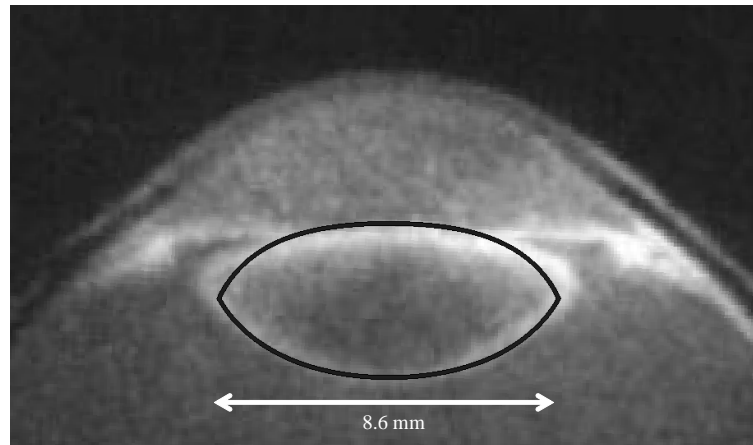


Figure 2.5: The idealised lens profile used by Abolmaali *et al.* (2007) (Black outline), the profile shape can be seen to be an inaccurate representation of the lens when compared to an MRI image of the relaxed lens (Adapted from Figure 1 of Strenk *et al.*, 1999), principally due to the sharp point at the equator.

created areas within the lens with altered material properties to represent the changes that would occur after laser surgery.

A different approach is to analyse what effects various lens parameters have on the deformations that occur. Abolmaali *et al.* (2007) carried out a sensitivity study, varying a number of lens parameters sequentially whilst the remaining parameters remained at a baseline value, to see what effects they would have on overall lens deformation. Van de Sompel *et al.* (2010) and Wilde (2011) performed a similar analysis, although restricted to adjusting the material properties. Martin *et al.* (2005) and Liu *et al.* (2006) introduced vitreous pressure in some models to study the effects on deformations, whilst Liu *et al.* (2005) and Hermans *et al.* (2006) tested different zonular arrangements.

2.4.1.1 Boundary conditions

The boundary conditions of an FEA model describe the loads (forces or displacements applied to the components) and restraints (restrictions to the degrees of freedom of the components). Hitherto, there have been two methods of applying loads to the accommodation models; displacements to the ciliary body or forces applied to the lens capsule.

For those models that apply a displacement, the only load required is on the representation of the ciliary body. The displacement value used typically comes from the data of Strenk *et al.* (1999). For those models using force application directly on the capsule, the amount of force required to deform the lens is usually defined within the study. Hermans *et al.* (2006) purpose was to estimate the amount of force required to deform the lens with an iterative process, varying the force until the deformations matched expectations.

Belaidi & Pierscionek (2007) and Lanchares *et al.* (2012) ran initial models to establish the force required, before those force values were used in further models to meet the aims of the study.

In those studies where the vitreous was included, a further load was required to simulate the pressure, with differing methods of application used, from a single value (e.g. Liu *et al.*, 2006) to a varying pressure along the posterior surface (e.g. Martin *et al.*, 2005).

The constraints of a model are required to ensure that there is no excess movement of the system. In an axi-symmetric model, the central axis cannot move radially, but can still move vertically. It was not clear in all studies how each model was constrained, but where specifications were given, it appears a typical restraint was to restrict ciliary body movement to only radial movement (e.g. Lanchares *et al.*, 2012). It was specified in a number of studies that axial movement of the lens was restricted, but not detailed how it was achieved (e.g. Liu *et al.*, 2005 and Hermans *et al.*, 2006).

2.4.2 Verification of results

Being able to produce a model that deforms suitably visually is not enough, the changes that occur need to be analysed so that meaningful results can be obtained. One method of doing this is to compare key parameters of the model to measured parameters from studies *in vivo*. The methods hitherto have either based the verification on comparing to power changes within the lens or to changes in lens parameters, such as the thickness or curvature change.

The most common method has been in comparing to measured power changes of the eye, using the thick lens formula to calculate the power change in the FEA model (Equation 2.2).

$$OpticalPower = \frac{(n_l - n_a)}{r_a} + \frac{(n_l - n_a)}{r_p} - \frac{t(n_l - n_a)^2}{r_a r_p n_l} \quad (2.2)$$

where n_l is the refractive index of the lens, n_a is the refractive index of the aqueous and vitreous, r_a is the radius of curvature of anterior surface, r_p is the radius of curvature of posterior surface and t is the axial thickness of the lens. The lens thickness and curvature values can be easily extracted from the FEA models, allowing the power before and after deformation to be calculated. Using the thick lens formula simplifies the optical calculation by attributing a single refractive index to the lens. As discussed in Chapter 1 there is actually a gradient refractive index within the lens. To factor this in some authors

have instead used ray tracing to calculate the power change. Ray tracing involves computing the path of individual light rays through an optical system. It can take into account a gradient refractive index as well as more complex shapes, rather than two surface curvatures. The first use in an accommodation model was by Breitenfeld *et al.* (2005) who used a linear Gaussian beam ray trace, although the refractive index used was not specified. Van de Sompel *et al.* (2010) performed ray tracing using a parabolic representation of the gradient refractive index layers. Riehemann *et al.* (2011) used a commercial ray tracing package and used the deformed FEA lens profiles representing stages of dis-accommodation as part of a model eye. An equivalent refractive index was incorporated, which used a different refractive index value for each state of dis-accommodation across the whole lens, rather than separating it into refractive index layers.

The alternative method for verifying results is to compare individual parameters to measured values, for example, Burd *et al.* (2002) simply compared the equatorial displacement of the lens to the expected value as defined by Strenk *et al.* (1999) in establishing a suitable zonular deformation value. However, a more comprehensive method was established by Hermans *et al.* (2006), where a cost function was used to compare multiple values at a time. A number of parameters were selected for comparison and each of these parameters from the deformed model was given a squared error, these errors were added up into the cost function, then the inputted forces that resulted in the lowest cost function were deemed to be the most accurate force estimation.

2.5 Results

The results of the studies are related to the individual aims, as shown in Table 2.1 (Page 52). These results can be analysed in terms of the accommodative theory supported, the magnitude of the zonular forces, what the causes of presbyopia are attributed to and what potential changes can be made to the lens to treat or prevent presbyopia. A few studies were simply used to establish whether a proposed model would be suitable for modelling the accommodation system (e.g. Burd *et al.*, 2002; Ljubimova *et al.*, 2008). In each case, it was declared a suitable method, although there was a general agreement that there was a lack of data on many aspects of the accommodative system

2.5.1 Accommodation

Broadly the various studies results fall into two categories, those that support the Helmholtz theory of accommodation, and those that support the Schachar theory. For the former studies, the results show that

after instigating the zonular traction the lens will decrease in power due to thickness decreasing and the anterior and posterior curvature changing (e.g. Burd *et al.*, 2002; Hermans *et al.*, 2006; Wilde, 2011). In the latter studies the results showed that increased zonular displacement resulted in a power increase (e.g. Liu *et al.*, 2005; Abolmaali *et al.*, 2007). When analysing these results, the starting lens shape needs to be considered due to the differences between accommodative theories.

Liu *et al.* (2005) used the same geometric model as Burd *et al.* (2002), but found that displacement of the ciliary body point resulted in an increase in power, rather than a decrease. The results show the thickness of the lens decreases as with Burd *et al.* (2002), however, the anterior curvature increases and the posterior decreases compared to an anterior and posterior decrease with Burd *et al.* (2002). The two studies measured the curvature across different radii, with Burd *et al.* (2002) measuring the curvature up to 0.8 mm from the axis and Liu up to 0.6 mm, which could have an effect on results. Liu *et al.* (2006) used the same model again, but this time found that there was a decrease in power when using the same set up as Burd *et al.* (2002). However, when using three ciliary body attachments for the zonules, the results supported Schachar's theory with the model showing an increase in thickness and power, albeit a small increase. The curvature changes of this model match the results of Burd *et al.* (2002) but show a decrease in curvature of both surfaces.

It is interesting to note where deformations as a result of zonular traction deviate from the typical results. Abolmaali *et al.* (2007) modelled a number of lens arrangements finding that all set ups had an increase in optical power with zonular displacement, regardless of whether the lens model was set up to represent Helmholtz or Schachar. However, when looking at the thickness changes only when the model was set up with a single equatorial zonule did the thickness increase, for all other arrangements the thickness decreased, which usually indicates a decrease in power (e.g. Burd *et al.*, 2002). The changes in curvature were not given for these models so a definite answer cannot be given. Curvature changes and thickness changes were given for the idealised lens model that was used, which supported the theory of Schachar, however as shown in Figure 2.5 this is an unrealistic representation of the lens, so results using this need to be treated with caution.

Belaidi & Pierscionek (2007) found support for both theories; the difference in which theory was supported was down to the age of the lens (which affected the starting shape), the amount of zonular force applied and the stiffness distribution. For young lenses the results typically supported Schachar, other than a young homogenous lens with a high force which showed support for Helmholtz. Older lenses in any configuration showed support for Helmholtz.

Martin *et al.* (2005) compared the Helmholtz and Coleman theories by utilising pressure application on the lens to simulate the vitreous. The results showed that the Coleman theory would not produce the required power changes, however, it was not clear exactly how the models with pressure were simulated. It appears from the supporting figures that the model with the pressure applied started in the deformed shape, which would mean that any further deformations would not be able to produce high enough power changes. Therefore, the results need careful consideration.

2.5.2 Zonular forces

A number of studies have investigated the amount of zonular force needed to achieve the required shape and power changes during accommodation. With a force established, comparisons could be made to *in vitro* studies that have been carried out (e.g. Fisher, 1977; Manns *et al.*, 2007; Michael *et al.*, 2012).

Fisher (1977) proposed that the force applied by the zonule was close to 0.01 N with very little change with age, which was similar to Michael *et al.* (2012). Manns *et al.* (2007) found that the force ranged from 0.008 N/D in a young eye to 0.02 N/D in an old eye. In those studies that measured the force applied by the zonules, the force was found to be higher with Burd *et al.* (2002) calculating the force to be the highest (0.08 N - 0.1 N), Hermans *et al.* (2008) the lowest (0.03 N to 0.06 N) and Hermans *et al.* (2006) and Lanchares *et al.* (2012) inbetween.

2.5.3 Presbyopia

A number of studies have investigated what changes with age in the accommodative components contribute to the development of presbyopia, typically through multiple age models but also by varying a few key parameters. Abolmaali *et al.* (2007) used the latter method, varying key parameters above and below a baseline value to see the effect on power change. From this analysis the development of presbyopia was given as the decline in the maximum amount of force that could be applied by the zonules. However, the results of the study also showed that an increase in lens stiffness would also cause the required decrease in optical power with age; this was not supported as a potential cause of presbyopia by the authors due to a lack of data showing suitable stiffness changes in a young eye to account for a 10 D decrease in accommodative ability by 40 years of age (see Figure 1.13).

Weeber & van der Heijde (2007) proposed that the change in stiffness gradient was the cause of accommodative decline compared to previous accommodative amplitude studies (such as those illustrated in

Figure 1.13), although a constant shape lens outline was used (equivalent to a 40 YO lens) combined with a consistent zonule arrangement, with only the stiffness and zonule displacement altered, so these factors need to be considered. An additional model was run analysing the effect of increased lens stiffness (60 YO) when the zonule displacement was increased to cause the equatorial displacement to match that of a young lens (20 YO). It was found that the surface curvatures did not change, which was attributed to the material in the cortex sliding over the stiff nucleus. This was explored further in a later study (Weeber & van der Heijde, 2008), where it was found that the strain in the nucleus was high in young lenses, but low in old lenses. This was due to the deformations only occurring in the equatorial region of the cortex in older lenses, not affecting the surface curvatures and therefore power.

Hermans *et al.* (2008) found that the force that can be applied to the lens was consistent with age, or may even increase slightly with age. This indicates that the cause for the accommodative decline is lenticular as the amount of force remains consistent, but the amplitude still reduces.

Van de Sompel *et al.* (2010) investigated the importance of the mechanical properties and geometry of the lens in accommodation. It was found that modifying the geometry of an older (45 YO) lens led to an increase in power change during accommodation; the altered model used the 29 YO lens shape with the 45 YO material properties. When the material properties were modified, using the 45 YO lens shape with 29 YO material properties, there was little improvement in power change indicating that the geometry of the lens was key in the development of presbyopia. It was not specified if the capsule properties were altered, but the indications were that the capsule was not altered.

Lanchares *et al.* (2012) investigated the stiffness values that were required so that a 40 and 50 YO lens would match the required lens deformations when a constant zonular force was applied. It was found that the required stiffness increased with age, supporting the theory that stiffness increase in the lens is the cause for presbyopia.

As part of the study into lens deformation Wilde (2011) simulated two models with mixed properties, one with a 29 YO shape but 45 YO mechanical properties and the other with the opposite. It was found that the decline in power change could be attributed to the change in stiffness parameters alone. However, the capsule thickness was the same in both age models, which could have had an impact on the deformations induced.

2.5.3.1 Presbyopia treatments

One area of FEA modelling which is of interest in future models is the replication of surgical techniques to try to improve the accommodative ability of the eye (see Section 1.3.3). In the literature, there have been only a couple of models that have investigated any of these techniques.

The first was by Breitenfeld *et al.* (2005) who modelled a simple representation of a lens with femtosecond laser microcuts. The model with these cuts offered a slight improvement over a normal lens model. A more in depth analysis was carried out by Wilde (2011), where three different cutting patterns were tested. A model using radial cuts was seen to give the most benefit, but again the improvement was slight over a normal lens.

2.6 Areas for Improvement

From analysing the current state of FEA modelling of the accommodative system there are a number of areas for development:

In terms of geometric and material modelling the latest data needs to be utilised, as there has been an over reliance on data that has been shown to be inaccurate (e.g. Fisher, 1971 material properties, Burd *et al.*, 2002 lens model) in previous studies. Any models developed need to be adaptable so that multiple scenarios can be examined, which will require the modelling methods to be able to replicate different ages of lens as well as accommodated and relaxed versions of the components modelled. The material properties need to reflect the complexity of the components, utilising more complex constitutive equations than simple linear elastic isotropic representations. In addition, methods of representing the more complex stiffness distribution within the lens combined with replication of the age related changes will be required. Finally, attempts need to be made to improve on the current zonular modelling methods to allow for a more accurate representation of the changes that occur with accommodation. Incorporating these improvements will allow for a thorough investigation of accommodation and presbyopia development to be conducted, in particular, how the relationship between the accommodative components changes with age.

Chapter 3

Geometry

3.1 Introduction

When modelling a structure using FEA, each component of the structure requires a defined geometry. To establish what data there are available to produce the geometric descriptions of the accommodative system components the existing data sources need to be analysed (Section 3.2), before the proposed modelling methods for the lens (Section 3.3), capsule (Section 3.4) and zonules (Section 3.5) will be detailed.

For clarity accommodation refers to the crystalline lens changing from its relaxed (low power, distance vision), or un-accommodated, state to its accommodated (high power, near vision) state. Dis-accommodation is the reverse.

3.2 Measured Data

A wide range of measurements have been established for the different components using a range of different methods. Before analysing the different measurements of the individual components, the different imaging methods will be summarised. The measurements will be split into *in vivo* and *in vitro* measurements and where possible, relaxed and accommodated states; with any appropriate age related changes detailed.

3.2.1 Imaging Methods

Table 3.1 (Page 80) gives an overview of the principal methods of measurement along with what each can measure and any common errors that can occur.

A number of these methods have been used to measure geometric parameters in the accommodated state (see Tables 3.2 to 3.7). If the accommodative ability of patients was not recorded and it was only assumed that patients were able to accommodate to the targets used, measurement inaccuracies could occur due to over or underestimations of the accommodative ability, which needs to be considered when looking at accommodative changes.

3.2.2 Crystalline lens measurements

The crystalline lens is the key component of the accommodation system due to the shape changes it can undergo. The key features of the lens that need to be modelled are the thickness, diameter and surface curvatures, all of which need to be adapted for accommodated and relaxed *in vivo* lens models. The internal lenticular structure also needs to be modelled so that the material properties can be distributed accurately.

3.2.2.1 Thickness

Table 3.2 (Page 81) gives an overview of the main measurements of the lens thickness, covering some of the historic data used in FEA studies, such as Brown (1973), as well as more recent data (Sheppard *et al.*, 2011).

It is clear that there is an increase in thickness in the relaxed state of approximately 0.02 mm per year. With accommodation, an increase is seen of approximately 0.05 mm per dioptre of accommodation, although this increase does appear to reduce with age by approximately 0.5 μm per year (Dubbelman *et al.*, 2005).

For measurements made *in vitro* the lens is free of any external forces which could represent the lens in its accommodated state, if the Helmholtz theory is followed (Dubbelman *et al.*, 2005). The data does suggest this, with measurements *in vitro* showing a larger thickness than *in vivo* measurements, and an increase in thickness with age. The influence of the capsule may cause the lens to form a more spherical shape than what can be formed *in vivo*, which will be discussed in Section 3.2.2.2.

Internal thickness changes

Further detail can be found when analysing the thickness changes internally rather than as an overall change. As discussed in Section 1.2.3.1 the lens is formed of a number of layers which are a result of the layering of fibres through life. Dubbelman *et al.* (2003) measured the thickness of the internal layers using

Table 3.1: Summary of the main imaging methods used in measuring accommodative components, giving detail on measurements available as well as any potential errors.

Imaging Method	Measureable parameters	Method	Principal Use	Errors
Scheimpflug Photography	Cornea (Thickness, curvature), Anterior Chamber depth, Lens (Thickness, curvature) – Only central portion of lens measurable	Slit lamp beam used with a perpendicular camera, imaging the optic section produced	<i>In vivo</i>	Two types of distortion, the first due to the tilt of the camera, the second due to imaging through multiple optical surfaces (Dubbelman et al. 2005)
Magnetic Resonance Imaging (MRI)	Whole lens	Magnetic field used to alter the nuclear spins of protons within tissues, these can then be visualised	<i>In vivo</i>	No optical distortions. Artefacts can arise from subject eye movements
Ultrasound	Lens thickness, Anterior Chamber depth (A-Scan), Ciliary muscle (B-scan)	Acoustic pulses used to generate reflections from the measurable components.	<i>In vivo</i>	
Shadowphotogrammetry	Whole lens	Shadow projected from lens onto a screen for measurement Laser light sources used to generate positive interference, can be combined into 2-dimensional cross sections.	<i>In vitro</i>	In vitro measurements
Optical coherence tomography (OCT)	Cornea, Lens, ciliary muscle	Reflections of light from the different optical surfaces allow calculation of geometric parameters	<i>In vivo</i>	Distortion due to light passing through optical surfaces
Ophthalmometry (Purkinje images)	Lens curvatures		<i>In vivo</i>	Subject eye movement

Table 3.2: Summary of crystalline lens thickness measurements. Age related changes are given where possible, otherwise values are the mean value found. * indicates change per dioptre of accommodative response, A = Age.

	Study	Imaging Method	Number of eyes	Age (Years)	Lens Thickness (mm)
<i>In vivo</i> Relaxed	Brown (1973)	Photography	4	11 - 43	3.95 - 4.66
	Strenk <i>et al.</i> (1999)	MRI	25	22 - 83	2.9276 + 0.0238A
	Dubbelman <i>et al.</i> (2001)	Schiempflug	90	16 - 65	0.93 + 0.024A
	Kirschkamp <i>et al.</i> (2004)	Ultrasonography	9	20 - 38	3.7
	Koretz <i>et al.</i> (2004)	Schiempflug	62	18 - 50	3.088 + 0.0194A
	Fea <i>et al.</i> (2005)	MRI	25	18 - 50	2.944 + 0.0193A
	Jones <i>et al.</i> (2007)	MRI	88	20 - 79	4.23
	Jones <i>et al.</i> (2007)	MRI	44	18 - 59	3.31 + 0.0180A
	Atchison <i>et al.</i> (2008)	Ultrasonography	102	18 - 69	3.1267 + 0.02364A
	Richdale <i>et al.</i> (2008)	OCT	22	36 - 50	3.14 + 0.021A
	Hermans <i>et al.</i> (2009)	MRI	5	18 - 35	3.66
	Hermans <i>et al.</i> (2009)	Schiempflug	5	18 - 35	3.684
	Kasthurirangan <i>et al.</i> (2011)	MRI	15	19 - 29	3.69
	Kasthurirangan <i>et al.</i> (2011)	MRI	15	60 - 70	4.66
	Sheppard <i>et al.</i> (2011)	MRI	19	19 - 30	3.75
	Richdale <i>et al.</i> (2013)	MRI	26	30 - 50	3.68 + 0.027A
	<i>In vivo</i> Accommodated	Brown (1973)	Photography	4	11 - 43
Koretz <i>et al.</i> (1997)		Schiempflug	82	18 - 70	0.043*
Strenk <i>et al.</i> (1999)		MRI	25	22 - 83	3.5955 + 0.0144A
Kirschkamp <i>et al.</i> (2004)		Ultrasonography	9	20 - 38	3.9
Dubbelman <i>et al.</i> (2005)		Schiempflug	65	16 - 51	0.058 - 0.0005A*
Jones <i>et al.</i> (2007)		MRI	26	18 - 33	0.05*
Richdale <i>et al.</i> (2008)		OCT	22	36 - 50	0.051*
Hermans <i>et al.</i> (2009)		MRI	5	18 - 35	0.061*
Hermans <i>et al.</i> (2009)		Schiempflug	5	18 - 35	0.045*
Sheppard <i>et al.</i> (2011)		MRI	19	19 - 30	0.08*
Kasthurirangan <i>et al.</i> (2011)		MRI	15	19 - 29	4.02
Richdale <i>et al.</i> (2013)		MRI	26	30 - 50	0.065*
Moffat <i>et al.</i> (2002a)		MRI	18	14 - 82	4.9 + 0.181A
Jones <i>et al.</i> (2005)		Scanning laser	20	7 - 82	4.87 + 0.00326A
Schachar (2005)		MRI	20	7 - 82	4.77 + 0.00477A
Rosen <i>et al.</i> (2006)		Photography	41	3 - 58	4.3817 - 0.1024A + 0.0032A ² - 0.00002A ³
Rosen <i>et al.</i> (2006)		Shadowphotogrammetry	37	20 - 99	3.97 + 0.0123A
<i>In vitro</i>					

densitometry on Scheimpflug photography, using the Oxford method of distinguishing the layers (Sparrow *et al.*, 1986). It was found that the cortex region increases with age seven times more than the nucleus region, with the anterior part of the cortex increasing in thickness 1.5 times more than the posterior region. However, parts of the cortex region did not show any changes at all, with all the changes in thickness with age coming in the C2 region (illustrated in Chapter 5).

In vitro Glasser & Campbell (1999) measured the increase in thickness in the anterior and posterior portions of the lens, finding that the anterior portion increases slightly with age. The posterior thickness was more stable and the ratio between anterior and posterior thickness remained stable at approximately 0.7. Rosen *et al.* (2006) found a similar ratio between the anterior and posterior axial thicknesses (0.7), which remained constant with age; however, the posterior thickness also appeared to increase in thickness quicker than the anterior. Glasser & Campbell (1999) showed that the capsule had an impact on measurement, as when the capsule was removed both the anterior and posterior portions of the lens showed larger increases with age.

With accommodation, the thickness increase of the lens was primarily attributed to changes in the nucleus region. Although there was evidence that there may be a slight decrease in cortical thickness, typically, there appeared to be no change (Dubbelman *et al.*, 2003).

The differences between anterior and posterior portions of the lens can be seen in surface curvature and volume changes, as will be discussed in Section 3.2.2.3 and Section 3.2.2.5.

3.2.2.2 Diameter

In vivo the diameter of the lens (Table 3.3, page 84) has been shown to remain stable (Jones *et al.*, 2007; Richdale *et al.*, 2013), decrease (Strenk *et al.*, 1999) and increase (Kasthurirangan *et al.*, 2011) in the relaxed state with age. The variation in these measurements could be indicative of measurement problems, such as MRI resolution. The way the lens fibres are laid down, where the fibres move from the anterior of the lens and differentiate at the equator (Section 1.2.3.2), would suggest that the lens diameter would increase with age.

In vitro studies were consistent in showing an increase in diameter with age, which would appear to match what is expected. The issue with *in vitro* measurement, as discussed in section Section 3.2.2.2, is that the lens is free of any external force. As a result of this, the capsule may cause the lens to form an artificially spherical shape, which it could not form *in vivo*. The measurements *in vitro* do appear to show

consistently lower diameter values than measurements from MRI of accommodated lens diameters, which would support this theory. Further support for this theory would be that the lens changes dimensions if the capsule is removed; Fisher (1971) found very little change in dimensions when the capsule was removed from lenses, whereas Glasser *et al.* (2001) showed that with the capsule removed from *in vitro* lenses there was an increase in diameter, although this increase reduced with age. Careful consideration of diameter measurements is therefore needed.

In vivo measurements of accommodated lens diameters were more consistent with the majority of studies showing that the lens decreased in diameter with accommodative demand (e.g. Richdale *et al.* (2013)), although the study of Schachar *et al.* (1996) found the opposite, but accommodation was pharmacologically induced which could produce errors.

3.2.2.3 Surface curvature

The surface curvatures contribute to the power changes that occur in the eye and vary between anterior and posterior surfaces (Table 3.4 and Table 3.5, pages 85 and 86). From *in vivo* measurements, there was general agreement that the curvature decreases with age, becoming more spherical. With accommodation, the anterior curvature also decreases.

For the posterior surface there was more debate. With age, it has been shown that the posterior curvature decreases (Dubbelman & Van der Heijde, 2001), increases (Koretz *et al.*, 2004; Kasthurirangan *et al.*, 2011) and has no change (Atchison *et al.*, 2008; Richdale *et al.*, 2013). With accommodation, there has been more agreement that the posterior surface curvature decreases and becomes more spherical.

In vitro studies show the surfaces appear to be much more curved, which can be attributed to the lens being outside the influence of the zonules, as discussed previously (Section 3.2.2.2).

3.2.2.4 Anterior Chamber Depth

The anterior chamber depth (ACD) (distance between the cornea and crystalline lens) provides a key indicator on whether there is any anterior or posterior movement of the lens with age or accommodation. Table 3.6 (Page 88) gives an overview of the measurements made and it shows that with age there was agreement that the ACD decreases.

However, there was disagreement on the movement of the posterior pole with both age and accommodation. The change in ACD describes the movement of the anterior surface but combined with data on the

Table 3.3: Summary of crystalline lens diameter measurements. *indicates changes per dioptre otherwise measurements are the mean values found. A = Age.

	Study	Imaging Method	Number of eyes	Age (Years)	Equatorial Diameter (mm)
<i>In vivo</i> Relaxed	Strenk <i>et al.</i> (1999)	MRI	25	22 - 83	9.3609 - 0.0047A
	Fea <i>et al.</i> (2005)	MRI	88	20 - 79	9.43
	Jones <i>et al.</i> (2007)	MRI	44	18 - 59	9.33
	Atchison <i>et al.</i> (2008)	MRI	15	18 - 29	9.03
		MRI	15	60 - 69	9.31
	Hermans <i>et al.</i> (2009)	MRI	5	18 - 35	9.58
	Kasthurirangan <i>et al.</i> (2011)	MRI	15	19 - 29	9.03
		MRI	15	60 - 70	9.31
	Sheppard <i>et al.</i> (2011)	MRI	19	19 - 30	9.49
	Richdale <i>et al.</i> (2013)	MRI	26	30 - 50	9.42
<i>In vivo</i> Accommodated	Schachar <i>et al.</i> (1996)	Ultrasound	6	20 - 34	+0.068*
	Strenk <i>et al.</i> (1999)	MRI	25	22 - 83	8.3622 + 0.0104A
	Jones <i>et al.</i> (2007)	MRI	44	18 - 59	-0.067*
	Hermans <i>et al.</i> (2009)	MRI	5	18 - 35	-0.037*
	Kasthurirangan <i>et al.</i> (2011)	MRI	15	19 - 29	8.71
	Sheppard <i>et al.</i> (2011)	MRI	19	19 - 30	-0.09*
	Richdale <i>et al.</i> (2013)	MRI	26	30 - 50	-0.075*
	Glasser & Campbell (1999)	Photography	19	5 - 96	6.195 + 0.047 × FocalLength
	Moffat <i>et al.</i> (2002a) (Decapsulated)	MRI	18	14 - 82	8.8 + 0.189A
	Jones <i>et al.</i> (2005)	Scanning laser MRI	20 20	7 - 82 7 - 82	7.94 + 0.0203A 8.14 + 0.0176A
<i>In vitro</i> Unstretched	Schachar (2005)	Photography	41	3 - 58	7.1505 × A ^{0.0696}
	Rosen <i>et al.</i> (2006)	SP	37	20 - 99	8.7 + 0.0138A

Table 3.4: Anterior crystalline lens radius of curvature measurements. *changes per dioptre of accommodation **measured as curvature, 1/Radius. A = Age.

	Author	Imaging Method	Number of eyes	Age (years)	Radius of curvature (mm)
<i>In vivo</i> Relaxed	Brown (1974)	Photography	100	-	16.82 – 0.104A
	Dubbelman & Van der Heijde (2001)	Schiempflug	102	16 - 65	12.9 – 0.057A
	Koretz <i>et al.</i> (2001)	Schiempflug	100	18 - 70	11.155 – 0.02004A
	Kirschkamp <i>et al.</i> (2004)	Purkinje	9	20 - 38	12.3
	Koretz <i>et al.</i> (2004)	Schiempflug	62	18 - 50	13.95 – 0.076A
		MRI	25	18 - 50	13.48 – 0.081A
	Atchison <i>et al.</i> (2008)	Purkinje	102	18 - 69	12.283 – 0.0438A
		MRI	5	18 - 35	11.45
	Hermans <i>et al.</i> (2009)	Schiempflug	5	18 - 35	12.15
	Sheppard <i>et al.</i> (2011)	MRI	19	19 - 30	11.89
<i>In vivo</i> Accommodated	Koretz <i>et al.</i> (2002)	Schiempflug	100	18 - 70	-0.60 + 0.009A*
	Kirschkamp <i>et al.</i> (2004)	Purkinje	9	20 - 38	8.6
	Dubbelman <i>et al.</i> (2005)	Schiempflug	65	16 - 51	-0.61*
		Schiempflug	11	22 - 36	graphical decrease
	Rosales <i>et al.</i> (2006)	Purkinje	11	22 - 36	graphical decrease
		MRI	5	18 - 35	-0.51*
	Hermans <i>et al.</i> (2009)	Schiempflug	5	18 - 35	-0.64*
	Sheppard <i>et al.</i> (2011)	MRI	19	19 - 30	-0.63*
	Pierścionek (1995)	Photography	5	35 - 72	7.4
	Glasser & Campbell (1999)	Photography	19	5 - 96	4.278 + 0.0168A + 0.00257A ²
<i>In vitro</i> Unstretched	Moffat <i>et al.</i> (2002a)	MRI	18	14 - 82	0.14 – 0.0007A**
	Schachar (2004)	Corneal Topography	30	33.6	10.5
	Manns <i>et al.</i> (2004)	Corneal Topography	13	46 - 93	10.15
		Scanning laser	20	7 - 82	0.163 – 0.00109A**
	Jones <i>et al.</i> (2005)	MRI	20	7 - 82	0.1363 – 0.00069A**
	Rosen <i>et al.</i> (2006)	Shadowphotogrammetry	37	20 - 99	7.5 + 0.046A

Table 3.5: Posterior crystalline lens radius of curvature measurements. *changes per dioptre of accommodation **measured as curvature, 1/Radius. A = Age.

	Study	Imaging Method	Number of eyes	Age (Years)	Radius of curvature (mm)
<i>In vivo</i> Relaxed	Brown (1974)	Photography	100	-	-8.719 + 0.015A
	Koretz <i>et al.</i> (2001)	Scheimpflug	100	18 - 70	-8.267 + 0.02025A
	Dubbelman & Van der Heijde (2001)	Schiempflug	65	16 - 65	-6.2 + 0.012A
	Kirschkamp <i>et al.</i> (2004)	Purkinje	9	20 - 38	-6.1
	Koretz <i>et al.</i> (2004)	Schiempflug	62	18 - 50	-6.436 + 0.0106A
		MRI	25	18 - 50	-5.368 - 0.0078A
	Atchison <i>et al.</i> (2008)	Purkinje	102	18 - 69	-7.1857 + 0.0076A
	Hermans <i>et al.</i> (2009)	MRI	5	18 - 35	6.11
		Scheimpflug	5	18 - 35	5.82
	Kasthurirangan <i>et al.</i> (2011)	MRI	15	19 - 29	-5.66
MRI		15	60 - 70	-6.08	
MRI		19	19 - 30	6.12	
<i>In vivo</i> Accommodated	Koretz <i>et al.</i> (2002)	Schiempflug	100	18 - 70	0.25 - 0.003A *
	Kirschkamp <i>et al.</i> (2004)	Purkinje	9	20 - 38	-5.3
	Dubbelman <i>et al.</i> (2005)	Schiempflug	65	16 - 51	-0.13* (37)
		Schiempflug	11	22 - 36	graphical decrease
	Rosales <i>et al.</i> (2006)	Purkinje	11	22 - 36	graphical decrease
		MRI	5	18 - 35	-0.14*
	Hermans <i>et al.</i> (2009)	Schiempflug	5	18 - 35	-0.16*
		MRI	15	19 - 29	-5.08
	Sheppard <i>et al.</i> (2011)	MRI	19	19 - 30	-0.15*
		MRI	19	19 - 30	5.32
<i>In vivo</i> Unstretched	Pierscionek (1995)	Photography	5	35 - 72	-8.0 (11)
		Photography	19	5 - 96	-3.143 - 0.0536A + 0.0004173A ² (19)
	Moffat <i>et al.</i> (2002a)	MRI	18	14 - 82	-0.25 + 0.0014A**
		Corneal Topography	30	33.6	-6.8
	Manns <i>et al.</i> (2004)	Corneal Topography	13	46 - 93	-2.313 - 0.05A
		Scanning laser	20	7 - 82	-0.183 + 0.00061A**
	Jones <i>et al.</i> (2005)	MRI	20	7 - 82	-0.1777 + 0.00067A**
		Shadowphotogrammetry	37	20 - 99	-5.5

change in axial length or lens thickness, the movement of the posterior surface can be measured. With age, there was support for the posterior pole moving backwards with age (Tsorbatzoglou *et al.*, 2007; Atchison *et al.*, 2008; Kasthurirangan *et al.*, 2011), but Richdale *et al.* (2013) showed evidence that the posterior pole was stable through life.

With accommodation, there was agreement that the ACD decreases in depth, but again, there were differing views on the movement of the posterior pole. Drexler *et al.* (1997) measured the anterior and posterior pole positions during accommodation and found that the posterior pole moves backwards with accommodation whilst the anterior pole moves forwards, with the anterior change being three times that of the posterior; also supported by Dubbelman *et al.* (2005). Ostrin *et al.* (2006) found that 73% of subjects showed posterior pole movement, and that anterior pole movement accounted for 75% of the change in lens thickness. Kasthurirangan *et al.* (2011) found that the posterior pole showed no movement with accommodation, although suggested that MRI resolution and the supine position of subjects may cause measurement errors. Finally, Du *et al.* (2012) found evidence for there being movement of the posterior pole, with the increase in lens thickness being larger than the decrease in ACD.

3.2.2.5 Other measurements

The measurements detailed so far are the typical measurements required to build a geometric representation of the lens. However, there have been additional measurements made of the volume, surface area and cross sectional area that could be beneficial for ensuring developed lens models are accurate (Table 3.7, page 90).

There has been general agreement that the volume of the lens increases with age and that the change in volume is not evenly distributed through the lens. Measurements indicate that the volume change is limited to the cortex (Koretz *et al.*, 2001) and that the majority of the volume change is limited to the anterior portion of the lens (Strenk *et al.*, 2004), which matches with the thickness changes discussed in Section 3.2.2.1.

Where there was disagreement was in the changes that occur with accommodation. Strenk *et al.* (2004) measured a volume increase with accommodation, which was also supported by Sheppard *et al.* (2011), whereas Hermans *et al.* (2009) measured no volume change with accommodation, although only 5 subjects were measured. In terms of surface area, there was agreement that the surface area decreased with accommodation, but the difference in opinion on the volume change led to disagreement on the compressibility of the lens.

Table 3.6: Anterior Chamber Depth measurements *includes cornea thickness **indicates change per dioptre of accommodative response. A = Age.

	Study	Imaging Method	Number of eyes	Age (Years)	Anterior chamber depth (mm)	Anterior segment length (mm)
In vivo Related	Drexler <i>et al.</i> (1997)	Partial coherence interferometry	10	25 - 39	3.091	-
	Koretz <i>et al.</i> (2004)	Scheimpflug	62	18 - 50	-0.0215A + 4.274	-0.0043A + 7.446
		MRI	25	18 - 50	-0.0215A + 4.351	0.0063A + 7.051
	Kirschkamp <i>et al.</i> (2004)	Ultrasound	9	20 - 38	3.6	-
		MRI	31	20 - 29	3.73	-
	Fea <i>et al.</i> (2005)	MRI	12	60 - 69	3.05	-
			32	< 30	3.578	7.355
	Tsorbatzoglou <i>et al.</i> (2007)	Partial coherence interferometry	37	31 - 44	3.324	7.364
			32	> 45	3.242	7.556
			102	18 - 69	3.857 - 0.0106A*	6.976 + 0.0132A
Atchison <i>et al.</i> (2008)	Ultrasound	15	Young	3.69	7.38	
Kasthurirangan <i>et al.</i> (2011)	MRI	15	Old	3.24	7.9	
		26	30 - 50	3.58 - 0.031A	-	
In vivo Accommodated	Drexler <i>et al.</i> (1997)	Partial coherence interferometry	10	25 - 39	3.091 (mean change - 186 μ m)	-
	Kirschkamp <i>et al.</i> (2004)	Ultrasound	9	20 - 38	3.4	-
		Scheimpflug	102	16 - 65	-0.048 + 0.0004A**	-
	Ostrin <i>et al.</i> (2006)	Ultrasound	22	21 - 30	-0.063 - 0.051 \times <i>AccAbility</i>	-0.039 + 0.017 \times <i>AccAbility</i>
			32	< 30	-0.08	0.029
	Tsorbatzoglou <i>et al.</i> (2007)	Partial coherence interferometry	37	31 - 44	-0.064	0.039
			32	> 45	-0.03	-0.023
	Kasthurirangan <i>et al.</i> (2011)	MRI	15	19 - 29	3.38	7.40

In measurements made *in vitro*, the same age trends were seen as *in vivo*, but additional measurements of surface area by Urs *et al.* (2009b) indicate that there is an increase in capsule tension corresponding to an increase in surface area with age.

3.2.3 Capsule

The exact role that the capsule plays in accommodation is equivocal (Section 1.2.3.2), therefore it is essential to replicate it along with any variation in thickness around the capsule profile.

The capsule follows the lens outline, therefore measurements that have been made have concentrated on the changes in thickness. Table 3.8 gives an overview of studies that have provided data on the changes in the capsule thickness. Figure 1.5 showed an example of the thickness variation from Fincham (1925), illustrating the change in thickness around the capsule, although this is believed to be a combination of the data from Fincham (1925) and Salzmann (1912) (Barraquer *et al.*, 2006). More recent studies have measured the thickness at different points and across ages. Figure 3.1 shows the variation in thickness between the measurements of Fisher & Pettet (1972) and Barraquer *et al.* (2006).

There has been a general agreement that the anterior capsule thickness is greater than the posterior, which was established with the early measurements of Salzmann (1912) and Fincham (1937). Subsequent studies that measured just parts of the capsule also supported these findings. Krag & Andreassen (2003a) observed the thickness of capsule sections approximately 1.6 mm from the anterior and posterior poles, finding that the anterior capsule thickened with age before 70 years old where it then stabilised or declined. The posterior thickness remained stable with age. Ziebarth *et al.* (2005) measured the thickness at the anterior and posterior poles, finding that the anterior was thicker than the posterior, using two measurement methods (Table 3.8).

Where there has been uncertainty is in where the thickness varies in the anterior and posterior sections, and how this changes with age. The study of Fisher & Pettet (1972) showed the anterior capsule increasing with age, both at the pole and at the zonular insertion point, whilst the equatorial and posterior sections were more stable. The posterior capsule thinned from 1 mm from the equator to the pole, with the posterior pole thickness remaining stable through life. The thickest portion of the capsule was initially at the equator, but by the onset of presbyopia the anterior zonular insertion was thickest.

The most recent study by Barraquer *et al.* (2006) provided thickness values at multiple regions around the lens and in line with previous studies, found that the anterior capsule was thicker than the posterior

Table 3.7: Summary of other lens measurements. *indicates changes per dioptre of accommodation. CSA = Cross Sectional Area, A= Age (Years).

	Study	Imaging Method	Number of eyes	Age (Years)	Volume (mm³)	CSA (mm²)	Surface Area (mm²)	Weight (mg)
<i>In vivo</i> Relaxed	Koretz <i>et al.</i> (2001)	Scheimpflug	100	18 - 70	Increases with age	-	-	-
	Strenk <i>et al.</i> (2004)	MRI	25	22 - 50	-	19,660 + 0.131A	-	-
	Hermans <i>et al.</i> (2009)	MRI	5	18 - 35	160.1	25.9	175.9	-
	Sheppard <i>et al.</i> (2011)	MRI	19	19 - 30	154.72	-	157.72	-
<i>In vivo</i> Accommodated	Strenk <i>et al.</i> (2004)	MRI	25	22 - 50	-	21,827 + 0.1A	-	-
	Hermans <i>et al.</i> (2009)	MRI	5	18 - 35	160.2	27.1	167.5	-
		MRI	5	18 - 35	-	0.2*	-1.4*	-
	Sheppard <i>et al.</i> (2011)	MRI	19	19 - 30	0.65*	-	-0.54*	-
<i>In vitro</i>	Rosen <i>et al.</i> (2006)	Shadow photogrammetry	37	20 - 99	0.91 × LensWeight	-	-	164 + 1.45A
	Urs <i>et al.</i> (2009b)(2 curve method)	Shadow photogrammetry	27	6 - 82	131.6 + 1.35A	24.9 + 0.14A	145.2 + 0.8A	-

Table 3.8: Capsule thickness measurement studies.

Study	Method	Number of eyes	Age (Years)	Summary of results
Salzmann (1912)	<i>In vitro</i> measurement	14	7 - 56	Anterior and posterior poles thicken with age, equator thickens then reduces. Two thicker sections, the first between anterior pole and equator, second between equator and posterior pole. Anterior capsule is thicker overall than the posterior
Fincham (1937)	Light microscopy	3	N/A	Similar results to Salzmann, slightly thinner measurements
Fisher & Pettet (1972)	<i>In vitro</i> micrometer measurement	32	1 - 70	Similar shape see as in previous studies, however, the anterior capsule grew throughout life whilst the equator stabilised in older eyes
Krag <i>et al.</i> (1997)	<i>In vitro</i> micrometer measurement	67	0.7 - 98	Measurements taken approximately 1.6mm from the poles, with evidence for a thicker anterior capsule than posterior with the anterior capsule showing progressive growth until 70 YO before stabilising. The posterior pole remained stable with age
Ziebarth <i>et al.</i> (2005)	Non-contact <i>in vitro</i> measurement and Histological measurement	22	40 - 92	Anterior capsule is thicker than posterior at the poles with both sets of measurements
Barraquer <i>et al.</i> (2006)	Photomicroscope image measured manually after enlarged images were printed	26	12 - 103	Similar overall shape as previous studies. Some differences to previous studies found. First, the maximum anterior thickness was at the mid periphery. Second, additional thinning found in the anterior capsule before the equator. Third the posterior peripheral thickening was less than in previous studies. Finally, anterior thickness increase throughout life was restricted to the anterior pole, with the mid periphery stabilises after 70 YO.

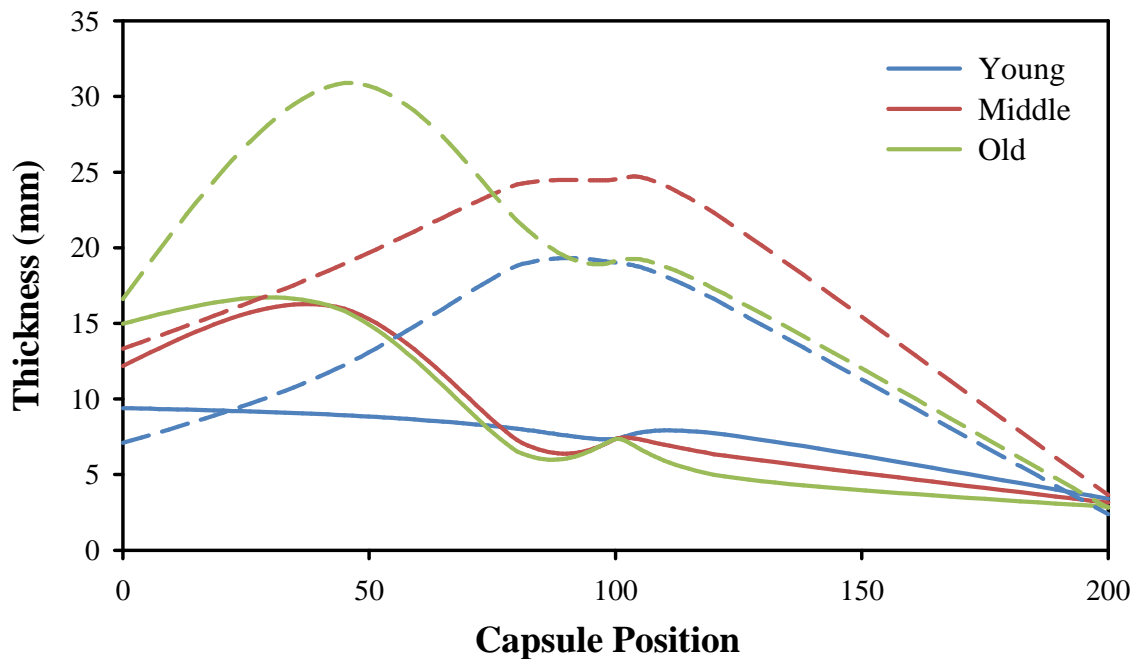


Figure 3.1: Comparison of capsule thickness variations. 0 represents the anterior pole, 100 the equator and 200 the posterior pole. The solid lines indicate the measurements of Barraquer *et al.* (2006) (20, 50 & 0 YO) and the dotted lines indicate the measurements of Fisher & Pettet (1972) (22, 37 & 77 YO).

with the anterior section growing with age whilst the posterior section was more stable. In terms of the thickness variation around the capsule, there were some differences to previous studies; first, the maximum thickness in the anterior section was always in the mid periphery, apart from in older lenses where it was at the anterior pole. Second, there was a thinning found in the anterior section just before the equator, appearing to correspond to the anterior zonular insertion. Third, a posterior “mound” was not found consistently and where seen was of a modest size. Finally, the anterior pole was found to thicken throughout life, whilst the mid anterior capsule thickened with age but then stabilised. These results would indicate that the anterior portion of the capsule increases in influence throughout life, compared to the more stable peripheral thickness, potentially aiding in changing the lens shape in older eyes.

3.2.4 Zonules

Although there have been a number of studies that have analysed the zonular arrangement (e.g. Nankivil *et al.*, 2009 and Lütjen-Drecoll *et al.*, 2010), there have been fewer studies that provide any measurements of aspects of the zonular arrangements. In previous FEA models the zonules are typically modelled in three groups (see Section 2.2.4) running from the lens to a single point representing the ciliary body. The

data shows that this is a simplification of how the zonules are actually arranged (see Section 1.2.3.3). To ensure that the existing measurements to be discussed are clear, a consistent description of the different zonular groups is needed. Figure 3.2 shows a simple representation of the different zonular groups and the naming convention that will be followed.

For the zonular structure to be modelled accurately the ciliary body also needs to be considered, therefore, the known measurements of the ciliary body will also be discussed in the current section.

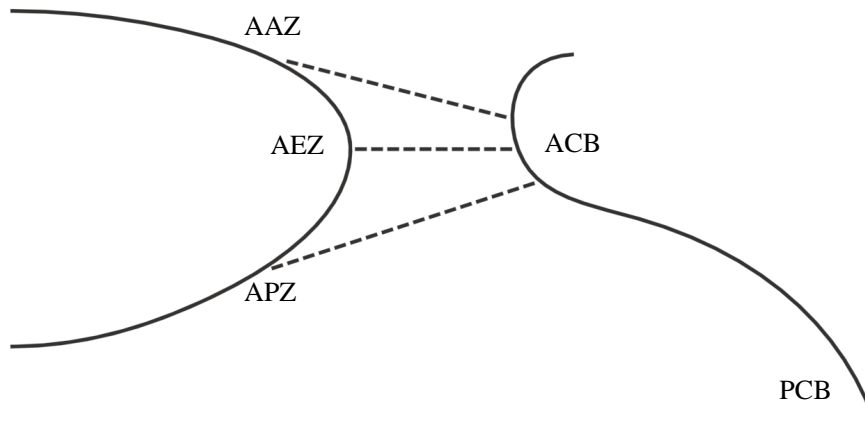


Figure 3.2: Illustration of zonule groupings and nomenclature. AAZ = Anterior zonule attachment, anterior group. AEZ = Equatorial zonule attachment, anterior group, APZ = Posterior zonule attachment, anterior group, ACB = Anterior ciliary body, PCB = Posterior ciliary body.

3.2.4.1 Lens attachment points

The measured changes in anterior insertion (AAZ zonule insertions) are detailed in Table 3.9 and illustrated in Figure 3.3, showing the similarity in trends.

Table 3.9: Measurements of the attachments of the zonular bundles to the crystalline lens.

Study	Anterior Position (mm from equator)	Results
Farnsworth & Shyne (1979)	$(0.0124 \times Age) + 0.0311$	Distance between zonular insertion and equator increases with age
Sakabe <i>et al.</i> (1998)	$(0.0079 \times Age) + (0.202 \times Diameter) - (0.041 \times Axial\ length) + 0.0114$	Anterior zonular insertion increases in distance from equator, zonular free zone decreases with age

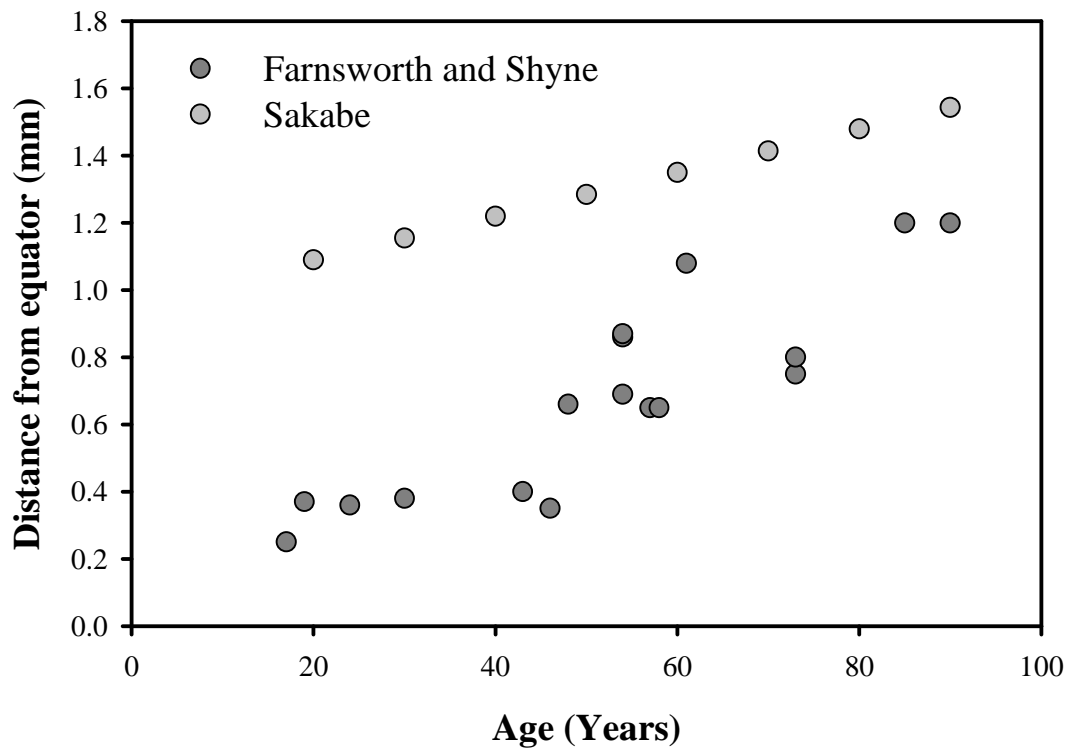


Figure 3.3: Comparison between the AAZ lens attachment movements with age, the lens diameter value needed to define the Sakabe *et al.* (1998) position was taken from Strenk *et al.* (1999) and the axial length from Atchison *et al.* (2008).

The posterior zonular attachments have not been measured in as much detail due to the difficulties in imaging them. Most FEA studies have modelled the posterior attachments as being the same distance from the equator as the anterior attachments (e.g. Burd *et al.*, 2002). Ljubimova *et al.* (2008) quoted a figure of 0.22 mm from the equator, based on data from Gorban & Dgiliashvili (1993), but the method of finding this value was unable to be verified.

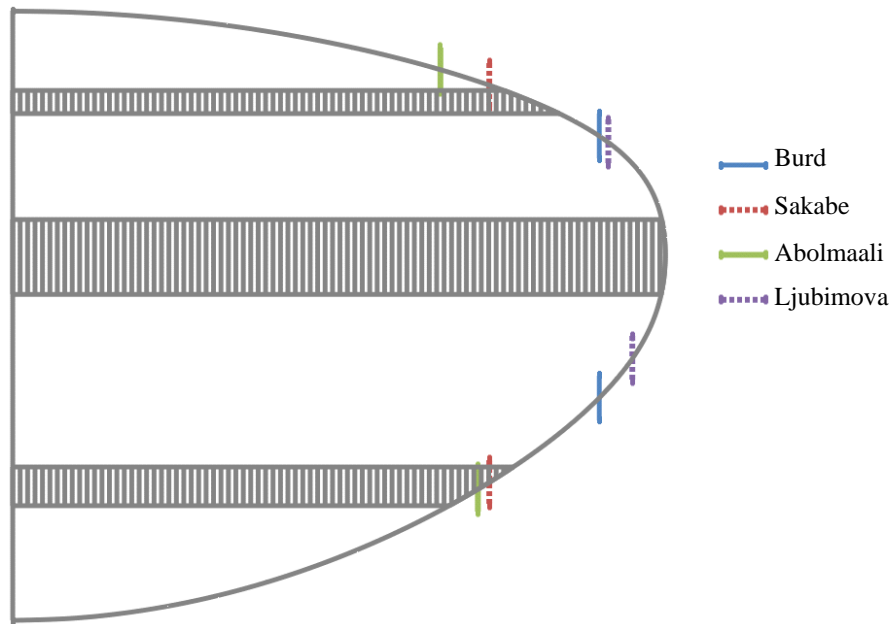


Figure 3.4: Illustration of the AAZ, AEZ and APZ zonular attachment locations on the lens, showing the positions of Burd *et al.* (2002), Sakabe *et al.* (1998), Abolmaali *et al.* (2007) and Ljubimova *et al.* (2008). The shaded bands represent the size of the zonular attachment zones according to Streeten (1977).

Figure 3.4 illustrates the typical locations of the various attachment positions used in previous FEA studies (based on the studies of Burd *et al.*, 2002; Ljubimova *et al.*, 2008; Lanchares *et al.*, 2012) on a representative 33 YO lens. The bands shown represent the size of the attachment areas according to Streeten (1977). The anterior insertion area is about 0.3 - 0.4 mm wide, whilst the equatorial and posterior areas are 0.4 - 0.5 mm. Sakabe *et al.* (1998) stated that the zonular free area decreases with age, indicating that the zonules cover a larger area with increased age; however, no data was given for this change.

3.2.4.2 Ciliary body measurements

A few studies have attempted to measure the ciliary body (and the ciliary muscle) to aid in the understanding of how it changes with age and accommodation. Tables 3.10 (Page 96) to 3.12 give an overview of the different measurements that have been made.

Table 3.11: Changes in key ciliary body measurements with age.

Study	Key Findings
Pardue & Sivak (2000)	CM Length decreases with age, CM Width increases with age
Strenk <i>et al.</i> (2010)	CM thickness increases with age (0.49 mm – 0.68 mm)
Sheppard & Davies (2011)	CM thickness increases with age
Kasthurirangan <i>et al.</i> (2011)	Distance from lens to CB decreases with age (Mean 0.43 mm)
Richdale <i>et al.</i> (2013)	no change in thickness with age

Table 3.10: Summary of key ciliary body (CB) and ciliary muscle (CM) measurements. All measurements taken *in vivo* unless otherwise stated in the method column.

Study	Method	Measured section	Subjects	Age (Years)	Anterior thickness (mm)	Posterior Thickness (mm)	Length (mm)
Pardue & Sivak (2000)	<i>In vitro</i>	CM	8	0 - 78	0.47	-	3.87
Bailey <i>et al.</i> (2008)	AS-OCT	CB	53	8 - 15	0.899	0.326	-
Ernst (2010)	AS-OCT	CB	63	18 - 39	1.16	0.5	-
Strenk <i>et al.</i> (2010)	MRI	CB	40	22 - 91	0.427	-	-
Sheppard & Davies (2011)	AS-OCT	CM	50	19 - 34	0.535	0.152	4.63
Buckhurst <i>et al.</i> (2013)	AS-OCT	CM	63	18 - 40	0.558	0.172	-
Richdale <i>et al.</i> (2013)	AS-OCT	CB	26	30 - 50	0.87	-	-

Table 3.12: Changes in key ciliary muscle measurements with accommodation.

Study	Key Findings
Strenk <i>et al.</i> (2010)	CM Thickness change with accommodation is constant throughout life (0.085 mm)
Sheppard & Davies (2010)	CM length decreases with accommodation, CM25 increased, CM50 and CM75 remained constant
Sheppard & Davies (2011)	CM25 increases with accommodation, constant increase with age nasally, reduced change temporally CM25 increases by 7.1 μm per D of accommodation
Kasthurirangan <i>et al.</i> (2011)	Distance from lens to CB does not change with accommodation
Richdale <i>et al.</i> (2013)	Increase anteriorly, decrease posteriorly

From Table 3.10 it can be seen that there are differences in the reported thicknesses, which can be attributed to three main factors. First, the different methods of imaging used, second, the differing ways in which the ciliary muscle has been distinguished from the ciliary body and finally, the different measurement positions. For example, the thickness measurements of Ernst (2010) are a lot higher than for Sheppard & Davies (2010); Ernst (2010) appears to have measured the overall ciliary body shape, whilst Sheppard & Davies (2010) measured just the ciliary muscle. The difference between these values could be attributed to the multi-layered aspect of the ciliary body, as discussed in Section 1.2.3.4.

In terms of measurement positions Bailey *et al.* (2008) measured the ciliary muscle thickness at 1, 2 and 3 mm from the scleral spur, compared to Sheppard & Davies (2011) who measured at 25, 50 and 75% along the ciliary muscle length. The two methods would produce different values, but the latter method would be consistent across different ciliary muscle lengths.

In terms of average measurements there was a general agreement that the ciliary muscle was thickest anteriorly (around 1 – 2 mm from the scleral spur) and that there was a progressive thinning posteriorly. Most studies found that the anterior thickness increased with age, however Richdale *et al.* (2013) found no change in thickness.

During accommodation all studies found that there was an increase in anterior thickness, but there was disagreement on posterior changes with Sheppard & Davies (2010) finding no change and Richdale *et al.* (2013) finding a decrease. The changes during accommodation did not appear to change significantly with age.

The measurements so far have concentrated on the ciliary muscle; there are additional measurements that have measured the ciliary body as a whole, using UBM or MRI, shown in Table 3.13. Combining these two sets of data should be able to give a good estimation of the ciliary body shape, as well as the changes

3.2 Measured Data

that it undergoes during accommodation (Section 3.5.3).

Table 3.13: Summary of *in vivo* studies that have measured the movement of the ciliary body with age and accommodation. CM = Ciliary muscle.

Study	Num of Subjects	Age (Years)	Method	Key findings
Strenk <i>et al.</i> (1999)	25	22 - 83	MRI	CM contraction remains constant throughout life, CM diameter in un-accommodated state decreases with age
Stachs <i>et al.</i> (2002)	12	-	UBM	CM centre of gravity shifts in a range of 0.04 - 0.26 mm towards the lens equator, with a small decrease with age
Strenk <i>et al.</i> (2006)	48	22 - 91	MRI	CM remains active throughout life
Sheppard & Davies (2010)	50	19 - 34	OCT	CM has an anterior and centripetal shift with accommodation
Kasthurirangan <i>et al.</i> (2011)	30	19 - 70	MRI	Circumlental space does not change with accommodation, decreases with age
Richdale <i>et al.</i> (2013)	26	30 - 50	OCT	CM has a mean diameter of 11.84 mm, no change with age, decrease with accommodation (-0.105 mm)

The work of Strenk *et al.* (1999) has been widely used for defining the movement of the ciliary body for FEA studies (Section 2.4), finding that the ciliary body diameter decreases with accommodation. The measurements also show that this decrease was constant with age, although the diameter in the relaxed state decreased with age. Strenk *et al.* (2000) showed further evidence of this, measuring the circumlental space and finding a decrease with age. The later study (Strenk *et al.*, 2006) backed up these measurements, although in all cases where the diameter was actually measured on the MRI images was not clear.

Stachs *et al.* (2002) measured the overall movement of the centre of gravity of the ciliary body finding an inwards movement, although it was less than that measured by Strenk *et al.* (1999). The measured changes also showed a small decrease with age, although the changes were pharmacologically induced which could cause potential inaccuracies. Sheppard & Davies (2010) showed support of this, hypothesising that measured thickness changes indicate that there was an anterior and inwards shift of the muscle mass, but a definition of this movement was not given.

Kasthurirangan *et al.* (2011) measured the distance between the lens and ciliary body finding that the distance between the two remained constant with accommodation, but decreased with age, supporting the other measurements by indicating an anterior thickening of the ciliary body in both cases.

3.2.4.3 Zonule thickness

Although descriptions of the overall zonular arrangement have been given by a range of authors, descriptions of the zonular fibres themselves have been scarcer. Bornfeld *et al.* (1974) investigated the zonules using scanning electron microscopy (SEM) on a young and an old lens, finding that zonule fibres are made of fibrils of 1 to 2 μm in diameter which form bundles from 10 to 20 μm in diameter. The smaller fibrils were also seen to traverse the distance between the larger fibres. Streeten (1977) also used SEM to investigate the zonules (utilising 30 human lenses), finding that the anterior and posterior zonules insert into the capsule in bundles 25 to 60 μm in diameter, whilst the equatorial bundles are 10 to 15 μm in diameter. The individual fibrils making up the bundles were measured as being 35 to 55 nm in diameter.

More recently, there have been a number of abstracts that have detailed thickness values. Reed *et al.* (2003) states that the mean thickness of the zonules was 6.8 μm , whilst Lamar *et al.* (2004) found that the zonule thickness varied from 6 to 35 μm midway between the lens and ciliary body, although the specifics could not be obtained. Lamar *et al.* (2005) used SEM and found that the thickness of the anterior zonules was approximately 3 times the posterior zonules and 10 times the equatorial zonules.

With the lack of data on thickness values, previous FEA models have instead estimated the zonular thickness by manually adjusting the stiffness values of the zonules until the deformations of the lens match a measured value (e.g. Burd *et al.*, 2002). To represent the fact that there are differences between the thickness of the zonular groups the stiffness values have been applied in a ratio, with Burd *et al.* (2002) using 6:1:3 for the anterior, equatorial and posterior zonules respectively based on the work of Farnsworth & Shyne (1979). Liu *et al.* (2005) set the anterior and posterior zonules to be three times the stiffness of the equatorial zonules, based on data from Rao & Wang (2002).

Weeber & van der Heijde (2008) used data cited from Kaczurowski (1964), where the diameter of the anterior zonules was 50 μm and the equatorial and posterior zonule diameter was 40 μm . The number of fibres in each group was different from previous studies with the split being 100:50:135, giving the posterior group the most fibres.

3.2.5 Summary

3.2.5.1 Accommodation and presbyopia theories

In Chapter 1, the various proposed theories of accommodation and presbyopia were discussed. The evidence for and against these theories in terms of geometric changes can now be summarised.

The majority of measured geometric changes in the lens and ciliary body support the Helmholtz theory, in that the lens increases in thickness and curvature and reduces in diameter in response to an inwards ciliary body movement.

Schachar's theory relies on the equator of the lens increasing with accommodation, which was only seen in a single *in vivo* study. It was also seen *in vitro*, but the errors that could arise from these have been discussed previously. Additionally, the overall shape of the lens in the Schachar theory (Section 1.2.2) does not match up with the more spherical lens shapes that are observed *in vivo*, as shown in Section 3.3.

The theories of Coleman and Santos (Section 1.3) rely on the movement of the posterior pole during accommodation, which from Section 3.2.2.4 is not agreed on with evidence for both posterior and anterior movements of the pole.

In terms of presbyopia development it is difficult to deduce whether one theory is more valid than another, as the geometric changes all illustrate the changes with age that occur. To aid in establishing the causes of presbyopia, the modelling that will be carried out in Chapter 6 will be of more use.

The geometry of the accommodation system has been well studied with the majority of parameters needed for modelling being well measured and agreed on (e.g. lens thickness and anterior curvature). However, there are a number of areas where there is disagreement in the literature, in particular on the posterior lens curvature and movement and the lens diameter, which will need to be considered when analysing future models. The lack of data on the zonules and ciliary body also impacts on developing a model suitable for FEA.

3.3 Crystalline lens model

In Chapter 2 an overview of the different models of the accommodative system used in FEA models was given. In addition to those models, there have been other methods developed to describe the components of the accommodation system. It is beyond the scope of this project to develop a new crystalline lens modelling method, therefore a choice of a suitable method from the literature is needed. The selected method needs to be able to be defined by measurable parameters as well as model a range of ages in both accommodated and relaxed states.

3.3.1 Existing models

Three principal methods of modelling the lens were detailed in Section 2.2.1 based on a small selection of source data. Table 3.14 gives a summary of these methods as well as other methods that have been proposed in the literature to model the complete lens. Smith *et al.* (2009) and Giovanzana & Talu (2012) conducted reviews of various methods of modelling the lens, both reporting on the difficulty in specifying a model suitable for representing the lens. Therefore, any models that are proposed need to be compared at different ages to ensure that they are suitable.

Table 3.14: Summary of crystalline lens modelling methods used in the literature. Whether a method is suitable is determined by 1. Ability to replicate the method 2. Ability to model based on measurable parameters.

Study	Source Data	Modelling Method	Suitable	Curves to describe lens
Kasprzak (2000)	Geometric constraints	Conic Sections	N	2
Burd <i>et al.</i> (2002)	Scheimpflug	5th order Polynomials, Circular end cap	N	3
Chien <i>et al.</i> (2003)	MRI	Cosine Function	N	2
Smith (2003)	Geometric constraints	Figuring Conic	Y	2
Kasprzak & Robert Iskander (2006)	Geometric constraints	Hyperbolic Cosine	Y	1
Weeber 2006	Geometric constraints	Conic Section, Circular Cap	N	3
Hermans <i>et al.</i> (2006)	Geometric constraints	Conic Sections	N	4
Hermans <i>et al.</i> (2009)	Geometric constraints	Conic Sections	Y	4
Smith <i>et al.</i> (2009)	MRI	Generalised Conic	N	2
Urs <i>et al.</i> (2009a)	Shadow Photogrammetry	2 Polynomial methods	N	1,2
Urs <i>et al.</i> (2010)	Shadow Photogrammetry	10th order fourier series	N	1
Giovanzana & Talu (2012)	Geometric constraints	Cosine function	Y	2
Kim <i>et al.</i> (2011)	OCT	Fourier cosine	N	1

Each modelling method uses different parameters to define the lens equations. Where possible the terms will be standardised to those defined in Figure 3.5 with definitions in Table 3.13.

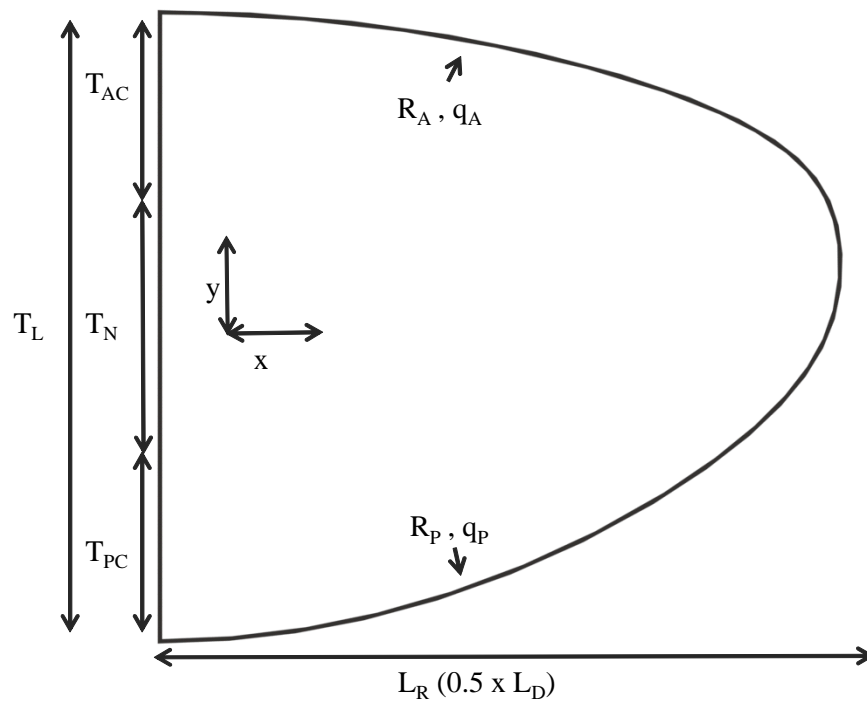


Figure 3.5: Standard nomenclature for describing lens parameters, with definitions given in Table 3.15.

Table 3.15: Lens parameter labels and units, as illustrated in Figure 3.5.

Lens Parameter	Label	Units
Axial Lens Thickness	T_L	mm
Equatorial Diameter	L_D	mm
Equatorial Radius	L_R	mm
Age	A	years
Anterior radius of curvature	R_A	mm
Posterior radius of curvature	R_P	mm
Anterior asphericity	q_A	-
Posterior asphericity	q_P	-
Nucleus thickness	T_N	mm
Cortex thickness anterior	T_{AC}	mm
Cortex thickness posterior	T_{PC}	mm

In Section 2.2.1.2 existing modelling methods were detailed with the limitations highlighted. A comparison between potential methods for the current model is now required to ensure that an appropriate model is selected. Table 3.14 shows that only a few methods are suitable, in that they are defined by measurable parameters and able to model both accommodated and relaxed lenses. The two most recent of these models were selected (Hermans *et al.*, 2009; Giovanzana & Talu, 2012) to be compared.

Hermans model

The model first proposed in Hermans *et al.* (2006) was later adjusted (Hermans *et al.*, 2009), giving equations 3.1 and 3.2 for the central portion of the lens.

$$x = \sqrt{\frac{2(y - y_{0ant})}{c_{ant}}} \quad x \leq 2 \text{ mm and } y \geq 0 \text{ mm} \quad (3.1)$$

$$x = \sqrt{\frac{2(y - y_{0pos})}{c_{pos}}} \quad x \leq 2 \text{ mm and } y \leq 0 \text{ mm} \quad (3.2)$$

Where y_{0ant} and y_{0pos} are the crossing points of the anterior and posterior surfaces with the lens axis and c_{ant} and c_{pos} are equivalent to 1/radius of curvature. Equation 3.3 defines the periphery of the lens with the c and k values for the anterior and posterior portions being defined by equations 3.4 to 3.7.

$$x = L_R - \frac{cy^2}{1 + \sqrt{(1 - kc^2y^2)}} \quad (3.3)$$

$$c_{ant-eq} = \frac{L_R - x_1}{y_1 [c_{ant}(L_R - x_1)x_1 + y_1]} \quad (3.4)$$

$$k_{ant-eq} = \frac{y_1 [2c_{ant}(L_R - x_1)x_1 + y_1]}{(L_R - x_1)^2} \quad (3.5)$$

$$c_{post-eq} = \frac{L_R - x_2}{y_2 [c_{post}(L_R - x_2)x_2 + y_2]} \quad (3.6)$$

$$k_{post-eq} = \frac{y_2 [2c_{post}(L_R - x_2)x_2 + y_2]}{(L_R - x_2)^2} \quad (3.7)$$

Giovanzana model

Giovanzana *et al.* (2011) developed their method from the work of Chien *et al.* (2003) adapting the curve generating method to be defined by geometric constraints. The lens can be modelled with two curves, one

for the anterior surface and one for the posterior. The anterior curve is defined using equations 3.8 - 3.13.

$$z_a(u) = (b_{0a} + b_{1a}(\pi - u)^2 + b_{2a}(\pi - u)^4) \cos \theta \quad (3.8)$$

$$y_a(u) = a_a \sin \theta \quad (3.9)$$

$$a_a = L_R \quad (3.10)$$

$$b_{0a} = T_{AC} \quad (3.11)$$

$$b_{1a} = \frac{1}{2} \left(t - \frac{L_R^2}{R_a} \right) \quad (3.12)$$

$$b_{2a} = \frac{5}{24} T_{AC} - \frac{1}{12} \frac{L_R^2}{R_A} - \frac{1 + q_a}{8} \frac{L_R^2}{R_A^3} \quad (3.13)$$

An alternate form of b_{2a} was proposed in Giovanzana *et al.* (2011) removing the need for q_a to be defined, shown in Equation 3.14.

$$b_{2a} = -\frac{1}{\pi^2} \left(T_{AC} - \frac{L_R^2}{R_A} \right) \quad (3.14)$$

The posterior surface was defined using equations 3.15 - 3.20.

$$z_p(u) = (b_{0p} + b_{1p}u^2 + b_{2p}u^4) \cos \theta \quad (3.15)$$

$$y_p(u) = a_p \sin \theta \quad (3.16)$$

$$a_p = L_R \quad (3.17)$$

$$b_{0p} = T_{PC} \quad (3.18)$$

$$b_{1p} = \frac{1}{2} \left(T_{PC} + \frac{L_R^2}{R_P} \right) \quad (3.19)$$

$$b_{2p} = b_{2a} + 2 \frac{\pi^2 + 8}{\pi^4} (T_{AC} - T_{PC}) - 2 \frac{L_R^2}{\pi^2} \left(\frac{1}{R_A} + \frac{1}{R_P} \right) \quad (3.20)$$

Both of these models would appear to be suitable however, a comparison between them was needed.

3.3.2 Model comparison

To decide which model would be used for the models proposed in Chapter 6, three age lenses (20, 40 and 60 years old) would be made using the two methods each in accommodated and relaxed forms. These would then be compared in terms of anterior and posterior curvature across a 3 mm aperture, to avoid using the curvature at the poles.

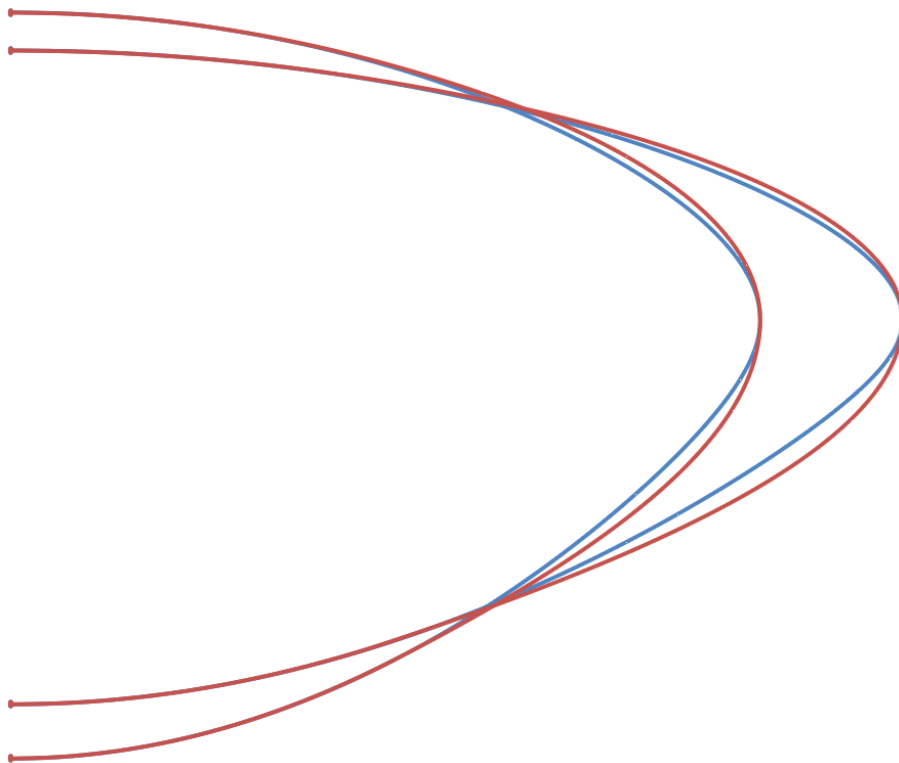
3.3.2.1 Data used to create models

The different sources of data for the lens parameters have been discussed (Section 3.2.2). From this, the data in Table 3.16 was selected as these definitions allowed age related relaxed and accommodated models to be defined.

Table 3.16: Data used to create models, taken from Section 3.2. A = Age, AccAbility = the accommodative ability at Age A, taken from the data of Duane (1922).

Parameter	Relaxed	Accommodated
L_R	$((-0.0047A) + 9.3609)/2$	$(((-0.0047A) + 9.3609)/2) - (0.067 \times acc\ ability)$
T_L	$0.0238A + 2.9276$	$0.0144A + 3.5955$
<i>Anterior Half Lens</i> <i>Posterior Half Lens</i>	0.7	0.7
R_A	$12.9 - 0.057A$	$R_A + ((0.009A - 0.6) \times acc\ ability)$
R_P	$-6.2 + 0.012A$	$R_P + ((0.25 - 0.003A) \times acc\ ability)$
q_A	$-5.4 + 0.03A$	$(-5.4 + 0.03A) - (0.5 \times acc\ ability)$
q_P	$-5 + 0.07A$	$-5 + 0.07A$

Figure 3.6 shows an example of the accommodated and relaxed forms of a 20YO lens using both the Hermans and Giovanzana methods.

**Figure 3.6:** Example of the accommodated and relaxed form of a 20 YO lens defined using the Hermans (Red) and Giovanzana (Blue) methods. An accommodative change of 11D was assumed, as according to Duane (1922).

The Giovanzana model was defined using Equation 3.14 as utilising Equation 3.13 resulted in an unrealistic outline in the accommodated state in a young lens.

3.3.2.2 How do the models compare?

Once each model of the lens was created, the anterior and posterior curvatures were calculated using MatLab. Circles were fitted to the anterior and posterior surfaces across a 1.5 mm portion (representing a 3 mm aperture) using the method proposed by Taubin (1991), with the process repeated for both relaxed and accommodated models to calculate the change in curvature.

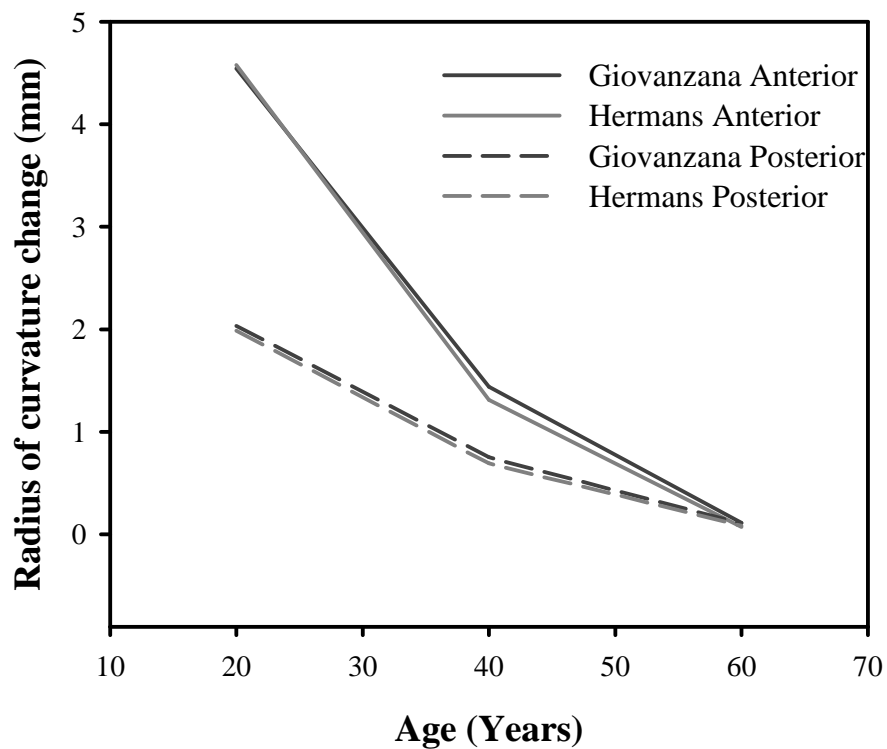


Figure 3.7: Change with age of the decrease in curvature between the relaxed and accommodated states of the Hermans and Giovanzana models.

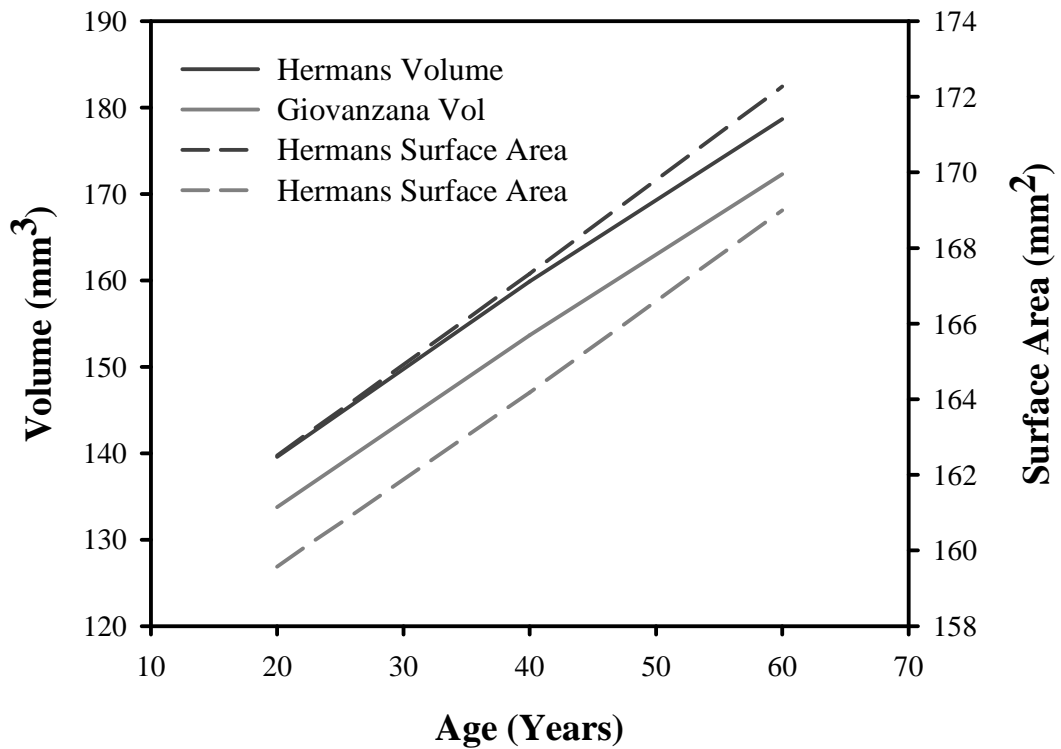


Figure 3.8: The volume and surface area changes with age of the Hermans and Giovanzana models in the relaxed state.

Figure 3.7 shows the change in the radius of curvature in each method, with both methods producing similar results. Figure 3.8 shows the volume and surface area for relaxed models, which compares well with measured data (see Table 3.7). The main difference between the methods is in the shape at the periphery of the lens (Figure 3.6), with the Giovanzana method producing a more pointed profile than the Hermans method. Figure 3.9 shows the curvature changes around the lens profile, where it can be seen that the Giovanzana method produces a slightly smoother profile than the Hermans method.

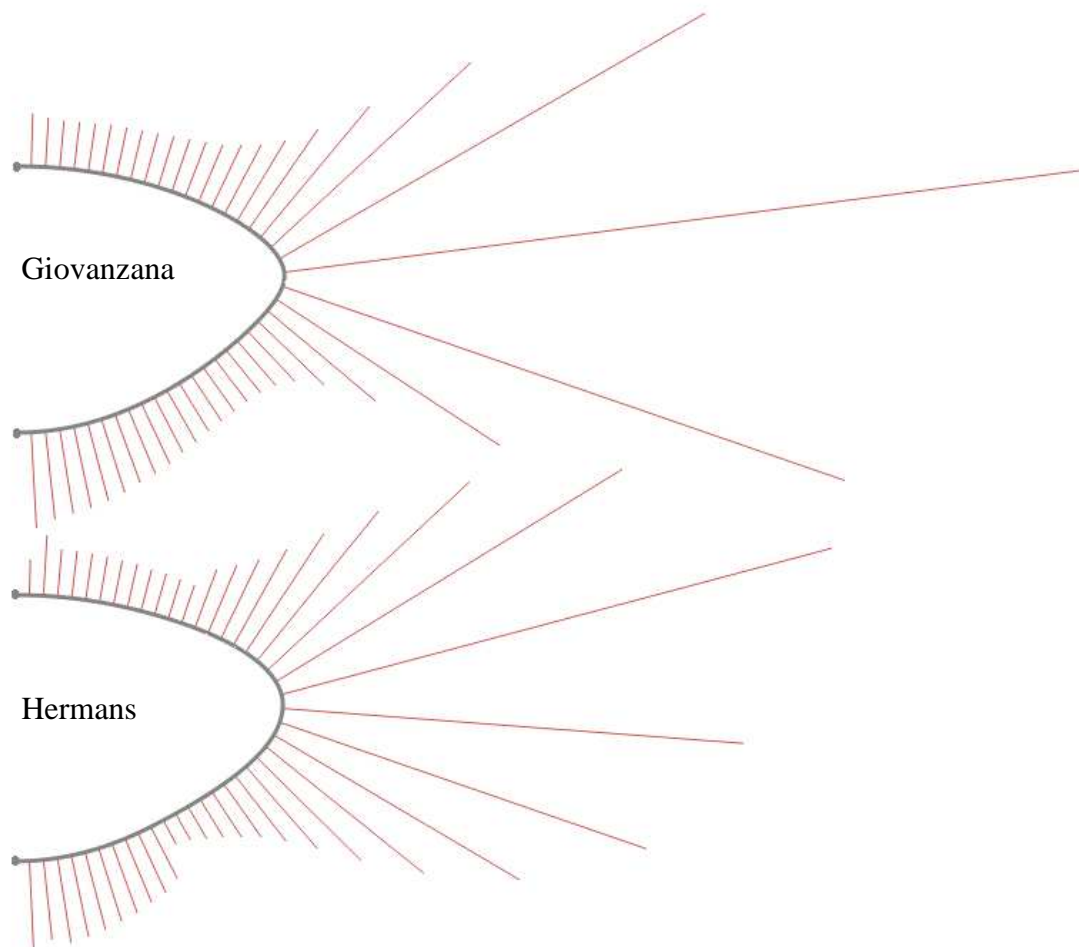


Figure 3.9: Comparison between the curvature changes around the profile of a 20 YO accommodated lens modelled with the Giovanzana and Hermans methods, with the length of the red lines illustrating the amount of curvature at that point.

Both methods are comparable in terms of curvature change, volume, smoothness and adaptability however, when the profiles are compared to whole lens images seen *in vivo* with MRI (e.g. Koretz *et al.*, 2004; Strenk *et al.*, 2005), a more rounded profile would be appropriate in representing the lens therefore, the Hermans method is selected.

3.3.3 Internal structure

To ensure that the material properties of the lens can be modelled suitably (Chapter 2, Chapter 4), a method of defining the different internal regions of the lens was needed. To avoid the issue of a sharp point being created (Section 2.2.2), the percentage reduction method utilised by Abolmaali *et al.* (2007) was adopted, using the data of Dubbelman *et al.* (2003) (Table 3.17).

Table 3.17: Data used to define internal structure, from Dubbelman *et al.* (2003). Z = Zone, with the lens split into 8 zones along the axial length.

Parameter	Definition
Z1	0.28
Z2	$0.23 + 0.012A$
Z3	0.34
Z4	$0.73 + 0.0016A$
Z5	$0.74 + 0.0011A$
Z6	0.31
Z7	$0.18 + 0.0076A$
Z8	0.17
Lens thickness	$Z1+Z2\dots+Z8$
Nucleus	$Z3+Z4+Z5+Z6$
Ant Cortex	$Z1+Z2$
Pos Cortex	$Z7 + Z8$

Dubbelman *et al.* (2003) provided data on the changes in thickness of the internal layers with accommodation, which can be adapted to model the internal changes with accommodation if required (Table 3.18).

Table 3.18: Change in internal thickness with accommodation, taken from Dubbelman *et al.* (2003).

Age (Years)	Ant Cortex	Nucleus	Pos Cortex	Acc. Amplitude (D)
	Change in mm			
19	0.005	0.035	0	8.29
25	0.008	0.043	0.001	7.15
31	0.005	0.038	-0.001	6.01
37	0	0.04	-0.001	4.87
43	0.001	0.043	0.001	3.73
49	-0.008	0.036	-0.012	2.59

The values defined in Tables 3.17 and 3.18 were used to establish the scaling factor required to reduce the outer lens shape down. However, a centre point around which to scale was required as the 0,0 point of the lens was not a suitable scaling point due to being too far towards the anterior part of the lens. The scaling point was defined by utilising the internal thickness data of Dubbelman *et al.* (2003) to provide a translation value for moving from the 0,0 point of the lens outline (Equation 3.21).

$$Scale\ Translation = (T_{AC} + NucMiddle) - T_{Anterior} \quad (3.21)$$

Where

$$NucMiddle = T_N/2 \tag{3.22}$$

$$T_{Anterior} = \frac{Anterior\ Half\ Lens}{Posterior\ Half\ Lens} \times T_L \tag{3.23}$$

3.3.4 Summary

A range of different lens modelling methods have been detailed to date, both within FEA models of accommodation and for other purposes. To ensure that the proposed method for the current study was suitable (see Section 2.6) it needed to be able model a range of different age lenses both in accommodated and relaxed states, through the use of measurable parameters. In addition, the final lens shape produced needed to replicate the overall lens shape as seen *in vivo* well, and be adaptable to represent the internal structure variation. The proposed method detailed in the current sections met all these criteria.

3.4 Proposed capsule model

From the sources of thickness data discussed previously, the study of Barraquer *et al.* (2006) was selected for the modelling process due to the age related parameters defined. To define how the thickness at key points around the capsule varied with age Barraquer *et al.* (2006) used Equation 3.24, with the parameters needed given in Table 3.19.

$$CapsuleThicknessPoint = m2 \times Age^2 + m1 \times Age + n \tag{3.24}$$

Table 3.19: Capsule thickness parameters from Barraquer *et al.* (2006) for defining Equation 3.24.

Position on Capsule	Equation 3.24 parameters		
	n	m1	m2
Anterior pole (p0)	7.53	0.093	0
Anterior maximum (p45)	0.219	0.515	-0.004
Anterior minimum (p80)	8.535	-0.025	0
Equator (p100)	7.352	0	0
Posterior maximum (p120)	8.649	-0.046	0
Posterior pole (p200)	3.581	-0.009	0

A method of modelling an area which represents the capsule was created. Using the lens outline that

was detailed previously (Section 3.3), the thickness values defined using Equation 3.24 can be used to offset the lens outline to create an area within the outer lens shape. The first test of this showed that only using the six points defined in Table 3.19 resulted in an irregular line. Therefore, additional points around the capsule were required to ensure a smooth offset curve. To define these additional points the thickness values were plotted against relative position, as in Figure 3.1, and additional thickness values were interpolated from a fitted spline curve. To produce the capsule curve the normal-to line was found at each capsule thickness coordinate on the outer lens curve then, the thickness for this position could be found along the normal line to give a new coordinate, which could then be used to generate the curve (Figure 3.10).

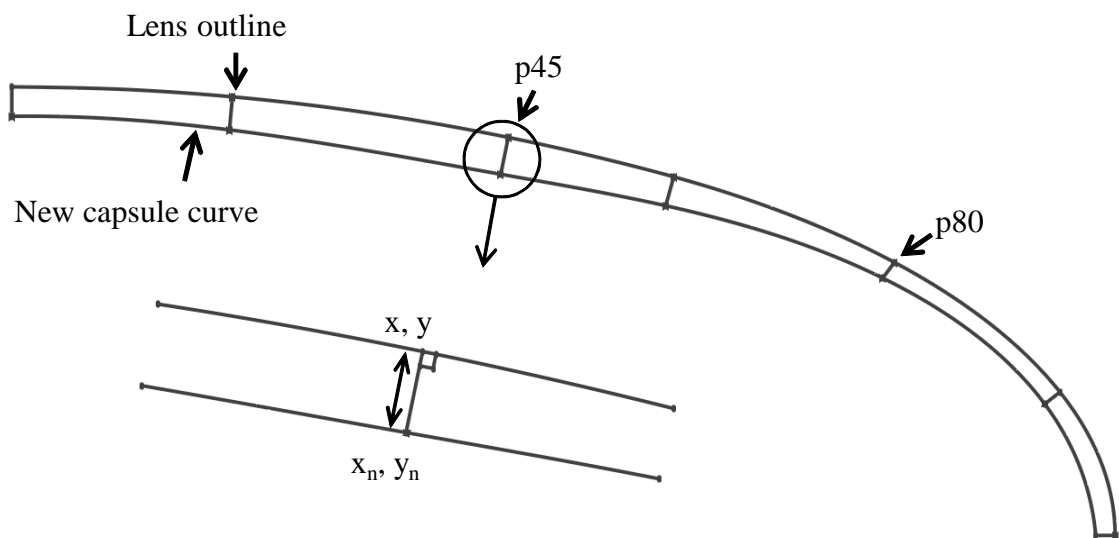


Figure 3.10: Illustration of the method used to define the capsule thickness variation. The anterior portion of a 40 YO lens is shown, with the capsule thickness increased by a factor of 10 for clarity. Detail is shown of the p45 thickness location, illustrating the perpendicular line used to generate a new set of x and y co-ordinates.

Using this method a unique capsule thickness can be defined for each age of lens modelled, ensuring consistency in the modelling methods. The method also allowed for custom thickness variation profiles to be defined, allowing for investigations into the capsule thickness to be conducted in future models.

3.5 Proposed zonule model

The weaknesses of existing zonular models have been discussed (Section 2.2.6) as well as the differing views on how the zonules may be arranged (Section 1.2.3.3). Using the existing data discussed in Section 3.2, a more comprehensive zonular model was developed.

3.5.1 Zonular Arrangement

To be able to model the zonular arrangement a better understanding of the arrangement of the zonules between the lens and ciliary body was needed, which would enable a hypothesis on the ciliary body attachments to be made, of which there was a lack of measured *in vivo* or *in vitro* data. The different arrangements in the literature have been discussed in Section 1.2.3.3 therefore, the key features that are most agreed will be detailed here before a general schematic of how the zonules can be arranged will be given.

In terms of lens attachments there was evidence for four attachment locations: anteriorly (AAZ, see Figure 3.2) (Sakabe *et al.*, 1998), at the equator (AEZ) (Ludwig *et al.*, 1999) and two posterior attachments (APZ1 and APZ2). The APZ1 attachment is located approximately the same distance from the equator as the AAZ attachment (Ludwig *et al.*, 1999), with the APZ2 attachment occurring at Weigers ligament closer to the centre of the lens (Nankivil *et al.*, 2009; Lütjen-Drecoll *et al.*, 2010).

Each of these anterior attachment regions have a corresponding attachment location on the ciliary body, with the AAZ, AEZ and APZ1 attachments running from the lens to the anterior ciliary body (ACB), whilst the APZ2 attachment appears to run to the posterior ciliary body (PCB) (Lütjen-Drecoll *et al.*, 2010), with a secondary attachment to the ACB. The most likely arrangement of the zonules, developed for the current study, is shown in Figure 3.11.

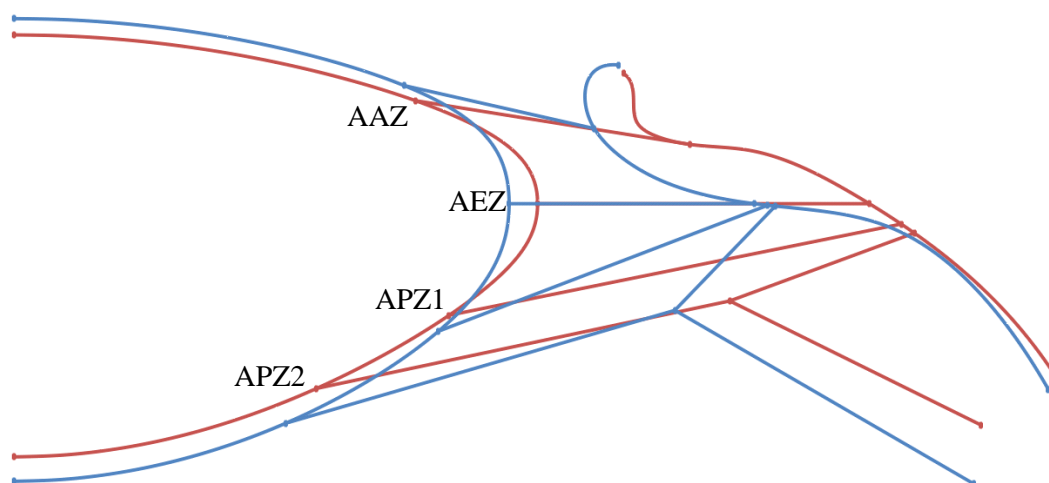


Figure 3.11: Proposed zonule arrangement based on analysis of the literature, showing the accommodated (Blue) and relaxed (Red) states. The schematic shows the four zonular bundles and the connections to both lens and ciliary body.

Compared to the existing methods of representing the zonular arrangement in FEA models (Section 2.2.4), the novel proposed arrangement allowed for a number of improvements. First, four zonular bundles were

proposed, adding the APZ2 zonule bundle to the established AAZ, AEZ and APZ1 bundles commonly used as a reflection of the *in vivo* data available. By adding the APZ2 zonule bundle, replicating the pull of the vitreous zonule, it was hypothesised that the movement of the lens will be controlled ensuring that the only loads and restraints needed on the model are the zonular displacements, improving on previous methods where artificial restraints were added to restrict anterior/posterior movement (see Section 2.4.1.1).

Second, each zonular bundle had a separate point representing the attachment to the ciliary body, rather than the typical single point. This allowed for the ciliary body points to be arranged in a manner that depicts the difference in movement between zonular bundles, as a result of both the anterior/posterior and radial movements of the ciliary body during accommodation (see Section 3.2.4.2). Previous models have been limited in either using a single displacement point or, if multiple points are used fixing them in a vertical, flat pattern (see Section 2.2.4). Overall, the proposed method ensured that the zonules were more representative of the *in vivo* structure than methods used in previous FEA models.

3.5.2 Attachment Points on Capsule

For the proposed model, attachment locations were needed for the AAZ, AEZ, APZ1 and APZ2 attachments. There was known data for the AAZ location (Sakabe *et al.*, 1998), and it was proposed that the AEZ was positioned on the widest point of the lens. However, a method of defining the posterior attachments was needed.

3.5.2.1 APZ attachment locations

Typically the APZ1 attachment has been positioned at the same distance from the equator as the AAZ (e.g. Burd *et al.*, 2002), an assumption followed here due to there being no direct measurements to dissuade this idea.

For the APZ2 attachment, assumed to adhere to Weiger's ligament (e.g. Nankivil *et al.*, 2009), a method of defining its position for multiple ages was needed. Weiger's ligament stems from the interface of the capsule and vitreous, meaning an assumption was made that it comes off tangentially from the capsule, based on the fact that the vitreous and capsule are in contact. Bergua & Kuchle (2002) illustrated the zone of wieger as covering a band of the posterior lens surface, extending from close to the first posterior attachment to a short distance from the posterior pole, as illustrated in Figure 3.12.

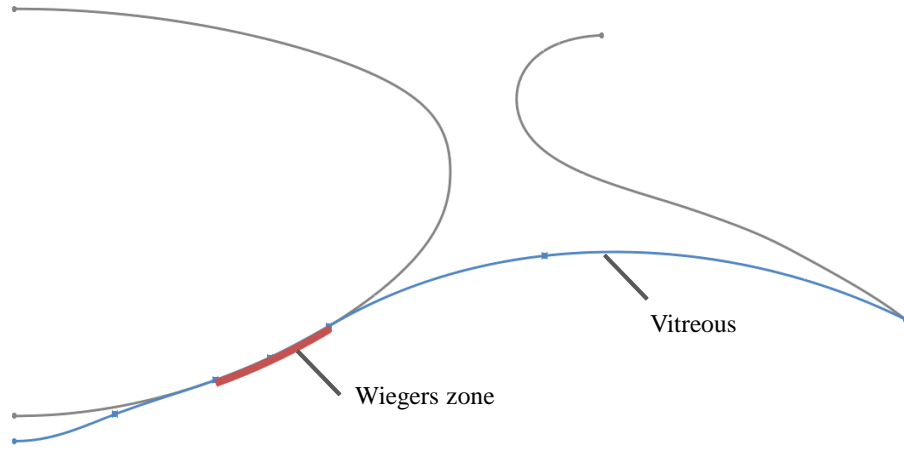


Figure 3.12: Illustration of the zone of Wieger, adapted from Bergua & Küchle (2002).

As an initial definition the location of APZ2 was defined as being halfway between the APZ1 attachment and the posterior lens pole. The AAZ equation was from Sakabe *et al.* (1998):

$$AAZ, APZ1 = (0.0079 \times A) + (0.202 \times L_D) - (0.041 \times Axial\ Length) + 0.0114 \quad (3.25)$$

$$APZ2 = \frac{L_R - APZ1}{2} \quad (3.26)$$

These definitions have been developed based on cadaver lenses, which could be assumed to represent the accommodated lens (see Section 3.2.2). It was assumed that these equations hold true for accommodated and relaxed lens states.

To define the axial length of the eye, Equation 3.27 was used, taken from Atchison *et al.* (2008):

$$Axial\ Length = 22.984 + 0.0113A \quad (3.27)$$

3.5.3 Attachment points on the ciliary body

As discussed previously, a model of the ciliary body was needed so that the zonular arrangement could be modelled effectively. A summary of the data that can be used to create the model will be given, before the actual model is detailed.

3.5.3.1 Ciliary body shape

As far as the author is aware, there has been one study that has used a model of the ciliary body in an FEA model (Stachs *et al.*, 2006). An approximation of the ciliary body was created based on UBM imaging, although there was only a representation of one eye and the zonules modelled did not replicate the more complicated arrangement that is proposed here. Therefore, a more comprehensive model was required.

The first step in creating the model was to define the basic shape of the ciliary body. A number of studies have imaged the ciliary body, with the most comprehensive images coming from Pardue & Sivak (2000) whose *in vitro* images give an idea of the whole shape, and Sheppard & Davies (2010) where the shape *in vivo* can be seen. The MRI images of Strenk *et al.* (1999) also provide a rough idea of the basic shape. From these, the basic shape of the ciliary body has the form shown in Figure 3.13.

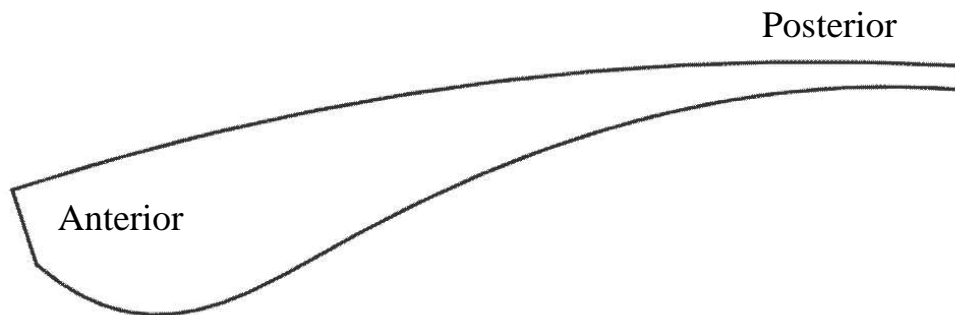


Figure 3.13: The basic shape of the ciliary body, based on images from Pardue & Sivak (2000), Strenk *et al.* (1999) and Sheppard & Davies (2010).

With the basic outline defined the measured thickness values can be applied, taken from the data discussed in Section 3.2.4.2. There were some differences in the measured thickness values, which was attributed to the different measurement methods (Section 3.2.4.2). Stachs *et al.* (2002) demonstrated how the ciliary processes can have an impact on the thickness of the ciliary body therefore, it was assumed that the measurements of Sheppard & Davies (2010) correspond to the underlying ciliary muscle, and the measurements of Ernst (2010) correspond to the total ciliary body including processes. Using this assumption to guide the creation of the model, any manipulation of the ciliary muscle values would alter the ciliary body shape.

3.5.3.2 Ciliary body position

Strenk *et al.* (2010) measured the distance between the ciliary muscle apex and the corneal apex, finding

that the distance decreased with age, which can be used to position the ciliary body vertically. The horizontal position can be defined through either the ciliary body ring diameter or the circumlental space, both of which have been measured (Kasthurirangan *et al.*, 2011; Richdale *et al.*, 2013). Measurements of the ciliary body ring diameter were not clear on where the measurements were made, therefore, the reduction of circumlental space was adapted. Kasthurirangan *et al.* (2011) stated a decrease of 0.43 mm between 20 and 60 years old (assumed to be a linear decrease), although this can be verified in the initial modelling phase (Chapter 6).

Finally, how the ciliary body is orientated needs to be defined. A composite of two MRI images from Strenk *et al.* (1999), showing an accommodated and unaccommodated ciliary body and lens, was made to consider how they are related which would allow the ciliary body to be angled correctly, establishing the dimensions required (see Figure 3.14).

3.5.3.3 Changes with accommodation

The base measurements (Table 3.10) would allow a model to be generated however, the individual measurements would need to be altered to show the changes that occur with accommodation. The two basic changes that occur are the thickening of the ciliary muscle and the movement of the ciliary body closer to the lens. Both thickness and movement have been measured, but the two sets of measurements do not combine together well.

In terms of thickness changes there are measured changes anteriorly, with no change reported for the posterior ciliary muscle. Based on the measurements of Sheppard & Davies (2010), the anterior thickness increases by 7.1 μm per dioptre of accommodation (0.071 mm for 10 D of accommodation), assuming a linear change.

When it comes to the movement of the ciliary body, the two main sources have been Strenk *et al.* (2006) and Stachs *et al.* (2002). Strenk's measurement of the diameter change in the ciliary body showed a large change (a mean value of 0.64 mm), but the measurement position is not clear. Stachs *et al.* (2002) reported a centre of gravity shift that was smaller (approximately 0.2 mm). Stachs also showed differences between movement with and without the ciliary processes.

Kasthurirangan *et al.* (2011) measured the circumlental space finding that it did not change with accommodation, with the ciliary body movement matching the change in lens diameter, which is approximately 0.05 mm per dioptre.

The increase in ciliary muscle thickness does not match with the assumed inwards movement however, one explanation of this is in the shape of the anterior portion of the ciliary body. MRI studies have not been detailed enough to give a really clear image of the ciliary muscle, which is why OCT images have been used. With these images the anterior portion of the ciliary body is not clear due to obstruction by the iris, hence most measurement of thickness come from 2 mm away from the scleral spur. In a study on Rhesus monkeys, Croft *et al.* (2009) showed a large movement in the anterior portion of the ciliary body, whilst the more posterior portions showed little change. If this same mechanism occurs in humans, which was assumed to be the case, the two sets of measurements could be combined into one model. Some evidence for this can be seen in the *in vitro* study of Pardue & Sivak (2000) where a clear bulge in the anterior portion can be seen. The measured muscle changes could also indicate a shift in muscle mass anteriorly, indicating an anterior bulge, unseen in OCT imaging. Sheppard & Davies (2010) hypothesised that the measured ciliary muscle changes in their study (increase in anterior thickness and decrease in length) indicate an anterior and inwards shift of the ciliary muscle that would support this idea.

3.5.3.4 Changes with age

The changes with age have been more widely agreed on (Section 3.2.4.2), therefore the thickness changes of Sheppard & Davies (2010) were used for the anterior change whilst posterior thicknesses remained constant. The distance between lens and ciliary body changes with age as according to Kasthurirangan *et al.* (2011). The contraction with accommodation was linked to the age related decline in lens diameter change with accommodation.

All the measured data combined allowed a CB model showing changes with age and accommodation to be created, which enabled the CB attachments to be modelling in a more complex manner than in previous FEA studies.

3.5.4 Constructing the model

The basic outline was given in Figure 3.13 and this can be supplemented with the data summarised previously. Table 3.20 summarises all the parameters needed to define the ciliary body model, along with their definitions.

Figure 3.14 shows the MRI composite used to combine the basic outline with a representation of the lens in SolidWorks, allowing the orientation of the ciliary body to be defined by angles between the equatorial

line and the CMT lines.

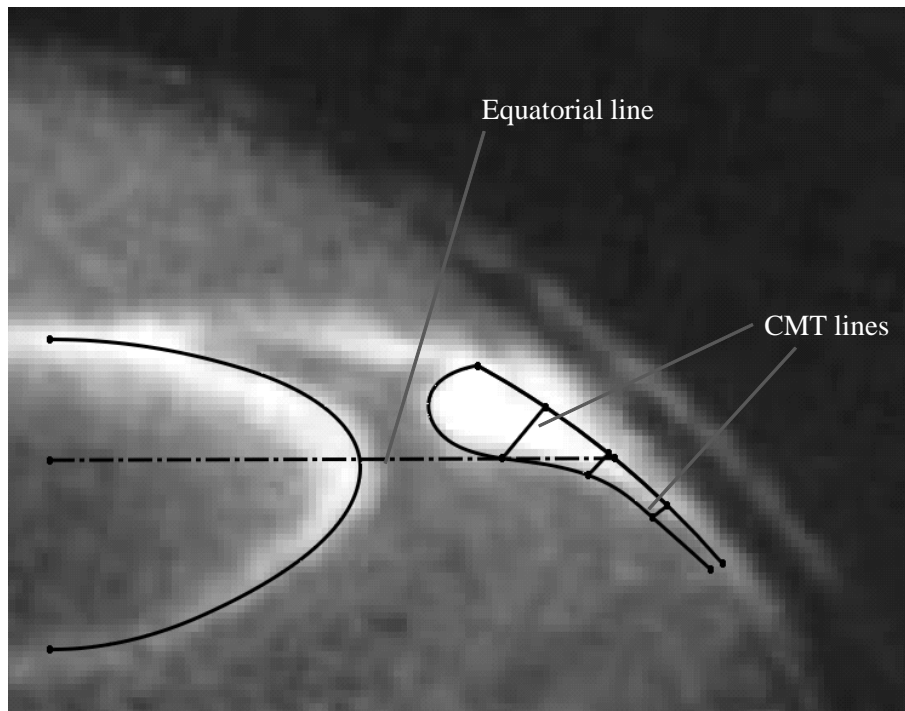


Figure 3.14: Illustration of the method used to orientate the ciliary body model, using the equatorial line and CMT (Ciliary muscle thickness) lines. The MRI image was adapted from Figure 1 of Strenk *et al.* (1999).

With the orientation defined the values defining the distance from the lens equator, the vertical distance from the cornea and the thickness changes with accommodation (as they are relative to the lens) were applied (Figure 3.15). Once this was established, all the parameters could be varied for age and accommodation to create a ciliary body model for use in generating the zonular arrangement.

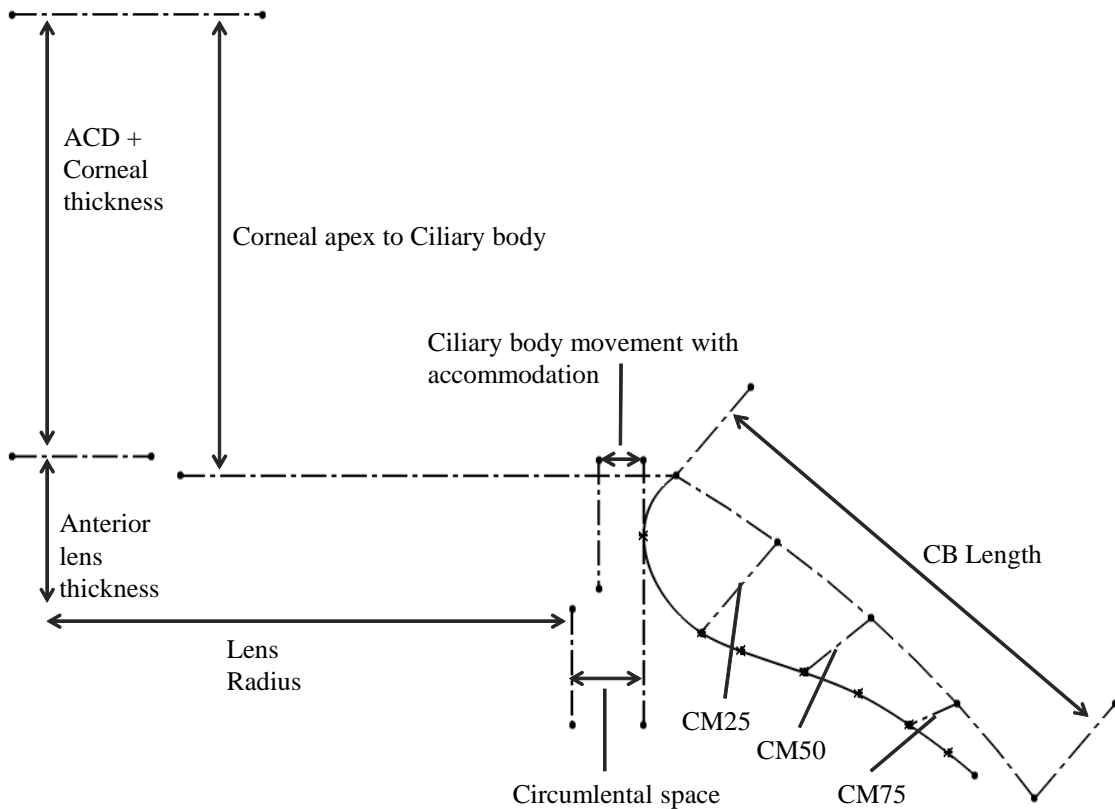


Figure 3.15: Proposed ciliary body model with defining parameters shown.

3.5.5 Final zonule arrangement

With a ciliary body model defined, the final zonule arrangement proposed previously could be fully defined. The first stage of this was to model the lens attachment locations, using the equations from Section 3.5.2. The next stage was to define the direction of travel. At this stage two methods were proposed, which would be tested in Chapter 6 to establish which method was appropriate as to date no measurements of the angle of attachments had been made. The first method was based on the AAZ, APZ1 and APZ2 zonules attaching to the lens tangentially, an assumption based on the fact that when the lens is in its accommodated form the zonules are positioned in their most expanded state, pulling on the lens. The second method was based on the zonules attaching in a more horizontal position, therefore, an angle of 4 degrees was defined between the tangent line and zonule line.

For the APZ2 zonule the zonule does not run straight from the lens to the ciliary body instead, *in vivo* the zonule has been shown to pass over the vitreous and attach to the posterior ciliary body, pinned by a zonule running from the anterior ciliary body (Section 1.2.3.3). For modelling in FEA only the section running from the lens to the “pinning” zonule was needed. As an initial method the pinning zonule was positioned

Table 3.20: Parameters needed to build ciliary body model shown in Figure 3.15.

Parameter	State		Source
	Relaxed	Accommodated	
Axial Length (AL)	$22.984 + 0.0113A$	-	Atchison <i>et al.</i> (2008)
L_D	$9.3609 - 0.0047A$	$(9.3609 - 0.0047A) - (0.067 \times \text{AccAbility})$	Strenk <i>et al.</i> (1999); Jones <i>et al.</i> (2007)
AAZ, APZ1	$(0.0079A) + (0.202L_D) - (0.041AL) + 0.0114$		Sakabe <i>et al.</i> (1998)
APZ2	$((\frac{L_D}{2}) - APZ1) \times 0.33$		-
CMT1	$((0.0035A) + 0.427) + 0.603$	$((0.0035A) + 0.427) + 0.603 + (0.0071 \times \text{AccAbility})$	Strenk <i>et al.</i> (2010); Ernst (2010); Sheppard & Davies (2011)
CMT2	$0.313 + 0.517$		
CMT3	$0.171 + 0.329$		
Ciliary muscle length	4.63	$4.63 - 0.065A$	Sheppard & Davies (2010)
ACD	$-0.0215A + 4.351$	-	Koretz <i>et al.</i> (2004)
Corneal thickness		$0.5667 - 0.00077A$	Atchison <i>et al.</i> (2008)
Anterior shift	-	0.05	Sheppard & Davies (2010)

by a line running tangential from the lens to the ciliary body. The pinning zonule was then formed from a line running perpendicular from the ciliary body at that point (Figure 3.16). The length was defined by eye initially, allowing the APZ2 zonule to be defined. Further refinement will be carried out in Chapter 6.

With the direction defined, the ciliary body attachment locations need to be defined. The AEZ was attached to the lens equator at an angle, which was visually chosen to represent a ciliary body attachment between the AAZ and APZ1 attachments.

The zonule arrangement was needed to estimate the displacement values of the zonules. To define these values, the accommodated and relaxed zonules were modelled. To define the ciliary body attachment points for the relaxed zonules, the angle of attachment was visually adjusted, depending on the assumed thickness change the lens would undergo. For example, in a young lens with a large thickness change the relaxed zonules were assumed to be almost horizontal, whereas in an old lens there would not be much change from the accommodated state.

To define the zonule coordinates and displacement values, the accommodated lens was shifted vertically so that the differences in anterior thickness between accommodated and relaxed lenses was three times that of the posterior thickness difference (Section 3.2.2.1). The zonules were then positioned, allowing the displacement values to be defined.

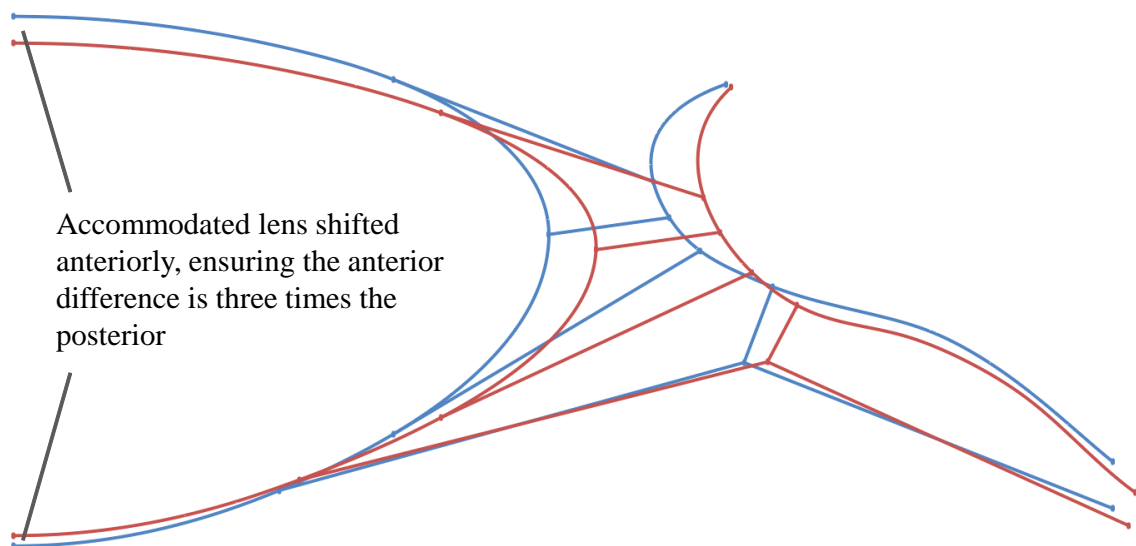


Figure 3.16: Final zonular arrangement where the blue outlines represent the accommodated model and the red lines represent the relaxed model. The anterior shift of the accommodated lens is highlighted.

3.5.6 Zonule thickness

The final aspect of modelling the zonules was the thickness of the zonular bundles and the connection between the zonules and the lens. As discussed previously, the zonules are made of bundles of zonular fibrils, which interlace with the capsule and lens epithelium. The thickness of the zonular fibres has been measured to be between 6 and 60 μm , made up of smaller fibrils that have been measured as being between 10 nm and 1 μm (Section 3.2.4.3). These fibres are bundled into groups which vary in number (and therefore thickness) between the different zonular groups (AAZ, AEZ, APZ). The bundles insert into the capsule, although the size of the insertion area varies between the different insertion regions. With the ambiguity over what the thickness of the different regions should be, different models will be simulated in ANSYS to ensure appropriate values are selected, which will be covered in Chapter 6.

3.5.7 Summary

The combination of a novel zonule arrangement model and ciliary body model allows for a more complete description of the zonular displacement to be defined, ensuring that induced deformations are likely to be more representative of the changes seen *in vivo*. The methods also allowed for multiple ages to be modelled, ensuring consistency with the proposed lens and capsule models. Finally, the methods could be adapted to explore the importance of the attachment angles and ciliary body position and movement, ensuring that the complete accommodative geometric model is capable of exploring accommodation and presbyopia in detail.

Chapter 4

Material Properties

4.1 Introduction

Chapter 2 gave a brief introduction to the material properties that have been used in previous FEA models. The current chapter will explore the various sources of data that have been used in more detail before highlighting the initial properties to be used in the proposed accommodation model. An overview of how a materials behaviour can be defined will be given in addition to a summary of the main constitutive models relevant to the current study.

4.2 Defining Material Behaviour

Material properties are used to quantify how a material reacts under different loading conditions. For the purposes of the current investigation the properties related to the elasticity of a material are relevant.

An elastic material will deform under external loads, but once those loads are removed the material will return to its original state, due to the internal forces in opposition to the external loads. There are a number of different elastic moduli which can be used to define an elastic material and three moduli are commonly used: the elastic modulus (E), sometimes referred to as the Young's modulus, the shear modulus (G) and the bulk modulus (K). These three constants can be related using Equation 4.1, where ν is the Poisson's ratio. For isotropic, linearly elastic behaviour, two independent moduli are required.

$$E = 2G(1 + \nu) = 3K(1 - 2\nu) \quad (4.1)$$

For materials that are assumed to be incompressible, such as the crystalline lens, the Poisson's ratio approaches 0.5 (Section 2.3.1).

Deformations with linear isotropic materials are simple to define as stress is related to strain by a constant, the stiffness of the material. However, the materials relevant to this study are typically more complex, as they usually exhibit non-linear behaviour with evidence for there being anisotropic properties as well. In addition, linear materials are often assumed to have small strains which are not seen in the accommodative components. Therefore, the constitutive model relevant to accommodation will need to represent non-linear effects and large strain, with the potential for anisotropy.

4.2.1 FEA Representation

To be able to describe how a material will behave in an FEA simulation, constitutive equations are used to relate stress to strain, using material properties (or parameters). Section 2.3 covered the models that have been used previously, with the most basic model being the linear elastic constitutive model where stress (σ) is related to strain (ϵ) by:

$$\{\sigma\} = [D]\{\epsilon\} \quad (4.2)$$

Where D represents a stiffness matrix (for an axisymmetric model):

$$\begin{bmatrix} \sigma_r \\ \sigma_z \\ \sigma_\theta \\ \tau_{rz} \end{bmatrix} = \frac{E}{(1+\nu)(1-2\nu)} \begin{bmatrix} 1-\nu & \nu & \nu & 0 \\ \nu & 1-\nu & \nu & 0 \\ \nu & \nu & 1-\nu & 0 \\ 0 & 0 & 0 & \frac{1-2\nu}{2} \end{bmatrix} \begin{bmatrix} \epsilon_r \\ \epsilon_z \\ \epsilon_\theta \\ \gamma_{rz} \end{bmatrix} \quad (4.3)$$

The ideal approach for the accommodative components would be to use a fully anisotropic model, however, as will be shown in the current Chapter, there was insufficient data to fully determine the required parameters.

A more appropriate method is to use hyper-elasticity, which is a method of modelling materials that have a non-linear stress strain relationship, but are elastic, isotropic and incompressible. The neo-Hookean hyper-elastic constitutive model is represented by two material parameters, μ and k , which are equivalent to G and K at small strains. Adopting this constitutive model for accommodative components will therefore allow measured material parameters discussed in this Chapter to be utilised. The strain energy function is

given in Equation 4.4, with the relationship between d and k given in Equation 4.5.

$$W = \frac{\mu}{2} (\bar{I}_1 - 3) + \frac{1}{d} (J - 1)^2 \quad (4.4)$$

$$d = \frac{2}{k} \quad (4.5)$$

4.2.2 Units

ANSYS is a dimensionless system; therefore, all inputs need to be consistent. The methods used for generating the geometry of the proposed models have utilised mm for definitions therefore, all material properties also need to be in terms of mm. In the literature, a range of units have been used to describe material parameters therefore, in the comparison sections in the current chapter the units will be standardised. In the final model, all units will be converted to be based on mm.

4.3 Measured Data

Compared to the measurements that have been made of the geometric parameters of the accommodative components, there was a paucity of data on the material properties. Table 4.1 gives an overview of the principal studies relevant to the current study, with an overview of the methods and subjects used.

To be able to develop an FEA model of the accommodation system that can investigate presbyopia, an understanding of how the material properties change with age is needed therefore, those studies that provide age related data are of particular interest.

4.3.1 Crystalline lens material properties

The studies into the material properties of the crystalline lens will be discussed in terms of the material testing method utilised, detailing the primary findings and their relevance to the current study, before an overall comparison between the findings is given.

4.3.1.1 Lens Spinning

The lens spinning test was pioneered by Fisher (1971) as an alternative to compression tests on lenses, due to the lens fibres being less disrupted by spinning. The principal was that the lens was spun about its axis

Table 4.1: Summary of studies measuring the material properties of the accommodative components. All studies are *in vitro*, unless stated otherwise. *indicates diabetic samples **indicates cataract samples.

Study	Component Tested	Number of Samples	Age Range (Years)	Method
Fisher (1971)	Lens	40	0.4 - 67	Spinning
Beers & Van Der Heijde (1994)	Lens (<i>in-vivo</i>)	24	15 - 44	Velocity of Sound
Glasser & Campbell (1999)	Lens	19	5 - 96	Compression
	Lens (De-capsulated)			
Subbaram <i>et al.</i> (2002)	Lens	19	30 - 64	Brillouin light scattering
Heys <i>et al.</i> (2004)	Sectioned Lens	18	14 - 76	Indentation
Weeber <i>et al.</i> (2005)	Sectioned Lens	39	18 - 90	Compression
Hollman <i>et al.</i> (2007)	Lens	3	40	Bubble based acoustic force
		9	63 - 70	
Weeber <i>et al.</i> (2007)	Sectioned Lens	10	19 - 78	Indentation
Bailey <i>et al.</i> (2010)	Lens	29	30 - 70	Brillouin light scattering
Reißet <i>et al.</i> (2011)	Lens	1	70	Brillouin light scattering
Sharma <i>et al.</i> (2011)	Lens	44	17 - 24	Compression
		16	18 - 36	Shear Displacement
Schachar <i>et al.</i> (2011)	Nucleus	52		
		117		
Wilde <i>et al.</i> (2012)	Lens (De-capsulated)	117	12 - 87	Spinning
Chai <i>et al.</i> (2012)	Lens Nucleus	22	34 - 63	Spinning
Fisher (1969)	Capsule	-	-	Biaxial Inflation
Krag <i>et al.</i> (1997)	Capsule (Anterior)	67	0.7 - 98	Uniaxial Loading
Krag & Andreassen (2003b)	Capsule (Posterior)	25	1 - 94	Uniaxial Loading
		15	58 - 96	Inflation
Pedrigi <i>et al.</i> (2007)	Capsule	6	29 - 81	Biaxial Inflation
		6	44 - 77*	Biaxial Inflation
Ziebarth <i>et al.</i> (2011)	Capsule (Anterior)	18	33 - 79	AFM
Choi <i>et al.</i> (2012)	Capsule (Anterior)	8	59 - 85**	AFM
Fisher (1986)	Zonule	-	15 - 45	Stretching
Assia <i>et al.</i> (1991)	Capsule and Zonule	40	52 - 85	Manual Stretch
Van Alphen & Graebel (1991)	L,C,Z,CM,Choroid	13	0 - 80	Uniaxial Loading
Manns <i>et al.</i> (2007)	L,C,Z,CB,Sclera	20	1 - 78	Stretching
Michael <i>et al.</i> (2012)	Zonule	16	47 - 97	Stretching

at a set speed, which would cause the lens to decrease in thickness while increasing in diameter. These changes can be related to the spinning force, which can be seen to approximate the forces experienced in accommodation. The deformations were captured through photography so that the estimations of the Young's modulus across the lens could be made. The material properties obtained using this method can also be utilised in the constitutive models proposed in Section 4.2.

Fisher calculated the Young's modulus in the polar and equatorial regions of the lens, based on the changes in thickness and diameter respectively. The calculations were carried out assuming that the lens could be approximated by an infinite number of homogenous disks spinning about their axis, each with a Poisson's ratio of 0.5. The nucleus was approximated as a spherical structure within the cortex and the interface between the nucleus and cortex was assumed to only be partly attached, and the capsule was assumed to have little or no effect on the lens. Fisher's results showed that the nucleus stiffness remained stable until about 35 years old, where it then began to increase. The cortex increased with stiffness until the age of 40 to 50 years old, where it began to decrease. The cortex was consistently stiffer than the nucleus, until the age of 70 where both nucleus and cortex had the same stiffness.

A detailed analysis of Fisher's test was carried out by Burd *et al.* (2006) which showed that there were a number of modelling errors made by Fisher. The main issues were with the spinning disks model, which led to wrong estimations of the ratio of the Young's modulus for the nucleus and the cortex, and the ignoring of the capsules effects in the analysis. This led to a new spinning test being proposed (Burd *et al.*, 2011), which would eliminate the erroneous assumptions made by Fisher. The model was used by Wilde (2011) to establish a new set of stiffness values for the lens.

The new test had two main improvements over Fisher's experiment. Firstly, the imaging systems were able to synchronise image capture so consistent images could be obtained, as well as reducing image blur. Secondly, the spinning tests were conducted on de-capsulated lenses, reducing the complexity of obtained stiffness values. To obtain the stiffness values an FEA model was used, replicating the spinning test, where the initial outlines of the lens samples were input from photographs then stiffness values were varied until the deformed outlines matched the imaged deformation. This was done with three different descriptions of the stiffness distribution within the lens: a homogenous model, a nucleus-cortex model and an exponential model. The results showed that the stiffness of the lens increases with age. The homogenous profile showed a very slow increase up until approximately 25 YO, before a linear increase up to 60 YO. The nucleus-cortex and exponential profiles both showed the stiffness in the nucleus region was initially lower than the cortex, until around 45 YO when this reversed. The exponential model showed

a much higher central stiffness in the older lenses than either of the other models.

A further experiment was carried out by Chai *et al.* (2012), using the same procedures as Wilde *et al.* (2012), but only on lens nuclei. The results followed the same trends as the nucleus-cortex models used by Wilde *et al.* (2012) with the results showing an exponential increase in stiffness of the nucleus with age, although no younger lenses were tested.

4.3.1.2 Lens indentation

A different approach to spinning whole lenses has been to use indentation tests on lens sections. Conducting these tests allows for detailed information on the material properties of the lens structure, although it does cause localised disruption of the lens substance. The method does allow for the stiffness in different regions of the lens to be tested across a range of ages, providing suitable material parameters to be used in the proposed constitutive models.

Heys *et al.* (2004) used indentation tests on cores taken from lens samples to establish the shear modulus across the lens. The results showed an increase in stiffness in both the lens centre and periphery with age, although the increase at the centre was higher (450 times compared to 20 times). The stiffness profile in a young lens indicated that the shear modulus at the centre of the lens was slightly higher than at the periphery, which reversed in the old lens with the periphery being much higher than the centre. There are a number of issues with the testing by Heys *et al.* (2004) which could have an impact on results. First, the equations used assume the lens is an incompressible, isotropic elastic material; second, the lens samples were frozen; third, the displacement of the indenter was described as being approximately 0.75 mm, a substantial indentation in a half of a lens (approximately 2 mm) which would appear to cause strains that would cause rupture within the lens (Wilde *et al.*, 2012); and finally, the most peripheral of measurements were carried out at a distance of 3.5 mm, which is a lot less than the actual lens periphery (which approaches 4 – 4.5 mm, see Section 3.2.2.2).

A later test on non frozen lenses was carried out (Heys *et al.*, 2007) reporting stiffness values for the nucleus region of the lens only. The results indicated that non frozen lenses were stiffer than frozen ones, but that a similar age related increase in stiffness was observable as in Heys *et al.* (2004). Measurements were also carried out on lenses that had been heated, finding that the shear modulus increased with heating.

Another indentation study was carried out by Weeber *et al.* (2007), where whole lenses were halved along the equator before indentation. It was found that the centre of the oldest lens was a 1000 times stiffer than

the youngest, whilst the periphery was 100 times stiffer. In the younger lens, the centre was softer than the periphery but this reversed with age. As with Heys *et al.* (2004), the lenses were frozen prior to the tests being carried out which, as discussed can impact on results. In addition, the correction factor used to correct for the disturbance caused by the indenter was not certain to cause appropriate adjustments to the measured properties.

4.3.1.3 Lens compression and shearing

The simplest methods of measuring a materials stiffness are to use a stretching or compression test, relating the force used to deform the sample to the displacements caused. In relation to the crystalline lens, compression tests have principally been used to look at the viscosity of the whole lens and have not provided data suitable for use in the proposed constitutive models however, the results can be used to support findings from other tests. Both Glasser & Campbell (1999) and Sharma *et al.* (2011) conducted compression tests on whole lenses across a range of ages, finding that the amount of resistance that the lens gave to compression increased with age. Sharma showed that de-capsulated lenses had less of an increase in resistance with age than en-capsulated lenses.

Weeber *et al.* (2005) performed alternate compression tests using dynamic mechanical analysis (DMA) on lens sections across a range of ages. The study found that the viscosity of the lens increases with age; however, the whole lens was assumed to be isotropic and homogenous as well as the samples used being frozen. In an effort to compare with the results of Fisher (1971), the Young's modulus was calculated to be 2 kPa for a 40 YO lens which was similar to the results of Fisher.

Schachar *et al.* (2011) conducted a shearing deformation test on both lens nucleus and cortex samples. The results showed that the mean elastic shear modulus was lower than the mean viscous shear modulus, indicating that lenses under 40 YO can be described as being over damped. The results seemed to show no difference between the material from nucleus and cortex samples. A small increase in shear modulus was seen with age, although the authors believed that this was not enough to account for the accommodation decrease seen across the same age, hypothesising that the accommodative decrease is due to an increase in equatorial diameter (see Section 1.2.2 for Schachar's theory of accommodation).

4.3.1.4 Acoustic methods

Hollman *et al.* (2007) obtained Young's modulus data from whole lens samples using a femtosecond laser to create micro bubbles at various radial distances within the lenses. A two element ultrasound transducer was then used to apply an acoustic radiation force to the bubbles, with the resultant displacements measured by the second element. The results indicated that the Young's modulus of a middle aged lens was consistent across its width, whilst in an old lens the Young's modulus declines from the lens centre to the periphery. The results for human lenses had a large amount of variation, not seen in tests on porcine lenses, but the reasons for this were not known.

4.3.1.5 Brillouin Light Scattering

A final method of obtaining material properties of the crystalline lens is Brillouin light scattering (BLS), which uses the interaction between light and acoustic modes within a medium to obtain its material properties, used in establishing values of the bulk modulus in the crystalline lens, relevant for the proposed constitutive models of the lens. Bailey *et al.* (2010) used this method and found that the bulk modulus of the nucleus was greater than the cortex, but neither was age dependant; the measurements were carried out along the central axis of the lens. The method relies on the refractive index being defined, in this case two distinct values for the nucleus and cortex, which if not defined accurately could have an impact on results. A single *in vitro* lens study by Reißet *et al.* (2011) found similar results with the bulk modulus higher in the nucleus than the cortex, with similar results found by Scarcelli & Yun (2012) in the first *in vivo* use, although there was no distinction between nucleus and cortex. BLS was also used by Subbaram *et al.* (2002) where the average bulk modulus of the nucleus was higher than the cortex, although the methods were not examinable.

4.3.1.6 Comparison of results

Each method of mechanical testing obtains the material properties of the lens in different positions and orientations. For example, indentation tests measured properties axially approximately halfway through the lens, whereas the spinning tests calculated material properties in the anterior and equatorial positions of the lens as shown in Figure 4.1. The differing measurement positions will have an impact on the measured properties if, as expected, the lens exhibits anisotropic material behaviour.

In addition, the material property values calculated are dependent on the constitutive models assumed in

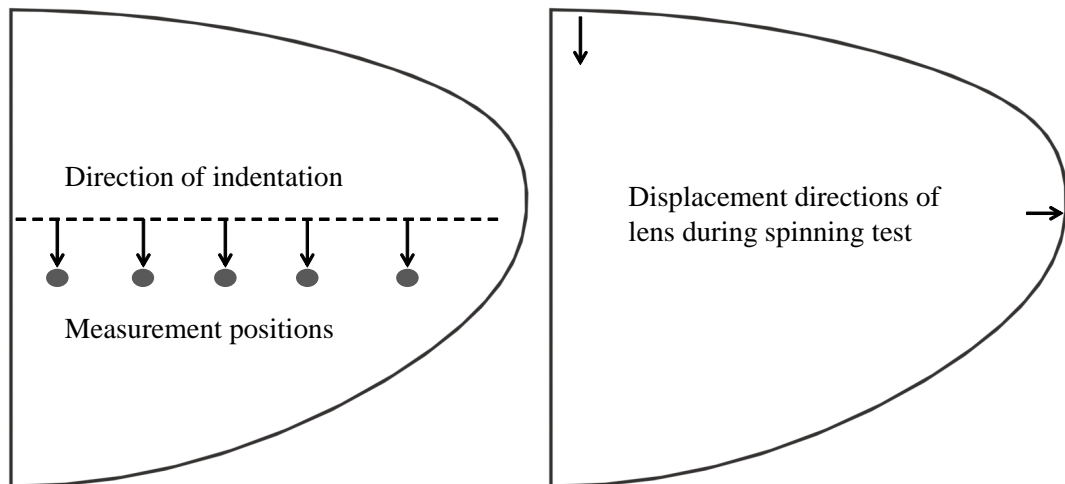


Figure 4.1: Illustration of the measurement positions within the lens in indentation studies (Left) and the locations and displacement directions used in measurement in spinning lens studies (Right).

the individual tests (e.g. an isotropic elastic material as used by Heys *et al.*, 2004), which will also impact on results if no anisotropy is assumed. Therefore, the comparisons made are to investigate the relative changes with age and measurement position within the lens. For consistency, the results from each study were standardised to shear modulus values in Pa, with any conversion calculated using Equation 4.1 and assuming a Poisson's ratio of 0.49. For those studies that provide data on positions within the lens, the data was based on relative position with the lens diameter defined as according to Rosen *et al.* (2006) (see Table 3.3).

The comparison between studies will be completed in stages. First, those studies that analysed the variation in properties across the lens (e.g. Weeber *et al.*, 2007 and Wilde *et al.*, 2012) will be compared. Second, those that provide data on properties in the nucleus and cortex (e.g. shear modulus data Fisher, 1971 and bulk modulus data Bailey *et al.*, 2010) will be compared.

Stiffness Gradient

Figure 4.2 shows a comparison between the stiffness gradient results of Weeber *et al.* (2007) and Wilde *et al.* (2012). Heys *et al.* (2004) also gave some representative results for a middle aged and old lens in terms of Young's modulus and radial position. The stiffness profiles of Weeber *et al.* (2007) were taken from their Figure 7, manually fitted by the author to be replicated in Figure 4.2 (see Section 4.4.1 for further detail on the manual fitting).

There are some general aspects which all studies agree on; first, that the shear modulus increases with age; second, that the variation of the shear modulus alters with age; and finally, in an older lens, the inner part

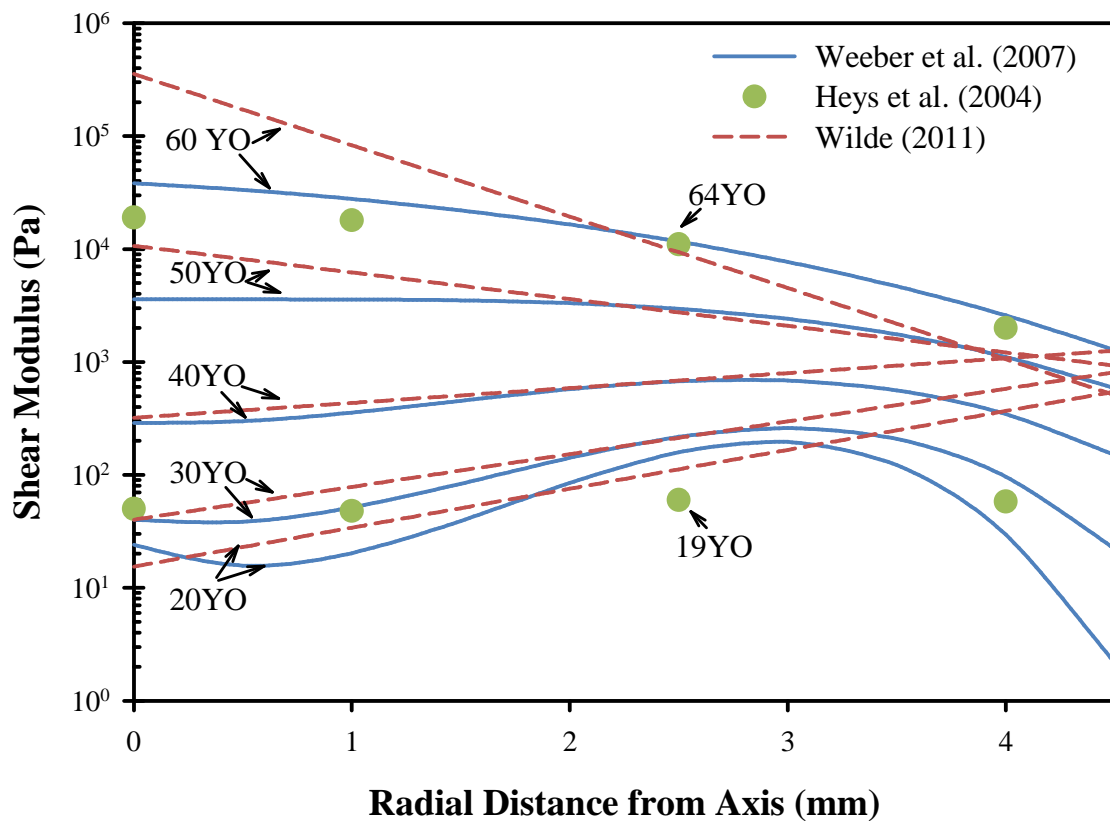


Figure 4.2: Comparison of the variation in shear modulus with radial position.

of the lens has a higher shear modulus than the outer portion.

Where these studies varied was in how the shear modulus varies with position. Heys *et al.* (2004) showed limited variation in the younger lens, where the shear modulus was consistent with position. Weeber *et al.* (2007) showed a much more varied stiffness profile, whereas Wilde *et al.* (2012) showed an increase across the lens. With the increase in age however, Weeber *et al.* (2007) showed a smoother change across the lens with a reversal of the difference in shear modulus. The fits used by Weeber *et al.* (2007) were to illustrate general trends with the data showing a large amount of variation, indicating that the curves in Figure 4.2 may not be representative of the exact stiffness profile.

As discussed, the results of Wilde *et al.* (2012) seemed to show a particularly high shear modulus for the centre of an old lens, whilst also showing no change from a younger lens at the periphery. As a result of the higher shear modulus values in the centre, Wilde proposed that for an older lens the material properties should only be represented by nucleus and cortex regions. Another aspect of interest is the shear modulus values of the 50 and 60 YO lens at the very edge of the lens, where they are a lot lower than in younger lenses, indicating a reduction in stiffness with age, which will need consideration when modelling.

Nucleus-Cortex

Figure 4.3 shows a comparison between those studies where the shear modulus was measured for the nucleus and cortex. The age related changes in the nucleus and cortex as defined by Wilde (2011) using their model D are also shown

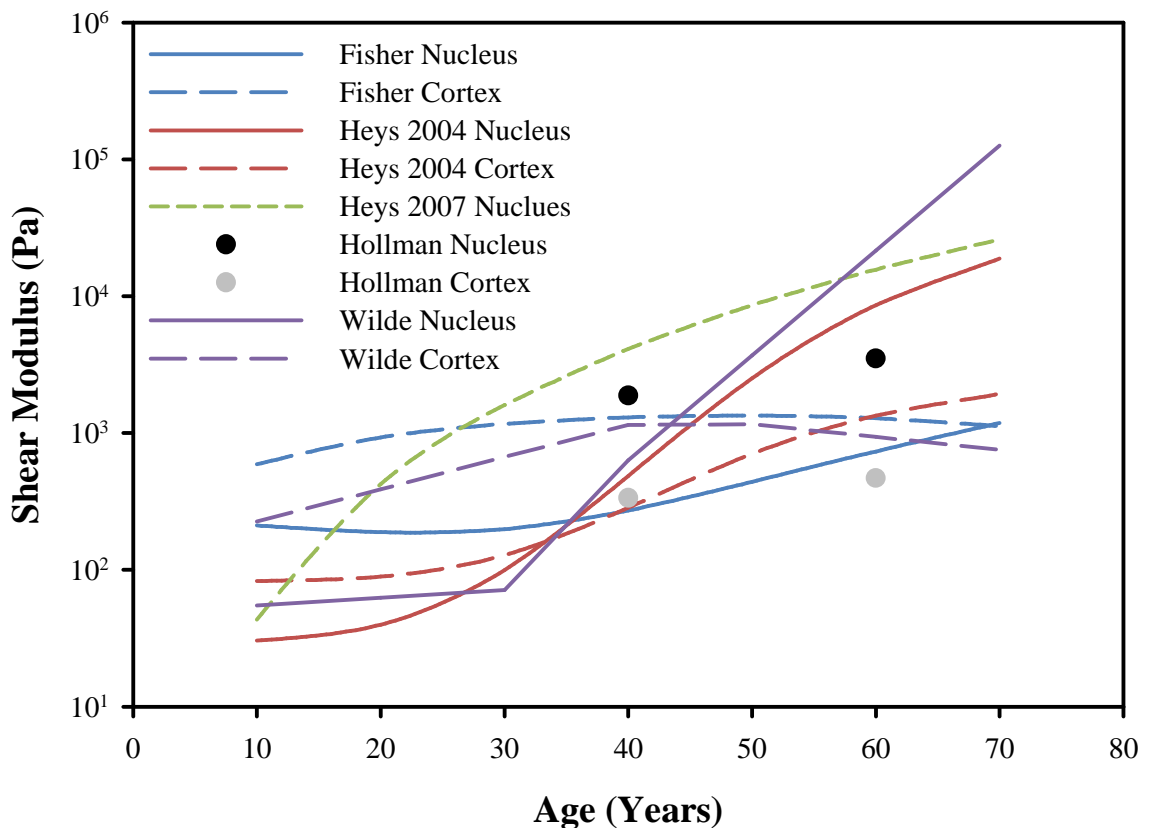


Figure 4.3: Comparison of studies that measured nucleus and cortex properties.

Overall, there appeared to be agreement that the nucleus stiffens with age, although the rate of stiffness increase varies. It would appear there is a general agreement between studies that the cortex has an initial stiffness increase before it begins to stabilise or decline, again with different rates of stiffness increase. Finally, the nucleus appears to initially have a lower stiffness than the cortex, but this reverses with age. The differing rates of stiffness increase are likely due to the difference in measurement methods and assumptions made on constitutive models, as discussed previously.

The main disagreement between studies is in the age at which the nucleus becomes stiffer than the cortex; the results of Fisher (1971) indicated that it was not until 70 YO whilst Heys *et al.* (2004) showed that the nucleus becomes stiffer than the cortex around 35 YO, Wilde *et al.* (2012) (model D) showed it was approximately 44 YO with Hollman *et al.* (2007) having all measurements illustrate the nucleus is stiffer

than the cortex.

To compare to the stiffness gradient results, the relationship of Heys *et al.* (2004) matches that of Weeber *et al.* (2007) and Wilde *et al.* (2012) (model E), where in younger eyes, the nucleus is less stiff than the cortex, but with age, this reverses.

Bulk Modulus

In addition to those studies that measured the shear modulus of the nucleus and cortex, the work of Bailey *et al.* (2010) and Subbaram *et al.* (2002) established bulk moduli values for the same regions, both finding that the bulk modulus was higher in the nucleus than the cortex, although no age related changes were seen.

As a comparison, the shear modulus measured in other studies could be used to calculate the bulk modulus, assuming the material is isotropic, using Equation 4.1. The nature of this relationship dictates that the accuracy of the Poisson's ratio is important, i.e. the closer to 0.5 the ratio approaches, the larger the difference between shear and bulk moduli. To ensure a consistent comparison, a Poisson's ratio of 0.49999 was chosen for all conversions. Table 4.2 gives a comparison between the direct measurements of bulk modulus to two methods of calculating the bulk modulus from measured shear moduli.

Table 4.2: Comparison of Bulk modulus values from the literature. N = Nucleus, C = Cortex.

Study	Lens Area	Bulk Modulus (Pa)		
		20 YO	40 YO	60 YO
Bailey <i>et al.</i> (2010)	N	2.790E+09	2.790E+09	2.790E+09
	C	2.360E+09	2.360E+09	2.360E+09
Subbaram <i>et al.</i> (2002)	N	3.790E+09	3.790E+09	3.790E+09
	C	2.800E+09	2.800E+09	2.800E+09
Wilde (2011)	N	2.694E+04	4.239E+05	5.129E+04
	C	3.146E+05	1.062E+06	7.543E+05
Wilde (2011)	N	1.347E+06	2.120E+07	2.564E+09
	C	1.573E+07	5.310E+07	3.771E+07

It can be seen from Table 4.2 that studies that measured the bulk modulus directly found higher bulk moduli values than when the bulk modulus was calculated from measured shear modulus values. As a result, the specification of the bulk modulus will require careful consideration.

4.3.2 Capsule

Compared to the lens, there were fewer studies that have been used as a source in defining the capsule material properties in FEA models (Section 2.3.2), however, the capsule's material properties have been

studied extensively.

4.3.2.1 Inflation

Fisher (1969) clamped 4 mm diameter anterior capsule sections to allow them to be deformed under fluid pressure. The elastic modulus could be calculated from the relationship between applied pressure and volume; assuming first that the capsule behaves in a linear elastic manner, second, the strains applied in each axis would be equal, and finally, the capsule thickness would remain constant. The results showed that the Young's modulus decreased with age in an almost linear fashion.

Danielsen (2004) used a similar method to Fisher (1969), also assuming that the capsule was isotropic and had a constant thickness. Stress and stiffness were calculated at a strain value of 0.1 and the values found were higher than in Fishers test, although the values calculated for maximum stress at rupture were comparable.

Pedrigi *et al.* (2007) performed another inflation test, but using a different method. In this case, the lens was removed whole from the eye. A number of micro spheres were then placed on the anterior portion of the eye, which would be used to record displacement using a video camera. The displacement was caused by fluid pressure, with the fluid injected at the joint of the capsule and cortex. The displacement of the micro spheres was measured and combined with an FEA model to establish hyper-elastic material properties, with the regional variation around the capsule taken into account. It was established that the capsule exhibited non-linear and anisotropic behaviour, and it was found that the stiffness in the circumferential direction increased over the meridional direction, the closer to the equator the measurements were made.

4.3.2.2 Stretching

Assia *et al.* (1991) performed stretching tests on capsule samples using a modified vernier calliper to stretch the samples to rupture point. The mean stretching capability was 62%, with all samples showing the ability to be stretched. There was no statistically significant relation to age found, but capsules younger than 70 YO did have a lower elasticity than those above 70 YO. The test was conducted in a simplistic manner with measurements appearing to be made by hand, which could compromise the result, although as no material parameters were defined.

Krag *et al.* (1997) performed stretching tests on anterior capsule sections, and later, on posterior capsule sections (Krag & Andreassen, 2003b). The anterior sections were obtained from the central, zonular free,

anterior region and a ring of the capsule was excised using a laser. The posterior sections were obtained in a similar fashion. The capsular rings were placed over two pins, which were able to move along an axis to deform the samples. A constant stretching force was applied to these pins, with constant measurement of the force applied and the resultant deformations. The Krag tests allowed the calculation of load-strain graphs, showing the mechanical response of the capsule. These allowed the calculation of the elastic modulus of the capsule, at a strain value of 10% which is comparable to the strains encountered *in vivo*, where it was found that the elastic modulus increased with age. There was little difference between the anterior and posterior capsule samples, although the posterior samples had a slightly lower elastic modulus.

4.3.2.3 Atomic force microscopy

Atomic force microscopy (AFM) can be used to examine the elasticity of a material using nano indentation. A cantilevered beam is used for the indentation, forced into the sample with the corresponding deflection measured. This force indentation relationship allows the calculation of the Young's modulus of the sample.

Ziebarth *et al.* (2011) used capsule sections taken from the anterior lens (a 5 mm diameter section was removed) and the measurements were carried out in the centre of the sample. The epithelial cells that lie between the capsule and lens were removed before measurements were taken. The results showed that the Young's modulus of the capsule increased with age.

Choi *et al.* (2012) used anterior capsule quarter sections, measuring material properties on both the anterior and posterior sides of the capsule sections, although the measurement positions were not detailed. A force-distance curve was produced, allowing the stiffness of the capsule sections to be calculated. The elastic modulus was then calculated from the stiffness and tip diameter. The results for the anterior side were found to be consistently higher than the posterior, although there appeared to be discrepancies between the text and table results.

4.3.2.4 Other capsule tests

In a number of other tests, the influence of the capsule was measured, although no material properties defined. In the spinning lens test of Fisher (1971) it was indicated that the presence of the capsule resulted in a decrease of 20% on axial thickness change, although there were no detailed results on this.

Ziebarth *et al.* (2008) measured the impact of the capsule using an *in vitro* accommodation stretcher, where the lens, capsule, zonules, ciliary body and sclera were stretched together, both with and without the lens contents. The whole system was stretched by 4 mm, an amount selected as giving appropriate diameter change in the lens. It was found that there was no change in force needed to deform an empty capsule with age, whereas with the lens intact, the force increased with age. Comparing the load in the two cases showed that in young eyes, the force applied by the ciliary muscle is almost completely transferred to the lens. In older lenses, this dropped to 20%, indicating that the capsule is able to transfer force into old age, but the lens itself loses the ability to change.

Burd *et al.* (2011) and Wilde *et al.* (2012) compared spinning lens measurements between en-capsulated and de-capsulated lenses finding that the capsule has a restrictive effect; reducing the slope of the load-stretch graph by approximately 30%. The results also indicated that the capsule often enhanced the axial thickness changes in older lenses, whilst the diameter change was restricted in almost all cases.

In the compression tests of Sharma *et al.* (2011), comparisons were made between en-capsulated and de-capsulated studies and it was found that en-capsulated lenses stiffened faster with age than de-capsulated lenses as well as had a higher induced load to achieve 10% deformation.

4.3.2.5 Comparison of results

Figure 4.4 shows a comparison between those studies that measured the elastic modulus of the capsule, where it can be seen that there is a large variation in the measured data. The data from Krag & Andreassen (2003a) was extracted and fit with a linear trend line as a comparison between the anterior and posterior measurements, although there was considerable scatter on the results.

The methods of measurement could be the cause of variation between studies, for example, between the inflation and stretching tests of Fisher (1969) and Krag & Andreassen (2003a). In particular, the lower results for Ziebarth *et al.* (2011) and Choi *et al.* (2012) could be an indication of the compressive nature of AFM, with Pedrigo *et al.* (2007) demonstrating the anisotropic nature of the capsule, the properties in compression could be very different to those measuring using inflation or stretching.

Pedrigo *et al.* (2007) measured the anisotropy of the capsule, making comparisons to other studies difficult, but a comparison carried out within their own study did compare to the 10% strain results of Krag & Andreassen (2003a). To enable the comparison, Pedrigo took results from the mid-capsule region, a similar location to the measurement positions of Krag & Andreassen (2003a), as well as converting the results

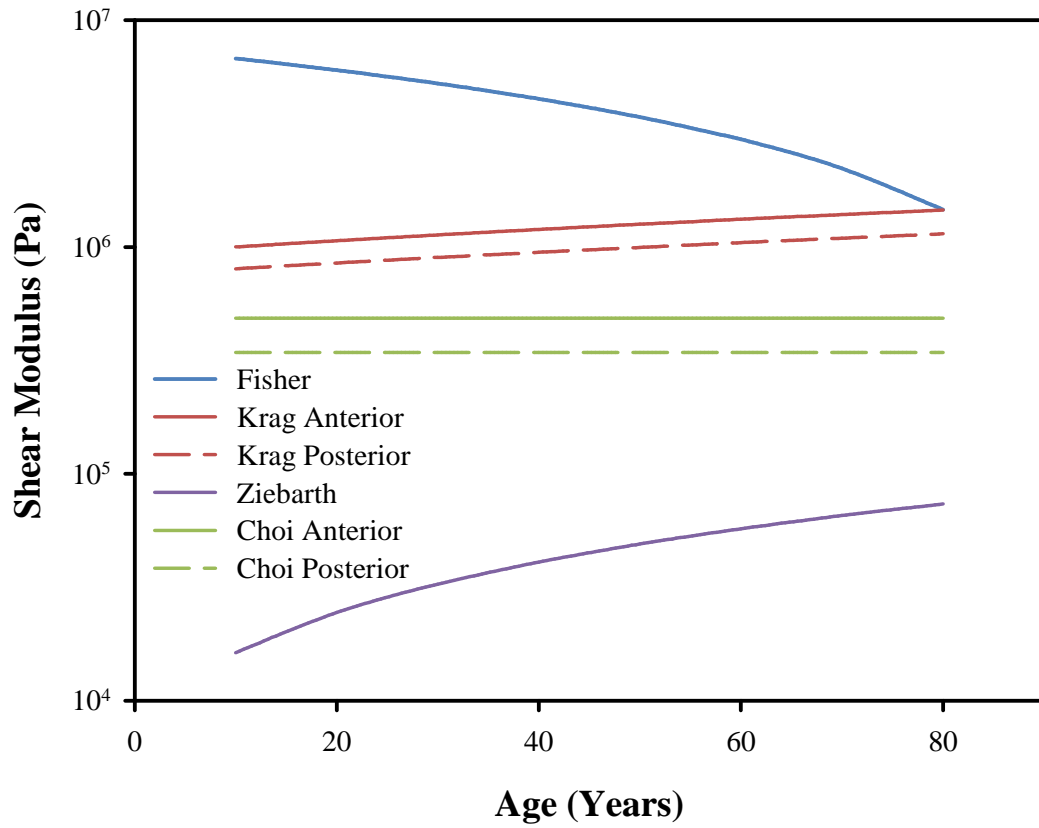


Figure 4.4: Comparison of the studies of the capsule material properties. Fisher (1969), Krag & Andreassen (2003a), Ziebarth *et al.* (2007) and Choi *et al.* (2012).

to show the stress measured as force per original area to match the data of Krag & Andreassen (2003a). The overall comparison showed a similar elastic modulus, albeit slightly higher. This was backed up by a comparison by Burd (2009) where the work of Pedrigi *et al.* (2007) and Fisher (1969) were compared, finding that the results of both are consistent with each other.

In those studies that have measured the influence of the capsule using other methods, it appears that the presence of the capsule has an obvious effect on the changes that the lens undergoes. From spinning studies, the capsule has a restrictive effect on the changes in thickness and diameter, which can also be seen in compression studies, where higher loads were required to induce similar deformations. The capsule was also seen to retain its ability to transmit force into old age. These observations point towards the capsule having an effect throughout life, which may not necessarily be affected by potential changes in elastic modulus.

4.3.3 Zonules

Compared to the lens and capsule, there has been a paucity of testing on the material properties of the zonules. As a result, a number of FEA models developed different methods of estimating the material properties. An overview of the measured properties will be given, before analysing the methods used in FEA models.

4.3.3.1 *In vitro* measurements

Fisher (1977) conducted two tests where the zonular properties were estimated. The first was a stretching study, where the ciliary body, zonules and lens were all extracted from the eye before being radially stretched to simulate accommodation. The changes that occurred in shape were photographed and then measured. The second was part of the spinning lens test discussed earlier (Section 4.3.1.1).

The spinning test was conducted to find the spinning speed that gave the same thickness change as was achieved in the stretching test, allowing the load that was applied in the stretching test to be estimated under the assumption that the loads to induce similar thickness changes are comparable. It was then reported by Fisher (1986) that the Young's modulus of the zonules required to cause the previous measured changes remained constant with age at approximately 350 kPa. It is unlikely that the forces in the stretching test and spinning test are comparable, which would make this value suspect.

Stretching tests were also conducted by Assia *et al.* (1991), who showed that the zonules had a high capability for stretch before rupture, with a decrease in the maximum stretch with age.

Van Alphen & Graebel (1991) performed uniaxial stretching tests on the anterior eye, testing a number of accommodative components. The ciliary body, zonules and lens were tested by stretching them as a unit with the applied load and resultant deformations recorded, with the relationship between the applied load and the extension of the zonules used to calculate the Young's modulus of the zonules. There was a large variation in the values reported, but for a 52 YO eye the Young's modulus was 1500 mN/mm².

A recent paper by Michael *et al.* (2012) used another lens stretching experiment to estimate material properties of the zonules in presbyopes. The accommodative structure was intact for the experiment, with the sclera attached to the stretching device. The applied force and measured strain and elongation were recorded, allowing the spring constant and elastic modulus of the zonules to be calculated. The Young's modulus was shown to be slightly age related, with a younger lens (47 – 60 YO) having a Young's modulus

of 340 mN/mm² and an older lens (83 – 97 YO) 270 mN/mm², with the spring constants being 80.3 and 53.2 mN/mm respectively.

4.3.3.2 FEA model estimations

Burd carried out manual adjustments of zonular thickness on an initial FEA model until the deformations of the lens equator matched the measurements of Strenk *et al.* (1999). The zonules were assumed to vary in thickness between anterior, equatorial and posterior groups in a ratio of 6:1:3 and the stiffness values established were 0.066:0.011:0.033 N/mm², with no age related changes.

Liu *et al.* (2005) modelled the zonules as being springs using the same three sets of zonules as Burd *et al.* (2002), and the spring stiffness was set to 0.6:0.2:0.6 N/mm.

Wilde (2011) adapted the Burd *et al.* (2002) method for an updated material constitutive model, establishing a shear modulus value of 763.1 kPa spread across an altering cross sectional area.

4.3.3.3 Comparison of results

To be able to perform a comparison, the spring constant and Young's modulus was calculated for each study. From the measurements of Michael *et al.* (2012), it was assumed that the cross sectional area could be set to 0.43 mm² with an initial zonule length of 1.82 mm. Assuming that a 10% strain results in a 0.182 mm elongation and that the zonules are isotropic and elastic, the force and stress could be calculated for each study; which would then allow the spring constant and Young's modulus to be calculated from the force-elongation and stress-strain graphs respectively.

Table 4.3 summarises the results and it can be seen that there is a considerable spread, although a number of studies have specified the elastic modulus to be close to 300 mN/mm².

Table 4.3: Comparison of the calculated spring constant and elastic modulus values from both *in vitro* and FEA models.

Study	Spring Constant (mN/mm)	Elastic Modulus (mN/mm ²)
Fisher (1986)	82.7	340
Van Alphen & Graebel (1991)	354	1500
Burd <i>et al.</i> (2002)	66	279
Liu <i>et al.</i> (2005)	600	2539
Wilde (2011)	537	2274
Michael <i>et al.</i> (2012)	80.3	340

4.3.4 Summary

The crystalline lens has been well studied and it has been shown that it increases in stiffness with age. There is enough data to be able to produce a basic representation of how the stiffness varies with both position and age, however, there are a few key aspects of the material properties of the lens that have not been measured. The key information missing is on any anisotropy within the lens, despite the different load conditions used in the different material testing methods (e.g. spinning lens compared to lens indentation, see Section 4.3.1.6), there is not sufficient data to be able to give a suitable approximation of the potential anisotropy present.

For the capsule, there was evidence for its non-linear and anisotropic nature, although not enough data to be able to fully replicate this for multiple ages. Although the data on the elastic modulus varies, there is enough data for an initial representation in the proposed FEA model.

Finally, for the zonules, it was clear that they are linearly elastic and able to stretch a large amount, but it will be difficult to capture this due to the complexities of establishing the amount of zonules in the individual bundles that attach to the capsule. However, the data can be used to aid in a initial approximation of the zonular behaviour.

4.3.4.1 Evidence for accommodation and presbyopia theories

In terms of accommodation theories, there is little in the analysis of material properties of the lens to aid in defining which theories are most appropriate. However, the studies on the zonules have not shown any indication that the zonules would be able to compress the lens, as hypothesised by Wilson (1993).

From the theories of the presbyopia discussed in Section 1.3, there was sufficient evidence to support those theories that suggest lens stiffening may be cause of presbyopia and the data suggests that the zonules are able to transmit force throughout life, which would support the theories that suggest the ciliary muscle continues to have an effect throughout life. Further work is needed to understand how the variation of key material properties may affect the accommodation process.

4.4 Data used for Model

The material parameters that are required for modelling the accommodative system were established in Section 4.2. The measured data discussed in Section 4.3 was used to provide initial estimations of the val-

ues to use in representing the accommodative components. For each component, the essential properties to capture will be discussed before the selected data is detailed.

4.4.1 Crystalline lens

The essential features to capture of the lens are that it increases with stiffness with age and that the stiffness profile varies across the lens. So that the hyper-elastic constitutive model can be used, the shear and bulk moduli across the lens are needed.

Weeber *et al.* (2007) and Wilde *et al.* (2012) both provided data that appear to match well; therefore, methods of adapting both of these data sets will be established. In Chapter 6, the data of Wilde was used initially, and if necessary, the data of Weeber could be utilised to establish if there is a significant difference between them.

For the shear moduli values, Weeber's data had to be extracted from their Figure 7, fitting curves to the individual ages using MatLab. The measurements were all taken up to 4 mm from the sample centre, meaning that the peripheral values are extrapolated. 5th order polynomials (Equation 4.6) were fitted to each age, up to 4.5 mm from the lens centre, with the parameters defined in Table 4.4.

$$f(A) = p_1A^4 + p_2A^3 + p_3A^2 + p_4A + p_5 \quad (4.6)$$

Table 4.4: Parameters to define the shear modulus as according to Weeber.

Parameter	Age (Years)				
	20	30	40	50	60
p1	0.001016	-0.00038	0.000193	-0.00073	-0.00077
p2	-0.1648	-0.08248	-0.04223	-0.00817	0.001624
p3	0.8348	0.4163	0.1828	0.01425	-0.04314
p4	-0.7447	-0.2261	-0.04799	-0.00741	-0.0968
p5	-1.619	-1.396	-0.5407	0.5561	1.583

The data of Wilde *et al.* (2012) was obtained directly from Equation 4.7.

$$\mu = \mu_0^{1-\hat{\zeta}} \mu_1^{\hat{\zeta}} \quad (4.7)$$

where μ_0 is the central shear modulus and μ_1 is the peripheral shear modulus, $\hat{\zeta}$ represents the relative distance from the center, equivalent to ζ/ζ_0 , where ζ is the length of a point on a line running from the

centre to the edge and ζ_0 is the total length of that line. The values of shear moduli were age related with Equation 4.8 used to define the shear modulus, using the parameters in Table 4.5.

$$\log_{10} \mu_x = \begin{cases} b_1 (A - A_0) + c & A \leq A_0 \\ b_2 (A - A_0) + c & A > A_0 \end{cases} \quad (4.8)$$

Table 4.5: Parameters to define the shear modulus values for Equation 4.8 as according to Wilde (2011).

	Centre	Exterior
A0	35.594	43.166
b1	0.04154	0.0191
b2	0.15222	-0.03796
c	1.8357	3.1772

From Section 4.3.1.6, it was clear that the bulk modulus of the lens, either as a whole or split into sections, is a lot higher than the shear modulus. As an initial estimate, it was assumed that the bulk modulus was equivalent to 1000 times the shear modulus, following Wilde (2011).

4.4.2 Capsule

The capsule has been shown to be non-linear and anisotropic, however, there was not enough data to fully model this. Utilising the neo-Hookean model requires the specification of the shear and bulk moduli. As shown in Section 4.3.2, there was more variation in capsule material properties than with the properties of the lens, however, the initial properties were taken from the work of Krag & Andreassen (2003a), who defined the age related function for anterior elastic modulus shown in Equation 4.9. The function applied to capsules 35 YO or younger as there was no significant change found above that age.

$$CapsuleEM = 0.03 \times (Age - 35) + 1.45 \text{ For } A \leq 35 \quad (4.9)$$

To be able to use the hyper-elastic constitutive model, the elastic modulus was converted to shear modulus using Equation 4.1, and the bulk modulus was set to be 1000 times the shear modulus, as with the lens.

4.4.3 Zonules

The zonules have been measured as being linear elastic and therefore, a linear elastic constitutive model was chosen to represent them. There has been considerable variation in the material properties established;

however, it appears that there is little variation with age.

The final representation of the zonules was not established at this stage, instead, an initial set of material properties was needed. The data of Michael *et al.* (2012) was used initially, with the elastic modulus set to be 340 N/mm^2 . The Poisson's ratio was set to 0.4999.

To enable the zonules to be modelled completely, the thickness of each bundle required definition, to ensure that the force passed from the displacement of the zonule to the lens was suitable. The thickness that was utilised will be discussed in Chapters 5 and 6, utilising both the elastic modulus proposed here and the thickness data explored in Section 3.2.4.3.

4.4.4 Summary

Compared to the geometric parameters used, the material properties were all measured *in vitro*, and it was unknown exactly how the *in vitro* data compares to the *in vivo* behaviour. Therefore, the material parameters were an approximation, and for the purposes of the current model provided a baseline dataset to use. The lens and capsule data chosen were successfully integrated into previous FEA models, which supported the selections made. Incorporating the stiffness variation across the lens also ensured that the proposed material parameters complemented the proposed geometric modelling method, combining to produce an overall improved FEA model.

Chapter 5

Procedure

5.1 Introduction

With the material properties and geometry selected, the procedures that will be followed in Chapter 6 needed to be established. The basic theory of finite element analysis relevant to the current study will be discussed, before a breakdown of the additional features of an FEA model, other than the geometry and material properties, will be given. The actual modelling methods that will be followed can then be discussed. The commercial FEA program ANSYS (Research Mechanical version 14.0) was utilised for all the studies conducted in Chapter 6, therefore the theory and methodologies discussed in the current Chapter are based on available methods in this program.

5.2 Finite element theory

Modelling accommodation is more complex than basic static structural analysis in a number of ways. First, non-linear geometry changes are present in the form of large strain. Secondly, as covered in Chapter 4, there are non-linear material properties present, in the form of hyper-elasticity. Finally, the models that will be used will be represented as being axisymmetric.

5.2.1 Geometric non linearity

Simple static, elastic analysis assumes that there is infinitesimal strain within the model, however, in modelling the accommodation process, there is expected to be a finite strain present (e.g. the lens thickness reduces by 10% in a 30 YO eye, as measured by Koretz *et al.*, 1997) and at some locations strains will be higher than 10%. When strains of such magnitude are present, the change in geometry that occurs during

deformation cannot be ignored and the study becomes a large (or finite) strain analysis, where the stiffness is a function of the displacement.

ANSYS uses an updated Lagrangian method to simulate static non-linear geometric studies, where it is assumed that all variables (e.g. stress, strain, displacement, material parameters) are solved and known at a step time, t . The displacements applied to the model then become the primary unknowns and linearized simultaneous equations are then solved to provide a solution at a step time $t + \Delta t$. Element formulations based on the principle of virtual work are used to derive the simultaneous equations (Chapter 3, ANSYS, 2010b).

5.2.2 Material non linearity

The strain energy function used for representing the hyper-elastic models used for the lens and capsule (Equations 4.4 and 4.5) is a scalar function of the right Cauchy-Green deformation tensor, whose derivative determines the Piola-Kirchhoff stress tensor (Chapter 4, ANSYS, 2010b).

5.2.3 Axisymmetry

The overall shape and loading conditions present in the accommodative system can be approximated as being axisymmetric, allowing the lens to be described by cylindrical co-ordinates ($R; \vartheta; Z$), where the Z axis is aligned with the symmetry axis in the lens. It was therefore assumed that the stress and strain, due to the loading and geometry, did not vary with ϑ reducing the modelling to two dimensions as well as simplifying the computational demand.

5.3 ANSYS Modelling Procedures

The geometric models (Chapter 3) and material properties (Chapter 4) have been defined, along with the basic assumptions used in defining the FEA model. The next stage was to define how those methods would be adapted into an ANSYS model with a number of different experiments proposed in Chapter 6. These are split into initial testing, to ensure new modelling methods are suitable, and the full accommodation model, to investigate the overall aims of the thesis. Although there are individual differences in modelling methods related to the geometry and material properties, further discussed in Chapter 6, there will also be common elements across the studies which will be detailed in the current chapter. Each study conducted would be a static study, with the large deformation option selected.

5.3.1 Element Choice

The choice of element for modelling each component of the accommodative system is controlled by the modelling procedures used. In the current model, the choices of hyper-elasticity, axisymmetry and large deformations mean that only specific elements can be selected. Table 5.1 summarises the elements used for the three components of the model, with the lens and capsule elements being defined as quadrilateral and being formulated using the pure displacement formulation.

Specification of zonule elements is complicated by the limited *in vivo* data on the behaviour of the zonules during accommodation. It was known that the zonules connect to the lens in bundles (see Chapter 1), however, for a 2D axisymmetric study, this cannot be replicated. A suitable alternative was to represent the zonules as thin “sheets”, one for each zonular group. For the purposes of the current model, the zonule elements needed to be able to represent the changing thickness, and therefore stiffness, in the appropriate number of zonular bundles; in addition to transmitting the loads from the displacement of the zonule end point to the lens. Shell elements were proposed to represent the zonules, as they allowed for all of the requirements to be met. To ensure that the elements were suitable, the transmission of forces will be confirmed in Chapter 6 when the zonules are first modelled, as well as ensuring that there is little or no bending within the elements.

Table 5.1: Elements used for representing the different components of the accommodation model.

Component	Element Name	Type
Lens, Capsule	PLANE183	8 node structural solid
Zonules	SHELL208	2 node axisymmetric shell

To enable the zonule to be represented by shell elements the thickness needs to be defined. In the current model this was achieved by using shell section controls, one for each zonule bundle, defining a constant thickness along the zonule length.

5.3.2 Geometric Definition

The first step in defining a model was to build the geometric representation. For each age lens model used in Chapter 6, the relaxed and accommodated lens outlines were generated with MatLab using the Hermans method defined in Section 3.3. The outlines were imported to SolidWorks, where they were combined with the corresponding ciliary body model defined using the data in Table 3.20. Both were then utilised to model the zonular structure, using the steps outlined in Chapter 3. The co-ordinates of the

accommodated zonule endpoints were then extracted and used to input the zonules into ANSYS. The lens outlines were used to generate the internal curves (see Section 3.3.3) and all curves were then imported directly into ANSYS after being defined in MatLab.

The capsule was defined as a separate area within the lens. The method defined in Section 3.4 was used to generate the keypoints of the capsule curve, which were then imported to ANSYS so that the capsule curve could be generated, allowing the area to be defined.

5.3.2.1 Internal structure models

As part of the modelling in Chapter 6, different internal structure models will be tested. The basic method of scaling down the outer lens shape and positioning the scaled areas was given in Section 3.3.3. Further detail will be given here on the different internal structure models that will be used in Chapter 6, as well as how the data from Section 3.3.3 will be utilised.

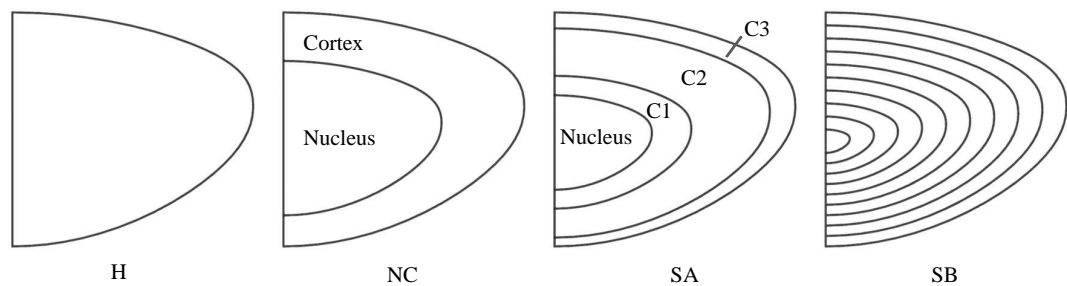


Figure 5.1: Internal Structure representations. H = Homogenous, NC = Nuclues-Cortex, SA = Stiffness gradient A, SB = Stiffness Gradient B.

Figure 5.1 illustrates the four internal structure models. The first internal structure model (Designated with the H prefix) was a homogenous lens, with no internal variation. The second (NC) was based on the nucleus-cortex models used in the literature (e.g. Burd *et al.*, 2002, see Section 2.2.2). The scaling factor was calculated by comparing the thickness of the nucleus to the overall thickness of the lens using the data from Table 3.17. The scaled nucleus was positioned using the anterior cortical thickness to locate the top vertex of the nucleus. The centre point calculated from the nucleus here was used as the centre point for scaling in the next two models.

The SA model was based on the different internal areas observed *in vivo* by Dubbelman *et al.* (2003), which are similar to the internal areas observed by Taylor *et al.* (1996) *in vitro* (see Section 1.2.3.1). Four areas were used to define the internal structure, grouped by Dubbelman *et al.* (2003) into the C1, C2,

C3 and nucleus areas (see Figure 5.1). To allow these areas to be modeled, the changes with age and accommodation are required, defined by Dubbelman based on 8 zones (Table 3.17). How these zones related to the internal areas detailed in Figure 5.1 is detailed in Table 5.2, with the total thickness of the zones used to calculate the scaling factor.

Table 5.2: Lens areas and equivalent zones from the densitometry analysis of Dubbelman *et al.* (2003), see Section 3.2.2.1.

Lens area	Equivalent zones
C1	Zone 1 + Zone 8
C2	Zone 2 + Zone 7
C3	Zone 3 + Zone 6
Nucleus	Zone 4 + Zone 5

The final SB model was based on the method used by Weeber & van der Heijde (2007), where 10 shells were used, each 10% smaller than the last. The central scaling point was defined as for the NC model.

5.3.3 Material Property definition

The properties defined in Chapter 4 were assigned to the appropriate areas, ensuring the units were adjusted to ensure consistency (see Section 4.2.2). The zonules and capsule required only the properties described in Chapter 4 to be assigned to the appropriate area of the model, however, for the lens, the definition of the material properties was dependent on the internal structure model used.

To define the material properties for each section of the different internal structure models, the data from Wilde *et al.* (2012) was used, as defined in Chapter 4. The shear modulus was calculated at 10 relative positions within the lens structure, measured radially from the centre (0.05 – 0.95), and these values were then adapted for the different internal models. For the H model, an average was taken of all shear modulus values. The NC model was split, with the nucleus values taken from 0.05 to 0.65 measurements and the cortical values taken from the 0.75 to 0.95 regions. The same process was used for the SA model, with the regions for each section defined by the measurements of Dubbelman *et al.* (2003). The SB model used the 10 values.

5.3.4 Mesh Generation

With the material properties and geometry defined, the mesh could be generated. The lens and capsule areas were meshed as being bonded together, with the free element mapping method utilised and size controls were used. A constant element size was assigned to the lens areas, with a smaller element size required when the capsule area was used to prevent element shape warnings to do with the aspect ratio of the elements. The zonules were meshed with single elements. An example of the mesh generated is shown in Figure 5.2.

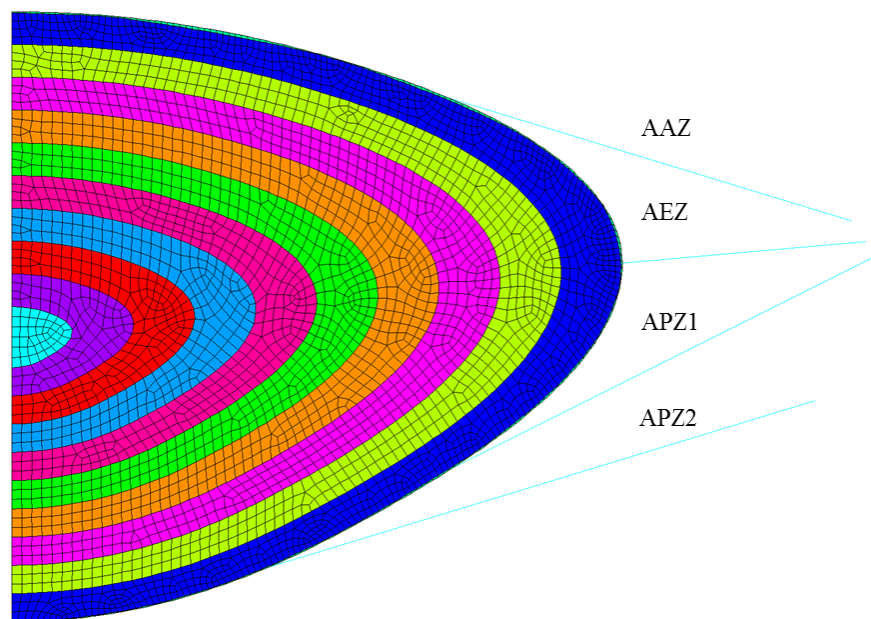


Figure 5.2: Illustration of the mesh generated for a 20 YO lens model using the free element mapping method, the colours illustrate the different material property regions that are meshed individually.

The number of elements used in meshing can have an effect on the results of an FEA model, therefore, what element size is suitable for the models used in Chapter 6 needed to be established. For an accurate analysis, an element size is defined as being suitable when further reduction causes no change in the results. However, due to the variance present in the definitions of the geometry and material properties in the current models, absolute accuracy is not needed; therefore, the element size chosen needs to simply demonstrate that it is of a suitable size. This will be achieved using a mesh convergence study, repeated when different modelling methods are introduced (e.g. addition of the capsule to the model). The mesh will be reduced iteratively until the results converge to within 2% of the previous value and then an appropriate element size from all of the ones simulated will be selected.

5.3.5 Loads and Restraints

The final part in building the model is to define what loading forces will be applied and how the model is constrained. There are two analysis procedures that will be conducted in Chapter 6, the spinning test and the displacement test.

5.3.5.1 Spinning studies

One method of investigating the material properties of the lens is to spin the lens about its central axis, a method discussed in Chapter 4. The purpose is to induce deformations that are similar to those seen *in vivo* with accommodation, a reduction in thickness and an increase in diameter. Although the forces present with spinning are unlike those found with accommodation they will enable investigations into material property distributions to be conducted.

When using the spinning set up, the crystalline lens will be simulated as being spun freely in space. A rotational velocity of 1000 rpm will be applied to the lens, a speed chosen in the original studies of Fisher (1971) and Wilde *et al.* (2012), as this induces deformations similar to those found *in vivo*. The speed is defined as a global rotational velocity within ANSYS, with a value of 104.72 radians/s.

To ensure that equilibrium is reached, the lens will need to be constrained on the vertical axis, which will be achieved by applying a zero displacement constraint on the bottom vertex of the lens model. To enable a rotational velocity to be applied, each material property used needs to have a density defined, which was set to be 1058.98 kg/m³ (Bellows, 1944) following the similar study of Wilde (2011).

5.3.5.2 Displacement studies

To be able to replicate the accommodation process using available data the most appropriate method is to displace a representation of the zonular fibres, commonly used in existing FEA accommodation models (see Chapter 2). The reason for approaching the problem this way is due to the uncertainty of the forces involved in changing the lens shape. Using a representation of the zonules and displacing the ends by a set distance, which can be approximated from *in vivo* data, allows a more accurate simulation to be conducted.

The loads will be applied to the end of each zonular bundle representation, in the form of x and y displacement values. These would be calculated from the zonule model generated in SolidWorks (Section 5.3.2).

The displacement applied to the end of the zonules will apply a force to the connection to the capsule, in turn applying forces to the lens itself, inducing the appropriate lens deformations. The use of the proposed zonule structure should ensure that no further restraints are required.

Zonule attachment

The zonules are modeled with different elements to the lens and capsule and require a method of attaching them to the lens body. Although there is evidence for the zonules passing through the capsule and interlacing with the lens cortex (Hiraoka *et al.*, 2010), there is currently not enough data to be able to replicate this. Therefore, it was decided to attach the zonules by combining the degrees of freedom (x, y and rotation) of the zonule and capsule nodes, as shown in Figure 5.3.

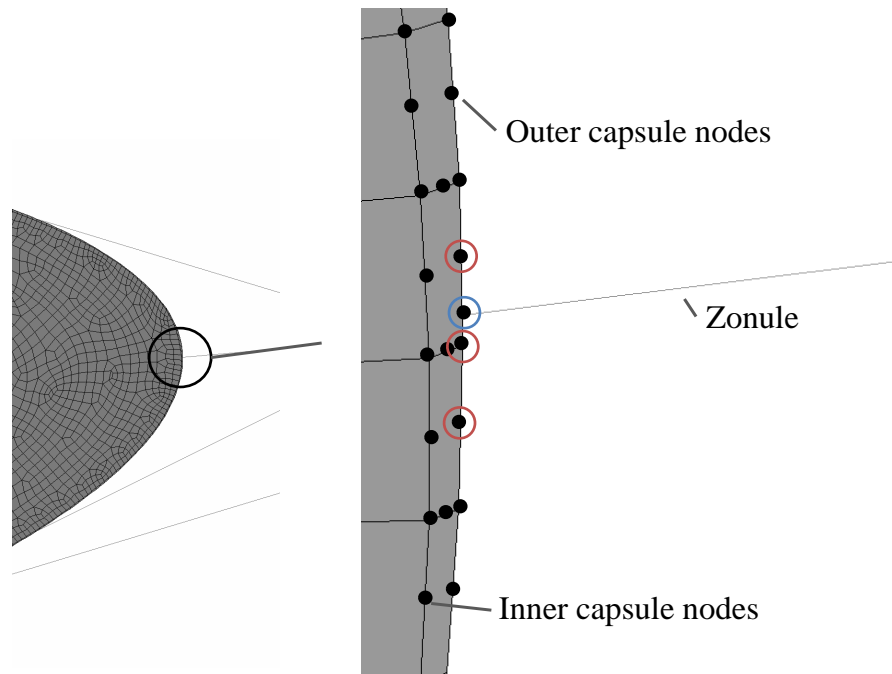


Figure 5.3: Illustration of the zonule node (Blue circle) connection to the capsule nodes (red circles) for the equatorial zonule, with detail on where the nodes (which form the individual elements, denoted by Black dots) are located on the model.

5.4 Results Extraction

To establish whether the deformations of the different models are actually representative of the changes that occur *in vivo*, a method of comparing key parameters from the models to measured values is required. The most appropriate method in the case of the models proposed in the current study is to extract the displacements in terms of the nodal x and y coordinates, in both the original and deformed state. Different

aspects of the deformations can be obtained by extracting only those nodes relevant, for example, to enable calculation of the thickness, diameter and surface curvature changes, only those nodes on the outer lens edge are needed. The x and y coordinates can also be used to generate a 3D representation of the lens in both original and deformed conditions to enable surface area and volume calculations. The thickness and diameter changes were extracted from the displacements of the anterior, posterior and equatorial poles, taking into account the original positions. The nodal points were analysed in MatLab to give the final changes.

To measure the change in surface curvature, the radius of curvature was calculated before and after deformation for the anterior and posterior surfaces. Circles were fitted to each surface using MatLab, utilizing a circle fitting function based on the work of Taubin (1991). Starting from the anterior and posterior poles, nodal points up to 1.5 mm from the poles were extracted from the outer lens shape, an aperture similar to those utilised in a number of FEA models for curvature estimations (e.g. Burd *et al.*, 2002 and Lanchares *et al.*, 2012), and fitted with planar circles, giving the radius of curvature.

5.4.1 Detailed Results

The measurements detailed so far will enable the performance of models to be well understood, however, to aid in establishing a complete picture of how the model is behaving, additional comparisons can be made to *in vivo* measurements of the movement of the lens; as well as the more complex measures of the thickness change that the lens undergoes during accommodation (Section 3.2.2).

The movement of the lens can be defined by the posterior pole displacement, extracted as the y displacement of the bottom node; and the equatorial movement, extracted as the y displacement of the node at the equator. The internal thickness changes can be split into the changes within the nucleus region, and in terms of the distribution of thickness change between the anterior and posterior poles. To obtain the nucleus change, an appropriate boundary line will need to be chosen, which will then allow the displacements of the anterior and posterior nodes aligned on the central axis to be extracted. For example, in the SB model, the boundary of area 7 would correspond to the nucleus region, as defined by Dubbelman *et al.* (2003) (see Figure 5.4). To obtain the distribution of thickness change between the anterior and posterior surfaces, the displacements of the anterior and posterior poles of the lens will be extracted and compared to the overall thickness change.

In addition to these geometric parameters, the stress and strain values distributed through the lens can be extracted using the post processing tools within ANSYS.

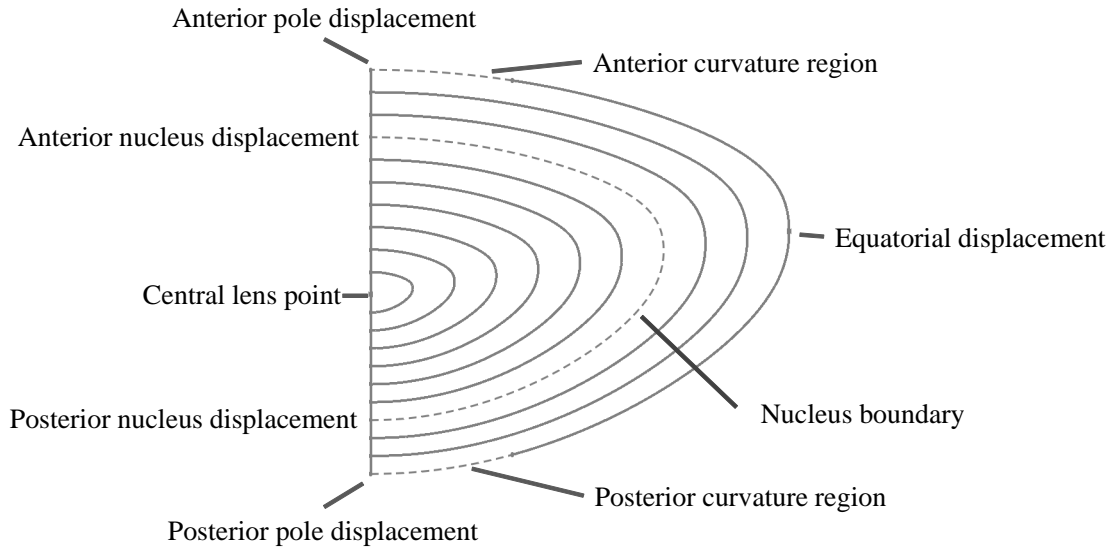


Figure 5.4: Illustration of where the displacement values for calculating thickness and movement changes are taken from.

The principal methods of verification used in the current study are related to the geometric changes, due to the comparison that can be made to measured *in vivo* data. However, it would be ideal when modelling the accommodation process to calculate the changes in power of the lens. Section 2.4.2 covered some of the methods used to estimate the power of the lens after simulation using FEA, with the most accurate method being to use ray tracing. To be able to obtain suitable results using this method, the appropriate refractive index values throughout the lens are required, across all the ages of lens that are analysed. It is beyond the scope of this study to develop a ray tracing system that incorporated the deformed lens shape combined with a suitable gradient refractive index. However, the optical power of the lens is a convenient method of discussing the geometric changes that the lens undergoes, as well as being a useful method of comparison between models. Therefore, the simpler, thick lens formula used by the majority of studies (Section 2.4.2) will be utilised where required, using Equation 5.1.

$$OpticalPower = \frac{n_1 - n_2}{r_a} + \frac{n_1 - n_a}{r_p} - \frac{t(n_1 - n_a)^2}{r_a r_p n_1} \quad (5.1)$$

where n_1 is the refractive index of the lens (1.42), n_a is the refractive index of the aqueous and vitreous (1.336), r_a is the radius of curvature of anterior surface, r_p is the radius of curvature of posterior surface and t is the axial thickness of the lens, with the same refractive index values as in previous studies (Schachar *et al.*, 1993; Burd *et al.*, 1999). Using the thick lens formula provides an oversimplification of the power changes that occur, principally due to the use of a single refractive index value for the lens, therefore

calculation of the lens power will principally be used as a method of comparison between different models, rather than to predict the optical ability of lens models.

5.4.2 Expected changes in geometry

Chapter 3 looked in detail at the various sources of data on the changes that the accommodative components undergo with both age and accommodation, principally to establish data to use in modelling the accommodative system. The data can also be used to ensure that the changes that the model will undergo match previous *in vivo* measurements.

For each of the key comparison values that will be extracted from the deformed models, there is a wide variation in the *in vivo* measurements. To assist a comparison to the measured data a range of data was plotted (Figure 5.5), representing the variation present (the sources are detailed in Table 5.3). The models will be representing the transition from the accommodated to relaxed state, therefore, the changes are opposite to those measured *in vivo* (typically measured transitioning from relaxed to accommodated) and will be altered to represent the appropriate change (e.g. Thickness will decrease rather than increase).

Table 5.3: Sources of data used in plotting the graphs in Figure 5.5. A indicates age in years. All measurements indicated the change per diopter of accommodative response, with the amount of accommodative response per year, used in defining the graphs in Figure 5.5, taken from the study of Duane (1922). Each graph in Figure 5.5 is formed of a maximum and minimum range of values, hence the use of two definitions in the table.

	Thickness (mm)	Diameter (mm)	Anterior radius of Curvature (mm/D)	Posterior radius of Curvature (mm/D)
Definition 1	$-0.0058(\pm 0.0007) - 0.00048(\pm 0.00025) * A$	0.067 ± 0.03	$0.59(\pm 0.0073) - 0.0092(\pm 0.00026) * A$	$0.13(\pm 0.06)$
Source	Dubbelman <i>et al.</i> (2005)	Jones <i>et al.</i> (2007)	Koretz <i>et al.</i> (2002)	Dubbelman <i>et al.</i> (2005)
Definition 2	-0.05 ± 0.024	0.037 ± 0.004	0.64 ± 0.1	0.16 ± 0.1
Source	Jones <i>et al.</i> (2007)	Hermans <i>et al.</i> (2009)	Hermans <i>et al.</i> (2009)	Hermans <i>et al.</i> (2009)

The first tests conducted in Chapter 6 will be using the spinning lens method (Section 5.3.5.1), therefore, to be able to measure the performance of the lens models in this case, a comparison to the data of Wilde (2011) was conducted, extracting the appropriate values from their Figure 8.5 and appendices, detailed in Chapter 6.

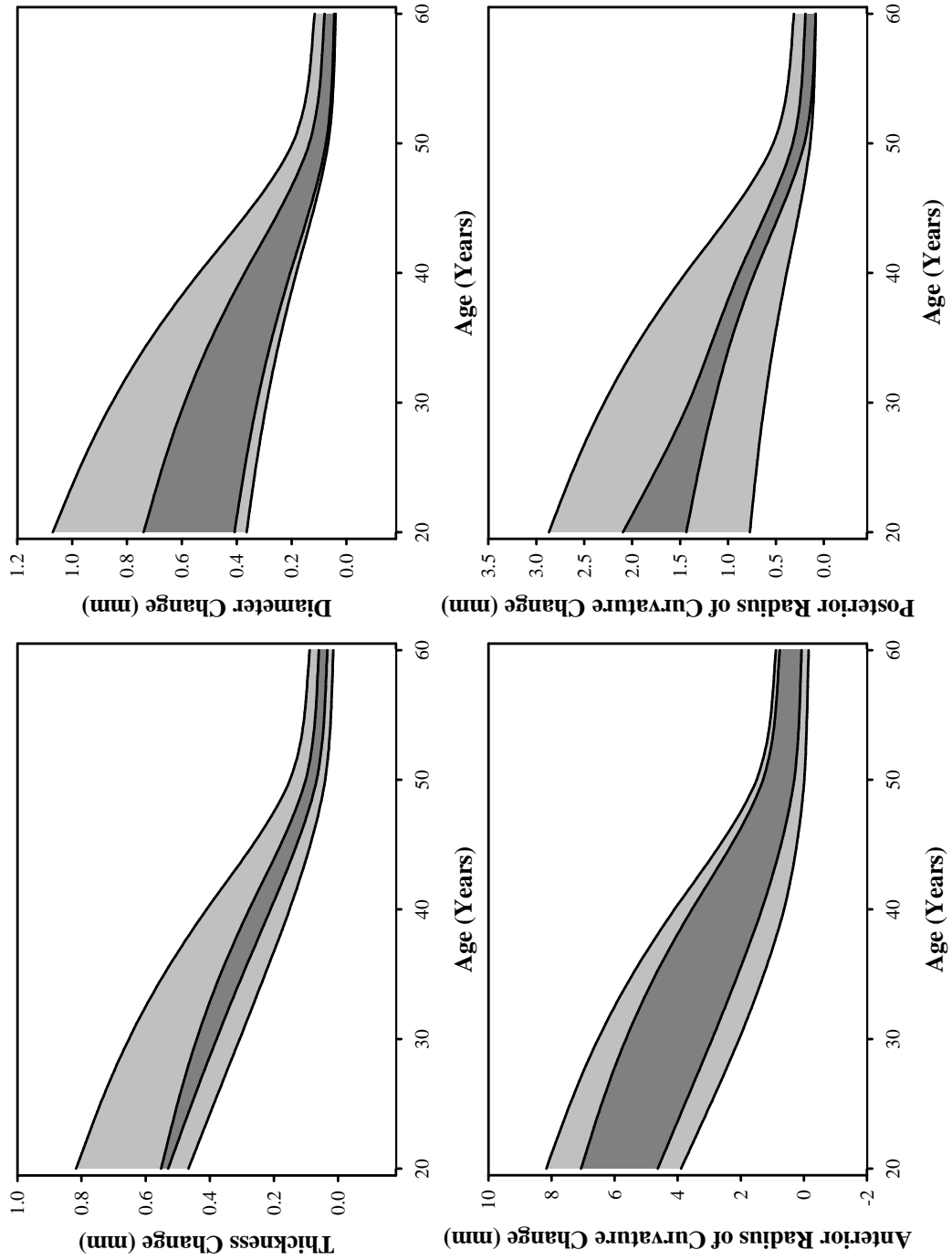


Figure 5.5: Graphs showing the variation in measurements of the changes in thickness, diameter, anterior radius of curvature, posterior radius of curvature with accommodative stimulus. The dark grey regions represent the boundary between maximum and minimum values, with the light grey regions representing the variation in the measurements.

Chapter 6

Modelling

6.1 Introduction

Using the methods established in Chapters 3, 4 and 5, a new finite element model of the accommodation system has been proposed to investigate the development of presbyopia; in addition to overcoming the weaknesses of previous models, as discussed in Chapter 2.

Due to the new modelling methods (e.g. the zonule model, Section 3.5), a series of initial tests were conducted to establish the suitability of the new methods and suggest any alterations that may need to be made. The updated modelling procedures were then used to produce three different age models of accommodation that were compared to both measured *in vivo* data, and previous FEA models. Once the suitability of the FE model was verified, the modelling procedures were then used in the main investigation of the thesis into presbyopia development. A final few models were then run to compare alternate theories of accommodation.

6.2 Initial model development

The initial model development was conducted in stages, each stage designed to evaluate a particular aspect of the model, beginning with the method of modelling the internal structure of the lens. The capsule was then introduced, before testing of the novel zonular arrangement. Final adjustments were then made to the overall modelling procedure.

6.2.1 Internal Structure

As shown in Chapter 2 the nucleus-cortex method of modelling the internal structure is the most prevalent, despite the emergence of data on the variations that occur within the lens; in terms of geometry (e.g. Dubbelman *et al.*, 2003) and material properties (e.g. Weeber *et al.*, 2007).

As part of a new spinning lens test Wilde *et al.* (2012) investigated the material property distribution within the lens using three internal structure models to infer stiffness parameters for the lens: an homogenous (H), nucleus/cortex (D) and exponential model (E). The results indicated that older lenses were best represented by the D model, whilst a younger lens was best represented by the E model, which shows the variability of different internal structure models. Although the spinning test produces changes that are unlike *in vivo* accommodation, it demonstrates the need to ensure that appropriate models are selected for FEA modelling.

To aid in ensuring an appropriate method is selected, four internal structure models were compared using a simulated spinning lens test. Three of the models used were similar to those used by Burd *et al.* (2011) and Wilde *et al.* (2012), with a new method proposed based on *in vivo* and *in vitro* data (see Figure 5.1). The capsule was not modelled and modelling results were compared to de-capsulated lens tests (Wilde *et al.*, 2012), as the current study is concerned only with comparing the difference between internal structure models.

6.2.1.1 Model set up

The modelling methods established in Chapters 3 and 5 were followed, defining four internal structure models (H, NC, SA and SB, see Section 5.3.2.1) for three ages, 20, 40 and 50 YO. The material properties were distributed as described in Section 5.3.3 and the procedure outlined in Section 5.3.5.1 was followed.

A mesh convergence study was conducted on the SB model, finding that the optimum global element edge length to utilise was 0.08 mm. The mesh initially had a global element edge length of 0.18 mm, and was reduced in steps of 0.02 mm. Convergence of lens thickness and curvature to within 1% of the previous edge was achieved using a 0.02 mm edge length (Figure 6.1).

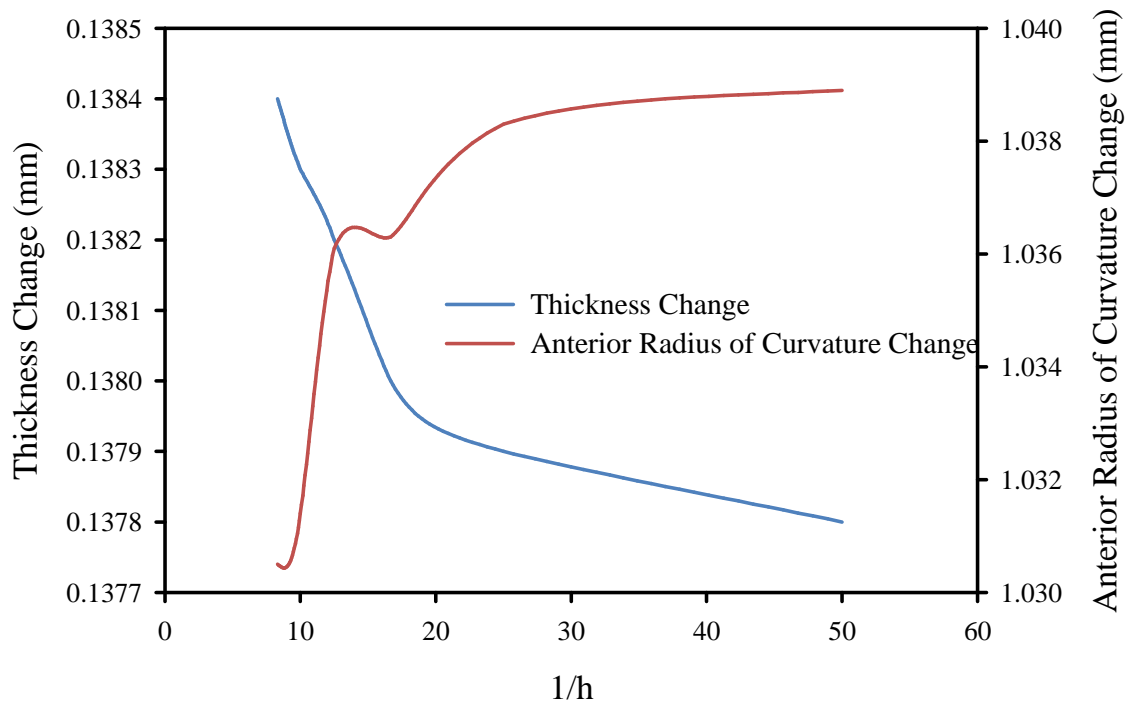


Figure 6.1: Mesh convergence of the thickness and anterior radius of curvature of the SB model. h = element edge length.

6.2.1.2 Results

The changes in shape undergone by the lens are illustrated in Figure 6.2. The measured thickness changes in each internal structure model are shown in Figure 6.3 for the rotational speed of 1000 rpm. There is a large difference between the changes in a young and old lens, which is to be expected due to the stiffer material properties in the older lenses. Also a larger amount of variation in the internal structure models is evident in the younger lens. However, the differences between structure models in the older lens are of more interest, because these ages are where the onset of presbyopia occurs, therefore Figure 6.4 and Figure 6.5 show the changes in thickness, curvature and power for the 40 and 50 YO lenses only. The changes in diameter were very similar for the NC, SA and SB models, with the H model deviating from these values.

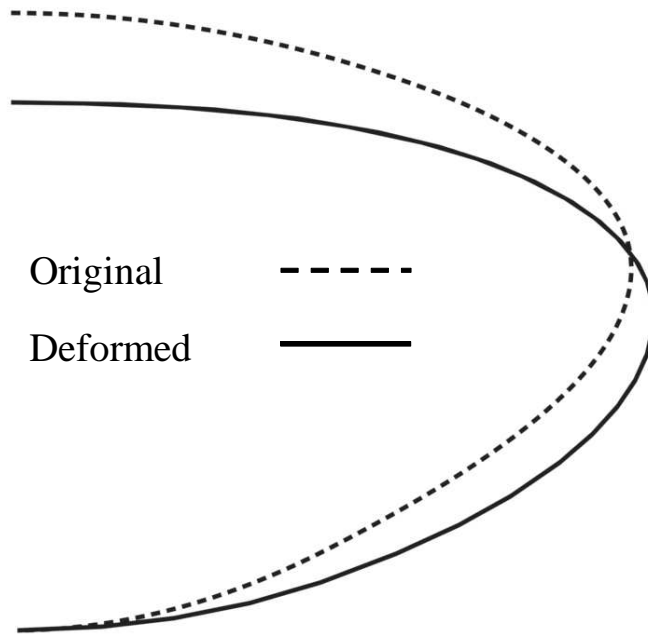


Figure 6.2: The deformation undergone by the lens after being spun at 1000 rpm, with the dotted line representing the lens before spinning and the solid line the lens after, showing the changes in thickness and curvatures.

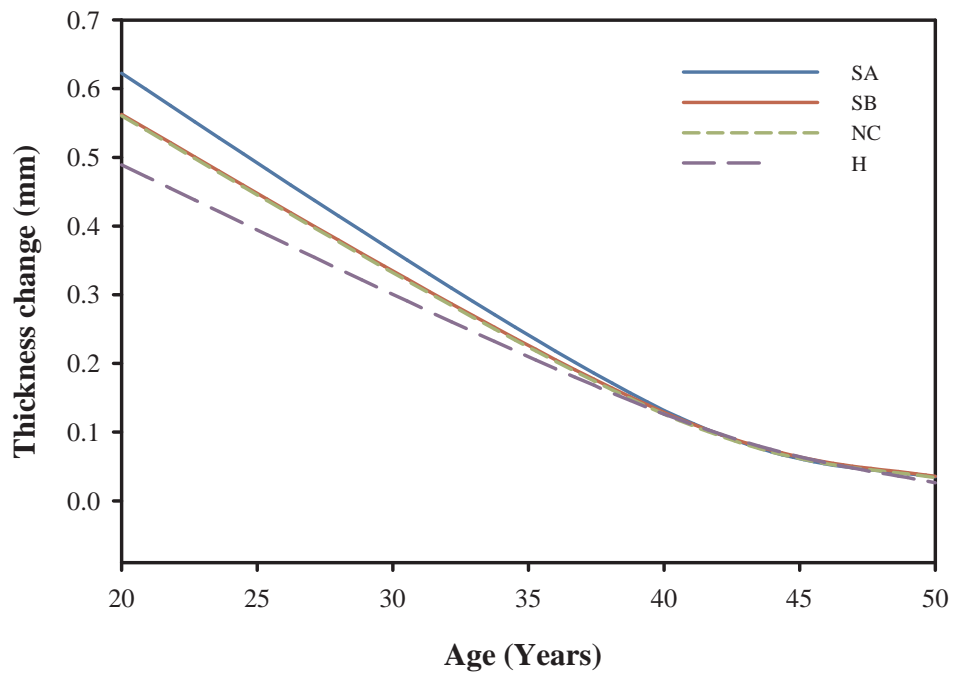


Figure 6.3: The decrease in axial thickness with age of each internal structure model for lenses spun at 1000 rpm.

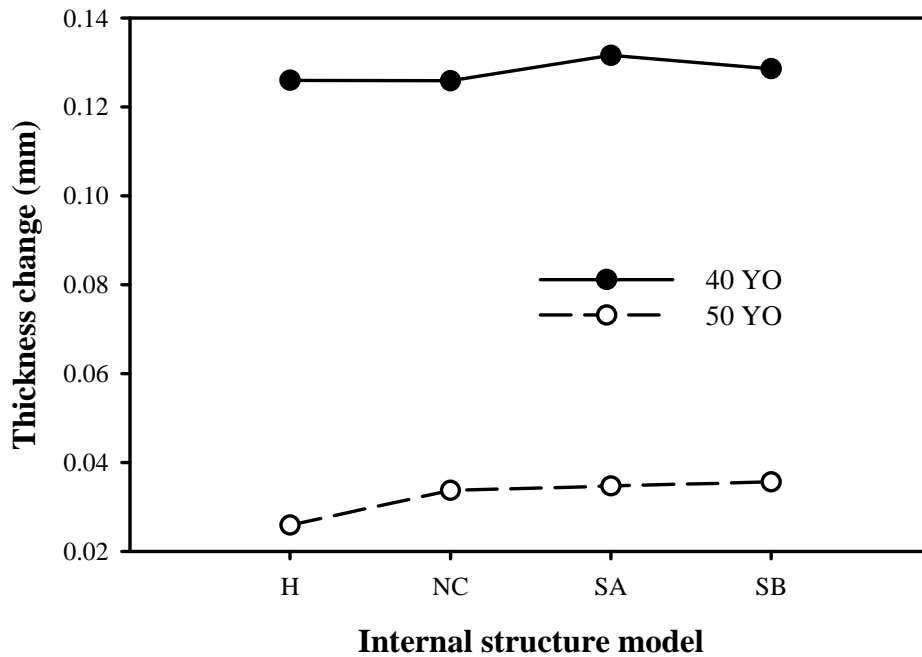


Figure 6.4: Comparison of the decrease in axial thickness for the different internal structure models at 40 and 50 YO for lenses spun at 1000 rpm.

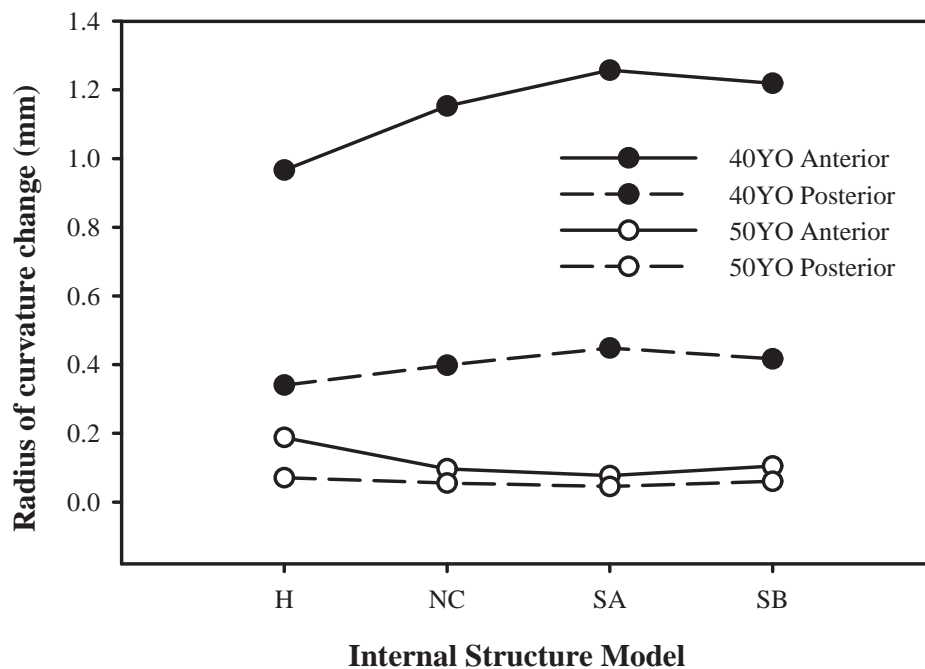


Figure 6.5: The changes in the radius of curvature of the anterior and posterior surfaces of each internal structure model at 40 and 50 YO for lenses spun at 1000 rpm.

There was a small variation between the thickness changes in the older lens models, but the key changes

were within the curvatures, as they have more of an impact on lens power. Aside from the H model, the SA model has the most variation between ages, although the SB model is similar.

To analyse the differences between FEA models more thoroughly, a comparison to the study of Wilde (2011) was made. In Wilde's study, a range of lenses were spun at the same speeds used in the current study. There are differences in the lens shapes due to the spinning structure, but the overall thickness changes are comparable. For young lenses, comparable to the 20 YO lens modelled, the thickness reduction was in the range 0.4 to 0.6 mm. The SA model falls outside this range while the other three models are in agreement. For lenses close to 40 YO, the thickness change was in the range 0.1 to 0.2 mm and for the 50 YO lens, the change was 0 to 0.1 mm. All models agree with these results for 40 YO and 50 YO lenses. In terms of diameter changes, all models had lower changes than the results of Wilde, which could be attributed to the support structure used in the experiment, however, an age related decrease was observed, as with Wilde.

In all models and ages, the H model deviates from the other models significantly, which can be expected due to modelling the lens as a single homogenous structure. In the other three models, the results are more consistent. In terms of curvature changes, both the SA and SB model have increased changes compared to the NC model, indicating that alteration of the internal structure will have an increased impact on surface curvatures, a significant aspect of power change.

As the distribution of load that occurs *in vivo* is considerably different from that used here and in the spinning lens experiments, further work is needed to understand which model is more suitable when subjected to *in vivo* conditions with forces applied through the zonules, which will be conducted in Section 6.2.5.

6.2.2 Initial Capsule Test

For the proposed model, the capsule thickness variation was modelled using an area within the lens outline (Section 5.3.2). To ensure that it could be implemented in the proposed model, a comparison to measured data was carried out by adding the capsule to the models tested in the Section 6.2.1. The measured data to compare against came from the study by Wilde (2011) (see Section 4.3.1.1), where additional spinning tests were carried out on en-capsulated lenses, so a comparison between them and de-capsulated lenses could be made in terms of thickness and diameter change. The presence of the support structure in the tests by Wilde (2011) would mean a direct comparison to those results is not possible; however, the general trends could be compared. Wilde (2011) found that in younger lenses, the capsule had a consistent

restrictive effect, reducing the thickness and diameter changes. In older lenses (over 40 YO) the capsule often enhanced the axial compression, although a consistent restriction of diameter changes was seen.

6.2.2.1 Model set up

Only the models for a 20 and 40 YO lens from the previous section were adapted, due to the low changes in thickness and diameter in the 50 YO lens. The SB stiffness distribution was used for the lens material properties. The capsular area was added, using the method outlined in Section 3.4, with the material properties defined as in Section 4.4.2. The procedure for a spinning lens study as outlined in Section 5.3.5.1 was followed. Two additional models were run for the 20 YO lens using alternate material properties (from Fisher, 1969; Ziebarth *et al.*, 2011) to see how they affected the results.

A new mesh convergence study was required due to the addition of the capsular area. The majority of the lens structure was the same as the previous models, therefore, it was decided to only vary the element size in the new capsular area. The optimum element edge length was 0.035 mm for the capsule. The initial element edge length was 0.04 mm, reducing in steps of 0.005 mm. Convergence of lens thickness and diameter to within 1% of the previous step using a 0.015 mm edge length was achieved.

6.2.2.2 Results

A comparison between the thickness and diameter changes of the en-capsulated and de-capsulated lens models with the results of Wilde (2011) can be seen in Table 6.1, with a representation of the difference in lens deformation given in Figure 6.6. The percentage changes in thickness were used for the comparison between models due to the differences in the geometric description of the lens.

Table 6.1: Comparison between the changes in en-capsulated (C) and de-capsulated lens (DC) models in the current test and from Wilde (2011). The changes are given in terms of percentage change in thickness due to the difference in the geometric description of the lens.

Study	Age (Years)	State	Thickness change (%)	Difference (%)	Diameter change (%)	Difference (%)
Wilde (2011)	20	C	6.54	-	2.41	-
Current			4.35		0.21	
Wilde (2011)		DC	15.36	8.82	5.89	3.48
Current			14.49	10.14	1.79	1.58
Wilde (2011)	40	C	2.62	-	0.58	-
Current			1.75		0.17	
Wilde (2011)		DC	2.58	-0.04	1.06	0.4
Current			3.49	1.74	0.46	0.29

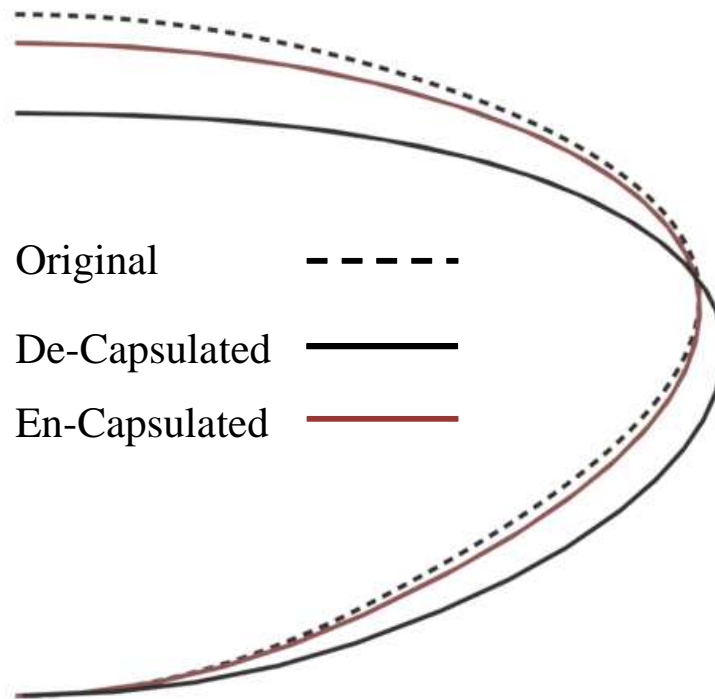


Figure 6.6: Comparison between the deformations undergone by an en-capsulated (Solid Grey) and de-capsulated (Solid Black) lens after being spun at 1000 rpm, with the dotted line representing the lens before spinning.

The changes between en-capsulated and de-capsulated lenses were similar for the young lens in terms of both thickness and diameter, but only for diameter in the old lens. The disparity could be a consequence of the support structure in the test of Wilde or the material properties used, therefore, an analysis was carried out using the material properties from the studies of Ziebarth *et al.* (2011) (lower shear modulus than Krag & Andreassen, 2003a) and Fisher (1969) (higher shear modulus than Krag & Andreassen, 2003a), as shown in Section 4.3.2. Using the data of Ziebarth *et al.* (2011) led to greater deformation whilst using the data of Fisher (1969) led to less deformation, in comparison to the changes of Wilde (2011), with no significant change in the trends observed in Figure 6.6.

6.2.2.3 Conclusion

The testing conducted on the capsule indicated that the modelling methods selected were suitable for the current modelling purposes. The addition of the capsular area, including the variation in thickness present, to the lens structure resulted in restrictions to both the thickness and diameter changes that were similar to those seen *in vitro*. A complete match for the changes measured *in vitro* was not found, which was most probably due to the anisotropy present in the capsule, although it could also have been a result of the disparity between the two geometric set ups. However, due to the lack of available data on the

anisotropic properties, the selected properties of Krag & Andreassen (2003a) would appear to be a suitable compromise for the proposed accommodation model. The spinning test is not fully representative of the conditions *in vivo*, therefore, further testing of the capsule combined with zonular structure was required (see Section 6.2.3).

6.2.3 Zonule testing

Having tested the initial models of the internal structure and capsule the proposed zonule model from Chapter 3 also needed to be tested to ensure that it performed as expected. The zonule model should undergo appropriate deformation and cause the required movement in the lens, based on available *in vivo* studies (see Section 3.2.2).

As covered in Chapter 2, the majority of existing models used a single point of displacement to cause the deformations within the lens, whereas the proposed model has four displacement points. The effect of the addition of the APZ2 zonule (See Section 3.5), which has not been included in any previous studies, also needed clarification. The first test was to compare the traditional zonule representation with the proposed model from Section 3.5, before further adjustments could be made.

6.2.3.1 Zonule methods comparison

To enable a comparison between the proposed model from Section 3.5 to the traditional model, three versions of a 40 YO lens were modelled (using the same geometry and material properties as in Section 6.2.2). Each model had the same attachment points on the lens itself, as defined in Section 3.5.2, but the zonule arrangement varied. Figure 6.7 illustrates the three models, ZA being the traditional model (similar to the methods of Burd *et al.*, 2002), ZB and ZC being the model proposed in Section 3.5, with the ZB model having the PZ2 zonule removed to match the models that used three zonules.

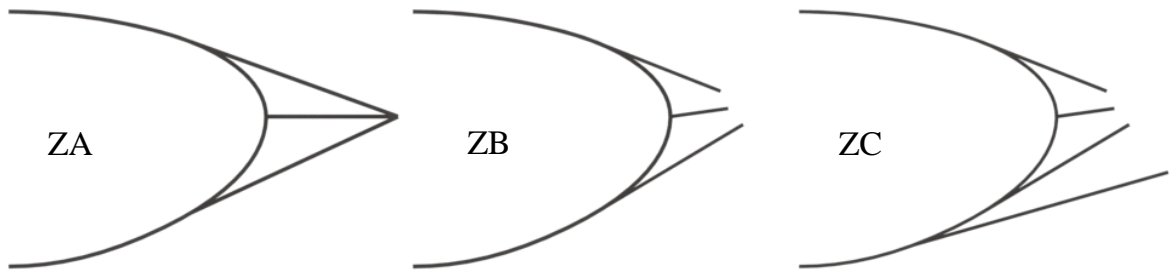


Figure 6.7: The three zonule models simulated in section 6.1.3.1. ZA = zonule model of Burd *et al.* (2002), ZB = The proposed zonule model without the PZ2 zonule, ZC = The complete proposed zonule model.

The displacement of the ciliary body point in the ZA model was constrained to have zero y movement and an axial movement as according to Kasthurirangan *et al.* (2011), where the circumferential space does not change with accommodation, therefore the zonular displacement is linked to the change in equatorial diameter.

$$\text{Zonule Displacement} = L_{Racc} - L_{Rel} \quad (6.1)$$

The second and third zonules models (ZB and ZC) are based on the zonule modelling method defined in Section 3.5, where both relaxed and accommodated zonules are modelled and the displacements are defined by the change between them. The movement of the ciliary body is defined using the same displacement value as in ZA. The procedure is as outlined in Section 5.3.5.2, with the individual displacement values of the zonular bundles given in Table A.1.

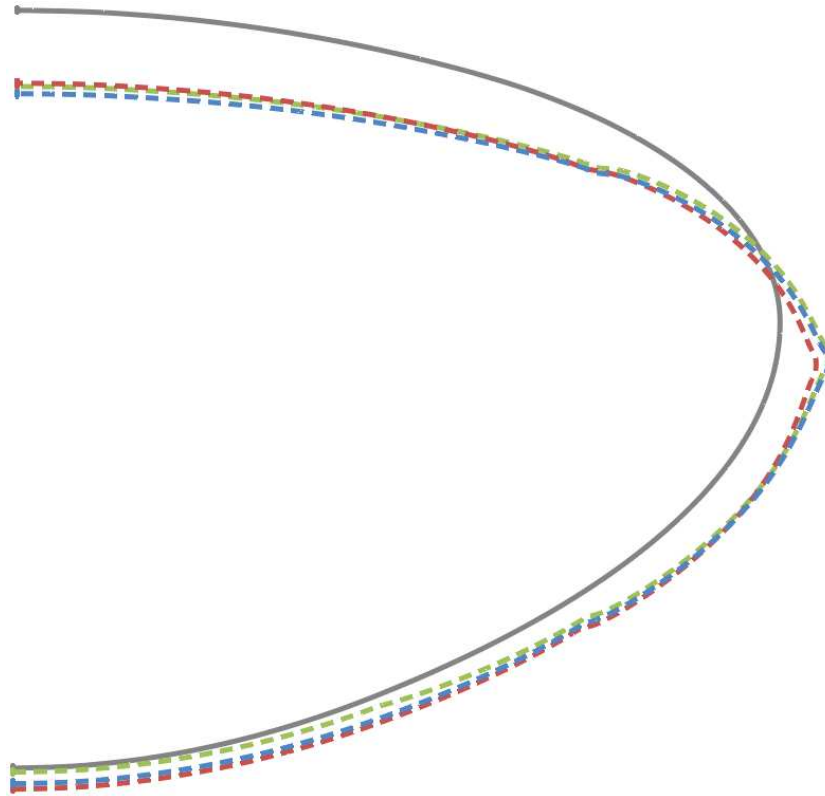


Figure 6.8: Deformations of the three zonule models from Section 6.2.3.1, showing the initial and deformed shapes for the individual displacement values given in Table A.1. ZA = Blue, ZB = Red, ZC = Green.

The deformations in the three models were similar (Figure 6.8), although the geometric changes in the ZA model were lowest (Table A.4). The key result from this comparison is the movement of the posterior surface. In Chapter 3 it was discussed how there was disagreement on whether the posterior pole moves forwards during accommodation or remains stationary, with accommodation being the change from far to near viewing. In the current models, the lens moves from near to far, which would require the posterior pole to move forwards, or remain stationary. The only model which satisfies this requirement is the ZC model. Utilising four zonule bundles would therefore appear to be the most appropriate method of simulating accommodation.

6.2.3.2 Test of base zonule model

To ensure that appropriate changes are induced, the proposed zonule model was tested at different ages. The same three ages will be used as in Section 6.2.1 and Section 6.2.2 with the same geometric and material properties as in Section 6.2.1, using the SB internal structure model. The zonules are modelled as described in Section 3.5 and for the ZC model in Section 6.2.3.1, resulting in three different sets of displacements for the three ages (see Table A.1). The section thickness remains constant with age, and

the thickness was distributed as 0.036:0.006:0.012:0.012 mm between the four zonule bundles, similar to previous FEA models (e.g. Burd *et al.*, 2002). The procedure from Section 5.3.5.2 was followed.

The deformed lens shapes, representing the relaxed state of the lens, are shown in Figure 6.9. Overall the shape changes seen appear to be suitable from visual inspection, with the change in shape reducing with age and there being little posterior movement of the lens. From the measured changes (detailed in Table A.4) the 20 YO model had too much thickness (by 0.41 mm) and curvature change (by 4 mm anteriorly, 0.2 mm posteriorly), the 40 YO model had too much thickness change (by 0.1 mm) and anterior curvature change (by 0.5 mm), whilst the 50 YO model had too little change in the posterior curvature (by 0.03 mm).

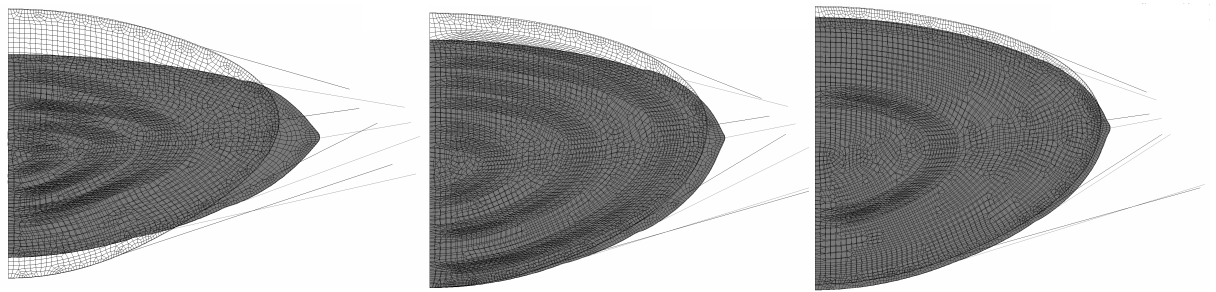


Figure 6.9: Comparison between the deformations in the three age models used in Section 6.2.3.2, with the 20 YO lens on the left, the 40 YO lens in the centre and the 50 YO lens on the right.

The proposed zonular model is inducing deformations that are approaching the actual changes that are expected, but there are still adjustments that are needed before the method can be considered a match for the objectives outlined in Chapter 2.

6.2.3.3 Defining the thickness and movement

Both the thickness of the zonular bundles as well as the displacements of the ciliary body lack data (see Section 3.2.4.2 and Section 3.2.4.3) therefore, the impact of varying both needs investigation so that the boundaries for these values can be defined.

It was assumed for the current test that the material properties of the lens, capsule and zonules were correct therefore, the discrepancy between the deformations measured and the expected changes arise from differences in the zonular thickness or displacement. Two simple tests were carried out; the first to establish which level of zonular displacement, with a constant section thickness, caused deformations that were close to expected. The second to see which section thickness variation caused suitable geometric changes.

Displacement test

It was outlined in Section 3.5.3 that there were differing views on the displacement of the ciliary body, with all the initial displacements modelled so far using the data of Kasthurirangan *et al.* (2011) (Method B, Equation 6.1 in the current test). Strenk *et al.* (1999) also measured the ciliary body movement, with the results showing the age related trend in Equation 6.2 (Method A in the current test), utilised in a number of existing FEA models (Chapter 2). Figure 6.10 illustrates the differences between proposals for the movement of the ciliary muscle, where it can be seen that there is a range of potential displacement values.

$$\text{Zonule Displacement} = 0.5129 - 0.00525 * A \quad (6.2)$$

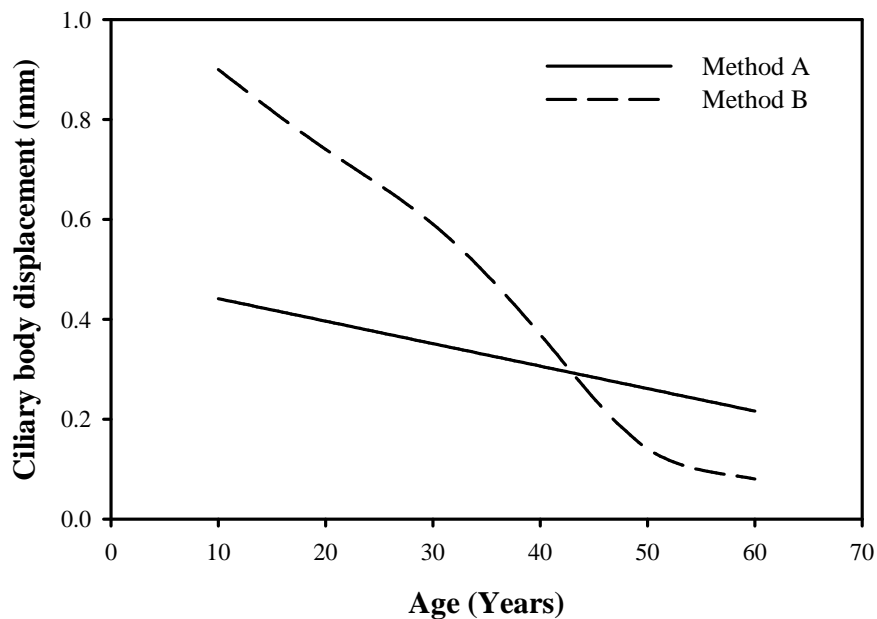


Figure 6.10: Illustration of the change in ciliary body displacement using method A based on a ciliary body displacement defined using Equation 6.2 and method B based on a ciliary body displacement defined using Equation 6.1.

By altering the geometric model to adopt alternate ciliary body displacements, new zonular displacements could be defined using the method detailed in Section 3.5.5.

The baseline geometry and material properties of the lens and capsule were taken from the models in Section 6.2.3.2, with only the zonular representation changing. A constant section thickness of 0.012 mm for the zonule bundles was used, combined with two variations on the displacements for each age lens.

For the 20 YO model, the results (Table 6.2) indicated that both displacement values did not produce suitable changes, but that Method A produced changes closer to what was expected. For the 40 YO model, both methods were very similar as a result of the similarity in displacement values (Figure 6.10), however method A induced a more appropriate thickness change. For the 50 YO models the displacement was closer to that of method A, with method B producing changes that were slightly too low. The overall axial movement of the lens was not suitable for all models, most likely due to the distribution of thickness between the zonules.

Table 6.2: The results of the displacement variation from Section 6.2.3.3. A *Indicates a change that was too high, a ** indicates a change that was too low, compared to measured *in vivo* data (Section 5.4.2).

Model	T _L change (mm)	L _R change (mm)	R _A change (mm)	R _P change (mm)
20_A	0.60*	0.38	3.72**	1.76
20_B	0.78*	0.53	6.20	2.11*
40_A	0.27	0.24	1.73	0.79
40_B	0.30*	0.27	2.09	0.78
50_A	0.10	0.21	0.51	0.18**
50_B	0.08	0.13	0.46	0.17**

Thickness test

The three age models from the previous section would then have the thickness distribution of the zonular groups adjusted, with three versions of the thickness distribution used as shown in Table 6.3. The distribution of thickness between the zonular bundles was taken from previous geometric studies, discussed in Section 3.2.4.3. The displacement of the ciliary body was defined using method A for all three ages.

Table 6.3: Zonule thickness values used in thickness test, showing the difference in thickness distribution used.

Zonule group	Thickness (mm)		
	Distribution 1	Distribution 2	Distribution 3
Anterior	0.036	0.025	0.012
Equator	0.006	0.012	0.006
Posterior 1	0.012	0.025	0.02
Posterior 2	0.012	0.012	0.012

Distribution 1 gave the best geometric changes overall (See Table A.4), although the thickness changes were still too high (by ≈ 0.1 mm) in the 20 and 40 YO models and the posterior curvature changes in the 50 YO model were too low (by 0.05 mm). The results therefore indicate that the anterior zonule thickness should be highest, followed by the posterior and then the equator. The PZ2 thickness is still an unknown at this stage, however, it is likely to be between the posterior and equatorial zonule bundle thickness.

6.2.3.4 Final zonule alterations

The testing conducted in Section 6.2.3.2 to Section 6.2.3.3 established that the zonule modelling method proposed in Chapter 3 induces deformations in the crystalline lens that are approaching the expected changes. The ciliary body displacement as defined using Equation 6.2 would appear to be suitable; however, the exact distribution of thickness between the zonule bundles required further investigation. Before the thickness distribution was explored, some additional assumptions in the current modelling methodology required testing.

It was stated in Chapter 3 that there were two potential methods of the positioning of the zonules in the accommodated state, the first by making them tangential to the lens surface and the second by attaching them at an angle to the tangential line. Two versions of the 40 YO model were modelled, to establish whether there was a difference between the two methods. Both models were deformed using the same displacement values for the zonule bundles, based on a ciliary body displacement defined using Equation 6.2.

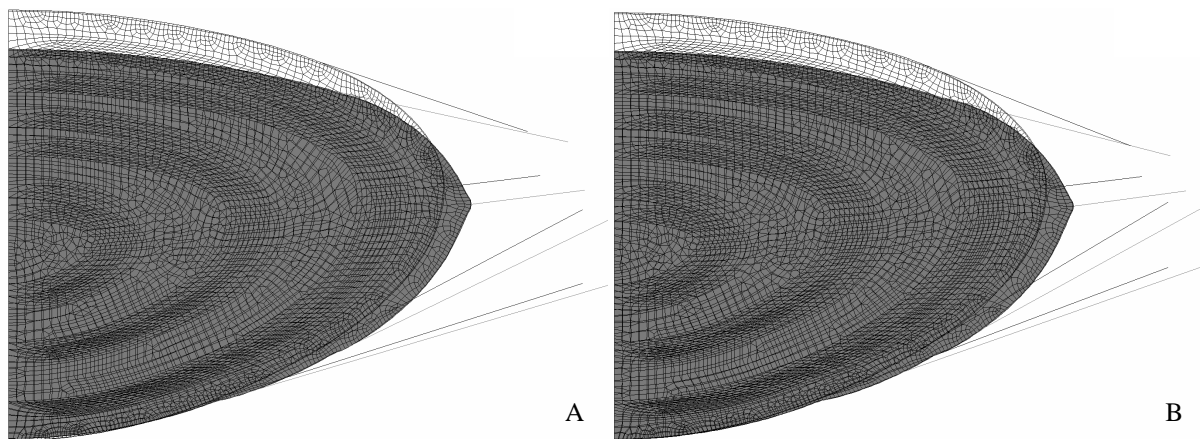


Figure 6.11: Comparison between the deformations in the 40 YO lens with two different zonule attachment methods based on a ciliary body displacement defined using Equation 6.2. A = Angled attachments, B= Tangential attachments.

Figure 6.11 shows the deformed outlines, showing how similar the two methods were, however, there was a slight improvement in the deformed shape using the angled attachments. This was principally due to a reduction in the amount of bunching that occurs at the zonule attachment points. Therefore, using an angled attachment was adopted for future models.

Part of the novel zonular modelling method proposed in (Section 3.5) was the use of four zonular bundles, with the proposed PZ2 zonule bundle used to represent the vitreous zonule. During the modelling conducted so far, it was found that the ciliary body attachment of the PZ2 zonule had an excessive migration along the ciliary body with age. In the current modelling methodology, the “pinning” zonule is positioned

using a line running tangent from the PZ2 lens attachment point (see Figure 3.11) and it was this that was causing the large axial migration.

The PZ2 zonule was assumed to run across the top of the vitreous. The shape of the vitreous was not known; however, it was assumed to form a shape similar to that shown in Figure 6.12 for the anterior portion of the vitreous. The pinning zonule was therefore altered to run from the ciliary body, close to the CT1 line, to the top of the vitreous, defined as being halfway between the PZ2 lens attachment and the bottom ciliary body point. Here, it would meet the PZ2 zonule running tangentially from the lens. With this alteration, the axial movement of the pinning zonule with age was reduced.

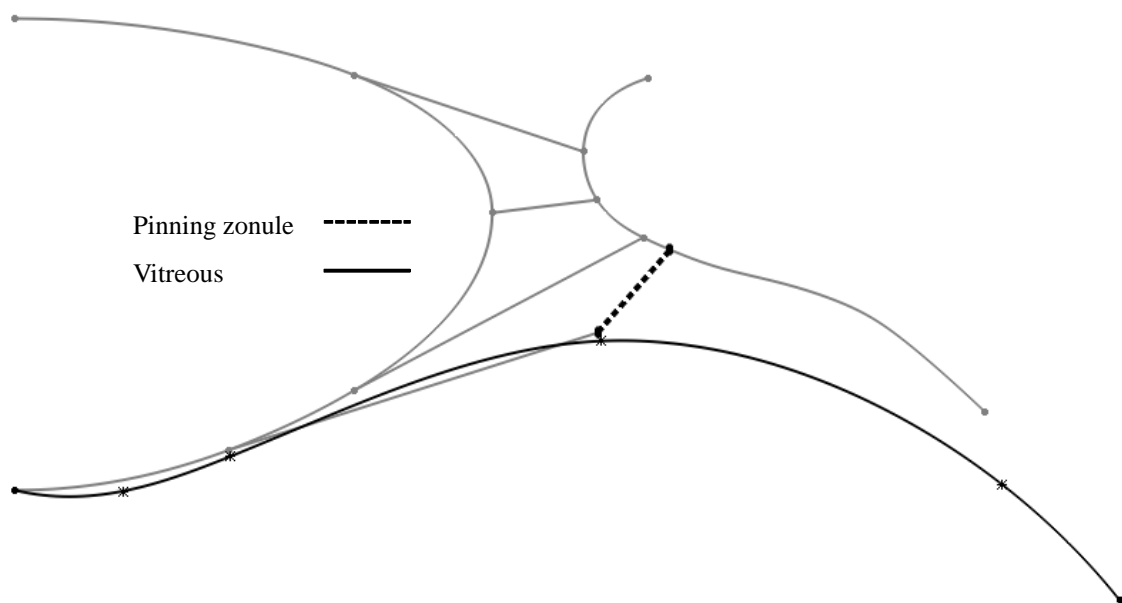


Figure 6.12: Illustration of the new modelling method for the PZ2 zonule in the 40 YO accommodated lens model. The black line indicates the vitreous with the dashed line indicating the altered pinning zonule.

The thickness of each zonule bundle and how the thickness varies across the bundles, was still uncertain. To aid in establishing an appropriate distribution, adjustments were made to the thickness values whilst also measuring the force applied by the ciliary body. It was assumed that the force applied by the ciliary muscle did not diminish significantly with age (e.g. Hermans *et al.*, 2008), but that the amount of ciliary body displacement reduces. Therefore, to maintain the same force, the zonular stiffness must increase, either from changes in the elastic modulus (shown to remain stable, or even reduce (Michael *et al.*, 2012)) or from the thickness, which has been less well studied (see Section 3.2.2.1). In previous FEA models (see Section 2.5.2), the force has been found to be between 0.03 N and 0.1N but not to change significantly with age.

Within ANSYS it is possible to extract the reaction forces on the four zonules (see Chapter 4) which was

done for the models used in Section 6.2.3.3, where the displacement reduced with age but the section thickness remained constant. The applied force in those three models (Table 6.4) showed a significant reduction with age; supporting the hypothesis that to retain the ciliary body force, the section thickness must increase with age. To test this hypothesis, as well as investigate the thickness distribution further, a number of new models were defined.

Table 6.4: Reaction forces calculated from the models used in Section 6.2.3.3, illustrating the reduction of force with age.

Model	Total Fx (N)
20_A	0.0737
40_A	0.0620
50_A	0.0488

Model set up

Three baseline models would be modelled (20, 40 and 50 YO), using the geometry and material properties of the lens and capsule from Section 6.2.3.3, with the ciliary body displacement defined using Equation 6.2. A new zonule arrangement for each age was modelled, based on the updated assumptions discussed previously.

A first iteration of the 20 YO lens would use a constant section thickness across the four zonule bundles (0.006 mm). Two subsequent iterations would double the thickness of the four zonule bundles. The resulting force and deformations from the three runs would then be used to establish a suitable zonule thickness distribution, based on the findings from Section 6.2.3.3.

When the 20 YO model performed satisfactorily, the section thicknesses were then applied to the 40 YO model and altered until the model matched the expected changes. The process was repeated using the final 40 YO thickness distribution applied to the 50 YO lens.

Results

The results of the initial 20 YO run are detailed in Table 6.5 and it was found that both the 0.012 and 0.024 mm thicknesses produced deformations close to expected changes, however, using a constant section thickness induced too much anterior movement.

By varying the section thickness between the four zonular groups, the overall movement was able to be controlled. Using 0.012 mm as a minimum thickness, the four zonular thicknesses were varied until the changes and lens movement were suitable. Repeating the process outlined previously, the thickness

Table 6.5: Results of the three iterations of zonular thickness in the 20 YO model.

Age (Years)	Iteration	Zonule bundle thickness (mm)	Net force (N)	Geometric changes
20	1	0.006	0.04	Too low
	2	0.012	0.069	Thickness too high, R_a too low
	3	0.024	0.11	Thickness too high, R_a too low

distributions were also established for the 40 and 50 YO models. The final thickness distributions varied with age (see Table A.2) and resulted in a ciliary body force that was constant with age. In terms of the geometric changes the results were not ideal, but provided a closer match across all ages than previous models (Table A.4), compared to measured *in vivo* data.

Conclusion of zonule testing

The final zonule arrangement established for the three ages did not provide a perfect match for the expected changes, principally due to high thickness changes; however, important data on how variation of the zonule bundle thickness affects the models was gained and it was decided to not continue alteration of those specific models. The current methodology for modelling the accommodative system requires alteration to the zonular thickness distribution before a final arrangement can be detailed, and using the information from the current section will aid in producing a suitable final definition in future models (Section 6.3.2).

6.2.4 Probabilistic Analysis

Due to the higher thickness changes that were occurring in the models tested so far, the influence of the material properties on the thickness change was investigated using probabilistic analysis (Chapter 3, ANSYS, 2010a). Within ANSYS, probabilistic analysis is a tool that takes a range of individual parameters (termed random inputs) input to a model and uses a statistical variation of these parameters to iteratively run updated versions of a model. How those random inputs are statistically relevant to a key change in the models (a random output) is then determined.

To run a probabilistic study, an existing model has to be re-made in such as way that ANSYS can repeatedly run the model without any further input. Each random input is defined as a single value with an appropriate statistical variation. The model is then run repeatedly using a slightly different input for each parameter in each iteration.

Two studies were carried out, both using the 40 YO model from Section 6.2.3.4 as the input model, adapted with the necessary changes needed for it to be run automatically.

6.2.4.1 Comparison of lens and capsule material properties

The first study used the lens and capsule material properties as the random inputs, using the properties for a 40 YO lens as defined in Chapter 4 as the baseline values. A Gaussian distribution was used to describe the variance in the data. The random output was the total thickness change of the lens.

Results

After running for 150 iterations, the results showed that the capsule shear modulus was the most significant parameter from the test (Figure 6.13), with layers 9, 4, 10 and 8 of the lens showing some significance. The results show that increasing the shear modulus of the capsule, layer 4 or layer 8 would result in an increase in thickness change, while increasing the shear modulus in layers 9 or 10 would reduce the thickness change.

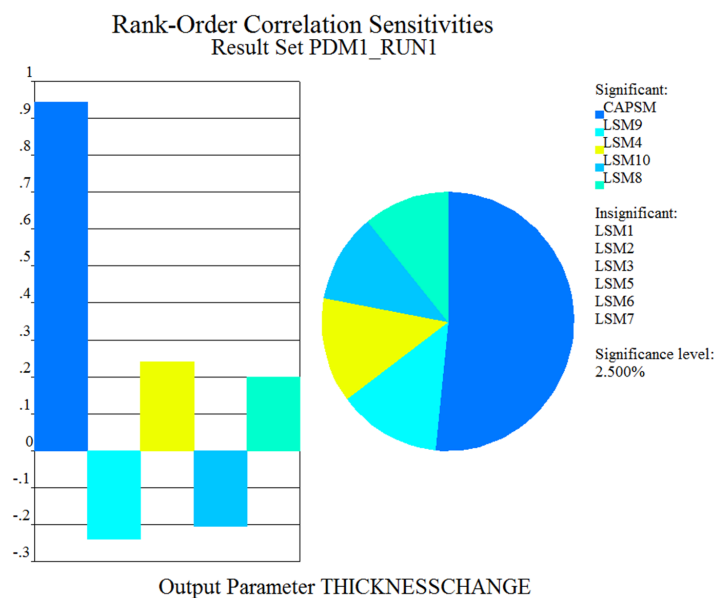


Figure 6.13: Results of probabilistic analysis 1, showing that the capsule and layers 9, 4, 10 and 8 are significant parameters in regards to the total thickness change.

6.2.4.2 Comparison of the capsule and zonule material properties

From Section 6.2.4.1, the influence of the capsule shear modulus was more significant to the thickness change than any alteration of the shear modulus of the internal layers. However, it has been established in Section 6.2.3 that the zonules also have an impact on the lens thickness change. A second analysis was conducted with the capsule and zonule material properties as the random inputs to investigate which has more influence, with the total thickness change and posterior pole movement as outputs.

6.2 Initial model development

The zonule elastic modulus was used as an input with a Gaussian distribution, meaning that the thickness distribution of the zonules would remain constant but the overall stiffness would be altered. The capsule material data was input as in Section 6.2.4.1.

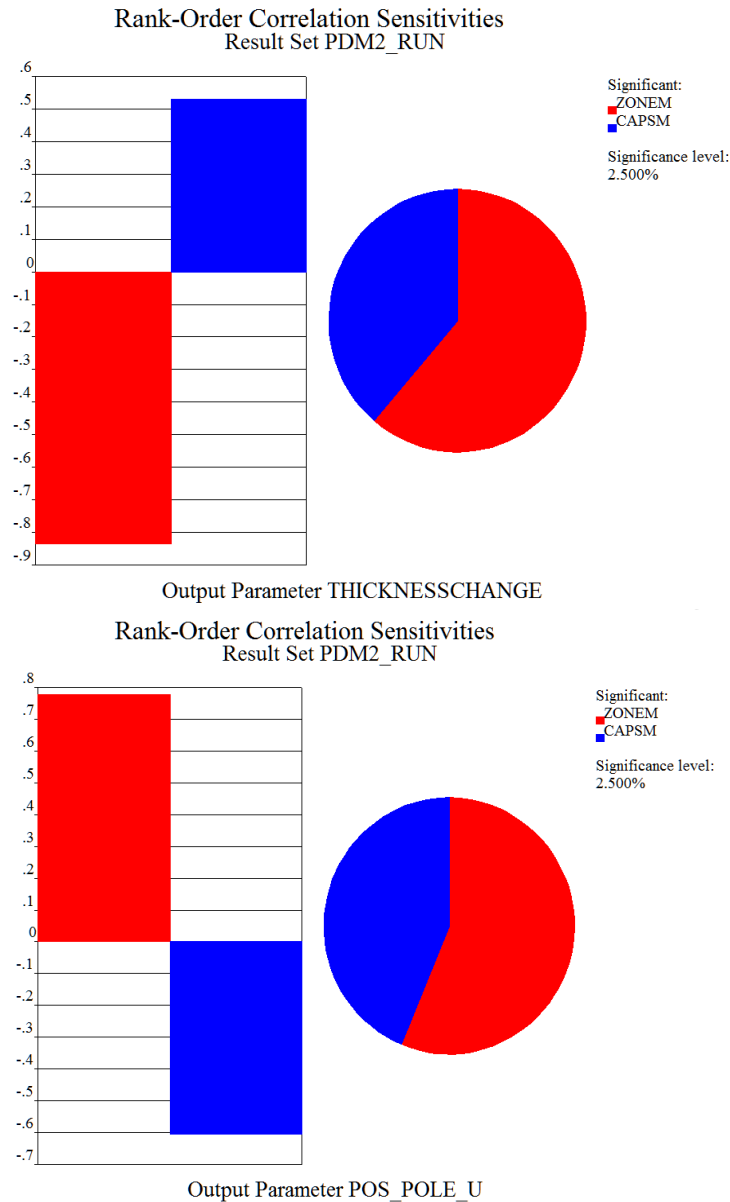


Figure 6.14: The results of probabilistic analysis 2, showing that the zonule elastic modulus was most significant for both outputs.

After running for 150 iterations, the results (Figure 6.14) showed that the zonule elastic modulus was marginally more significant for both outputs, although for the posterior movement an increase in the zonules elastic modulus would increase movement, whilst for the thickness change an increase in zonule elastic modulus would decrease the thickness change. The opposite was true for altering the capsule shear modulus in both cases.

The studies in Section 6.2.4.1 and Section 6.2.4.2 indicate that the capsule and zonules are key features of the model, and that alterations to either will have an impact on the models behaviour. Assuming that the alterations to the zonule elastic modulus alter the stiffness of the zonules, it is proposed that increasing the thickness of the zonules would have the same impact, similar to the findings in Section 6.2.3.4.

6.2.5 Internal structure test with zonules

The final part of the initial testing was to select the internal structure distribution to use in future models. Section 6.2.1 investigated the internal structure variation with a spinning test and it was shown that there was little difference between internal structure models. The loading conditions used in the study were not representative of the *in vivo* accommodation system, therefore, further comparison between internal structure models was needed using the zonular arrangement tested so far.

Using the best models from Section 6.2.3.4, which represent the SB model, combined with the SA and NC models used previously (Section 6.2.1) will allow deformations induced by zonular displacement to be compared between the different internal structure representations. The H model was not used, due to oversimplifying the internal structure. The procedure was the same as in the zonular tests detailed so far, with the material properties taken from Section 6.2.1.

In terms of thickness change, all three internal structure models were very closely matched across all ages (Figure 6.15 and Figure 6.16). The curvature changes had more variation (Figure 6.17), with the results for the 20 YO lens (not shown) showing a similar trend to the 40 YO lens, but with higher values.

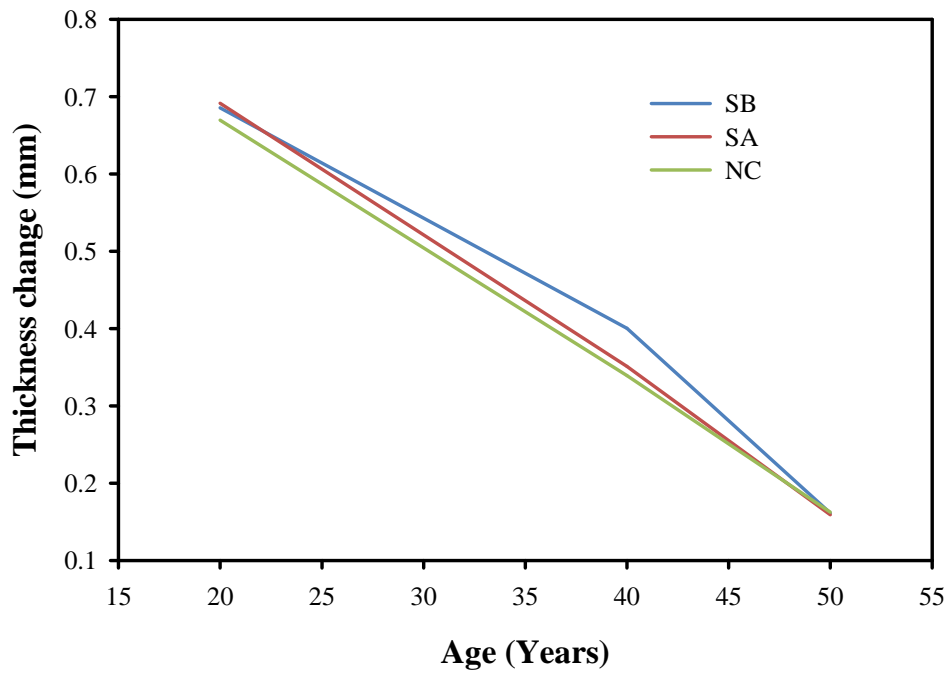


Figure 6.15: Thickness change in all internal structure models (with zonules) across all three ages.

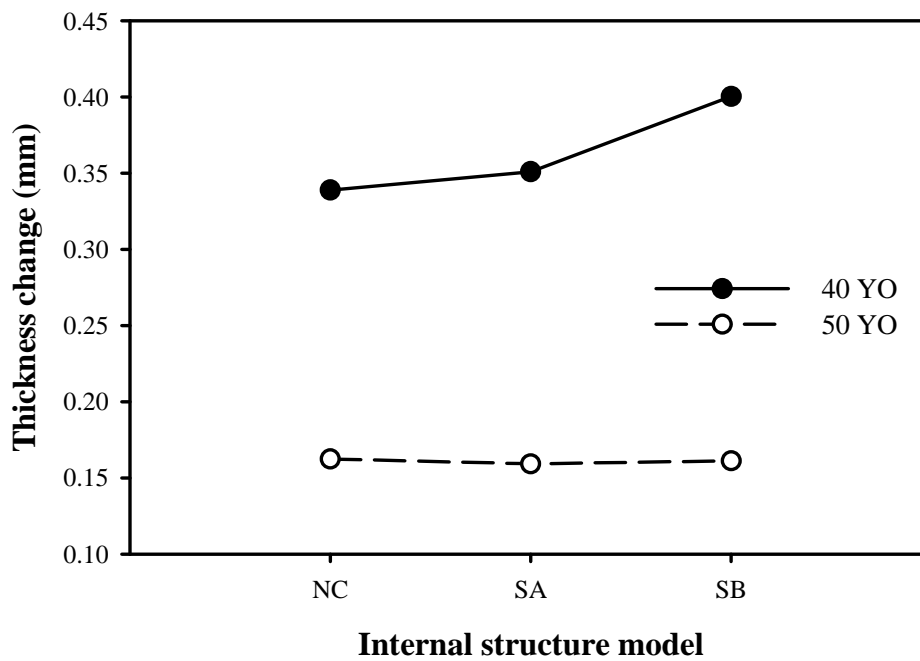


Figure 6.16: Thickness change of the 40 and 50 YO lens models with different internal structure models combined with the zonule structure.

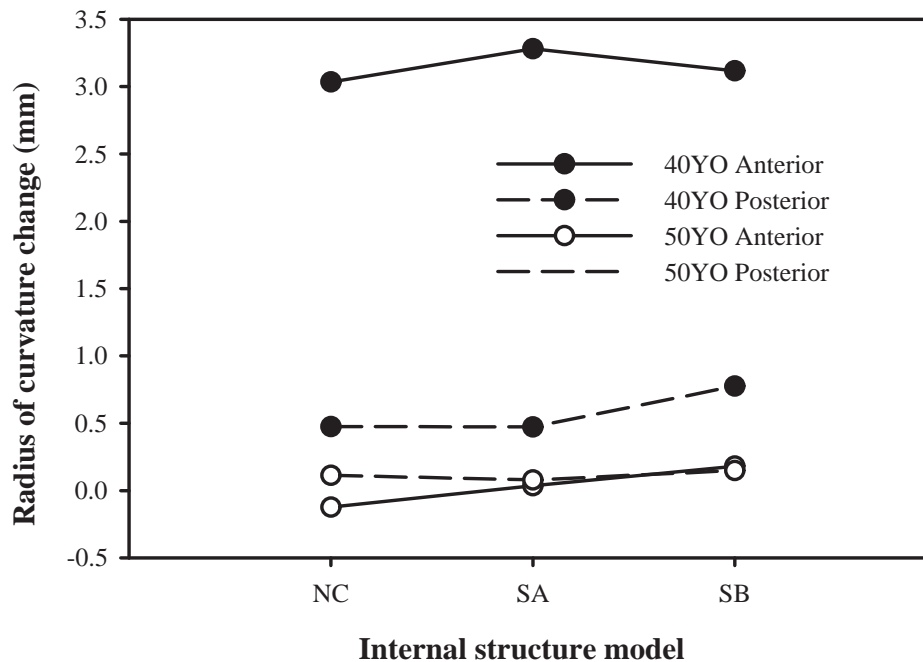


Figure 6.17: The curvatures changes of the 40 and 50 YO models with different internal structure models combined with the zonule structure.

The NC model can be discounted from future modelling methods, principally due to the low curvature changes in the 40 YO model, combined with a curvature decrease in the 50 YO model.

The SA and SB models again produced similar results, although the thickness change in the 40 YO SB model does have an increase over the NC and SA models, not seen in the 50 YO model. For the purposes of the current study, either the SA or SB model would appear to be suitable, however, due to the material data available, the SB model would be simpler to implement, therefore, it was selected for future modelling.

6.2.6 Summary of the model development

The principal purpose of the initial model development was to establish that the proposed modelling methods detailed in Chapters 3 to 5 resulted in an accommodation model that produced suitable changes in the crystalline lens at different ages. The secondary purpose was to elucidate any alterations that may be required to maximise the accuracy of the modelling methods, in addition to providing data on the key modelling parameters.

From the various tests conducted, it was shown that the proposed methods do produce suitable changes (i.e. they were a close match to measured *in vivo* data), but certain conditions would be needed in future

models:

1. The SB stiffness model should be used to represent the internal structure
2. The PZ2 zonule should be modelled according the definitions in Section 6.2.3.4
3. The zonule bundle thickness needs to increase with age, with the distributions between the bundles varying to ensure suitable movement of the lens.
4. The zonules should attach to the lens at an angle to reduce localised deformations.

6.3 Accommodation modelling

Using the information from Section 6.2, the proposed adaptations to the methods outlined in Chapters 3 – 5 were made, before three new accommodation models were defined. These three models were used, once they were shown to give suitable accommodative changes, to investigate how different age related changes impact on the accommodative process. The models in the current section will have additional results extracted to allow further comparison to data from the literature, as detailed in Section 5.4.1.

6.3.1 Models from baseline data

Three new age models were developed from the baseline data given in Chapter 3. The ages selected were 29 YO, 45 YO and 60 YO chosen so that comparisons to previous studies could be made, with the majority of previous work using similar ages (Section 2.4.1). The ages also represent different stages in the decline of accommodative ability with age (see Section 1.3).

The baseline models geometry was generated using the methods from Chapter 3, with the alterations to the zonular structure proposed in Section 6.2.3.4 made (e.g. PZ2 attachment redefined, zonules attach at an angle from the lens body). The ciliary body displacement was taken from the displacement values given by Equation 6.2. The section thickness variation was initially based on the values defined in Section 6.2.3.4.

Figure 6.18 illustrates the geometric representation used to establish the zonular positions and displacement for the three age models, with the displacement values for the three models detailed in Table A.1. The procedure from Section 5.3.5.2 was followed.

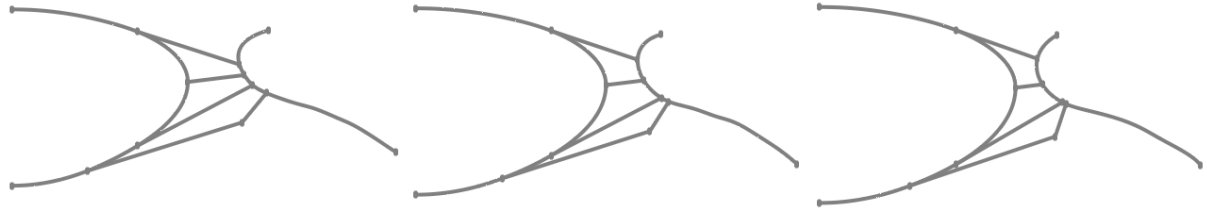


Figure 6.18: The zonular arrangements used in the 29, 45 and 60 YO models from Section 6.3.1.

6.3.1.1 Results of baseline models

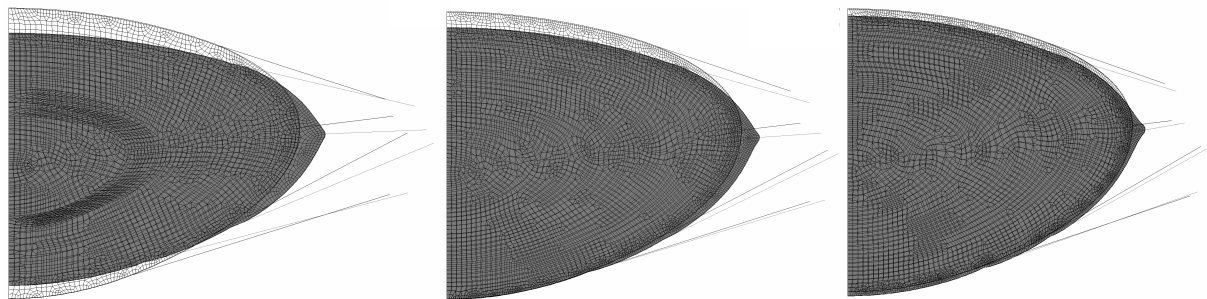


Figure 6.19: Results of the first run of the baseline 29, 45 and 60 YO models based on the ciliary body displacement defined using Equation 6.2.

In addition to the results that have been analysed so far, extra results were extracted from the deformed lenses in the current study (as detailed in Section 5.4.1). For the principal geometric changes, the initial run was favourable for the three models (Figure 6.19, Table A.5). There were discrepancies in the total force applied to the lenses and in the movement of the posterior pole, in particular in the 45 and 60 YO models. The 29 YO model appeared to be the most suitable, matching the expected changes in diameter and surface curvatures, only not matching the expected thickness change. The curvature change in the 60 YO model showed a decrease instead of an increase which would need to be altered. The 45 YO and 60 YO models both had problems with the overall movement, with the 45 YO lens having too much anterior pole movement and the 60 YO lens having a backwards movement of the posterior pole. The current internal thickness changes also appeared to diverge from the literature, in particular for the 60 YO lens, where it only accounted for 6% of the total change, compared to the expected majority (Section 3.2.2.1).

To remedy the current shortcoming, the findings from Section 6.2 were used to inform the alterations that are required. For the 29 YO lens, a reduction in force combined with a reduction in thickness change and more posterior movement would be preferred. For the 45 YO lens, a reduction in anterior pole movement and an increase in force was required. The 60 YO lens required the anterior curvature change to increase, combined with an increase in the force and anterior pole movement.

6.3.2 Model variations

Alterations to the models were carried out in stages; initially, only the zonule bundle thickness was altered, through alteration of the individual bundles or the thickness distribution of the bundles. If this failed to improve the model, the displacement values would be altered. A summary of the changes that were needed to be made will be given for each model, although these were established after iterative adjustments.

For the 29 YO model, the first changes were to the thickness of the zonules, as in Section 6.2.4 it was shown that decreasing the zonule stiffness (here via the thickness) potentially reduces the thickness change in the lens. A thickness reduction of 0.01 mm in each zonule bundle was found to provide suitable changes.

For the 45 YO model, the section thickness was increased for all zonules, again to adjust the stiffness, with the displacements of the anterior and equatorial zonules reduced in the y direction (Table A.1).

For the 60 YO model, the two alteration methods failed to improve the anterior curvature changes, therefore, alternative methods were required. The probabilistic modelling in Section 6.2 showed how the lens material and capsule material were significant factors in the changes in thickness. It was hypothesised that the reduction in anterior curvature was a result of the high central stiffness of the lens material, an aspect of the data of Wilde *et al.* (2012) discussed in Section 4.3.1.6. Due to this high central stiffness (evident by the 5% decrease in nucleus thickness in the initial model), the outer lens layers of the lens were being deformed in a way that resulted in an anterior curvature decrease. The material properties of Weeber *et al.* (2007) give a lower central stiffness, while maintaining a similar stiffness profile (see Figure 4.2, page 124), therefore, these properties were adopted to establish whether they would make a difference and it was found that this led to an anterior curvature increase. Subsequently, the thickness of the anterior and posterior zonular bundles was increased to provide suitable force application.

The final geometric changes achieved with the adjusted models are given in Table 6.6 with the deformed lens profiles illustrated in Figure 6.20. These adjusted models will be used to analyse theories of both accommodation (Section 6.3.3) and presbyopia (Section 6.4). A full breakdown of the material and geometric properties of each of the three models is given in Section A.3.

Table 6.6: The geometric and force changes during disaccommodation in the altered models of the 29, 45 and 60 YO models. Compared to the expected changes (Section 5.4.2) a * indicates a change that is too high and a ** indicates a change that is too low.

Parameter	29 YO	45 YO	60 YO
Thickness change (mm)	0.518*	0.244	0.065
Diameter change (mm)	0.342	0.263	0.090
Anterior radius of curvature change (mm)	3.613	1.073	0.050**
Posterior radius of curvature change (mm)	1.215	0.441	0.150
Total force (N)	0.089	0.086	0.083
Anterior pole movement (mm)	-0.346 (67%)	-0.186 (76%)	-0.057 (87%)
Posterior pole movement (mm)	0.172	0.058	0.008
Central movement (mm)	-0.0819	-0.0562	-0.0198
Equatorial axial movement (mm)	-0.0892	-0.0566	-0.0290
Nucleus thickness change (mm)	0.226 (44%)	0.0891 (37%)	0.0095 (15%)
Ratio of anterior to posterior thickness change	1.04	1.14	1.37
Volume change (mm ³)	-0.07	-0.41	-0.05
Surface area Change (mm ²)	9.98	6.86	2.84

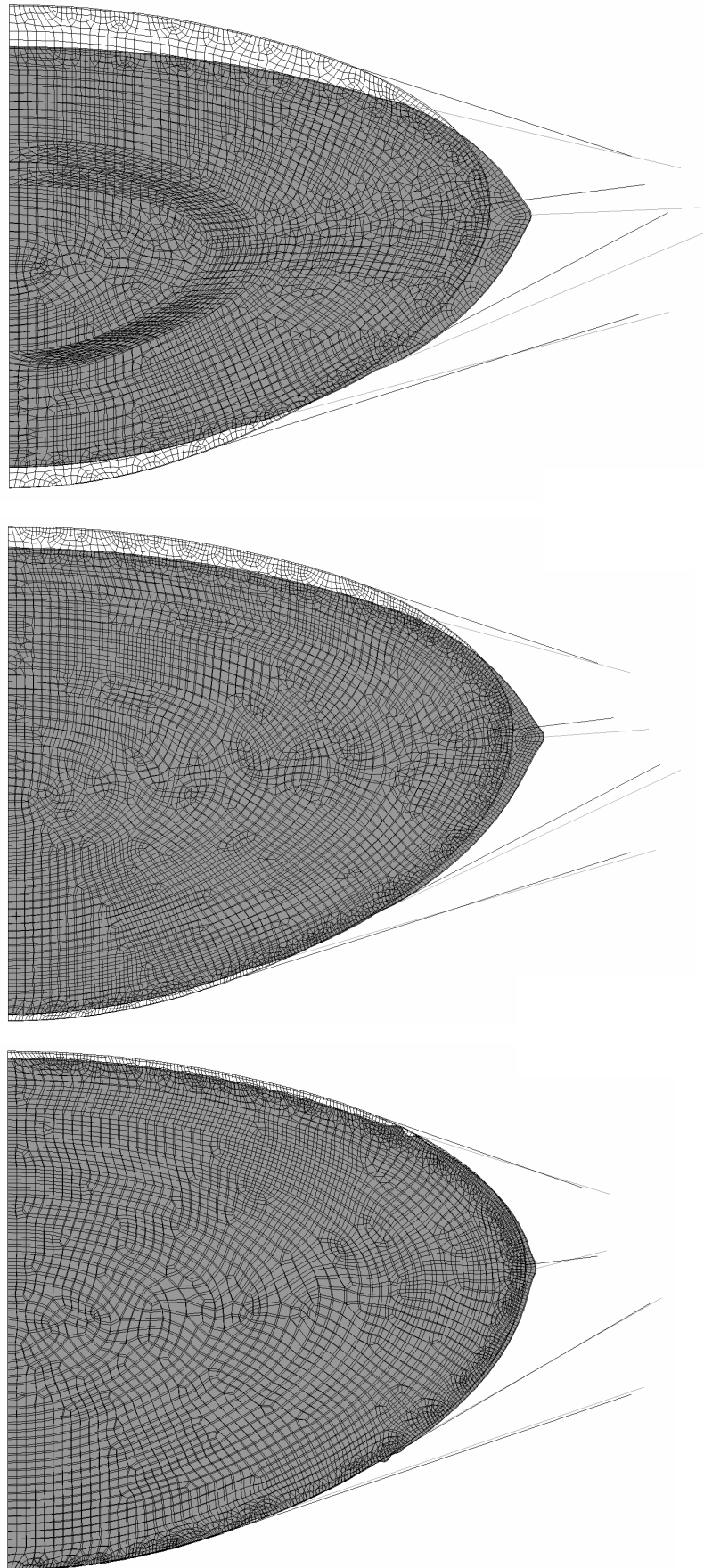


Figure 6.20: Deformations in the 29, 45 and 60 YO altered models (Section 6.3.2) based on a ciliary body displacement defined using Equation 6.2.

6.3.3 Analysis of accommodation

Before the main investigation into which parameters are key in the decline of accommodation (Section 6.4), a comparison of the current model to previous models and to measured *in vivo* data is needed.

6.3.3.1 Comparison to measured data

Chapter 3 gave a comprehensive overview of existing *in vivo* measurements of the accommodative system, which can now be used to evaluate the FEA models. To illustrate how the models compare to the literature, the graphs plotted in Section 5.4 showing the variation in data were used (Figure 6.21). The results of the current models were plotted on the graphs, along with the changes measured in previous FEA models, which will be discussed in Section 6.3.3.2.

All of the changes in the three ages fitted within the wider variation of the measured *in vivo* data, replicating the trends with age well. The thickness changes appeared to be higher than the mean values, a potential result of the material properties used, which will be discussed further in Section 6.3.3.2.

In addition to the four key measurements, additional data can be compared. The movement of the anterior and posterior poles matches what has been measured in the literature (Section 3.2.2.4) in that the anterior pole movement accounts for more of the thickness change than the posterior (67% - 87%). The overall movement of the posterior pole is a disputed aspect of accommodation (Section 3.2.2.4), however, it would appear that the posterior pole either remains constant, or moves backwards with accommodation. The current models show that the posterior pole moves forwards in all models.

A recent study by Croft *et al.* (2013) measured the movements of the lens equator, ciliary muscle and vitreous zonule during accommodation in 19 human subjects aged 19 – 65. The results supported the overall findings of the current study, in addition to providing insight into the modelling methods used. The lens equator was seen to move both anteriorly and inwards during accommodation, with both amounts reducing with age, matching the measurements of the equatorial change of the lens seen in the current models. The ciliary muscle thickness was also shown to increase with accommodation and was significantly linked to an increase in lens thickness. The attachment of the posterior zonule to the sclera was imaged and shown to move forwards with accommodation, with a link to the respective forwards movement of the lens equator, also seen in the current models.

The amount of force that can be applied by the ciliary muscle has been hypothesised to remain stable with age; which is supported by the current model, in addition to the testing conducted in Section 6.2. Previous

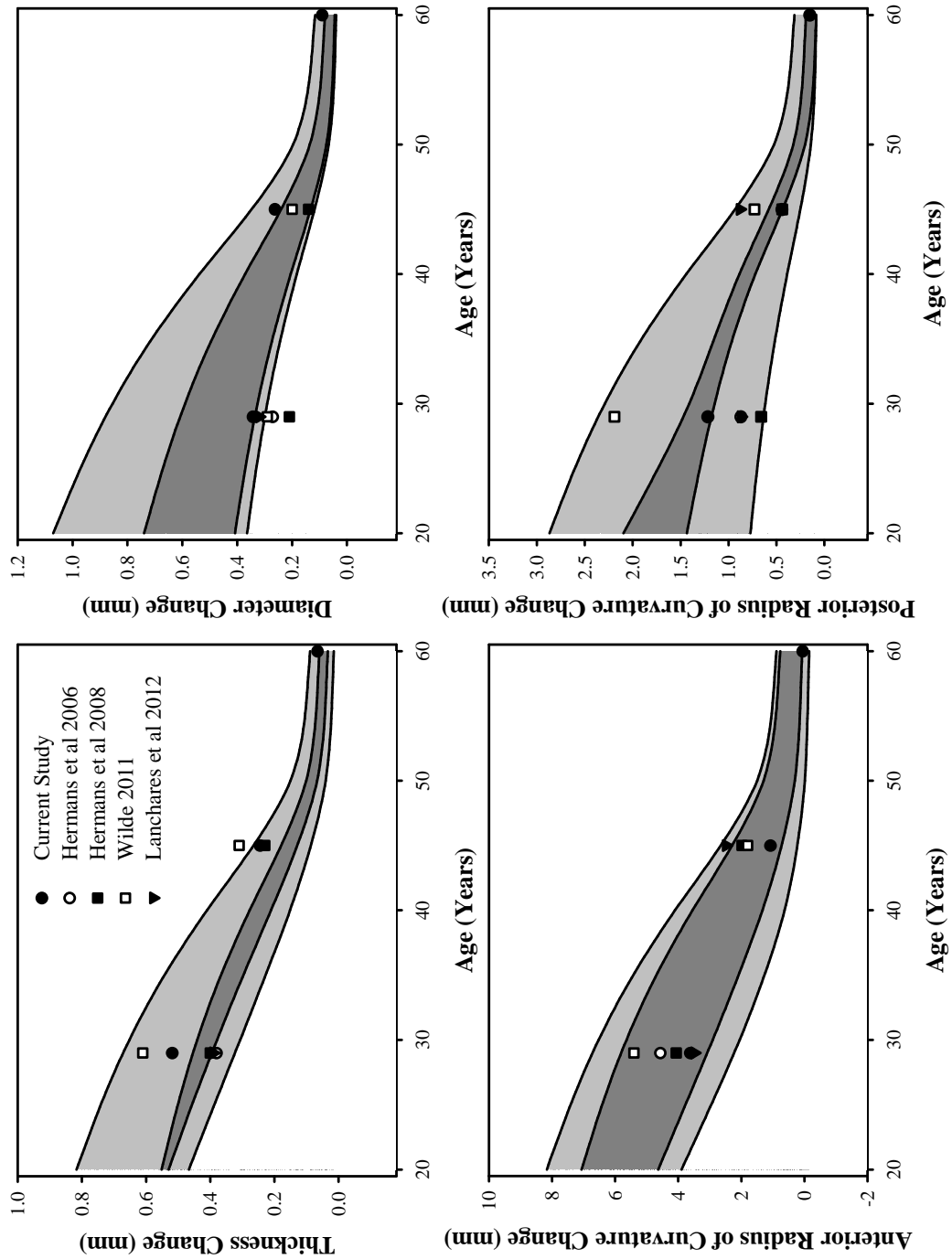


Figure 6.21: Comparison of the current model results to measured *in vivo* data, taken from Section 5.4.

measurements *in vitro* have shown similar force values (Manns *et al.*, 2007; Ziebarth *et al.*, 2008) to those measured in the current models.

The volume and surface area changes are disputed (Section 3.2.2.5), but the current model supports the measurements that show a volume increase combined with a surface area decrease with accommodation (e.g. Sheppard *et al.*, 2011).

There are some parameters that appear to have a deviation from measured data. The overall thickness changes appear to be consistently high at all ages, although they are within the wide variation measured (Figure 6.21). The internal thickness changes also deviate from measured data in two ways; firstly, in that the amount of thickness change within the nucleus reduces with age and secondly, that the contribution of the nucleus to the overall thickness change has a maximum of 44% in the 29 YO model. Dubbelman *et al.* (2003) showed that the nucleus is responsible for the majority of the thickness change, and that this does not change with age Section 3.2.2.1. Further analysis of the distribution of changes between the anterior and posterior portions of the lens shows that the change in thickness of the anterior half of the lens was consistently higher than the posterior half, and the contribution of the anterior half increased with age.

Two potential explanations for the discrepancy in internal thickness changes are the material properties used and the zonular arrangement. In Section 6.2.4 it was shown that the most significant contributors to the overall thickness change are the capsule and outer layers of the lens, indicating that the nucleus has less of an impact than the cortex. How the material properties change with age also would support this as the nucleus material properties stiffen, which would reduce its ability to decrease in thickness. In terms of the zonular arrangement, it is possible that the way the zonules are structured has an impact on the compressive forces distributed through the lens and that they are causing an excessive amount of thickness change. In addition, there is some obvious localised deformations at the zonular attachment locations on the 60 YO lens, with lesser deformations at the equatorial attachments in the 29 and 45 YO lenses, which could also be attributed to the zonular configuration.

6.3.3.2 Comparison to previous FEA models

A range of different ages and simulation methods have been utilised in previous FEA models (Chapter 2) however, there are a number of studies that have analysed similar age models to the current study, allowing a comparison to those studies to be made.

Changes in shape

The principal changes to compare are the changes in thickness, anterior curvature and posterior curvature. How much of the thickness change occurs in the nucleus is also a common measured parameter. The full set of results can be seen in Table A.6, but a comparison of the thickness, curvature and diameter changes to measured *in vivo* data can be seen in Figure 6.21.

Overall the current model compares well, showing similar changes in all regards with a better match to the curvature changes than previous models, although no changes in 60 YO lenses were reported in the literature. The thickness changes are higher than some previous models, but this could be a result of the differences in the representation of the material properties, with only the model of Wilde (2011) using a similar stiffness representation and obtaining higher thickness changes.

The contribution of the nucleus thickness change to the overall thickness change varies between previous FEA models, from 52% (Hermans *et al.*, 2006) to 80% (Wilde *et al.*, 2012) in a 29 YO lens, with the current 29 YO model having a change of 43%. For the 45 YO lens no other studies reported values, although Wilde (2011) inferred that both the 29 and 45 YO model did not match with the expected changes of Dubbelman *et al.* (2003). Weeber & van der Heijde (2008) gave the change in thickness of the nucleus as 0.07 mm/D for their 20 YO model, which is equivalent to approximately 0.03 mm/D in the current model (29 YO), although the power calculations may have an impact on the estimation (see Chapter 5). These findings show that the current model is not anomalous in terms of the internal thickness change, which would indicate further investigation into the apparent discrepancy between *in vivo* measurement and modelling is required.

Hermans *et al.* (2008) measured the change in surface area, finding that the 29 YO model had an increase of 6 mm² and the 45 YO model an increase of 5 mm², which compares to 9.98 mm² and 6.86 mm² in the current model.

In terms of the localised deformations, those models that have modelled the zonular structure also demonstrated similar localised deformations across different ages where deformed lens models were shown, for example, Figure 5 of Burd *et al.* (2002), Figure 2 of Weeber & van der Heijde (2008) and Figures 9.7 and 9.8 of Wilde (2011).

Lens movement

In all three age lenses modelled in the current section, the posterior pole had an anterior movement. In images of the deformed 29 YO lens from Burd *et al.* (2002), the anterior pole appeared to move twice as

much as the posterior. In the study of Hermans *et al.* (2006), the posterior and anterior pole movements appeared similar in magnitude, with no axial movement of the lens. The images from Wilde (2011) appear to show similar movements of both the 29 and 45 YO lens, with slightly too little posterior pole movement in the 45 YO model compared to *in vivo* measurements. Finally, the study of Lanchares *et al.* (2012) showed that the posterior pole appeared to have more movement than the anterior pole in the 30 YO model, although the lens was fixed and constrained from moving axially. Therefore, it would appear that the current model is the only model that is capable to recreating the known *in vivo* movement of the lens across multiple ages.

Ciliary body force

Figure 6.22 shows that the current model matches well with previous calculations of the amount of force transmitted to the lens by the ciliary muscle. The studies of Hermans *et al.* (2006) and Lanchares *et al.* (2012) inputted force values to an FEA model until the deformations matched what was expected, whilst the current study, Burd *et al.* (2002) and Wilde (2011) calculated the force based on the displacement of the zonules. As discussed in Section 6.3.3.1, these results compare well to *in vitro* experimental results.

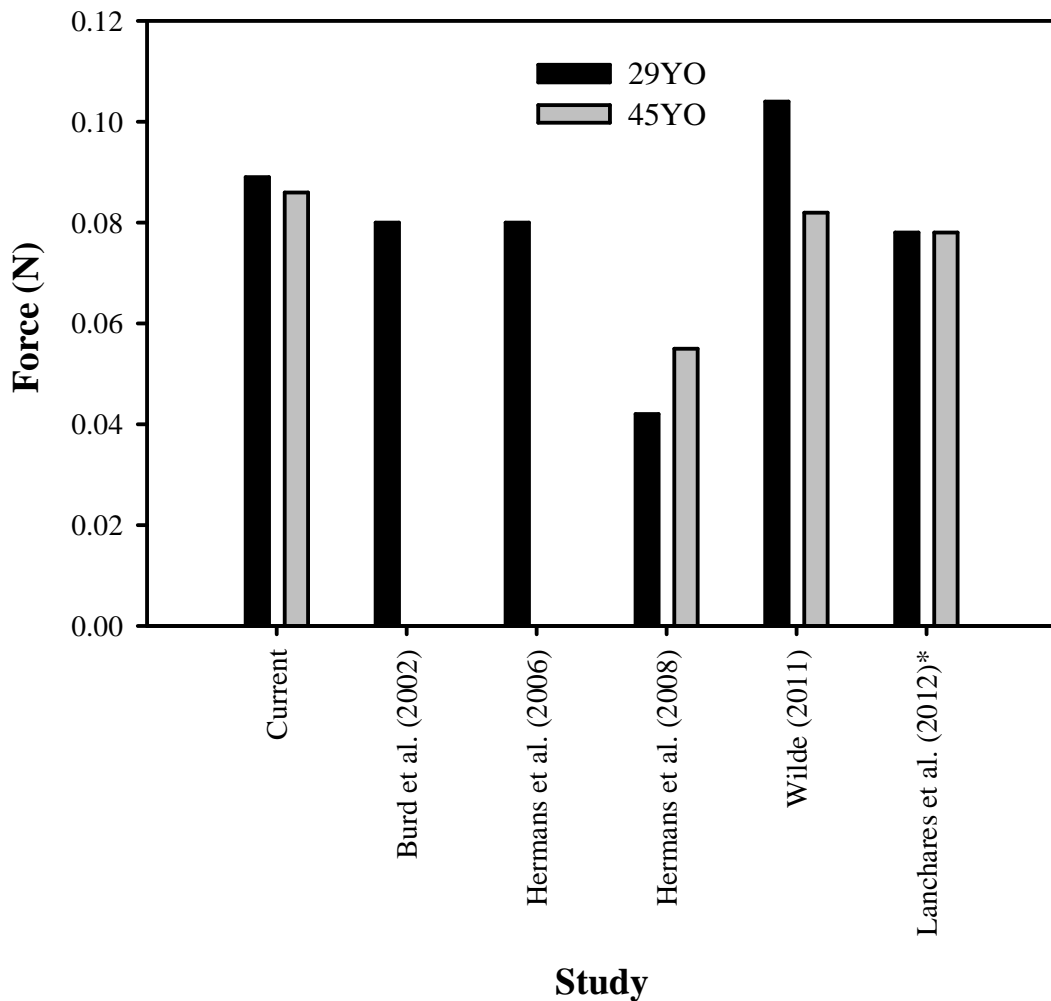


Figure 6.22: Comparison between the measured force values in the current and previous FEA studies. * The two models from this study were 30 YO and 40 YO.

Stress and Strain

The use of FEA allows for the internal stress and strain of deformed models to be visualised. The study of Hermans *et al.* (2006) showed that the von Mises stress (equivalent stress of all the normal and shear stresses) within the lens ranged from a maximum at the equator of $1.5e-03 \text{ N/mm}^2$ to a minimum in the central nucleus of $3.5e-05 \text{ N/mm}^2$. The majority of the higher stress was in the equatorial plane around the periphery of the lens.

In the Weeber & van der Heijde (2008) study, the strain distributions in both the x and y directions were plotted for 20, 40 and 60 YO lenses. In the x direction, the majority of strain was at the equatorial zonule attachment, however, the distribution through the lens changed with age. In the young lens, there was

more strain in the nucleus region, but this had disappeared in the old lens. In the y direction, a similar trend was seen, where in the young lens the strain varied along the y axis, with high values at both poles and centrally. The middle aged lens had lower central values but similar values at the poles. In the old lens, the strain was highest at the poles, with very little strain in the centre.

Lanchares *et al.* (2012) plotted the stress and strain for the capsule alone, as well as the stress distribution through the lens for a 30 YO lens. The stress within the lens was at a maximum at the equatorial zonule position ($5.5e-04 \text{ N/mm}^2$), with the maximum tensile stress along the optical axis of $1.9e-05 \text{ N/mm}^2$ and a compressive stress of $-2.5e-04 \text{ N/mm}^2$ in the nucleus region. The capsular stresses were higher, with the maximum stress in the posterior pole region of $1.6e-01 \text{ N/mm}^2$ (thinnest region), decreasing towards the lens equator with a stress of $8.2e-02 \text{ N/mm}^2$ (thickest region).

The stress distribution in the three lens bodies from the current study are shown in Figure 6.23, for both the first principal stress (A) and von Mises (B). Compared to Hermans *et al.* (2006), the stresses are lower for the 29 YO model, however, the distribution is similar with higher stresses at the periphery with low stress in the nucleus region. The first principal stresses in the 29 YO lens are a magnitude higher than for Lanchares *et al.* (2012), although the distribution follows a similar pattern in the current model. The differences in values in both comparisons are most likely due to the differences in material property distribution and force loading used, particularly due to both other models loading the lens with forces directly rather than using the displacement method. Figure 6.23 also shows the x (C) and y (D) axis strain distributions, to compare to the results of Weeber & van der Heijde (2008). The 29 and 45 YO models in the current study show a similar trend to the 20 and 40 YO models in Weeber's study.

The capsule stress had similar values to Lanchares *et al.* (2012), with a high stress at the posterior pole, which also decrease towards the equator (E, Figure 6.23). A second area of high stress was found close to the AZ attachment, not seen in Lanchares *et al.*, 2012, but a similar stress at the anterior pole was seen. The strain distributions were similar, both in terms of values and variation around the capsule (F, Figure 6.23), indicating that the capsule representation in both models was similar, with the principal differences found in the distribution and values of the lens material properties.

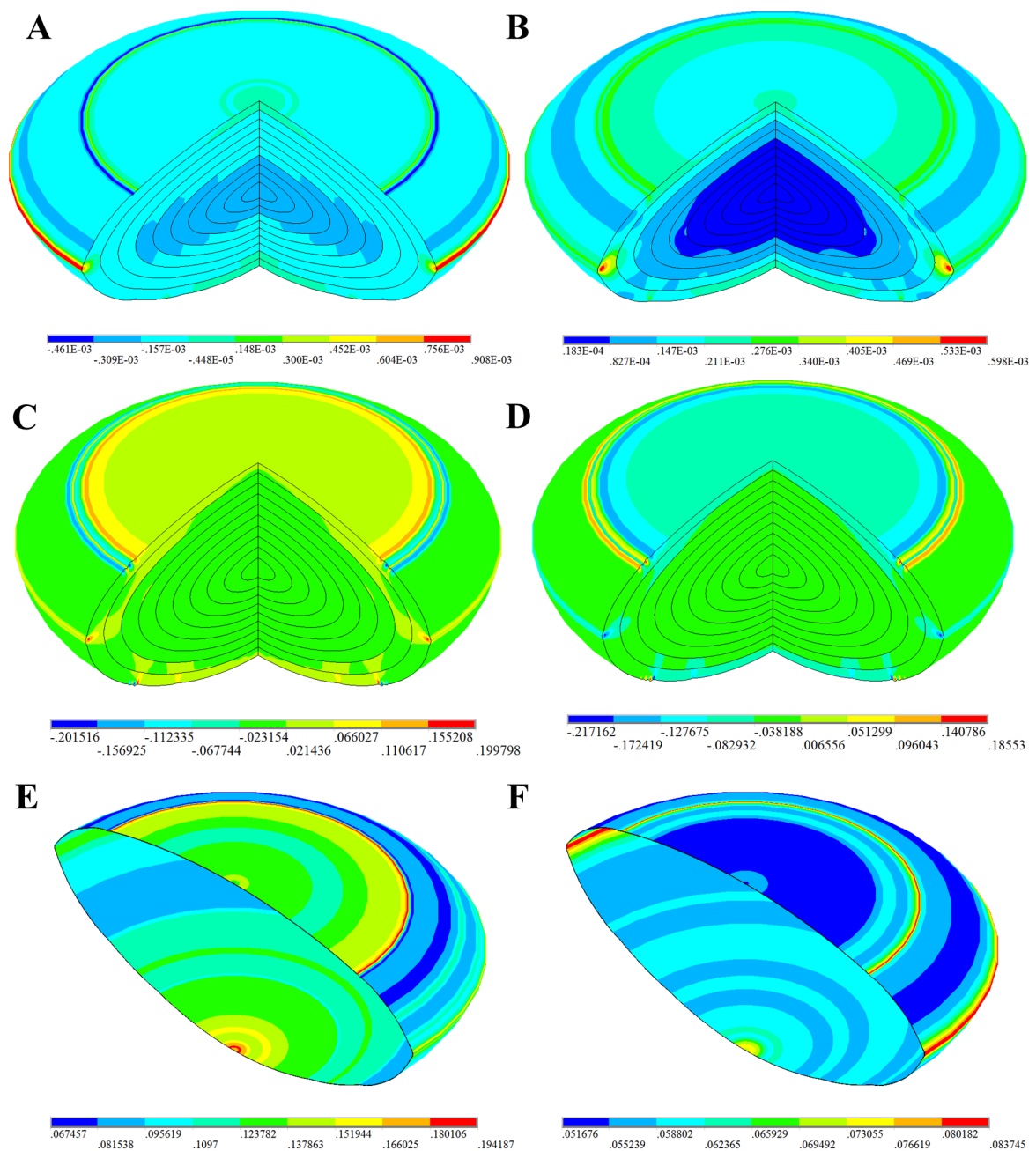


Figure 6.23: A: 1st Principal stress distribution in the 29 YO model B: Von Mises stress distribution in the 29 YO model. C: X axis strain in the 60 YO model D: y axis strain in the 60 YO model E: 1st Principal stress distribution in the 29 YO capsule F: 1st Principal strain distribution in the 29 YO Capsule. All models are shown utilising the symmetry expansion option in ANSYS, available due to the axisymmetric options used in the current models. All Stress values are in Pa.

6.3.4 Summary of accommodaion modelling

Overall the current model captures the majority of expected geometric changes that occur in the crystalline lens with accommodation and compares well with previous attempts at using FEA to model the accom-

modative system. The discrepancies present can be explained by the variation that is present in the data utilised to model the various components as well as the assumptions that have been made on aspects that have not been sufficiently measured hitherto, such as the material properties, as noted by Weeber & van der Heijde (2008); Wilde (2011) and Lanchares *et al.* (2012).

It is proposed that the model is suitable to be used in a further study that will investigate how the alteration of key aspects of the model will affect its accommodative ability to try to elucidate potential causes of Presbyopia.

6.4 Presbyopia modelling

Using the final three models from Section 6.3.2, individual parameters will now be altered to investigate the changes they cause to the accommodative ability on the model. So far, the optical capabilities of the lens models have not been measured, due to the limitations discussed in Section 5.4. However, to enable a method of comparison between the three baseline models from Section 6.3.2 and the deformations induced by the altered models in the current section, the power will be calculated, using the thick lens formula (Equation 5.1).

6.4.1 Variations to parameters of the baseline models

6.4.1.1 Material Property Variation

The first study will investigate altering the material properties, whilst keeping the geometry constant. First, only the lens properties will be altered, keeping the capsule and zonules constant. For example, the 29 YO model will have its lens material replaced with those of a 45 YO lens and then a 60 YO lens (Models 29_45M and 29_60M respectively). A second test will only alter the capsule properties (Models 29_45CM and 45_29CM), before alteration of both in a final test (Models 29_60LCM and 60_29LCM).

The purpose of altering the material properties is to establish how important they are in the development of presbyopia, as well as see if alteration of the properties in the old eye can increase the accommodative ability, information important in aiding development of accommodative restoration techniques (see Section 1.3.3). By only altering the capsule properties, insight into the role of the capsule with age can be gained, while alteration of both lens and capsule allows for a comparison to only altering the lens properties.

6.4.1.2 Displacement Variation

The second study will alter the displacements applied to the lens, with the lens geometry and material properties remaining constant. For example, a 29 YO lens can be combined with the ciliary body of a 60 YO lens to give the appropriate displacements for a 60 YO eye (29_60D). The zonules are remodelled for the new lens and ciliary body combination, however, the zonular thickness of the baseline model is retained. Additional models were run where the thickness of the zonules was adjusted to match the ciliary body model used, e.g. 29_60D+60ZA.

The purpose of altering the displacement of the ciliary body is to investigate the presbyopia theories that attribute the decline in accommodative ability to the changes in the ciliary body. For example, the Hess-Gullstrand theory (Section 1.3) is based on the force of the ciliary muscle remaining constant, with the only changes with age being in the lens, replicated in the current study by modelling an older lens with a younger ciliary body model.

6.4.1.3 Variation in lens attachments

It has been proposed by Koretz & Handelman (1986) that the zonular attachments move with age becoming more tangential (Section 1.3), a potential cause of accommodative decline. As part of the current modelling method, the zonules do move further away from the equator but to test the hypothesis of Koretz & Handelman (1986), the 29 YO model was adopted to give the 60 YO zonule positions (29_60ZA) which are further away from the equator. The ciliary body model of the 29 YO was retained, giving only a change in zonule attachment position. The result of this alteration was that the zonule attachments on the ciliary body spread further apart, giving a more horizontal application of displacement. A 60 YO model was also adapted to have the 29 YO zonule positions (60_29ZA) which are a lot closer to the equator, to see what impact that has. Again the ciliary body model of the 60 YO was retained. From this alteration, the zonule attachments moved closer together on the ciliary body resulting in a more vertical application of displacement.

6.4.1.4 Stiffness profile variation

It was discussed in the previous section how the thickness changes in the current models deviate from the literature. It was therefore decided to investigate how alteration of the stiffness profile in an old lens would affect the changes the lens undergoes. Using the 60 YO lens model, the crystalline lens material

properties would be reversed, meaning the inner nucleus values are now assigned to the outer cortex. Two variations, using the 29 YO material properties (60_29SV) and the 60YO material properties (60_60SV) were made.

6.4.2 Results of parameteric variations

The focus of the current study is on how changes to parameters of the baseline models affect the ability of the model to change shape and hence, power. Therefore, the results given in Table 6.7 (Page 197) show how the power changes in the altered models compare to the power change of the baseline model, with a full summary of the measured changes in Table A.7. The effect of variations to each of baseline models will be discussed before looking at how the current investigation compares to similar ones conducted in previous FEA models. How the results support the various theories of accommodation can then be explored.

6.4.2.1 29 YO

Alterations to the 29 YO model highlight which age related changes cause the largest decrease in accommodative ability (optical power change), highlighting the main drivers of presbyopia. Alteration of the material properties to match a 45 YO or 60 YO lens caused a decline, with the 60 YO material properties causing the largest change. Altering the zonular displacement caused less of a decrease in accommodative ability than changing the material properties, either with or without a corresponding alteration to the zonule thickness. When the zonule thickness was increased, and hence the force increased, the optical power decreased due to the change in force application; principally through a reduction in posterior curvature change. An increase in the distance between the zonule attachments and the equator also caused a reduction in accommodative ability.

Alteration of the capsule properties had some interesting results. When the capsule properties alone were aged, there was a slight decrease in accommodative ability (45CM). However, when both the internal lens and capsule material properties were increased to match a 60 YO lens (60LCM) the decrease in optical power was reduced, compared to alteration of the lens properties alone (60M). This showed that a young capsule cannot provide as good a force distribution as an old capsule; opposite to the findings of the 45CM model.

Table 6.7: The results of the presbyopia modelling in Section 6.4, principally showing the reduction in power change as a result of variation of key parameters. Key: Baseline models are taken from (Section 6.3). For the variation models, the number indicates the age followed by the type of the variation: M = Lens material, CM = Capsule Material, LCM=Lens and capsule materials, D = Displacement, ZA = Zonule attachments, SV = Stiffness profile. E.g. 29M indicates the baseline model was given a 29 YO lens material properties.

Baseline Model	Power Change (D)	Alteration model	Reduction in power change (D)	Other results of interest
29 YO	7.08	45M	-3.55	
		45CM	-0.23	
		45D	-2.10	0.062N Zonular force
		45D+ZT	-2.69	0.072N Zonular force
		60M	-6.39	
		60LCM	-6.37	
		60D	-2.69	0.043N Zonular force
45 YO	2.48	60D+ZT	-3.67	0.067N Zonular force
		60ZA	-1.42	Significant reduction in curvature change
		29M	1.45	
		29CM	-0.41	Increases thickness change
		29D	0.06	0.12N Zonular force
		29D+ZT	-0.08	0.096N Zonular force
		60M	-2.14	Anterior curvature decreases
60 YO	0.9	60D	-1.00	0.062N Zonular force
		60D+ZT	-1.13	0.074N Zonular force
		29M	1.59	
		29LCM	1.55	
		29D	-0.58	0.15N Zonular force
		29D+ZT	-0.55	0.095N Zonular force
		29SV	-1.06	Posterior curvature decreases
		29ZA	-0.47	
		45M	0.59	
		45D	-0.51	0.16N Zonular force
		45D+ZT	-0.52	0.12N Zonular force
60SV	0.58			

6.4.2.2 45 YO

For the 45 YO model altering the materials to match the 60 YO model caused a decrease in accommodative decline, as did using the 60 YO zonular arrangement, supporting the findings from alterations to the 29 YO lens. The accommodative ability of the 45 YO lens was improved when using the 29 YO material properties or zonular arrangement, although the latter had a small effect. When the zonule thickness was adjusted to match that of a 29 YO lens, the accommodative ability decreased reflecting a decrease in applied force.

Using the 29 YO capsule material properties resulted in a reduction in the accommodative ability, supporting the findings from the 29 YO model that the capsule is not as well suited at force distribution in a younger lens.

6.4.2.3 60 YO

For the 60 YO model, altering the zonule displacements to represent either a 29 YO or 45 YO lens resulted in a decrease in the accommodative ability, either with or without alterations to the zonule thickness, despite an increase in applied force over the baseline model. This appeared to be a result of changes in the amount of anterior curvature decrease.

Moving the zonule attachments closer to the lens equator also caused a reduction in accommodative ability, principally due to the zonules causing less curvature change and higher changes in equatorial diameter. Using the 29 YO material properties, but with the stiffness profile reversed, also resulted in a decrease in power due to it causing the anterior curvature to decrease; resulting in an increase in power with ciliary body movement.

Using the 29 and 45 YO material properties resulted in improvements to the accommodative ability, supporting the previous models. Reversing the material property distribution also increased the accommodative ability, indicating that a decrease in central stiffness may increase accommodative ability. Altering the lens and capsule properties to those of a 29 YO lens resulted in a smaller increase in accommodative ability, again suggesting that a young capsule cannot distribute forces.

6.4.3 Further variation

Two further adjustments to the baseline model were conducted, so that particular results found so far could be investigated further.

6.4.3.1 Further Material property variation

The results so far have indicated that the material properties have a larger effect on the accommodative ability than the displacement, therefore, three additional models were run where both the displacement and material properties were aged, while the lens shape remained constant: 29_60D+LCM, 29_45D+LCM and 60_29D+LCM.

The results of these further variations showed that using the young lens shape with a 45 YO displacement and material properties produced a higher decrease in accommodative ability than altering either alone. Using the 60 YO properties produced changes in between the alterations of the properties individually. With the old lens shape, using both the young material and displacement resulted in a larger increase in accommodative ability than altering either property alone. These results indicate the best method of restoring accommodative ability is to combine material changes with an increase in zonular displacement. In terms of ageing combining the material and displacement values appears to have less of an effect with increasing age, compared to alteration of the material properties alone, indicating that the material properties are the most significant.

6.4.3.2 Further capsule variation

The results of the capsule variations showed the importance of the capsule on the accommodative changes; therefore, a further investigation was carried out looking at how the thickness change with age impacts on the model.

Two further models were generated: 29_60CT+CM (Capsule Thickness and Capsule Material properties) and 60_29CT+CM. The results supported the previous hypothesis, with the model where the older capsule thickness and properties were used increasing the accommodative ability of the young lens shape, not seen with any previous adjustment. Using the young capsule thickness variation and material properties reduced the accommodative ability of the old lens by 0.45 D.

6.4.4 Comparison to previous FEA models

The studies conducted in the current section can be compared to previous FEA models which have conducted similar variations to baseline models.

Weeber & van der Heijde (2007) deformed their 60 YO model (modelled using a 40 YO lens shape with 60 YO material properties) by increasing the zonular displacement until the equatorial diameter change

matched that of a 20 YO lens. Even with the extra deformation at the equator, the anterior and posterior curvatures did not change, which was stated to be due to the cortex material sliding over the stiff nucleus. The 60_29D model comes closest to replicating the setup of Weeber, and the results showed that the anterior curvature decreased rather than increased (as typically seen with zonular movement), indicating a similar movement of the cortex material.

Van de Sompel *et al.* (2010) used similar lens alterations, combining a 29 YO lens shape with 45 YO material properties (referred to here as case 1), as well a 45 YO lens shape with 29 YO material properties (referred to here as case 2). It was found that reshaping the lens (case 1) was better than altering the material properties (case 2) in terms of accommodative ability. The results of the current study actually show the opposite, with the 29_45M (the same alterations as case 1) giving a lower power change compared to the 45_29M (the same alteration as case 2) model, which was supported by the changes seen in the 45_60M and 60_45M models, although Van de Sompel *et al.* (2010) only modelled a 29 and 45 YO lens. Wilde (2011) also produced altered models representing the same combinations as Van de Sompel *et al.* (2010), but finding the opposite results. The altered models closely matched the changes of the baseline models (e.g. 29_45M was close to the 45 YO model), indicating that the lens material is the most important factor in the accommodative decline. The results of the current study show the same trends.

Lanchares *et al.* (2012) used the zonular forces that were found to cause appropriate deformations in a 30 YO lens to input into a 40 and 50 YO lens and varied the material properties until the deformations in the new models were suitable. Appropriate deformations were induced with an increase in the stiffness of the nucleus and cortex, with the nucleus having a higher rate of change. In the current set up, the material properties are taken from *in vitro* measurements, but similar trends in stiffness increase were seen in the three age models in the current studies, which also matched expected changes supporting the findings of Lanchares.

6.4.5 Support for presbyopia theories

In Section 1.3 a number of theories on the development of presbyopia were discussed, which can now be analysed in terms of the changes seen in the current modelling. The Duane-Fincham theory is based on the ciliary muscle always reaching a maximum amount of contraction when accommodating, indicating that the reduced changes with age are due to the lens which is supported by the models demonstrating the material properties are a driving factor in accommodative decline (e.g. 29_45M and 29_60M), which will be further discussed later in this section.

The theory of Koretz & Handelman (1986) hypothesised that migration of the zonular attachments on the lens causes a reduction in the force applied by the ciliary body, reducing the ability of the ciliary body to alter the lens. The 29_60ZA model replicates this, showing that the inwards movement of the zonules did reduce the accommodative ability, although not by much. However, movement of the zonules closer to the equator in the 60_29ZA also produced an accommodative reduction. Therefore, this hypothesis cannot be refuted or supported from the current model, as the results appear to depend on the material properties of the lens model.

The modified geometric theory of Strenk *et al.* (2005) proposed that the reduction in accommodative ability is due to the reduction in circumlental space and a subsequent reduction in available zonular tension. The baseline models incorporate a reducing circumlental space in the modelling method, resulting in a smaller movement of the zonular fibres. In the initial models carried out in Section 6.2.3.2 the amount of force applied to the lens reduced due to the reduction in ciliary body movement, which would support the theory, however, the changes induced were not a match for what was expected. Therefore, the zonular tension was modelled to increase with age to induce appropriate changes in the lens with dis-accommodation. The 60_29D model should support this theory, in that it causes an increase in circumlental space, but the model predicts a power decrease going against the theory.

The models that adjusted the ciliary body displacement and zonule thickness are of interest. The results showed that reducing the ciliary body displacement in a young lens, regardless of whether the zonule thickness was increased or not, resulted in a decrease in applied force and accommodative ability (29_60D, 29_45D, 29_60D+ZT). In a middle age lens increasing the displacement resulted in an increase in force and an increase in accommodative ability, but if the force reduced, the accommodative ability reduced (45_29D, 45_29D+ZT). In an old lens, increasing the ciliary body displacement did not increase the accommodative ability, regardless of whether the force was increased (60_29D, 60_29D+ZT). In the old lens models, despite an increase in force, the accommodative ability still decreased due to the zonular attachments on an older lens.

Overall, the altered models run in Section 6.4 suggest that the material properties are the largest contributor to accommodative decline. When using a young lens shape, increasing the stiffness to match an older lens (e.g. 29_60M) caused a drop in the accommodative ability, while using an old lens shape with young lens material properties (e.g. 60_29M) caused an increase in accommodative ability. With both variations, the changes were the largest seen in any alteration. These results support the view that it is the stiffness of the lens that causes the decline in accommodative ability with age, as the increase in stiffness reduces the

effectiveness of the ciliary body and zonular structure.

The capsule has an important role, both in accommodation and its age related decline. From the initial alterations made to the baseline models, it was apparent that increasing the stiffness of the capsule as well as the stiffness of the lens reduced the amount of accommodative decline (29_60LCM). Also, alteration of the capsule stiffness in an old lens (e.g. 45_29CM) causes a reduction in the accommodative ability, indicating that the capsule stiffness increase with age is needed to cause a lens shape change. This was taken further in Section 6.4.3.2 by altering the thickness of the capsule as well as the stiffness, finding that increasing the age of the capsule in a young lens model (29_60CT+CM) provided an improvement in accommodation, not seen with any other alteration. Using a younger capsule on an older lens causes a reduction in the accommodative ability, supporting the idea that the capsule needs to change to be able to continue altering the lens shape. The reason for this, discussed in Section 1.2.3.2, is that the capsule acts as a force distributor and that with age it becomes more efficient at transferring the forces from the ciliary body, due to the stiffening of the lens.

6.4.5.1 Presbyopia correction

Section 1.3.3 discussed the various proposals for the restoration of accommodative ability, broadly divided into methods that replace the lens (IOLs and lens refilling) and methods that alter the existing lens substance (fs-laser treatment). The current modelling methods have been conducted assuming the lens is present, which is not the case with an IOL, therefore, the discussion will concentrate on lens refilling and fs-laser treatments, which both have a lens “body” present.

The results of the current study suggest that if the stiffness of the lens can be reduced, the accommodative ability of an old eye can be improved, provided the capsule retains its stiffness and thickness. Both lens refilling and fs-laser surgery aim to achieve this, using different methods.

Lens refilling uses a synthetic material of similar properties to the lens to replace the lens within the capsule. In principal, this could result in an overall lower stiffness; however, the procedure requires alterations to the capsule due to the need to inject a material into the capsular bag (Section 1.3.3), which is likely to alter the properties of the capsule. The current methods show that if the capsule stiffness is reduced the accommodative improvements are lessened (e.g. 60_29LCM compared to 60_29M), therefore, careful consideration of the capsular behaviour is needed.

Fs-laser surgery is based on the idea of cuts made internal to the lens increasing its flexibility. Although

not replicated by the current methods, it is proposed that any cuts made internally cause the stiffness to reduce, which has been shown to increase the accommodative ability. However, fs-laser surgery requires a focused area of the lens to be altered, which was not replicated in the material property alteration models (e.g. 60_29M) where the whole lens stiffness was altered. However, the 60_60SV model replicated a situation where the stiffness profile was altered, showing that having a lower stiffness nucleus resulted in an accommodative improvement which is more applicable in the case of fs treatment, with the 60_60SV model indicating an accommodative increase could be found.

The current modelling methods are not suitable in their current form to replicate surgical methods, however, they do lay the groundwork for future alterations to be made. The principal issue is in replicating the optical performance of the models before and after surgical treatments, as this will determine the effectiveness of either treatment method in the long term, in addition to accurately capturing the changes that occur as a result of the surgical method.

6.4.6 Presbyopia modelling summary

The current modelling method allows for in depth analysis of how individual parameters of the model affect the accommodative changes that occur. The results show that the material properties are the key parameter in the decline in accommodative ability, but that the capsule has a vital role. The results suggest that the most likely method of improving the accommodative ability in an ageing eye is to reduce the stiffness of the lens material, provided that the capsule stiffness is not altered; although increasing the stiffness of the capsule could be beneficial.

6.5 Alternative Accommodation models

Chapter 1 focused on the accommodative theory of Helmholtz, due to it being widely accepted as the most appropriate theory. Other theories have been proposed (Section 1.2.2), therefore, an additional investigation was conducted to try to replicate these and compare the results to the existing models from Section 6.3.

The two theories that will be modelled are those of Coleman and Schachar (Section 1.2.2). Previous FEA models have conducted similar tests (see Section 2.4.1), therefore, the majority of the inputs and alterations will be based on those models. In both cases, the 29 YO model from Section 6.3 will be

the base model. Comparisons to the measured data using the methods outlined in Section 5.4 will be conducted.

6.5.1 Model set up

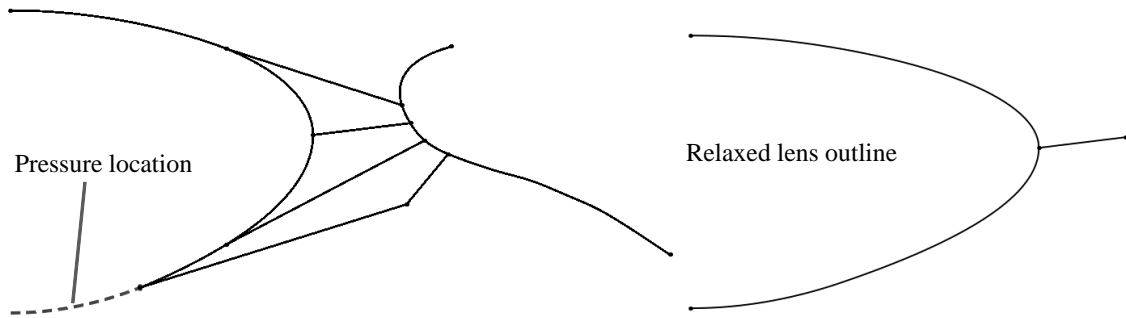


Figure 6.24: Illustration of the alterations to the baseline 29 YO lens to replicate the theories of Coleman (Left model) and Schachar (Right model).

To represent the theory of Coleman, a pressure on the posterior surface is required in addition to the zonular structure. Two models will be defined; the first will apply a pressure between the posterior pole and the APZ2 zonule lens attachment point (C_A, see Figure 6.24). The second model will apply the pressure between the posterior pole and APZ1 attachment point, with the APZ2 zonule being removed (C_B). Both cases are similar to models developed by Martin *et al.* (2005) to investigate the same theory. The initial pressure value will be taken from the study of Martin *et al.* (2005), using 225 Pa, applied as a constant across the posterior surface.

To represent the Schachar theory, alterations to the baseline model are needed. The theory is based on ciliary muscle contraction causing the equatorial zonule to apply traction on the lens, with the anterior and posterior zonule slackening. Therefore, the initial lens shape will need to be represented by the relaxed lens, as the accommodated lens shape is induced through traction from the relaxed state. In addition only the equatorial zonule will be modelled, as neither anterior nor posterior zonules function in the accommodative process. Two variations of this setup will be tested, the first using a flat equatorial zonule, S_A (replicating models in Schachar & Bax, 2001b and Abolmaali *et al.*, 2007) and the second using the equatorial zonule position from the baseline model, S_B (see Figure 6.24). The initial displacement applied to the flat zonule will be 0.2 mm (as in Abolmaali *et al.*, 2007) with the angled zonule having the same displacement as the baseline model. The thickness of the zonule will be set to 0.012 mm. A final model (S_C) was defined, using the material properties for the lens as in Abolmaali *et al.* (2007), with the rest of the model the same as S_B.

6.5.2 Results

Both versions of the Coleman model had similar results, with the diameter change being the only value that matched the expected changes. The anterior curvature had too little change, with the posterior curvature having too much change (see Figure 6.25). The lens had an overall anterior movement. The changes in the C_B were lower than the C_A model, but showed the same overall trends.

For the Schachar models, both the S_A and S_B models showed a decrease in thickness combined with increases in diameter and surface curvatures (see Figure 6.25), resulting in a decrease in optical power. Both models had an anterior movement of the lens body. The S_B model had slightly higher changes in all aspects compared to the S_A model. The S_C model showed that there was a thickness increase and a decrease in anterior curvature, not seen in the S_A and S_B model.

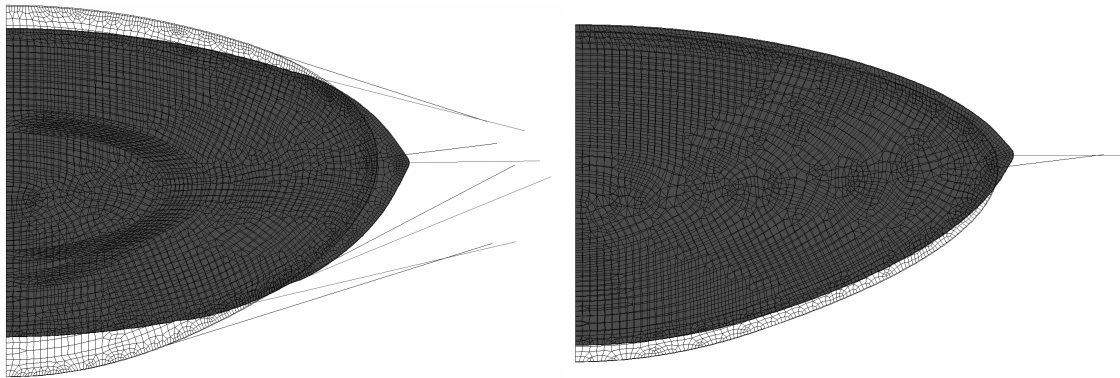


Figure 6.25: The deformations induced in the C_A and S_B models.

6.5.3 Analysis

The models run representing the Schachar and Coleman theories both did not match the required changes that are seen in the accommodative system (Section 3.2). The S_A and S_B models did not match with either the measured changes or those proposed by the Schachar theory, which is based on the lens forming a spindle shape with zonular contraction, with a steep central curvature section and lower curvature in the periphery of the lens. The S_C model did show a thickness increase, as in Schachar & Bax (2001b) and Abolmaali *et al.* (2007), but the spindle shape was not seen. The material properties of the S_C model also did not match any of the stiffness distributions measured *in vitro* (Section 4.3.1.6).

The Coleman models showed similar shape changes to the baseline models, however, there was too much anterior movement in the lens combined with increase posterior curvature changes due to the presence of

the posterior pressure. Models by Martin *et al.* (2005) showed similar results, that the set up following Coleman does not results in changes that match *in vivo* measurements.

Overall, neither of the altered models shows changes induced with accommodation that match what has been measured *in vivo*, indicating that the methods used in Section 6.3 and Section 6.4 following the Helmholtz theory are most appropriate for replicating accommodation.

Chapter 7

Conclusion

7.1 Introduction

In this chapter a summary of the whole thesis will be given, detailing to what extent the principal questions were answered and how the objectives defined in Section 1.4 were achieved. Suggestions for improvements and details of the future directions of research presented in this thesis are also included.

7.2 Comparisons to aims and objectives

The overall aim of this thesis was to investigate two fundamental questions:

1. What causes the crystalline lens to change shape?
2. What are the main contributing factors in the development of Presbyopia?

Both of these questions have been explored using a new finite element analysis model of the accommodation system, with both affirmations of existing ideas and new insights given. A number of objectives had to be completed in order to answer the principal aims.

7.2.1 Objective 1 - Development of a geometric model

To enable an improved model of the accommodation system to be developed, an understanding of the methods used to develop and run previous models was needed, which was achieved through the review of existing FEA models in Chapter 2. The majority of existing FEA models share a number of methodologies, either in terms of the crystalline lens model, zonular structure or material properties used. As a consequence, any limitations in one method were typically carried through to subsequent models that

adopted it. The key areas where existing models had limitations were in the internal structure of the lens (and therefore, the material property distribution, discussed in Section 7.2.2) and the zonular fibre arrangement.

In Chapter 3 a novel zonule model was proposed by incorporating a range of *in vivo* and *in vitro* data on the zonular structure and ciliary body. Four zonular bundles were modelled combined with a representation of the ciliary body, which could be altered to represent the accommodated and relaxed state, allowing estimations of the zonular displacements to be obtained (Section 3.5). In addition to the studies used to develop the model, recent data (Croft *et al.*, 2013) have supported the inclusion of the PZ2 bundle, with *in vivo* measurement highlighting the link between the vitreous zonules (which is represented by the PZ2 zonule) and the lens as an important aspect of accommodation.

To allow for the proposed model to fulfill its potential, a lens modelling method was selected that allowed for both accommodated and relaxed lens models to be generated for any age. Compared to previous methods used to model the lens, the selected method allowed for a range of ages to be modelled in both accommodated and relaxed states, through alteration of key parameters which could be measured *in vivo*. The method also produced appropriate lens shapes across all ages (Section 3.3.2). A new method of adapting measured capsule thickness data was proposed, defining a capsular area within the lens outline (Section 3.4). The final geometric consideration was the internal structure of the lens, which dictates how the material parameters are distributed through the lens. *In vivo* data were used to define a method of scaling the outer lens layer down to represent different internal layers, which will be discussed further in Section 7.2.2.

7.2.2 Objective 2 - Selection of appropriate material properties

Even with recent advancements in available material data for the lens, the majority of FEA models have persisted in using the data of Fisher (1971), leading to the use of a simplified nucleus cortex representation (Section 2.2.2). Fisher's data has since been shown to be based on inaccurate methodologies (Section 4.3.1.1), which, combined with recent data on the stiffness profile that exists in the lens, led to the adoption of an age related stiffness profile for the crystalline lens material properties (Section 4.4.1). To complement the use of recent material data, a hyper-elastic constitutive model was utilised to represent the lens, allowing the more complex behaviour of these components to be captured (Section 4.2).

The capsule modelling methods from previous studies have been consistent, leading to the use of a similar methodology. Although the capsule has known anisotropic properties, there was insufficient data available

to incorporate this accurately. Therefore, an isotropic hyper-elastic constitutive model, combined with suitable stiffness data (Section 4.4.2), was utilised to replicate the known constitutive behaviour of the capsule as precisely as possible.

The zonular material properties have been less well studied, leading to a variety of estimations used in previous FEA models. In the current study, the zonules were represented by a linear elastic model and modelled so that thickness values could be applied to individual bundles to control the stiffness. This allowed for customisation of the zonules in the modelling method, to ensure appropriate values could be selected for each age model (Section 4.4.3; Section 6.2.3.3).

In terms of the FEA methods used to simulate the accommodative process, a 2D axisymmetric large deformation static study was conducted, allowing for the large strain that is present in the accommodative process to be incorporated. Due to the proposed zonular arrangement, the only loads and restraints needed on the accommodative model are applied to the zonular bundles. Previous FEA models have had to include artificial restraints on the lens due to the zonular methods used, preventing movement of the lens. In the current method, the lens deformed purely from movement of the zonules, replicating *in vivo* conditions in a more suitable manner.

7.2.3 Objective 3 - Evaluation of proposed methods

The evaluation of the proposed models was conducted in two stages: the first stage (Section 6.2) was used to ensure the proposed modelling methods were appropriate, with alterations suggested where needed. The second stage (Section 6.3) was to evaluate the final modelling procedure against measured *in vivo* data.

7.2.3.1 Stage 1 - Development of the proposed model

In the first stage, a number of novel studies were conducted. Different internal structure models were analysed to ensure that an appropriate method would be used. The first analysis was conducted using an approximation of the spinning lens tests of Fisher (1971) and Wilde *et al.* (2012), comparing the deformations induced in four internal structure models (without the capsule present) to each other and to measured *in vitro* data (Section 6.2.1). It was found that the internal structure models that used a stiffness profile (SA and SB) were most suitable, which was further verified in a final test with the zonules integrated, conducted after the zonular structure was finalised (Section 6.2.5). The final result was that the

SB stiffness gradient was selected for all future modelling, with evidence that the nucleus-cortex model may over simplify modelling procedures.

To ensure the capsule modelling methodology was appropriate, the capsular area was first included on two different age lens models used in the spinning lens test (Section 6.2.2). *In vitro* testing had shown the capsule would restrict the changes in the spinning lens compared to de-capsulated lenses. The models showed that this did occur with the proposed capsule method, although there was not a complete match across all ages. The failure to match all ages may be due to limitations in the material data used. Further integration with the zonular model demonstrated that the capsule model provided suitable behaviour for the purposes of the current model.

Testing of the novel zonular arrangement first confirmed that it replicated the movement of the lens better than previous FEA models (Section 6.2.3.1). The testing then focused on establishing how the displacement and stiffness should be defined. Suitable ciliary body displacement values and zonule bundle thicknesses were found by utilising force calculations and comparisons to *in vivo* data (Section 6.2.3.3). Some minor alterations were then detailed to ensure the methodology represented the most appropriate zonular modelling procedure (Section 6.2.3.4), principally involving the adjustment of the zonule bundle thicknesses, ensuring that any thickness changes were within measured values (see Section 3.2.4.3)

A novel investigation into how statistical variation of the material properties affected the thickness change of the lens was conducted, using the probabilistic modelling methods in ANSYS (Section 6.2.4). Two studies were conducted, the first showed how the capsule stiffness had a larger significance than the internal layers of the lens (Section 6.2.4.1). The second study showed that the zonule and capsule stiffness were almost equal in significance with regards to thickness change and posterior pole movement, but had opposite effects on the thickness change if they were to be increased (Section 6.2.4.2).

7.2.3.2 Stage 2 - Accommodation modelling

After completion of the studies in Section 6.2, the methodologies were updated and a final three models were developed to replicate a 29, 45 and 60 YO lens. These were simulated to ensure that the models matched a detailed comparison to the expected changes that occur during accommodation, as well as to compare to previous FEA models to ensure that the proposed methods offer improvements. An initial study was conducted (Section 6.3.1), with some final alterations to the zonular arrangement completed, after which the performance of the models could be evaluated (Section 6.3.3.1 and Section 6.3.3.2).

Compared to measured *in vivo* data, the model performed well, matching the general trends with both age and accommodation of the posterior pole movement, curvature change, diameter change and ciliary body force. The parameters that deviated from the literature were the thickness change, with the overall thickness change being slightly high and the thickness distribution not matching *in vivo* measurements, with the thickness changes distributed between the nucleus and cortex regions rather than concentrated within the nucleus. Previous FEA models have also shown the internal thickness changes to be distributed through the lens, indicating that the issue could be a result of the material modelling methods used.

In comparison to previous FEA models, the current model compares well. Overall, the geometric changes had a better fit to measured data, but also had the best replication of the movement of the lens during the accommodation process. Differences were seen in the stress distributions, but this was a result of the differing material and loading conditions used. Overall, the modelling conducted in Section 6.2 and Section 6.3 demonstrated that the proposed modelling methodologies provide a suitable representation of the accommodation system.

7.2.4 Objective 4 - Parametric analysis

To meet the requirements of objective 4, and to explore the principal questions, a range of models were generated, each with an alteration to one of the three baseline models taken from Section 6.3. For example, the material properties of a 60 YO lens were used in the 29 YO baseline model, to examine how that change impacted on the accommodative ability of the model. Using alterations to one aspect of a model at a time allowed for direct comparisons to be made on how each alteration affected the deformations induced.

The parameter that had the highest impact on the accommodative ability was the material properties of the lens, where increasing the age in a young lens caused an accommodative decline and decreasing the age in an old lens caused an accommodative increase. Previous FEA models have shown similar findings and the results support various hypotheses from the literature on the root causes of presbyopia (Section 6.4.4). Adjustments to the material properties were the only changes that improved the accommodative ability of the baseline old lens, with the results also showing that changing the shape of an old lens is unlikely to have any benefits.

Novel investigations into capsular alterations were conducted, looking for the first time at how alteration of the capsule thickness and stiffness impacts on accommodation, finding that using an older capsule on a young lens actually causes an increase in accommodative ability, indicating that increasing the thickness and stiffness in an old capsule may have beneficial effects. The models also demonstrated that the younger

capsule is ineffective at distributing the forces induced by the zonules, indicating that the changes the capsule goes through with age are needed for accommodation to continue to be induced.

In terms of the current understandings of presbyopia development, a definitive answer could not be given on the exact cause, however, evidence was found both for and against a number of current theories. The overall indications are that presbyopia does have a lenticular origin, with only alterations to the lenticular parameters causing significant reductions in power in a younger lens. For ciliary body and zonule alterations, the results were not so clear. Decreasing the ciliary body displacement in a young lens, either with or without changing the zonule bundle thickness, caused a decrease in power change, mirroring a decrease in force application. Increasing the displacement in an old lens decreased the accommodative ability, despite increases in force applied. A possible explanation is that with a stiffer, larger lens, the zonules are less effective, so despite increased forces, reduced changes are seen, supporting a lenticular explanation of presbyopia. However, it would suggest that if the ciliary body force was to reduce with age, it could contribute to the accommodative decline.

An analysis of potential presbyopia treatments was not conducted due to the lack of data on the changes in both geometry and material behaviour that would occur as a result of any treatment. However, the indications are that if the stiffness of the lens was reduced, either as whole (e.g. 60_29M) or alteration of the stiffness profile (60_60SV), improvements to the accommodative ability could be gained, supporting the principals of lens refilling and femtosecond laser surgery. The indications are also that if the stiffness of the capsule could be altered, potential accommodative improvements could be gained.

A final few models were developed to try to simulate the accommodative theories of Coleman and Schachar, using basic alterations to the baseline model to replicate the different changes during accommodation. The results indicate that neither theory gives results that match expectations, supporting the Helmholtz theory.

7.3 Answers to principal questions of the thesis

The first principal question from Section 1.4 was in relation to the principal factors that cause the crystalline lens to change its shape. It is evident from the modelling conducted that the shape change that occurs is dependant on a combination of the crystalline lens material properties and the displacement of the zonular bundles. The material properties of the lens are the most significant aspect of the changes during accommodation. However, the importance of the zonular and capsular stiffness in the actions of the zonular displacement cannot be ignored.

The second principal question is of more interest and was in relation to how the change in material and geometric parameters with age contribute to the development of presbyopia. The indications are that the decline in accommodative ability has a lenticular origin and is a combination of a number of factors. From the modelling conducted, the material parameters of the lens are key, being the largest contributor to accommodative decline in a baseline young lens, but also demonstrating that alteration in an old eye could restore accommodative ability. The influence of the capsule was also demonstrated, showing how the increasing thickness of the capsule aids in delaying the accommodative decline. The contributions of the ciliary body and zonular arrangement to accommodative decline were not so clear, but the results still indicated a lenticular origin of presbyopia.

7.4 Suggestions for improvements and future directions

Although a good fit was found to the majority of *in vivo* measurements that the current models were compared to, there were a number of aspects that did not match what was expected. In addition, there was ambiguity in the studies looking at the root causes of presbyopia, which will require further investigation. The accommodation model developed in this thesis is based on a range of existing measurements of both material and geometric properties of the accommodative structures. Therefore, the aspects of the current model that do match with expectations could be explained by limitations in the available data, in particular in the material behaviour. A lack of *in vivo* measurements of the ciliary body and zonules, combined with the material property limitations led to assumptions being made on key modelling methodologies, as well as adoption of constitutive models that do not provide a complete description of the behaviour of the various components. Additional limitations are present in the FEA modelling methods, such as the simplified connection between the layers of the lens (currently modelled as bonded), the use of axisymmetry rather than a complete 3D model and the exclusion of other structures that may be relevant to accommodation. Therefore, future research should be split into two distinct areas:

1. Fundamental data;
2. FEA methods.

7.4.1 Fundamental data

The fundamental data used to define the current model could be improved in a number of ways. First, further data on the material properties of the accommodative structures is needed to develop the accom-

modation models. One method that could be used to obtain this data is through *in vitro* lens measurements, such as using mechanical stretchers to stretch the accommodative components, enabling analysis of the changes in the crystalline lens, zonules and ciliary body. Using a method such as this would enable the age related changes to be explored in more detail, in particular focusing on the material change in the post presbyopic eye, as future work will need to focus on methods of restoring accommodation in an ageing eye. One particular area of interest is in the apparent difference between the *in vivo* thickness change distribution and measured material property distribution, which can be explored through a combination of *in vitro* and *in vivo* imaging and material testing methods.

A second method of obtaining material data is through estimation of material properties using individualised FEA models. Due to the advances in *in vivo* imaging techniques (such as 3D MRI and AS-OCT), a more complete picture of subjects accommodative structures can be obtained. By using an individual subject's geometric data measured *in vivo* in both accommodated and relaxed states, personalised FEA models can be constructed. Deformations could then be induced in the FEA model based on the *in vivo* ciliary body measurements and the material parameters of the model altered until the deformed profile matches the measured changes. By repeating the process on a number of ages, the material properties can be compared between models and an estimation of appropriate values can be made, including investigations into potential anisotropic behaviour. The author has developed a method of analysing *in vivo* measurements of the ciliary body that would benefit this research direction (see Appendix B).

Continued advances in *in vivo* imaging can also be used to improve on the available population data of accommodative components geometry, in particular on the changes that occur during accommodation (e.g. 3d-OCT Gamba *et al.* (2013)). The use of MRI will potentially allow the majority of relevant changes to be captured using a single methodology, rather than combining a range of methodologies to obtain geometric data as utilised in the current study. Development of imaging methodologies that allow 3D data capture will also aid in building fully representative models, taking into account nasal and temporal asymmetry. New imaging techniques have the potential to improve on the known data on the refractive index distribution, aiding in optical modelling, discussed in the next section.

7.4.2 FEA Modelling methods

In terms of the FEA modelling method, using either future enhanced properties, or through refinement using existing data, a number of aspects can be improved. First of all, the basic FEA methods can be improved, by further investigation into element choices for the accommodative components and the con-

stitutive models used. These changes can be enhanced through further analysis of the deviations from the literature in the current model; such as the reasons for why the internal thickness changes do not match those measured (Section 6.3.3.1). Further refinement of the ciliary body model and zonular arrangement is needed, in particular in light of recent *in vivo* data in the literature. Another aspect that can be analysed is the use of a 3D compared to a 2D model, in particular in relation to how the zonular fibres would be modelled in 3D. The connections between the lens layers also need to be investigated, analysing whether friction between lens layers affects the accommodative behaviour. On top of the internal layers, whether the lens epithelium or suture sites have an effect on the accommodation mechanism can be investigated. The localised deformations at the zonular attachments in the current model would also need further work, ideally removing them entirely.

With improved data on the anterior eye, the influence of other accommodative components could be explored, such as the vitreous or iris. In addition, the evidence from the current model supports the idea that the capsule is a key aspect of accommodation, so further strengthening of the capsule modelling is needed, in particular in relation to its impact on potential accommodation restoration methods, where the capsule is altered due to surgical methods.

Finally, the change of the optical performance with accommodation needs more detailed analysis. The current methodology uses a very basic method of predicting the optical power, but this does not incorporate the gradient refractive index present within the lens. Therefore, more advanced methods of measuring optical performance need to be considered, such as ray tracing using internal region outlines of the deformed lens combined with a gradient refractive index.

7.5 Future applications

With more detailed FEA models of the accommodative components and accommodative system, a range of applications can be explored. First, a better understanding of accommodation and presbyopia can be gained, building on the work conducted in the current thesis. Secondly, investigations into accommodation restoration techniques can be conducted. Alterations to a baseline model can be made to replicate the changes that could be made through techniques such as lens refilling and fs-laser surgery.

One exciting avenue that would be beneficial to explore, if the potential benefits of accommodative restoration surgery are fully realised, is the use of personalised FEA models as part of the treatment process. By utilising available *in vivo* imaging techniques, all of the relevant geometric data can be gathered for a sub-

ject, allowing a personalised model to be generated. The individual material properties of that subject can then be established through the FEA model, and through adapting the FEA model, the most appropriate surgical techniques can be theoretically tested, before any actual surgical methods are utilised.

References

- Abolmaali, A., Schachar, R.A. & Le, T. (2007). Sensitivity study of human crystalline lens accommodation. *Computer Methods and Programs in Biomedicine*, 85(1), pp. 77–90.
- Ackermann, R., Kammel, R., Merker, M., Kamm, A., Tünnermann, A. & Nolte, S. (2013). Optical side-effects of fs-laser treatment in refractive surgery investigated by means of a model eye. *Biomedical Optics Express*, 4(2), pp. 220–229.
- ANSYS (2010a). *ANSYS Mechanical APDL Analysis Techniques Guide*, volume 3304.
- ANSYS (2010b). *ANSYS Mechanical APDL and Mechanical Applications Theory Reference*, volume 3304.
- Assia, E.I., Apple, D.J., Morgan, R.C., Legler, U.F. & Brown, S.J. (1991). The relationship between the stretching capability of the anterior capsule and zonules. *Investigative Ophthalmology & Visual Science*, 32(10), pp. 2835–2839.
- Atchison, D.A. (1995). Accommodation and presbyopia. *Ophthalmic Physiol Opt*, 15(4), pp. 255–272.
- Atchison, D.A., Markwell, E.L., Kasthurirangan, S., Pope, J.M., Smith, G. & Swann, P.G. (2008). Age-related changes in optical and biometric characteristics of emmetropic eyes. *Journal of Vision*, 8(4), pp. 1–20.
- Atchison, D.A. & Charman, W.N. (2010). Thomas Young's contribution to visual optics : The Bakerian lecture "On the mechanism of the eye". *Journal of Vision*, 10(12), pp. 1–16.
- Augusteyn, R.C. (2008). Growth of the lens: in vitro observations. *Clinical and Experimental Optometry*, 91(3), pp. 226–239.
- Bailey, M.D., Sinnott, L.T. & Mutti, D.O. (2008). Ciliary Body Thickness and Refractive Error in Children. *Investigative Ophthalmology & Visual Science*, 49(10), pp. 4353–4360.
- Bailey, S.T., Twa, M.D., Gump, J.C., Venkiteshwar, M., Bullimore, M.A. & Sooryakumar, R. (2010). Light-scattering study of the normal human eye lens: elastic properties and age dependence. *Biomedical Engineering, IEEE Transactions on*, 57(12), pp. 2910–2917.
- Barraquer, R.I., Michael, R., Abreu, R., Lamarca, J. & Tresserra, F. (2006). Human lens capsule thickness as a function of age and location along the sagittal lens perimeter. *Investigative Ophthalmology & Visual Science*, 47(5), p. 2053.
- Beers, A.P.A. & Van Der Heijde, G.L. (1994). Presbyopia and Velocity of Sound in the Lens. *Optometry & Vision Science*, 71(4), pp. 250–253.
- Belaidi, A. & Pierscionek, B.K. (2007). Modeling internal stress distributions in the human lens: Can opponent theories coexist? *Journal of Vision*, 7(11), pp. 1–12.
- Bellows, J.G. (1944). *Cataract and Anomalies of the Lens*. Kimpton.
- Ben-Nun, J. & Alió, J.L. (2005). Feasibility and development of a high-power real accommodating intraocular lens. *Journal of cataract and refractive surgery*, 31(9), pp. 1802–8.
- Bergua, A. & Küchle, M. (2002). Visualization of the hyalo-capsular ligament in the living eye. *Graefe's Archive for Clinical and Experimental Ophthalmology*, 240(6), pp. 503–5.

- Bernal, A., Parel, J.M. & Manns, F. (2006). Evidence for posterior zonular fiber attachment on the anterior hyaloid membrane. *Investigative Ophthalmology & Visual Science*, 47(11), p. 4708.
- Bito, L.Z. & Miranda, O.C. (1989). Accommodation and presbyopia. *Ophthalmology Annual*, pp. 102–128.
- Borja, D., Manns, F., Ho, A., Ziebarth, N., Rosen, A.M., Jain, R., Amelinckx, A., Arrieta, E., Augusteyn, R.C. & Parel, J.M. (2008). Optical Power of the Isolated Human Crystalline Lens. *Investigative Ophthalmology & Visual Science*, 49(6), pp. 2541–2548.
- Bornfeld, N., Spitznas, M., Breipohl, W. & Bijvank, G.J. (1974). Scanning electron microscopy of the zonule of Zinn. *Graefe's Archive for Clinical and Experimental Ophthalmology*, 192(2), pp. 117–129.
- Breitenfeld, P., Ripken, T. & Lubatschowski, H. (2005). Finite element method-simulation of the human lens during accommodation. In: *Therapeutic Laser Applications and Laser-Tissue Interactions II*, volume 586302 (eds. H. van den Bergh & A. Vogel), Munich, Germany.
- Brown, N. (1973). The change in shape and internal form of the lens of the eye on accommodation. *Experimental Eye Research*, 15(4), pp. 441–459.
- Brown, N. (1974). The change in lens curvature with age. *Experimental Eye Research*, 19(2), pp. 175–183.
- Buckhurst, H., Gilmartin, B., Cubbidge, R.P., Nagra, M. & Logan, N.S. (2013). Ocular biometric correlates of ciliary muscle thickness in human myopia. *Ophthalmic & physiological optics : the journal of the British College of Ophthalmic Opticians (Optometrists)*, 33(3), pp. 294–304.
- Burd, H.J. (2009). A structural constitutive model for the human lens capsule. *Biomechanics and Modeling in Mechanobiology*, 8(3), pp. 217–231.
- Burd, H.J., Judge, S.J. & Cross, J.A. (2002). Numerical modelling of the accommodating lens. *Vision Research*, 42(18), pp. 2235–2251.
- Burd, H.J., Judge, S.J. & Flavell, M.J. (1999). Mechanics of accommodation of the human eye. *Vision Research*, 39(9), pp. 1591–1595.
- Burd, H.J., Wilde, G.S. & Judge, S.J. (2006). Can reliable values of Young's modulus be deduced from Fisher's (1971) spinning lens measurements? *Vision Research*, 46(8-9), pp. 1346–1360.
- Burd, H.J., Wilde, G.S. & Judge, S.J. (2011). An improved spinning lens test to determine the stiffness of the human lens. *Experimental Eye Research*, 92(1), pp. 28–39.
- Candia, O.A., Zamudio, A.C. & Alvarez, L.J. (2010). Mechanical stretching forces oppose osmotic lens swelling. *Experimental Eye Research*.
- Chai, C.K., Burd, H.J. & Wilde, G.S. (2012). Shear modulus measurements on isolated human lens nuclei. *Experimental Eye Research*, 103(0), pp. 78–81.
- Charman, W.N. (2008). The eye in focus: accommodation and presbyopia. *Clinical and Experimental Optometry*, 91(3), pp. 207–225.
- Chien, C.H., Huang, T. & Schachar, R.A. (2003). A mathematical expression for the human crystalline lens. *Comprehensive Therapy*, 29(4), pp. 244–258.
- Choi, S., Lee, H.J., Cheong, Y., Shin, J.H., Jin, K.H., Park, H.K. & Park, Y.G. (2012). AFM Study for Morphological Characteristics and Biomechanical Properties of Human Cataract Anterior Lens Capsules. *Scanning*, 34(4), pp. 247–256.
- Coleman, D.J. (1986). On the hydraulic suspension theory of accommodation. *Transactions of the American Ophthalmological Society*, 84, pp. 846–868.
- Coleman, D.J. & Fish, S.K. (2001). Presbyopia, accommodation, and the mature catenary. *Ophthalmology*, 108(9), pp. 1544–1551.

- Croft, M.A., McDonald, J.P., Katz, A., Lin, T.L., Lütjen-drecoll, E. & Kaufman, P.L. (2013). Extralenticular and lenticular aspects of accommodation and presbyopia in human vs. Monkey eyes. *Investigative Ophthalmology and Visual Science*, IOVS-12-10846.
- Croft, M.A., McDonald, J.P., Nadkarni, N.V., Lin, T.L. & Kaufman, P.L. (2009). Age-related changes in centripetal ciliary body movement relative to centripetal lens movement in monkeys. *Experimental Eye Research*, 89(6), pp. 824–832.
- Cumming, J.S., Colvard, D.M., Dell, S.J., Doane, J., Fine, I.H., Hoffman, R.S., Packer, M. & Slade, S.G. (2006). Clinical evaluation of the Crystalens AT-45 accommodating intraocular lens. *Journal of cataract and refractive surgery*, 32(5), pp. 812–825.
- Danielsen, C.C. (2004). Tensile mechanical and creep properties of Descemet's membrane and lens capsule. *Experimental Eye Research*, 79(3), pp. 343–350.
- Danysh, B.P. & Duncan, M.K. (2009). The lens capsule. *Experimental Eye Research*, 88(2), pp. 151–164.
- Daxecker, F. (1992). Christoph Scheiner's eye studies. *Documenta Ophthalmologica*, 81(1), pp. 27–35.
- de Castro, A., Siedlecki, D., Borja, D., Uhlhorn, S., Parel, J.M., Manns, F. & Marcos, S. (2011). Age-dependent variation of the gradient index profile in human crystalline lenses. *Journal of Modern Optics*, 58(19), pp. 1781–1787.
- Drexler, W., Baumgartner, A., Findl, O., Hitzenberger, C.K. & Fercher, A.F. (1997). Biometric investigation of changes in the anterior eye segment during accommodation. *Vision Research*, 37(19), pp. 2789–2800.
- Du, C., Shen, M., Li, M., Zhu, D., Wang, M.R. & Wang, J. (2012). Anterior segment biometry during accommodation imaged with ultralong scan depth optical coherence tomography. *Ophthalmology*, 119(12), pp. 2479–85.
- Duane, A. (1922). Studies in monocular and binocular accommodation, with their clinical application. *Transactions of the American Ophthalmological Society*, 20, p. 132.
- Dubbelman, M. & Van der Heijde, G.L. (2001). The shape of the aging human lens: curvature, equivalent refractive index and the lens paradox. *Vision Research*, 41(14), pp. 1867–1877.
- Dubbelman, M., van der Heijde, G.L. & Weeber, H.A. (2001). The thickness of the aging human lens obtained from corrected Scheimpflug images. *Optometry and Vision Science*, 78(6), pp. 411–416.
- Dubbelman, M., Van der Heijde, G.L. & Weeber, H.A. (2005). Change in shape of the aging human crystalline lens with accommodation. *Vision Research*, 45(1), pp. 117–132.
- Dubbelman, M., Van der Heijde, G.L., Weeber, H.A. & Vrensen, G.F. (2003). Changes in the internal structure of the human crystalline lens with age and accommodation. *Vision Research*, 43(22), pp. 2363–2375.
- Ernst, L.E. (2010). *Ciliary Body Thickness and the Relationship to Refractive Error and Accommodative Function in Adults*. Master's thesis, Ohio State University.
- Fagerholm, P.P., Philipson, B.T. & Lindström, B. (1981). Normal human lens—the distribution of protein. *Experimental Eye Research*, 33(6), pp. 615–620.
- Farnsworth, P.N. & Shyne, S.E. (1979). Anterior zonular shifts with age. *Experimental Eye Research*, 28(3), pp. 291–297.
- Fea, A.M., Annetta, F., Cirillo, S., Campanella, D., De Giuseppe, M., Regge, D. & Grignolo, F.M. (2005). Magnetic resonance imaging and Orbscan assessment of the anterior chamber. *Journal of Cataract & Refractive Surgery*, 31(9), pp. 1713–1718.
- Fincham, E.F. (1925). The changes in the form of the crystalline lens in accommodation. *Transactions of the Optical Society*, 26(5), p. 239.

- Fincham, E.F. (1937). The Mechanism Of Accommodation. *British Journal of Ophthalmology*, Suppl. 8, pp. 5–80.
- Findl, O., Kiss, B., Petternel, V., Menapace, R., Georgopoulos, M., Rainer, G. & Drexler, W. (2003). Intraocular lens movement caused by ciliary muscle contraction. *Journal of cataract and refractive surgery*, 29(4), p. 669.
- Fisher, R.F. (1969). Elastic constants of the human lens capsule. *The Journal of Physiology*, 201(1), pp. 1–19.
- Fisher, R.F. (1971). The elastic constants of the human lens. *The Journal of Physiology*, 212(1), pp. 147–180.
- Fisher, R.F. (1977). The force of contraction of the human ciliary muscle during accommodation. *The Journal of Physiology*, 270(1), pp. 51–74.
- Fisher, R.F. (1983). Is the vitreous necessary for accommodation in man? *The British journal of ophthalmology*, 67(3), p. 206.
- Fisher, R.F. (1986). The ciliary body in accommodation. *Transactions of the ophthalmological societies of the United Kingdom*, 105, p. 208.
- Fisher, R.F. & Pettet, B.E. (1972). The postnatal growth of the capsule of the human crystalline lens. *Journal of Anatomy*, 112(Pt 2), pp. 207–214.
- Gambra, E., Ortiz, S., Perez-Merino, P., Gora, M., Wojtkowski, M. & Marcos, S. (2013). Static and dynamic crystalline lens accommodation evaluated using quantitative 3-D OCT. *Biomedical optics express*, 4(9), pp. 1595–609.
- Giovanzana, S., Savio, G., Meneghello, R. & Concheri, G. (2011). Shape analysis of a parametric human lens model based on geometrical constraints. *Journal of Modern Optics*, 58(19-20), pp. 1770–1780.
- Giovanzana, S. & Talu, S. (2012). Mathematical models for the shape analysis of human crystalline lens. *Journal of Modern Optics*, 59(1), pp. 26–34.
- Glasser, A., Croft, M.A. & Kaufman, P.L. (2001). Aging of the human crystalline lens and presbyopia. *International ophthalmology clinics*, 41(2), p. 1.
- Glasser, A. (2006). Restoration of accommodation. *Current Opinion in Ophthalmology*, 17(1), pp. 12–18
10.1097/01.icu.0000193069.32369.e1.
- Glasser, A. (2008). Restoration of accommodation: surgical options for correction of presbyopia. *Clinical and Experimental Optometry*, 91(3), pp. 279–295.
- Glasser, A. & Campbell, M.C.W. (1998). Presbyopia and the optical changes in the human crystalline lens with age. *Vision Research*, 38(2), pp. 209–229.
- Glasser, A. & Campbell, M.C.W. (1999). Biometric, optical and physical changes in the isolated human crystalline lens with age in relation to presbyopia. *Vision Research*, 39(11), pp. 1991–2015.
- Goldberg, D.B. (2011). Computer-animated model of accommodation and theory of reciprocal zonular action. *Clinical Ophthalmology*, 5, pp. 1559–1566.
- Gorban, A.J. & Dgiliashvili, O.A. (1993). *Microsurgery of an eye. Mistakes and complications*. Saint Petersburg: Gippokrat.
- Hermans, E., Dubbelman, M., van der Heijde, R. & Heethaar, R. (2007). The shape of the human lens nucleus with accommodation. *Journal of Vision*, 7(10), pp. 16 1–10.
- Hermans, E.A., Dubbelman, M., van der Heijde, G.L. & Heethaar, R.M. (2006). Estimating the external force acting on the human eye lens during accommodation by finite element modelling. *Vision Research*, 46(21), pp. 3642–3650.

- Hermans, E.A., Pouwels, P.J., Dubbelman, M., Kuijjer, J.P., van der Heijde, R.G. & Heethaar, R.M. (2009). Constant volume of the human lens and decrease in surface area of the capsular bag during accommodation: an MRI and Scheimpflug study. *Investigative Ophthalmology and Visual Science*, 50(1), pp. 281–289.
- Hermans, E.a., Terwee, T.T., Koopmans, S.a., Dubbelman, M., van der Heijde, R.G. & Heethaar, R.M. (2008). Development of a ciliary muscle driven accommodating intraocular lens. *Journal of Cataract & Refractive Surgery*, 34(12), pp. 2133–2138.
- Hettlich, H.J. (1996). Accommodative Lens Refilling. *Groningen: Pharmacia*, pp. 1–109.
- Heys, K.R., Cram, S.L. & Truscott, R.J. (2004). Massive increase in the stiffness of the human lens nucleus with age: the basis for presbyopia? *Molecular Vision*, 10, pp. 956–963.
- Heys, K.R., Friedrich, M.G. & Truscott, R.J.W. (2007). Presbyopia and heat: changes associated with aging of the human lens suggest a functional role for the small heat shock protein, α -crystallin, in maintaining lens flexibility. *Aging Cell*, 6(6), pp. 807–815.
- Hiraoka, M., Inoue, K.I., Ohtaka-Maruyama, C., Ohsako, S., Kojima, N., Senoo, H. & Takada, M. (2010). Intracapsular Organization of Ciliary Zonules in Monkey Eyes. *The Anatomical Record: Advances in Integrative Anatomy and Evolutionary Biology*, 293(10), pp. 1797–1804.
- Hollman, K.W., O'Donnell, M. & Erpelding, T.N. (2007). Mapping elasticity in human lenses using bubble-based acoustic radiation force. *Experimental Eye Research*, 85(6), pp. 890–893.
- Jones, C.E., Atchison, D.A., Meder, R. & Pope, J.M. (2005). Refractive index distribution and optical properties of the isolated human lens measured using magnetic resonance imaging (MRI). *Vision Research*, 45(18), pp. 2352–2366.
- Jones, C.E., Atchison, D.A. & Pope, J.M. (2007). Changes in lens dimensions and refractive index with age and accommodation. *Optometry & Vision Science*, 84(10), p. 990.
- Kaczurowski, M.I. (1964). Zonular fibers of the human eye. *American Journal of Ophthalmology*, 58, pp. 1030–1047.
- Kao, C.Y., Richdale, K., Sinnott, L.T., Ernst, L.E. & Bailey, M.D. (2011). Semi-Automatic Extraction Algorithm for Images of the Ciliary Muscle. *Optometry and vision science: official publication of the American Academy of Optometry*, 88(2), p. 275.
- Kasprzak, H.T. (2000). New approximation for the whole profile of the human crystalline lens. *Ophthalmic and Physiological Optics*, 20(1), pp. 31–43.
- Kasprzak, H.T. & Robert Iskander, D. (2006). Approximating ocular surfaces by generalised conic curves. *Ophthalmic and Physiological Optics*, 26(6), pp. 602–609.
- Kasthurirangan, S., Markwell, E.L., Atchison, D.A. & Pope, J.M. (2011). MRI study of the changes in crystalline lens shape with accommodation and aging in humans. *Journal of Vision*, 11(3).
- Kim, E., Ehrmann, K., Uhlhorn, S., Borja, D., Arrieta-Quintero, E. & Parel, J.M. (2011). Semiautomated analysis of optical coherence tomography crystalline lens images under simulated accommodation. *Journal of Biomedical Optics*, 16, p. 56003.
- Kirschkamp, T., Dunne, M. & Barry, J.C. (2004). Phakometric measurement of ocular surface radii of curvature, axial separations and alignment in relaxed and accommodated human eyes. *Ophthalmic and Physiological Optics*, 24(2), pp. 65–73.
- Koopmans, S.a., Terwee, T., Glasser, A., Wendt, M., Vilupuru, A.S., Vilipuru, A.S., van Kooten, T.G., Norrby, S., Haitjema, H.J. & Kooijman, A.C. (2006). Accommodative lens refilling in rhesus monkeys. *Investigative ophthalmology & visual science*, 47(7), pp. 2976–84.

- Koretz, J.F., Cook, C.A. & Kaufman, P.L. (1997). Accommodation and presbyopia in the human eye. Changes in the anterior segment and crystalline lens with focus. *Investigative Ophthalmology & Visual Science*, 38(3), p. 569.
- Koretz, J.F., Cook, C.A. & Kaufman, P.L. (2001). Aging of the human lens: changes in lens shape at zero-diopter accommodation. *Journal of the Optical Society of America A, Optics, Image Science, and Vision*, 18(2), pp. 265–272.
- Koretz, J.F., Cook, C.A. & Kaufman, P.L. (2002). Aging of the human lens: changes in lens shape upon accommodation and with accommodative loss. *Journal of the Optical Society of America A, Optics, Image Science, and Vision*, 19(1), pp. 144–151.
- Koretz, J.F. & Handelman, G.H. (1982). Model of the accommodative mechanism in the human eye. *Vision Research*, 22(8), pp. 917–927.
- Koretz, J.F., Kaufman, P.L., Neider, M.W. & Goeckner, P.A. (1989). Accommodation and presbyopia in the human eye—aging of the anterior segment. *Vision Research*, 29(12), pp. 1685–1692.
- Koretz, J.F. & Handelman, G.H. (1986). Modeling age-related accommodative loss in the human eye. *Mathematical Modelling*, 7(5-8), pp. 1003–1014.
- Koretz, J.F., Strenk, S.A., Strenk, L.M. & Semmlow, J.L. (2004). Scheimpflug and high-resolution magnetic resonance imaging of the anterior segment: a comparative study. *Journal of the Optical Society of America A, Optics and Image Science*, 21(3), pp. 346–354.
- Krag, S. & Andreassen, T.T. (2003a). Mechanical properties of the human lens capsule. *Progress in Retinal and Eye Research*, 22(6), pp. 749–767.
- Krag, S. & Andreassen, T.T. (2003b). Mechanical properties of the human posterior lens capsule. *Investigative Ophthalmology and Visual Science*, 44(2), pp. 691–696.
- Krag, S., Olsen, T. & Andreassen, T.T. (1997). Biomechanical characteristics of the human anterior lens capsule in relation to age. *Investigative Ophthalmology and Visual Science*, 38(2), pp. 357–363.
- Krueger, R.R., Kuszak, J., Lubatschowski, H., Myers, R.I., Ripken, T. & Heisterkamp, A. (2005). First safety study of femtosecond laser photodisruption in animal lenses: tissue morphology and cataractogenesis. *Journal of Cataract & Refractive Surgery*, 31(12), pp. 2386–2394.
- Krueger, R.R. (2002). "Retinal imaging" aberrometry: Author reply. *Ophthalmology*, 109(3), p. 406.
- Kuszak, J.R., Zoltoski, R.K. & Tiedemann, C.E. (2004). Development of lens sutures. *International Journal of Developmental Biology*, 48(8-9), pp. 889–902.
- Lamar, P.D., Acosta, A.C., Lee, W., Manns, F., Orozco, M., Augusteyn, R., Ho, A., Decker, S., Holden, B. & Parel, J.M. (2005). Zonular Architecture of the Crystalline Lens Examined ex vivo in a Lens Stretcher. *ARVO Meeting Abstracts*, 46(5), p. 737.
- Lamar, P.D., Decker, S., Acosta, A.C. & Parel, J.M. (2004). Anterior and posterior sem analysis of the zonular apparatus of human and non-human primates: a pilot study. *ARVO Meeting Abstracts*, 45(5), p. 59.
- Lanchares, E., Navarro, R. & Calvo, B.n. (2012). Hyperelastic modelling of the crystalline lens: Accommodation and presbyopia. *Journal of Optometry*, 5(3), pp. 110 – 120.
- Legeais, J.M., Werner, L., Abenhaim, a. & Renard, G. (1999). Pseudoaccommodation: BioComFold versus a foldable silicone intraocular lens. *Journal of cataract and refractive surgery*, 25(2), pp. 262–7.
- Lim, J.C., Walker, K.L., Sherwin, T., Schey, K.L. & Donaldson, P.J. (2009). Confocal microscopy reveals zones of membrane remodeling in the outer cortex of the human lens. *Investigative Ophthalmology & Visual Science*, 50(9), p. 4304.

- Liu, Z., Wang, B., Xu, X. & Wang, C. (2006). A study for accommodating the human crystalline lens by finite element simulation. *Comput Med Imaging Graph*, 30(6-7), pp. 371–376.
- Liu, Z., Boliang, W., Xiuying, X., Ying, J., Jiezhen, X. & Chunbo, B. (2005). Finite Element Modeling and Simulating of Accommodating Human Crystalline Lens. In: *Engineering in Medicine and Biology Society, 2005. IEEE-EMBS 2005. 27th Annual International Conference of the*, pp. 11–14.
- Lizak, M.J., Datiles, M.B., Aletras, A.H., Kador, P.F. & Balaban, R.S. (2000). MRI of the Human Eye Using Magnetization Transfer Contrast Enhancement. *Investigative Ophthalmology and Visual Science*, 41(12), pp. 3878–3881.
- Ljubimova, D., Eriksson, A. & Bauer, S. (2008). Aspects of eye accommodation evaluated by finite elements. *Biomechanics and Modeling in Mechanobiology*, 7(2), pp. 139–150.
- Ludwig, K. (2001). Chapter: Zonular apparatus, anatomy, biomechanics and coupling to the lens. In: *Current aspects of human accommodation* (eds. R. Guthoff & K. Ludwig), Heidelberg: Kaden Verlag, pp. 71–92.
- Ludwig, K., Wegscheider, E., Hoops, J.P. & Kampik, A. (1999). In vivo imaging of the human zonular apparatus with high-resolution ultrasound biomicroscopy. *Graefes Archive for Clinical and Experimental Ophthalmology*, 237(5), pp. 361–371.
- Lütjen-Drecoll, E., Kaufman, P.L., Wasielewski, R., Ting-Li, L. & Croft, M.A. (2010). Morphology and accommodative function of the vitreous zonule in human and monkey eyes. *Investigative Ophthalmology & Visual Science*, 51(3), p. 1554.
- Manns, F., Fernandez, V., Zipper, S., Sandadi, S., Hamaoui, M., Ho, A. & Parel, J.M. (2004). Radius of curvature and asphericity of the anterior and posterior surface of human cadaver crystalline lenses. *Experimental Eye Research*, 78(1), pp. 39–51.
- Manns, F., Parel, J.M., Denham, D., Billotte, C., Ziebarth, N., Borja, D., Fernandez, V., Aly, M., Arrieta, E., Ho, A. & Holden, B. (2007). Optomechanical Response of Human and Monkey Lenses in a Lens Stretcher. *Investigative Ophthalmology and Visual Science*, 48(7), pp. 3260–3268.
- Martin, H., Guthoff, R., Terwee, T. & Schmitz, K.P. (2005). Comparison of the accommodation theories of Coleman and of Helmholtz by finite element simulations. *Vision Research*, 45(22), pp. 2910–2915.
- McDonald, J.P., Croft, M.A., Vinje, E., Glasser, A., Heatley, G.A., Kaufman, P. & Sarfarazi, F.M. (2003). Sarfarazi elliptical accommodating intraocular lens (EAIOL) in rhesus monkey eyes in vitro and in vivo. *Investigative Ophthalmology and Visual Science*, 44(5), p. 256.
- McLeod, S.D., Vargas, L.G., Portney, V. & Ting, A. (2007). Synchrony dual-optic accommodating intraocular lens: Part 1: Optical and biomechanical principles and design considerations. *Journal of Cataract and Refractive Surgery*, 33(1), pp. 37–46.
- Menapace, R., Findl, O., Kriechbaum, K. & Leydolt-Koepl, C. (2007). Accommodating intraocular lenses: a critical review of present and future concepts. *Graefes archive for clinical and experimental ophthalmology = Albrecht von Graefes Archiv für klinische und experimentelle Ophthalmologie*, 245(4), pp. 473–89.
- Michael, R., Mikielwicz, M., Gordillo, C., Montenegro, G.A., Cortes, L.P. & Barraquer, R.I. (2012). Elastic properties of human lens zonules as a function of age in presbyopes. *Investigative Ophthalmology & Visual Science*, 53(10), pp. 6109–6114.
- Moffat, B.A., Atchison, D.A. & Pope, J.M. (2002a). Age-related changes in refractive index distribution and power of the human lens as measured by magnetic resonance micro-imaging in vitro. *Vision Research*, 42(13), pp. 1683–1693.
- Moffat, B.A., Atchison, D.A. & Pope, J.M. (2002b). Explanation of the Lens Paradox. *Optometry & Vision Science*, 79(3), pp. 148–150.

- Myers, R.I. & Krueger, R.R. (1998). Novel approaches to correction of presbyopia with laser modification of the crystalline lens. *Journal of refractive surgery*, 14(2), p. 136.
- Nankivil, D., Manns, F., Arrieta-Quintero, E., Ziebarth, N., Borja, D., Amelinckx, A., Bernal, A., Ho, A. & Parel, J.M. (2009). Effect of Anterior Zonule Transection on the Change in Lens Diameter and Power in Cynomolgus Monkeys during Simulated Accommodation. *Investigative Ophthalmology & Visual Science*, 50(8), pp. 4017–4021.
- Nishi, O. (1989). Refilling the lens of the rabbit eye after intercapsular cataract surgery using an endo-capsular balloon and an anterior capsule suturing technique. *Journal of cataract and refractive surgery*, 15(4), p. 450.
- Nishi, O., Nishi, K., Nishi, Y. & Chang, S. (2008). Capsular bag refilling using a new accommodating intraocular lens. *Journal of Cataract & Refractive Surgery*, 34(2), pp. 302–309.
- Nishi, Y., Mireskandari, K., Khaw, P. & Findl, O. (2009). Lens refilling to restore accommodation. *Journal of Cataract & Refractive Surgery*, 35(2), pp. 374–382.
- Ostrin, L., Kasthurirangan, S., Win-Hall, D. & Glasser, A. (2006). Simultaneous measurements of refraction and A-scan biometry during accommodation in humans. *Optometry and vision science : official publication of the American Academy of Optometry*, 83(9), pp. 657–65.
- Pardue, M.T. & Sivak, J.G. (2000). Age-Related Changes in Human Ciliary Muscle. *Optometry & Vision Science*, 77(4), pp. 204–210.
- Pedrigi, R.M., David, G., Dziezyc, J. & Humphrey, J.D. (2007). Regional mechanical properties and stress analysis of the human anterior lens capsule. *Vision Research*, 47(13), pp. 1781–1789.
- Piers, P.a., Manzanera, S., Prieto, P.M., Gorceix, N. & Artal, P. (2007). Use of adaptive optics to determine the optimal ocular spherical aberration. *Journal of cataract and refractive surgery*, 33(10), pp. 1721–6.
- PierścioneK, B.K. (1995). Age-related response of human lenses to stretching forces. *Experimental Eye Research*, 60(3), pp. 325–332.
- PierścioneK, B.K. & Chan, D.C. (1989). Refractive Index Gradient of Human Lenses. *Optometry & Vision Science*, 66(12), pp. 822–829.
- PierścioneK, B.K. & Weale, R.a. (1995). Presbyopia - a maverick of human aging. *Archives of gerontology and geriatrics*, 20(3), pp. 229–40.
- PierścioneK, B.K. (1993). In Vitro Alteration of Human Lens Curvatures by Radial Stretching. *Experimental Eye Research*, 57(5), pp. 629–635.
- Preußner, P., Wahl, J., Gerl, R., Kreiner, C. & Serester, A. (2001). Akkommodatives Linsenimplantat. *Der Ophthalmologe*, 98(1), pp. 97–102.
- Rao, H.Y. & Wang, L.T. (2002). An experimental study of stretching capability of zonules. *J Clin Ophthalmol*, 10(3), pp. 223–225.
- Reed, M.D., Thaker, R. & Guo, S. (2003). Ultrasound Biomicroscopic Changes of the Anterior Lens Capsule and Lens Zonule in Patients with Pseudoexfoliation. *ARVO Meeting Abstracts*, 44(5), p. 200.
- Reiß, S., Burau, G., Stachs, O., Guthoff, R. & Stolz, H. (2011). Spatially resolved Brillouin spectroscopy to determine the rheological properties of the eye lens. *Biomedical Optics Express*, 2(8), pp. 2144–2159.
- Richdale, K., Bullimore, M.A. & Zadnik, K. (2008). Lens thickness with age and accommodation by optical coherence tomography. *Ophthalmic Physiol Opt*, 28(5), pp. 441–447.
- Richdale, K., Sinnott, L.T., Bullimore, M.A., Wassenaar, P.A., Schmalbrock, P., Kao, C.Y., Patz, S., Mutti, D.O., Glasser, A. & Zadnik, K. (2013). Quantification of Age-Related and per Diopter Accommodative Changes of the Lens and Ciliary Muscle in the Emmetropic Human Eye. *Investigative Ophthalmology & Visual Science*, 54(2), pp. 1095–1105.

- Riehemann, S., Palme, M., Peschel, T., Kunert, K., Notni, G. & Blum, M. (2011). An accommodating opto-mechanical model of the aging human eye. *Journal of Modern Optics*, 58(19), pp. 1788–1803.
- Ripken, T., Oberheide, U., Fromm, M., Schumacher, S., Gerten, G. & Lubatschowski, H. (2008). fs-Laser induced elasticity changes to improve presbyopic lens accommodation. *Graefe's Archive for Clinical and Experimental Ophthalmology*, 246(6), pp. 897–906.
- Rohen, J.W. (1979). Scanning electron microscopic studies of the zonular apparatus in human and monkey eyes. *Investigative Ophthalmology and Visual Science*, 18(2), pp. 133–144.
- Rosales, P., Dubbelman, M., Marcos, S. & van der Heijde, R. (2006). Crystalline lens radii of curvature from Purkinje and Scheimpflug imaging. *Journal of Vision*, 6(10), pp. 1057–1067.
- Rosen, A.M., Denham, D.B., Fernandez, V., Borja, D., Ho, A., Manns, F., Parel, J.M. & Augusteyn, R.C. (2006). In vitro dimensions and curvatures of human lenses. *Vision Research*, 46(6-7), pp. 1002–1009.
- Sakabe, I., Oshika, T., Lim, S.J. & Apple, D.J. (1998). Anterior shift of zonular insertion onto the anterior surface of human crystalline lens with age. *Ophthalmology*, 105(2), pp. 295–299.
- Salzmann, M. (1912). *Anatomie und histologie des menschlichen augapfels im normalzustande: Seine entwicklung und sein altern*. F. Deuticke.
- Santos-Neto, E. & Alves, M.R. (2011). New concepts in accommodation and presbyopia. *Revista Brasileira de Oftalmologia*, 70(5), pp. 306–311.
- Scarcelli, G. & Yun, S.H. (2012). In vivo Brillouin optical microscopy of the human eye. *Optics express*, 20(8), pp. 9197–202.
- Schachar, R.A. (1992). Cause and treatment of presbyopia with a method for increasing the amplitude of accommodation. *Annals of Ophthalmology*, 24(12), pp. 445–447,452.
- Schachar, R.A., Abolmaali, A. & Le, T. (2006). Insights into the age-related decline in the amplitude of accommodation of the human lens using a non-linear finite-element model. *British Journal of Ophthalmology*, 90(10), pp. 1304–1309.
- Schachar, R.A. & Bax, A.J. (2001a). Mechanism of accommodation. *International ophthalmology clinics*, 41(2), p. 17.
- Schachar, R.A., Chan, R.W. & Fu, M. (2011). Viscoelastic properties of fresh human lenses under 40 years of age: implications for the aetiology of presbyopia. *British Journal of Ophthalmology*, 95, pp. 1010–1013.
- Schachar, R.A., Cudmore, D.P. & Black, T.D. (1993). Experimental support for Schachar's hypothesis of accommodation. *Annals of Ophthalmology*, 25(11), pp. 404–409.
- Schachar, R. & Bax, A. (2001b). Mechanism of human accommodation as analyzed by nonlinear finite element analysis. *Annals of Ophthalmology*, 33(2), pp. 103–112.
- Schachar, R., Tello, C., Cudmore, D.P., Liebmann, J.M., Black, T.D. & Ritch, R. (1996). In vivo increase of the human lens equatorial diameter during accommodation. *American Journal of Physiology. Regulatory, integrative and comparative physiology*, 40(3), pp. R670–R676.
- Schachar, R.a. (2004). Qualitative effect of zonular tension on freshly extracted intact human crystalline lenses: implications for the mechanism of accommodation. *Investigative ophthalmology & visual science*, 45(8), pp. 2691–5.
- Schachar, R.A. (2005). Growth patterns of fresh human crystalline lenses measured by in vitro photographic biometry. *Journal of Anatomy*, 206(6), pp. 575–580.
- Schachar, R.A. (2006). The Mechanism of Accommodation and Presbyopia. *International ophthalmology clinics*, 46(3), pp. 39–61.

- Schumacher, S., Oberheide, U., Fromm, M., Ripken, T., Ertmer, W., Gerten, G., Wegener, A. & Lubatschowski, H. (2009). Femtosecond laser induced flexibility change of human donor lenses. *Vision Research*, 49(14), pp. 1853–1859.
- Sharma, P.K., Busscher, H.J., Terwee, T., Koopmans, S.A. & van Kooten, T.G. (2011). A comparative study on the viscoelastic properties of human and animal lenses. *Experimental Eye Research*, 93(5), pp. 681–688.
- Sheppard, A.L. (2010). *In vivo analysis of ocular morphological changes during phakic accommodation*. Ph.D. thesis, Aston University.
- Sheppard, A.L. & Davies, L.N. (2010). In vivo analysis of ciliary muscle morphologic changes with accommodation and axial ametropia. *Investigative Ophthalmology & Visual Science*, 51(12), pp. 6882–6889.
- Sheppard, A.L., Bashir, A., Wolffsohn, J.S. & Davies, L.N. (2010). Accommodating intraocular lenses: a review of design concepts, usage and assessment methods. *Clinical and Experimental Optometry*, 93(6), pp. 441–452.
- Sheppard, A.L. & Davies, L.N. (2011). The Effect of Ageing on In Vivo Human Ciliary Muscle Morphology and Contractility. *Investigative Ophthalmology & Visual Science*, 52(3), pp. 1809–1816.
- Sheppard, A.L., Evans, C.J., Singh, K.D., Wolffsohn, J.S., Dunne, M.C.M. & Davies, L.N. (2011). Three-dimensional magnetic resonance imaging of the phakic crystalline lens during accommodation. *Investigative Ophthalmology & Visual Science*, 52(6), pp. 3689–3697.
- Smith, G. (2003). The optical properties of the crystalline lens and their significance. *Clinical & experimental optometry: journal of the Australian Optometrical Association*, 86(1), p. 3.
- Smith, G., Atchison, D.A., Robert Iskander, D., Jones, C.E. & Pope, J.M. (2009). Mathematical models for describing the shape of the in vitro unstretched human crystalline lens. *Vision Research*, 49(20), pp. 2442–2452.
- Sparrow, J.M., Bron, A.J., Brown, N.A.P., Ayliffe, W. & Hill, A.R. (1986). The Oxford clinical cataract classification and grading system. *International ophthalmology*, 9(4), pp. 207–225.
- Stachs, O., Martin, H., Behrend, D., Schmitz, K.P. & Guthoff, R. (2006). Three-dimensional ultrasound biomicroscopy, environmental and conventional scanning electron microscopy investigations of the human zonula ciliaris for numerical modelling of accommodation. *Graefe's Archive for Clinical and Experimental Ophthalmology*, 244(7), pp. 836–844.
- Stachs, O., Martin, H., Kirchhoff, A., Stave, J., Terwee, T. & Guthoff, R. (2002). Monitoring accommodative ciliary muscle function using three-dimensional ultrasound. *Graefe's Archive for Clinical and Experimental Ophthalmology*, 240(11), pp. 906–912.
- Stafford, M.J. (2001). The histology and biology of the lens. *Optometry Today*, pp. 23–30.
- Streten, B.W. (1977). The zonular insertion: a scanning electron microscopic study. *Investigative Ophthalmology and Visual Science*, 16(4), pp. 364–375.
- Streten, B.W. (2003). Chapter 14 anatomy of the zonular apparatus. In: *Duane's clinical ophthalmology* (eds. W. Tasman & E. Jager), Hagerstown: Lippincott Williams and Wilkins.
- Strenk, S.A., Semmlow, J.L., Strenk, L.M., Munoz, P., Gronlund-Jacob, J. & DeMarco, J.K. (1999). Age-related changes in human ciliary muscle and lens: a magnetic resonance imaging study. *Investigative Ophthalmology and Visual Science*, 40(6), pp. 1162–1169.
- Strenk, S.A., Strenk, L.M. & Guo, S. (2006). Magnetic resonance imaging of aging, accommodating, phakic, and pseudophakic ciliary muscle diameters. *Journal of Cataract & Refractive Surgery*, 32(11), pp. 1792–1798.

- Strenk, S.A., Strenk, L.M. & Koretz, J.F. (2005). The mechanism of presbyopia. *Prog Retin Eye Res*, 24(3), pp. 379–393.
- Strenk, S.A., Strenk, L.M. & Semmlow, J.L. (2000). High resolution MRI study of circumlental space in the aging eye. *Journal of Refractive Surgery*, 16(5), pp. 659–660.
- Strenk, S.A., Strenk, L.M., Semmlow, J.L. & DeMarco, J.K. (2004). Magnetic resonance imaging study of the effects of age and accommodation on the human lens cross-sectional area. *Investigative Ophthalmology and Visual Science*, 45(2), pp. 539–545.
- Strenk, S.a., Strenk, L.M. & Guo, S. (2010). Magnetic resonance imaging of the anteroposterior position and thickness of the aging, accommodating, phakic, and pseudophakic ciliary muscle. *Journal of Cataract & Refractive Surgery*, 36(2), pp. 235–41.
- Subbaram, M.V., Gump, J.C., Bullimore, M.A. & Sooryakumar, R. (2002). The Elasticity of the Human Lens. *Investigative Ophthalmology and Visual Science*, 43(12), pp. 468–.
- Taubin, G. (1991). Estimation of planar curves, surfaces, and nonplanar space curves defined by implicit equations with applications to edge and range image segmentation. *IEEE Transactions on Pattern Analysis and Machine Intelligence*, pp. 1115–1138.
- Taylor, V.L., Al-Ghoul, K.J., Lane, C.W., Davis, V.A., Kuszak, J.R. & Costello, M.J. (1996). Morphology of the normal human lens. *Investigative Ophthalmology & Visual Science*, 37(7), pp. 1396–1410.
- Truscott, R.J. (2009). Presbyopia. Emerging from a blur towards an understanding of the molecular basis for this most common eye condition. *Experimental Eye Research*, 88(2), pp. 241–247.
- Tsorbatzoglou, A., Németh, G., Széll, N., Biró, Z. & Berta, A. (2007). Anterior segment changes with age and during accommodation measured with partial coherence interferometry. *Journal of cataract and refractive surgery*, 33(9), pp. 1597–601.
- Urs, R., Ho, A., Manns, F. & Parel, J.M. (2010). Age-dependent Fourier model of the shape of the isolated ex vivo human crystalline lens. *Vision Research*, 50(11), pp. 1041–1047.
- Urs, R., Ho, A., Manns, F., Parel, J.M. & Magjarevic, R. (2009a). Model of the Isolated Ex-Vivo Human Crystalline Lens Using Cosine Functions. In: *25th Southern Biomedical Engineering Conference 2009, 15 - 17 May 2009, Miami, Florida, USA*, volume 24 (eds. A.J. McGoron, C.Z. Li & W.C. Lin), Springer Berlin Heidelberg, ISBN 978-3-642-01697-4, pp. 241–242.
- Urs, R., Manns, F., Ho, A., Borja, D., Amelinckx, A., Smith, J., Jain, R., Augusteyn, R. & Parel, J.M. (2009b). Shape of the isolated ex-vivo human crystalline lens. *Vision Research*, 49(1), pp. 74–83.
- Van Alphen, G. & Graebel, W.P. (1991). Elasticity of tissues involved in accommodation. *Vision Research*, 31(7-8), pp. 1417–1438.
- Van de Sompel, D., Kunkel, G.J., Hersh, P.S. & Smits, A.J. (2010). Model of accommodation: Contributions of lens geometry and mechanical properties to the development of presbyopia. *Journal of Cataract & Refractive Surgery*, 36(11), pp. 1960–1971.
- von Helmholtz, H. (1855). Uber die akkommodation des auges. *Archives of Ophthalmology*, 1, pp. 1–74.
- Weale, R.A. (2000). Why we need reading-glasses before a zimmer-frame. *Vision research*, 40(17), pp. 2233–2240.
- Weeber, H.A., Eckert, G., Pechhold, W. & van der Heijde, R.G. (2007). Stiffness gradient in the crystalline lens. *Graefe's Archive for Clinical and Experimental Ophthalmology*, 245(9), pp. 1357–1366.
- Weeber, H.A., Eckert, G., Soergel, F., Meyer, C.H., Pechhold, W. & van der Heijde, R.G. (2005). Dynamic mechanical properties of human lenses. *Experimental Eye Research*, 80(3), pp. 425–434.
- Weeber, H.A. & van der Heijde, R.G.L. (2007). On the relationship between lens stiffness and accommodative amplitude. *Experimental Eye Research*, 85(5), pp. 602–607.

- Weeber, H.A. & van der Heijde, R.G.L. (2008). Internal deformation of the human crystalline lens during accommodation. *Acta Ophthalmologica*, 86(6), pp. 642–647.
- Wilde, G.S., Burd, H.J. & Judge, S.J. (2012). Shear modulus data for the human lens determined from a spinning lens test. *Experimental Eye Research*, 97(1), pp. 36–48.
- Wilde, G.S. (2011). *Measurement of Human Lens Stiffness for Modelling Presbyopia Treatments*. Ph.D. thesis.
- Wilson, R.S. (1993). A new theory of human accommodation: cilio-zonular compression of the lens equator. *Transactions of the American Ophthalmological Society*, 91, pp. 401–16; discussion 416–9.
- Ziebarth, N.M., Wojcikiewicz, E.P., Manns, F., Moy, V.T. & Parel, J.M. (2007). Atomic force microscopy measurements of lens elasticity in monkey eyes. *Molecular Vision*, 13, p. 504.
- Ziebarth, N.M., Arrieta, E., Feuer, W.J., Moy, V.T., Manns, F. & Parel, J.M. (2011). Primate lens capsule elasticity assessed using Atomic Force Microscopy. *Experimental Eye Research*, 92(6), pp. 490–494.
- Ziebarth, N.M., Borja, D., Arrieta, E., Aly, M., Manns, F., Dortonne, I., Nankivil, D., Jain, R. & Parel, J.M. (2008). Role of the Lens Capsule on the Mechanical Accommodative Response in a Lens Stretcher. *Investigative Ophthalmology & Visual Science*, 49(10), pp. 4490–4496.
- Ziebarth, N.M., Manns, F., Uhlhorn, S.R., Venkatraman, A.S. & Parel, J.M. (2005). Noncontact Optical Measurement of Lens Capsule Thickness in Human, Monkey, and Rabbit Postmortem Eyes. *Investigative Ophthalmology & Visual Science*, 46(5), pp. 1690–1697.

Appendix A

Supporting data for Chapter 6

A.1 Zonule bundle data

Table A.1: Zonule displacements used in Chapter 6, divided into sections and models. All displacements in mm.

Section	Model	AAZ		AEZ		APZ1		APZ2	
		x	y	x	y	x	y	x	y
6.2.3.1	ZA	-	-	0.37	0	-	-	-	-
	ZB	0.4	-0.12	0.4	-0.12	0.41	-0.17	-	-
	ZC	0.4	-0.12	0.4	-0.12	0.41	-0.17	0.2	0.12
6.2.3.2	ZT1_20	0.79	-0.26	0.74	-0.2	0.61	-0.19	0.34	-0.14
	ZT1_40	0.4	-0.12	0.4	-0.12	0.41	-0.17	0.2	0.12
	ZT1_50	0.15	-0.12	0.19	-0.07	0.13	0	0.07	0.05
6.2.3.3	20_A	0.47	-0.26	0.51	-0.23	0.54	-0.24	0.35	-0.14
	20_B	0.79	-0.26	0.74	-0.2	0.61	-0.19	0.34	-0.14
	40_A	0.33	-0.1	0.34	-0.12	0.42	-0.19	0.26	-0.04
	40_B	0.4	-0.12	0.4	-0.12	0.41	-0.17	0.2	0.12
	50_A	0.29	-0.23	0.26	-0.06	0.1	0.06	0.14	0.08
	50_B	0.15	-0.12	0.19	-0.07	0.13	0	0.07	0.05
6.2.3.4	40_Ang	0.39	-0.1	0.43	-0.14	0.31	-0.07	0.31	0
	40_Tan								
	20	0.44	-0.14	0.46	-0.17	0.44	-0.16	0.4	-0.07
	40	0.37	-0.1	0.42	-0.1	0.21	-0.06	0.17	0.06
	50	0.25	-0.16	0.32	-0.08	0.2	-0.01	0.14	-0.01
6.2.5	20_NC/SA/SB	0.48	-0.2	0.46	-0.17	0.44	-0.16	0.34	-0.07
	40_NC/SA/SB	0.37	-0.1	0.42	-0.1	0.21	-0.06	0.17	0.06
	50_NC/SA/SB	0.25	-0.16	0.32	-0.08	0.2	-0.01	0.14	-0.01
6.3	29	0.41	-0.1	0.46	-0.19	0.39	-0.13	0.25	0.02
	45	0.27	-0.17	0.3	-0.15	0.16	-0.05	0.22	0.02
	60	0.18	-0.12	0.2	-0.04	0.09	-0.04	0.11	0.06

Table A.2: Zonule bundle thickness values used in Chapter 6. All values in mm.

Section	Model Age (Years)	AAZ	AEZ	APZ1	APZ2
6.2.3.4	20	0.03	0.012	0.018	0.012
	40	0.03	0.024	0.022	0.018
	50	0.035	0.024	0.03	0.025
6.3.1	29	0.03	0.012	0.018	0.012
	45	0.03	0.024	0.022	0.018
	60	0.035	0.025	0.03	0.025
6.3.2	29	0.029	0.011	0.017	0.011
	45	0.032	0.025	0.026	0.019
	60	0.045	0.025	0.045	0.035

A.2 Results data

Detailed results of all models run in Chapter 6, split into the different procedure methods used

Table A.3: Results of models using the spinning lens setup. Compared to the expected changes (Section 5.4.2) a * indicates a change that is too high and a ** indicates a change that is too low.

Section	Model	T _L change (mm)	L _R change (mm)	R _A change (mm)	R _P change (mm)
Section 6.2.1	20_H	0.489	0.188	3.600	1.185
	20_NC	0.561	0.152	6.302	2.106
	20_SA	0.623	0.149	8.494	2.984
	20_SB	0.563	0.139	7.627	2.182
	40_H	0.126	0.046	0.967	0.340
	40_NC	0.126	0.039	1.153	0.398
	40_SA	0.132	0.039	1.257	0.448
	40_SB	0.129	0.039	1.219	0.417
	50_H	0.026	0.009	0.188	0.071
	50_NC	0.034	0.019	0.096	0.055
	50_SA	0.035	0.019	0.077	0.045
50_SB	0.036	0.020	0.105	0.060	
Section 6.2.2	20_SBC	0.169	0.017	0.002	0.000
	40_SBC	0.073	0.015	0.001	0.000

Table A.4: Results of models run in Section 6.2 using the zonule displacement procedure. Compared to the expected changes (Section 5.4.2) a * indicates a change that is too high and a ** indicates a change that is too low.

Section	Model	T _L change (mm)	L _R change (mm)	R _A change (mm)	R _P change (mm)
6.2.3.1	ZA	0.29	0.20	2.69	0.70**
	ZB	0.37*	0.26	4.35*	0.80
	ZC	0.40*	0.27	4.01*	0.80
6.2.3.2	ZT1_20	0.96*	0.58	12.30*	2.24*
	ZT1_40	0.40*	0.27	4.01*	0.80
	ZT1_50	0.08	0.14	0.47	0.17**
6.2.3.3	20_A	0.60*	0.38	3.72**	1.76
	20_B	0.78*	0.53	6.20	2.11*
	40_A	0.27	0.24	1.73	0.79
	40_B	0.30*	0.27	2.09	0.78
	50_A	0.10	0.21	0.51	0.18**
	50_B	0.08	0.13	0.46	0.17**
	20_A_1	0.73*	0.37	6.90	1.67
	20_A_2	0.72*	0.42	5.16	1.96
	20_A_3	0.60*	0.33**	3.37**	1.94
	40_A_1	0.34*	0.22	2.96	0.77
	40_A_2	0.35*	0.26	2.42	0.90*
	40_A_3	0.27	0.20	1.55	0.83
	50_A_1	0.14	0.21	0.65	0.18**
	50_A_2	0.13	0.23	0.60	0.19**
50_A_3	0.09	0.17	0.48	0.19**	
6.2.3.4	40_Ang	0.40*	0.26	4.41*	0.80
	40_Tan	0.38*	0.26	3.48	0.62**
	20	0.65*	0.38	4.73	1.83
	40	0.40*	0.36	3.12	0.78
	50	0.16	0.29*	0.62	0.15**
6.2.5	20_NC	0.67*	0.39	3.86**	1.72
	20_SA	0.69*	0.39	4.13**	1.86
	20_SB	0.69*	0.39	4.12**	1.81
	40_NC	0.34*	0.28	3.03	0.47**
	40_SA	0.35*	0.29	3.28	0.47**
	40_SB	0.40*	0.36	3.12	0.78
	50_NC	0.16	0.29*	-0.12**	0.11**
	50_SA	0.16	0.29*	0.04**	0.08**
50_SB	0.16	0.29*	0.18**	0.15**	

Table A.5: Results of studies in Section 6.3. Compared to the expected changes (Section 5.4.2) a * indicates a change that is too high and a ** indicates a change that is too low.

Parameter	29 YO	45 YO	60 YO
T _L change (mm)	0.528*	0.241	0.051
L _R change (mm)	0.351	0.261	0.198
R _A change (mm)	3.624	0.981	-0.155**
R _P change (mm)	1.220	0.436	0.098
Total force (N)	0.092	0.082	0.057
Anterior pole movement (mm)	-0.346 (67%)	-0.233 (97%)	-0.133 (2.6%)
Posterior pole movement (mm)	0.182	0.0255	-0.085
Central movement (mm)	-0.076	-0.106	-0.089
T _N change (mm)	0.229 (43%)	0.088 (36%)	0.003 (5%)

Table A.6: Comparison of the changes in geometry in the current model in comparison to models from previous FEA models, from Section 6.3.3.2.

Age (Years)	Study	T _L change (mm)	R _A change (mm)	R _P change (mm)	T _N change (mm)	L _R change (mm)
29	Current	0.52	3.61	1.21	0.226	0.3420
	Burd <i>et al.</i> (2002)	-	6.26	0.81	-	-
	Hermans <i>et al.</i> (2006)	0.38	4.56	0.87	0.2 (52%)	0.27
	Hermans <i>et al.</i> (2008)	0.4	4.06	0.66		0.21
	Wilde (2011)	0.61	5.4	2.19	80%	0.29
	Lanchares <i>et al.</i> (2012)	0.39	3.49	0.87	0.234 (60%)	0.32
45	Current	0.24	1.07	0.44	0.09	0.2620
	Hermans <i>et al.</i> (2008)	0.23	1.98	0.44	0.06	0.14
	Wilde (2011)	0.31	1.8	0.73		0.23
	Lanchares <i>et al.</i> (2012)		2.48	0.88		

Table A.7: Results of the presbyopia models run in Section 6.4

Section	Baseline model	Model	T _L change (mm)	L _R change (mm)	R _A change (mm)	R _P change (mm)
6.4.1	29	45M	0.31	0.29	1.39	0.56
		45CM	0.49	0.33	3.38	1.18
		45D	0.38	0.23	2.39	0.76
		45D+ZT	0.40	0.28	2.40	0.57
		60M	0.09	0.22	0.00	0.17
		60LCM	0.09	0.22	0.01	0.17
		60D	0.29	0.17	2.05	0.65
		60D+ZT	0.38	0.20	1.92	0.39
		60ZA	0.49	0.33	2.94	0.86
	45	29M	0.39	0.28	2.84	0.77
		29CM	0.25	0.27	1.08	0.45
		29D	0.33	0.34	1.49	0.52
		29D+ZT	0.29	0.28	1.44	0.48
		60M	0.08	0.23	-0.11	0.16
		60D	0.18	0.21	0.70	0.32
		60D+ZT	0.20	0.21	0.72	0.27
	60	29M	0.33	0.12	2.90	0.16
		29LCM	0.34	0.12	2.96	0.13
		29D	0.11	0.26	-0.04	0.13
		29D+ZT	0.08	0.20	0.00	0.13
		29SV	0.29	0.11	1.58	-0.45
		29ZA	0.07	0.09	0.04	0.14
		45M	0.20	0.11	1.00	0.24
		45D	0.09	0.21	-0.04	0.16
		45D+ZT	0.08	0.21	-0.02	0.14
		60SV	0.07	0.04	0.64	0.35
		6.4.3	29	60D+LCM	0.05	0.12
45D+LCM	0.21			0.19	0.95	0.36
60CT+CM	0.52			0.29	5.06	1.03
60	29D+LCM		0.49	0.33	3.96	0.35
	29CT+CM		0.05	0.08	0.02	0.16

A.3 Further details of the accommodation models in Section 6.3.2

Table A.8: Material property data for the models used in Section 6.3.2.

Component		29		45		60	
		μ (N/mm ²)	d	μ (N/mm ²)	d	μ (N/mm ²)	d
Lens Region	0.05	4.26E-05	46.95	1.82E-03	1.10	0.036	0.055
	0.15	5.8E-05	34.48	1.75E-03	1.14	0.032	0.063
	0.25	7.9E-05	25.32	1.69E-03	1.18	0.026	0.076
	0.35	1.08E-04	18.52	1.63E-03	1.23	0.021	0.095
	0.45	1.47E-04	13.61	1.57E-03	1.27	0.016	0.124
	0.55	2E-04	10	1.51E-03	1.32	0.012	0.171
	0.65	2.73E-04	7.33	1.46E-03	1.37	0.008	0.247
	0.75	3.72E-04	5.38	1.41E-03	1.42	0.005	0.385
	0.85	5.07E-04	3.94	1.35E-03	1.48	0.003	0.645
	0.95	6.91E-04	2.89	1.31E-03	1.54	0.002	1.177
Capsule		0.432	4.63E-03	0.493	4.06E-03	0.493	4.06E-03

Table A.9: Geometric data for the lens outline and internal structure used in Section 6.3.2.

Parameter (in mm unless otherwise indicated)	29 YO	45 YO	60 YO
L_R	4.01	4.33	4.46
T_L	4.01	4.24	4.46
R_A	8.18	9.64	9.41
R_P	-4.38	-5.25	-5.40
q_A	-9.05	-5.84	-4.20
q_P	-2.9700	-1.85	-0.8
AccAbility (D)	9.05	3.58	1.20
Z1	0.28	0.28	0.28
Z2	0.58	0.77	0.95
Z3	0.34	0.34	0.34
Z4	0.78	0.80	0.83
Z5	0.77	0.79	0.81
Z6	0.31	0.31	0.31
Z7	0.40	0.52	0.64
Z8	0.17	0.17	0.17
Nucleus thickness	2.20	2.24	2.28
Anterior Cortex thickness	0.86	1.05	1.23

Table A.10: The capsule thickness values used in Section 6.3.2.

Parameter (all in mm)	29 YO	45 YO	60 YO
p0	0.0102	0.0117	0.0131
p45	0.0118	0.0153	0.0167
p80	0.0078	0.0074	0.0070
p100	0.0074	0.0074	0.0074
p120	0.0073	0.0066	0.0059
p200	0.0033	0.0032	0.0030

Table A.11: Geometric data for definition of the zonules and ciliary body used in Section 6.3.2. R = Relaxed, A = Accommodated.

Parameter (all in mm)	29 YO		45 YO		60 YO	
	R	A	R	A	R	A
Axial Length (AL)	23.31		23.49		23.66	
L_D	9.22	8.01	9.15	8.67	9.08	8.92
AAZ, APZ1	1.15		1.25		1.35	
APZ2	1.14		1.10		1.05	
CMT1	1.13	1.20	1.19	1.21	1.24	1.25
CMT2	0.83					
CMT3	0.5					
Ciliary muscle length	4.63	4.04	4.63	4.40	4.63	4.55
ACD	3.73	3.20	3.38	3.14	3.06	2.94
Corneal thickness	0.54		0.53		0.52	
Anterior shift		0.05		0.05		0.05
Corneal apex to ciliary body	4.44	4.46	4.30	4.34	4.17	4.22
Ciliary muscle movement		0.36		0.28		0.20

Appendix B

Ciliary body image analysis tool

B.1 Introduction

The Aston Longitudinal Assessment of Presbyopia (ALAP) study was run to try to quantify the changes in structure and optics during incipient presbyopia. A key part of the study was investigation into why some individuals become increasingly myopic during this period. The study was to be conducted over a 2.5 year period, collecting data from 58 emmetropic and myopic subjects aged 33 – 45 years, with data collected every 6 months.

One of the subsets of data collected was on the measurement of the ciliary muscle, in both relaxed and accommodated states, using the Visante OCT system. Although the Visante allows for measurement of the ciliary body, it was not designed for this purpose, therefore, measurements were taken by manually fitting callipers to subject images. It was decided that a more robust method was required for analysing these images. In particular, a study by Kao *et al.* (2011) had developed a semi-automated oct measurement tool to extract thickness measurements. However, the methods used appeared to measure the overall ciliary body thickness rather than the ciliary muscle, in addition to approximating the anterior thickness of the ciliary body. The thickness measurements used also were consistent in being measured 1, 2 and 3 mm from the scleral spur, not taking into account the changing length of the ciliary body with age (Sheppard & Davies, 2010).

It was therefore decided to develop a method of fitting curves to the ciliary muscle itself, in addition to measuring at 25, 50 and 75% of the ciliary muscle length.

B.2 Method

The first stage in the process was the adjustment of the original DICOM images that were extracted from the Visante. The raw images measured 1024 by 512 pixels and were in the RGB format (Figure B.1). The images had to be rotated by 90 degrees, before being resized to reflect the actual aspect ratio of the ciliary muscle, which was 512 by 1280 pixels (assuming a conversion of 128 pixels per mm) following Kao *et al.* (2011). A conversion to grey-scale was completed to reduce the complexity of the image. The resultant adjusted images had their histogram automatically adjusted to remove any excess noise in the image, as shown in Figure B.1.

To begin the curve fitting process, a number of points need to be defined by the user. The first was the location of the scleral spur (SS), followed by an approximation of the ending point of the ciliary muscle. Additional points highlighting the top and bottom of the ciliary muscle were also selected visually, at the midpoint between the SS and right hand boundary. These points were then used to form a mask, formed from two polynomials, so that only the relevant ciliary muscle region is used in the curve fitting process, removing the data from the rest of the image Figure B.1.

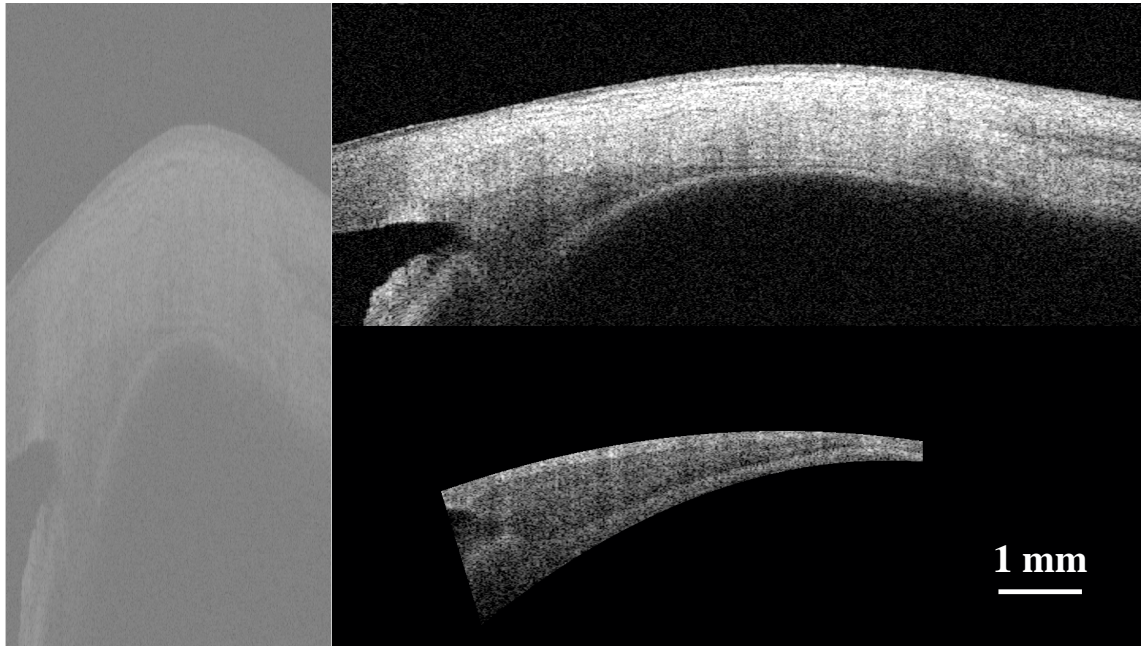


Figure B.1: Comparison between the original DICOM image (Left), its rotation and histogram adjustment (Top right) and the final region of interest (Bottom right).

With the relevant region extracted, the curve fitting process could be started. A block of 10 vertical lines, every 0.5 mm between the scleral spur and the ciliary muscle end point, were defined that passed through the ciliary muscle region. These lines were then split into two smaller lines, covering the top and bottom part of the ciliary muscle, and the pixel intensity values along the lines were then extracted. The intensity change along the line can then be established to find the boundary of the ciliary muscle, which is where there was a change in intensity. To define the boundary point, a second order fourier series was fitted to the intensity profile and then differentiated. The peaks of the curve could then be established for each of the 10 lines in the block, defining the crossing points. These points can then be used to define a polynomial curve for both the top and bottom edge of the ciliary muscle, as shown in Figure B.2.

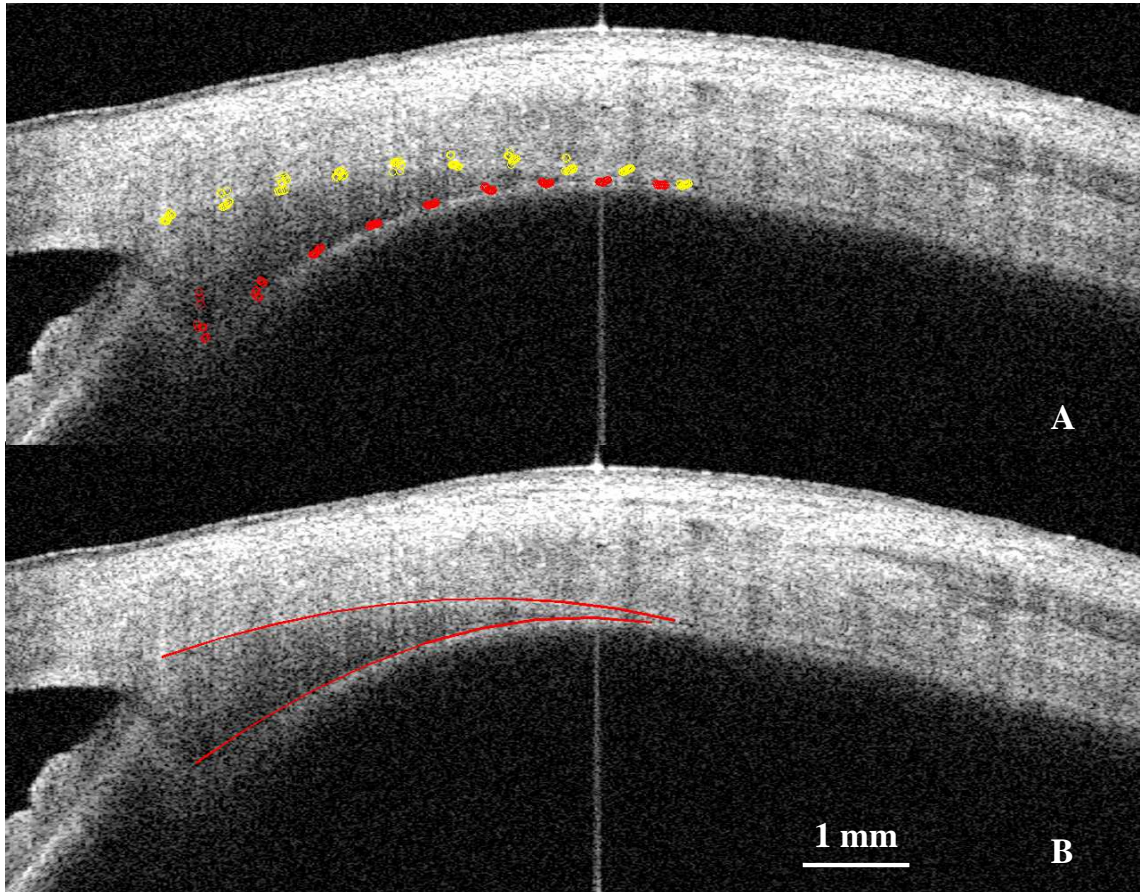


Figure B.2: Illustration of the points used to define the top and bottom of the ciliary muscle (A) and the resulted fitted curves (B).

To establish the actual measurement of the ciliary muscle thickness and length, the images needed to be dewarped to reflect the impact of the refractive index of the sclera and ciliary body, achieved through adjustment of the fitted curves. A curve was fitted to the sclera by converting the image to black and white and using the boundary edge detection algorithms in MatLab. The distance between the sclera and ciliary muscle top fit could then be adjusted to reflect the refractive index. The same process was repeated between the top and bottom ciliary muscle fits, allowing the final measurements to then be taken. The majority were straightforward, simply finding the distance between top and bottom curves, assuming a normal to relation between the measurement line and the top edge. However, the ciliary muscle length required a method of definition. It was decided that the ciliary muscle length could be established as the point where the top and bottom ciliary muscle fits began to separate.

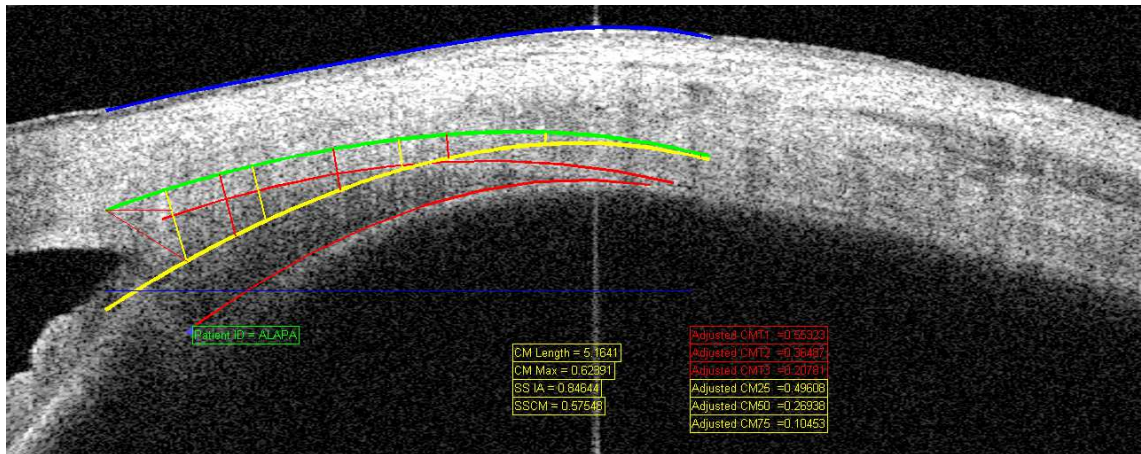


Figure B.3: Illustration of the final measurements. The two red curves represent the original fitted muscle, with the green and yellow curves representing the dewarped curve fits. The blue curve shows the top fit of the sclera, used for the dewarping of the ciliary muscle curves. The rest of the lines represent the measurement locations.

Additional code was written to account for the images where contact lenses were present (Figure B.4). The effect of refractive index due to a contact lens was assumed to be negligible; therefore, the contact lens was removed from the image before the measurements were taken.

B.3 Results

The tool was trial run on a range of images, with some images having artefacts to ensure that the program was robust enough to measure in all cases. Images with contact lenses were also tested. In those images that were clear with no artefacts or contact lenses, the analysis time was less than 1 minute.

With more complex images, such as those shown in Figure B.4, some addition code was written to allow the bottom ciliary muscle edge to be manually defined, as typically this was the edge that did not fit where artefacts were present. In those images where a contact lens was present, or the ciliary muscle edge was manually defined, the analysis time increased, but remained under 2 minutes.

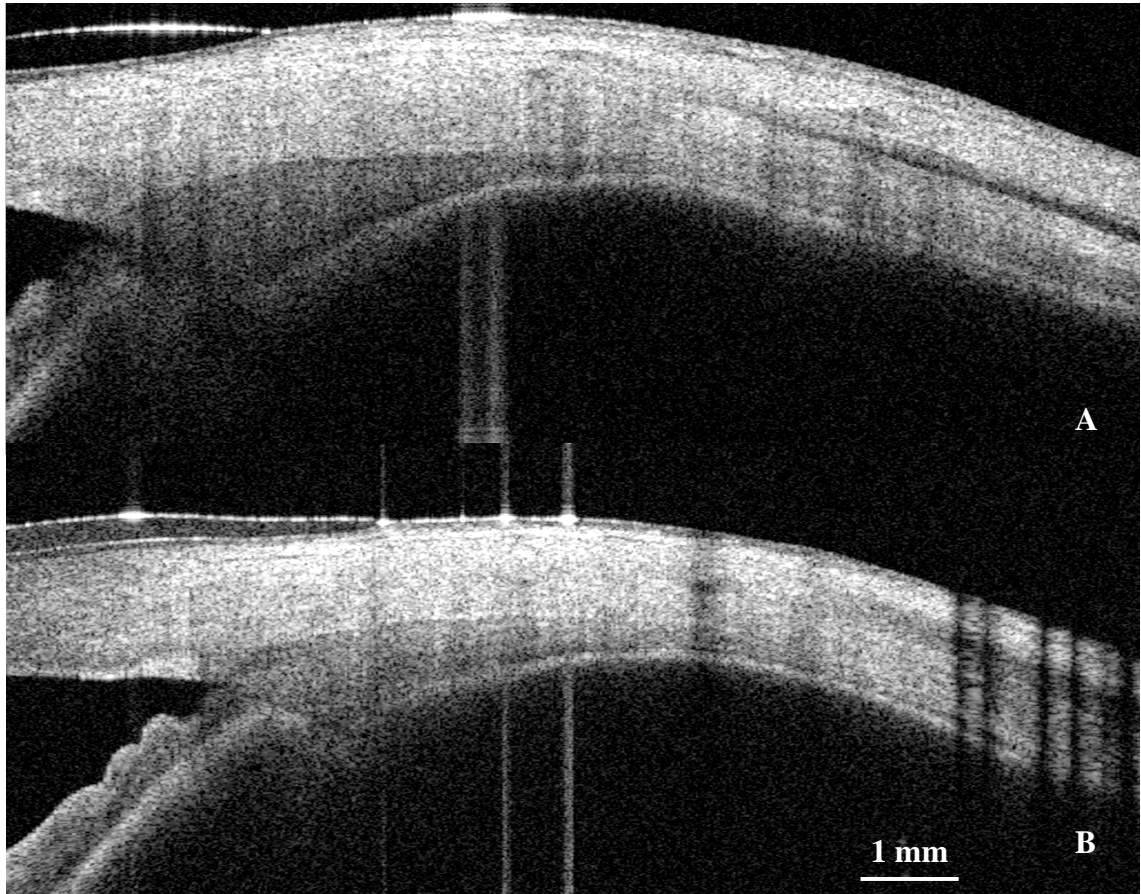


Figure B.4: Two examples of poor images, illustrating the presence of contact lenses and artefacts present.

A complete validation of the measurements was not conducted at the time of writing, but a set of images had been measured manually on the Visante, and it was proposed that the same images would be measured using the tool to compare the two sets of results.